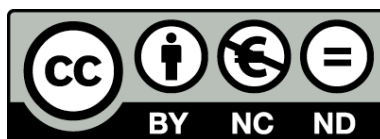




UNIVERSITAT DE  
BARCELONA

## Development and applications of photoswitchable muscarinic ligands

Fabio Riefolo



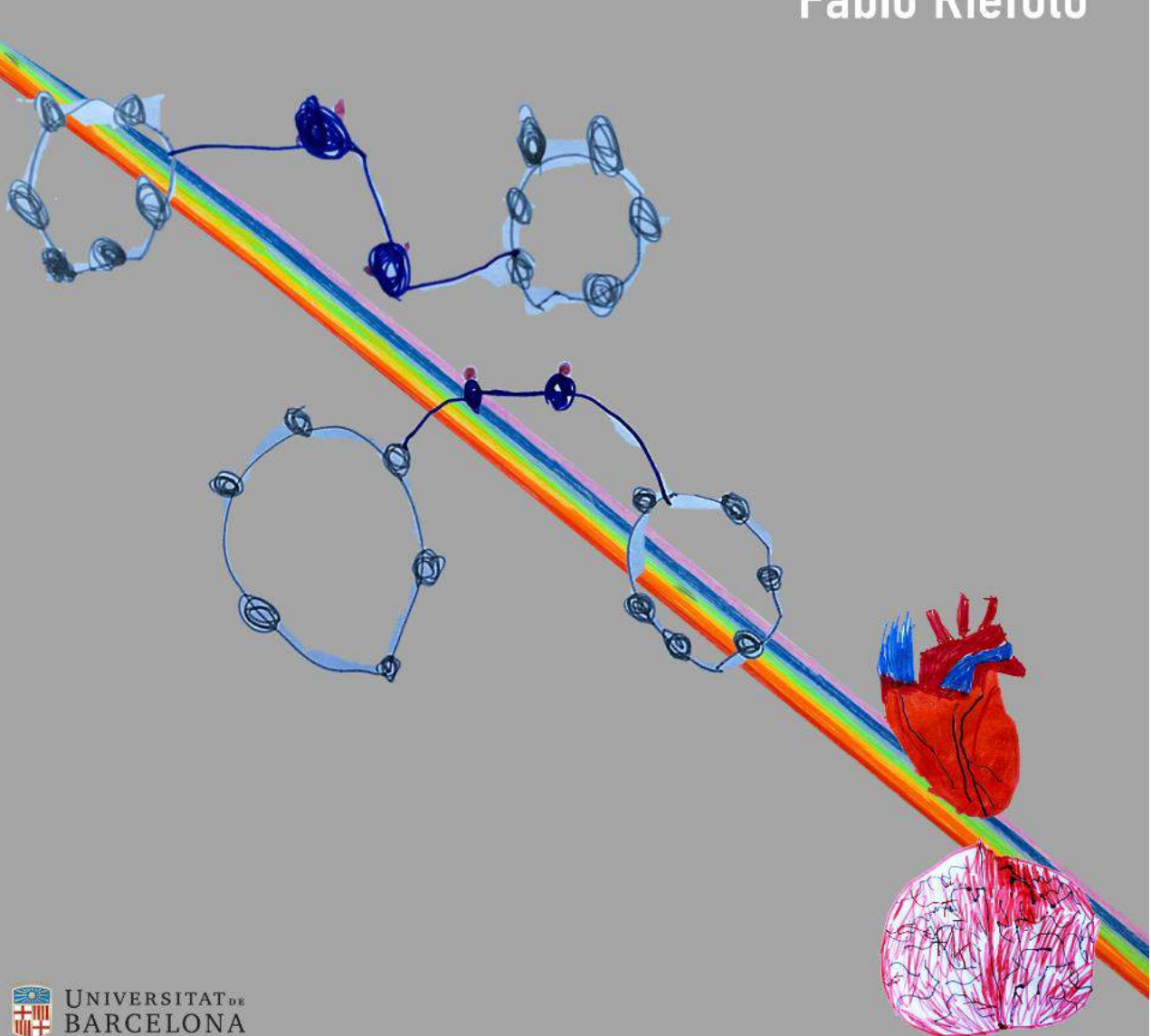
Aquesta tesi doctoral està subjecta a la llicència **Reconeixement- NoComercial – SenseObraDerivada 4.0. Espanya de Creative Commons.**

Esta tesis doctoral está sujeta a la licencia **Reconocimiento - NoComercial – SinObraDerivada 4.0. España de Creative Commons.**

This doctoral thesis is licensed under the **Creative Commons Attribution-NonCommercial-NoDerivs 4.0. Spain License.**

# DEVELOPMENT and APPLICATIONS of PHOTOSWITCHABLE MUSCARINIC LIGANDS

Fabio Riefolo







UNIVERSITY of BARCELONA

Doctoral Program in Organic Chemistry

*Biological Chemistry and Medicinal Chemistry*

PhD Thesis of Fabio Riefolo

2016-2020

**DEVELOPMENT and APPLICATIONS  
of PHOTOSWITCHABLE MUSCARINIC LIGANDS**

Director: Pau Gorostiza

ICREA Researcher Professor at the  
Institute for Bioengineering of Catalonia  
Nanoprobes and Nanoswitches Group

Tutor: Pedro Romea García

Professor at the University of Barcelona  
Department of Inorganic  
and Organic Chemistry

*Barcelona, June 2020*



*Alla mia famiglia,*



# TABLE of CONTENTS

Abbreviations.....	7
CHAPTER I – Introduction.....	9
Preface.....	11
1. Acetylcholine (ACh).....	13
1.1. Muscarinic Acetylcholine Receptors.....	17
1.1.1. General structure and intracellular activation mechanisms.....	17
1.1.2. M1, M3 and M5 receptor family.....	20
1.1.3. M2 and M4 receptor family.....	22
1.1.4. Conclusions about mAChRs intracellular signaling mechanisms.....	26
1.2. ACh binding site and activation of mAChRs: the orthosteric site.....	27
1.3. The Allosteric Site of mAChRs.....	33
1.4. Classification of the mAChRs, physiological functions and Pharmacology.....	40
1.4.1. Muscarinic acetylcholine receptor M1.....	41
1.4.2. Muscarinic acetylcholine receptor M2.....	43
1.4.3. Muscarinic acetylcholine receptor M3.....	45
1.4.4. Muscarinic acetylcholine receptor M4.....	46
1.4.5. Muscarinic acetylcholine receptor M5.....	47
1.5 Conclusions about mAChRs.....	47
2. Control of Protein Function using Light.....	49
2.1. The molecular photo-switches.....	52
2.1.1. Diarylethenes.....	53
2.1.2. Fulgimides.....	54
2.1.3. Spiropyrans/Merocyanines.....	55
2.1.4. Azobenzenes.....	56
2.2. Methods to photocontrol biological systems.....	65
2.2.1. Optogenetic.....	65
2.2.2. Photoswitchable tethered ligands (PTLs).....	66
2.2.3. Photopharmacology using caged compounds.....	69
2.2.4. Photopharmacology using photoisomerisable free ligands.....	72

2.3. Conclusions about photopharmacology.....	77
3. Objectives of the Thesis.....	79
CHAPTER II - Development of Orthosteric Photoswitchable Agonists to Control Muscarinic Receptors.....	81
General Introduction Chapter II.....	83
<i>Fluorination of Photoswitchable Muscarinic Agonists Tunes Receptor Pharmacology and Photochromic Properties.....</i>	85
Supporting Information.....	109
General Discussion Chapter II.....	119
CHAPTER III - Novel Photoswitchable Muscarinic Agonists Obtained by Molecular Hybridization of Orthosteric and Allosteric Ligands.....	121
General Introduction Chapter III.....	123
<i>Optical Control of Cardiac Function with a Photoswitchable Muscarinic Agonist.....</i>	127
Supporting Information.....	145
<i>Control of brain state transitions with a photoswitchable muscarinic agonist.....</i>	167
Supporting Information.....	191
General Discussion Chapter III.....	195
CHAPTER IV - Light-sensitive MI Muscarinic Antagonists Designed with a Novel "Crypto-azologization" Method.....	199
General Introduction Chapter IV.....	201
<i>Rational design of photochromic analogs of tricyclic drugs.....</i>	203
Supporting Information.....	219
General Discussion Chapter IV.....	249
CHAPTER V - Conclusions.....	253
BIBLIOGRAPHY.....	259
SUMMARY in Spanish.....	279

## Abbreviations

2D	Two-Dimensional
3D	Three-Dimensional
Abn	Azobenzene Derivatives Family
AA	Arachidonic Acid
aAB	Aminoazobenzene Derivatives Family
AC	Adenylate Cyclase
ACh	Acetylcholine
AChE	Acetylcholinesterase
ADP	Adenosine Diphosphate
Ala	Alanine
AMP	Adenosine Monophosphate
ANS	Autonomic Nervous System
Asn	Asparagine
Asp	Aspartate
ATCM	Allosteric Ternary Complex Model
ATP	Adenosine Triphosphate
ATSM	Allosteric Two-State Model
bAB	Diazocines or "Bridged Azobenzene" Family
BBB	Blood-Brain Barrier
cAMP	3',5'-cyclic Adenosine Monophosphate
CCh	Carbachol
ChAT	Choline Acetyltransferase
ChRs	Channelrhodopsins
CNS	Central Nervous System
CoA	Coenzyme A
Cys	Cysteine
DAG	Diacylglycerol
G	GTP-binding
GABA <sub>A</sub> R(s)	Ionotropic $\gamma$ -Aminobutyric Acid Receptor(s)
GIRKs	G Protein-Activated Inwardly Rectifying K <sup>+</sup> Channels
Gluk2	Glutamate Ionotropic Receptor Kainate type subunit 2
GPCR(s)	G Protein-Coupled Receptor(s)
GTP	Guanosine Triphosphate
IAI	Iper-Azo-Iper
IP <sub>3</sub>	Inositol Trisphosphate
IPX	Iperoxo
mAChRs	Muscarinic Acetylcholine Receptors
MAP Kinase	Mitogen-Activated Protein Kinases
mGluRs	Metabotropic Glutamate Receptors
MscI	Large-Conductance Mechanosensitive Channel
NA	Noradrenaline

nAChRs	Nicotinic Acetylcholine Receptors
NAI	Naphthalimide-Azobenzene-Iperoxo
NIR	Near-Infrared
NMS	N-Methylscopolamine
PA	Phosphatidic Acid
PAI	Phthalimide-Azobenzene-Iperoxo
PAP	Phosphatidate Phosphohydrolase
PCLs	Photochromic Ligands
PDE	Phosphodiesterase
Phe	Phenylalanine
PI	Photoiperoxo
PIP <sub>2</sub>	Phosphatidylinositol-4,5-bisphosphate
PKA	Protein Kinase A
PKC	Protein Kinase C
PLC	Phospholipase C
PLD	Phospholipase D
PNS	Peripheral Nervous System
ppAB	Push-pull Azobenzene Family
PSNS	Parasympathetic Nervous System
PTLs	Photoswitchable Tethered Ligands
SAR	Structure-Activity Relationship
Ser	Serine
SNS	Sympathetic Nervous System
Thr	Threonine
TMD	Transmembrane Domains
toAB	Tetra-ortho substituted Azobenzene Family
Trp	Tryptophan
Tyr	Tyrosine
UV	Ultraviolet
Val	Valine
Vis	Visible

**CHAPTER I**  
**Introduction**



# Preface

## Italy, Spain and Acetylcholine

Camillo Golgi (Italian, 1843-1926) is recognized as the greatest neuroscientist and biologist of his time. He studied medicine at the University of Pavia and became a biologist and pathologist famous for his works on the central nervous system.

Santiago Ramón y Cajal (Spanish, 1852-1934) is recognized as a pioneer of modern neuroscience and his drawings of brain cells are still largely in use for educational purposes. He graduated in medicine at the University of Zaragoza and became a neuroscientist, specialized in neuroanatomy, and he focused on the histology of the central nervous system.

In 1906, “in recognition of their work on the structure of the nervous system”, Golgi and Ramón y Cajal jointly received the Nobel Prize in Physiology or Medicine. They were the first persons of Italian and Spanish origin, respectively, who won a scientific Nobel Prize in Medicine.

During the 19<sup>th</sup> century Golgi discovered that brain cells could be colored using silver nitrate opening the door to essential studies of how the nervous system is structured. He believed in a nervous system made by a continuous and interconnected network of nerve cells, in disagreement with Ramón y Cajal’s opinion.

In 1877, Ramón y Cajal takes advantage of Golgi’s method to stain brain cells, achieving many groundbreaking results in the next years. One of his histological examinations proved that the nervous system is not an interconnected network, as Golgi supported, but it is constituted by

independent neuronal entities with a 20-40 nm gap in between, today known as the synaptic cleft. Such discovery proved that each brain cell is an independent entity and neuronal synapses are the places where the nerve impulses are transferred, from one neuronal entity to another.

Scientifically, until the early 20<sup>th</sup> century, it was assumed that the majority of the communications transferred between brain cells in the synaptic cleft was of electrical nature. However, the presence of such a gap discovered by Ramón y Cajal also suggested the existence of another type of communication, of chemical nature, via messengers traversing the synaptic cleft.

The presence of neurotransmitters, endogenous chemical messengers released by neurons in the synaptic space and that enable neurotransmission, was finally discovered in 1914 by a pharmacologist and physiologist, Sir Henry Hallett Dale (English, 1875-1968). Neurotransmitters existence was later confirmed in 1921, by a German pharmacologist, Otto Loewi (1873-1961).

In 1936, Dale and Loewi shared the Nobel Prize in Physiology or Medicine “for their discoveries relating to chemical transmission of nerve impulses”.

They identified for the very first time a neurotransmitter.  
The Acetylcholine.

## 1. Acetylcholine (ACh)

Acetylcholine (ACh) is one of the most abundant neurotransmitters in the central nervous system (CNS) and peripheral nervous system (PNS) of many types of animals, including humans. ACh is not only the most common chemical messenger, but it was also the very first neurotransmitter to be identified (Prado et al., 2017; Tansey, 2006). The name “acetylcholine” is derived from its chemical structure. It is made up of an ester of acetic acid and choline. The presence of the polar charged ammonium group avoids the penetration into lipid membranes of the body, thus peripheral administrations of the drug are not able to pass through the blood-brain barrier (BBB). Certain CNS neurons directly synthesize ACh by the enzyme choline acetyltransferase (ChAT) from the compound choline and the coenzyme acetyl-CoA. Acetylcholinesterase (AChE) is another enzyme that is abundant in the synaptic cleft and has the essential role to convert ACh into inactive metabolites choline and acetate ion. Therefore, AChE rapidly cleans the synapse from the presence of the neurotransmitter (**Figure 1**). Cholinergic synapses are those in which transmission is mediated by ACh. Precisely, all the parts in the body that are affected by ACh are stated as cholinergic (**Figure 2**).

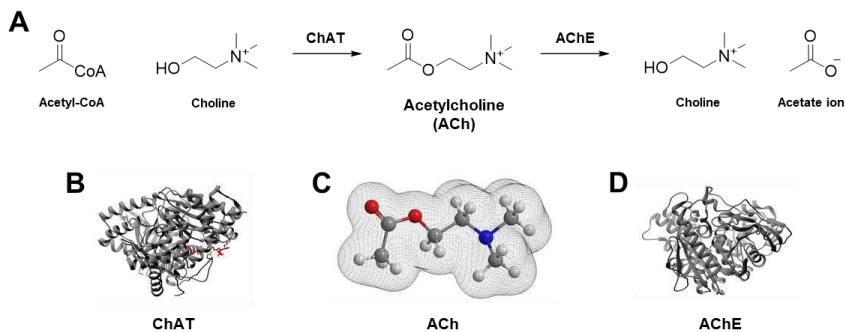


**Figure 1. Acetylcholine Synthesis and Metabolism.** A) Acetylcholine (ACh) is synthesized from acetyl coenzyme A (Acetyl-CoA) and choline by the enzyme choline acetyltransferase (ChAT). Neuronal acetylcholinesterase (AChE) inactivates the majority of ACh released in brain. B) 3D structure of the human ChAT (PDB code 2FY4). C) 3D structure of ACh in balls with a surface of charge density as a wire mesh. D) Crystal structure of human AChE (PDB code 4PQE).

The communication between the nervous system and the rest of the body is mediated by neuronal connections from the CNS with the PNS, muscles and glands. This is a very complex process involving a variety of interrelated mechanisms. Neurons communicate using a combination of chemicals and electricity. For communicating, they use the secretion of chemical messengers, called neurotransmitters, in the synaptic cleft or the direct transmission of intercellular signals through gap junctions at electrical synapses. The autonomic nervous system (ANS) is the branch of the PNS that controls the body's involuntary actions and visceral functions. Traditionally, the ANS is divided into the sympathetic nervous system (SNS) and the parasympathetic nervous system (PSNS). For both the systems, SNS and PSNS, the signals through the inter-neuronal connections can be driven by the action of the neurotransmitter ACh (Waxenbaum et al., 2019). Moreover, the postganglionic neurons in the PNS, as well as those of the SNS that innervate the sweat glands and the piloerector muscles, also transmit their signals to effector organs by the means of release of ACh. It binds to its ACh receptors on the target organs and performs its activity. All other postganglionic neurons of the SNS, however, mediate their communications through another neurotransmitter: noradrenaline (NA) (Huang and Thathiah, 2015; Prado et al., 2017). ACh is implicated in a vast range of functions. In the CNS, it predominantly enhances cognitive functions, such as learning and memory, alertness, attention (Hasselmo and Sarter, 2011). In the PNS, it activates skeletal muscles activities. In particular, ACh is the major neurotransmitter in the ANS, regulating vital functions like the heart rate, digestion, respiratory rate, pupillary response, urination, and sexual arousal (Prado et al., 2017; Schmidt and Thews, 1989). The ACh actions differ depending on the type of receptors through which it undergoes mediation. These receptors are classified as nicotinic (ionotropic) and muscarinic (metabotropic) receptors (**Figure 2**).

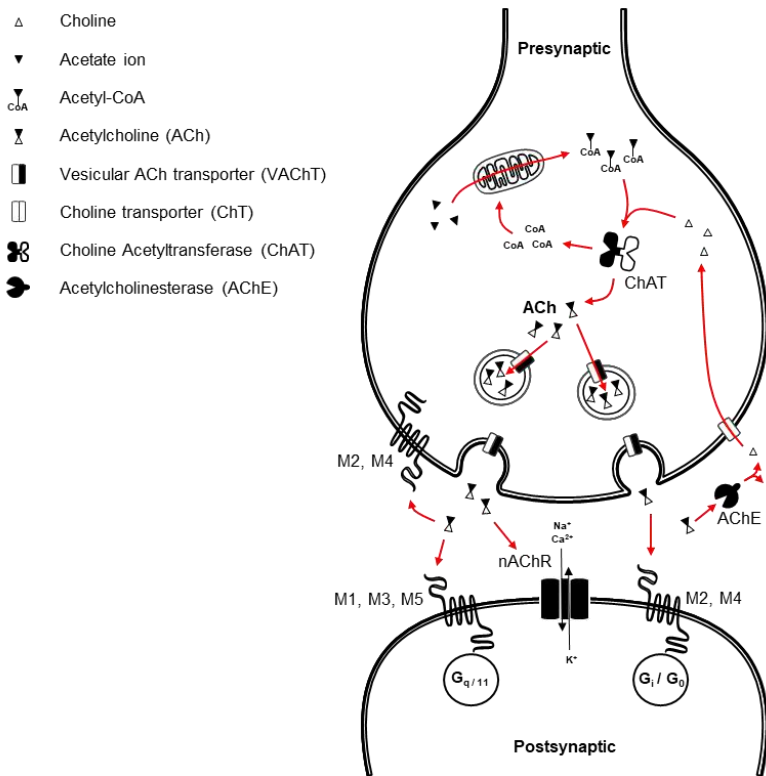
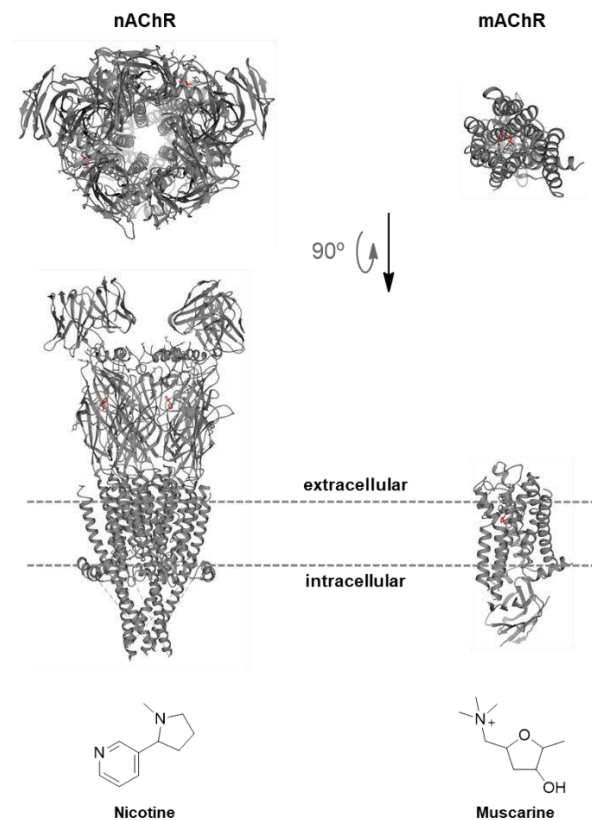


Figure 2. Schematic Cholinergic Synapse. Adapted from Cuello, 2009.

Nicotinic acetylcholine receptors (nAChRs) get their name from nicotine (Figure 3), the potent stimulant alkaloid that is naturally produced by the Solanaceae plants family and binds to the nicotinic receptor selectively (Itier and Bertrand, 2001; Purves et al., 2011). The nAChRs are considered the prototypic of the transmembrane ion-channel proteins group. This class of channel proteins are responsible for the fast synaptic transmission between neurons, and belong to the Cysteine (Cys)-loop ligand-gated ion channel superfamily. In response to the binding of a chemical ligand, such as ACh or nicotine, the receptor conformation changes in its open state, which leads to a flow of ions (such as Na<sup>+</sup>, K<sup>+</sup>, Ca<sup>2+</sup>, and/or Cl<sup>-</sup>) across the cell membrane. In particular, nAChRs are non-selective cation channels, permeable to Ca<sup>2+</sup>, Na<sup>+</sup> and K<sup>+</sup> ions (Beker et al., 2003; Purves et al., 2011; Weber et al., 2005). The nAChRs are exclusively found in the neuromuscular junction. Precisely, they are expressed in the cell membrane of the skeletal muscle fiber. Neuromuscular junction is a chemical synapse between a motor neuron and a muscle fiber. Here, ACh

is released from the motor neurons, diffuses across the synaptic cleft and activates nAChRs of the muscle fiber. This activation triggers muscle contraction. Moreover, nAChRs have a role in the immune system for regulating inflammatory processes (Lu et al., 2014), and, together with muscarinic receptors, are present in autonomic ganglion cells and neuronal cells from the CNS.

Muscarinic acetylcholine receptors (mAChRs) get the name from another natural product. This molecule is known as muscarine (**Figure 3**), was found in the mushrooms *Amanita muscaria* and selectively attaches to such receptors.



**Figure 3. nAChR, mAChR, Nicotine and Muscarine Chemical Structures.** The nAChR (PDB code 6PV7) and the mAChR (PDB code 4MQT) shown in side- and top-view (from the extracellular side) and fitted to the same scale, and the chemical structure of nicotine and muscarine.

The mAChRs belong to the large protein family of G protein-coupled receptor (GPCR). They are responsible for the slow modulation of synaptic transmission. In response to the binding of an agonist as ACh or muscarine, mAChRs activate internal signal transduction pathways and, finally, cellular responses. This slow synaptic modulation is mediated by the five members of the mAChRs superfamily, M1-M5 (Caulfield and Birdsall, 1998). These five subtypes of mAChRs are classified mainly on the basis of their different distribution, sequence homology, and the signaling transduction pathway they are coupled to, and will be described in detail in the following sections.

## **1.1. Muscarinic Acetylcholine Receptors**

### **1.1.1. General structure and intracellular activation mechanisms**

Muscarinic acetylcholine receptors are important members of the G protein coupled receptors (GPCRs) class A superfamily, also called rhodopsin-like superfamily. They are abundant and widely distributed throughout the CNS and the PNS. The mAChR subtypes were named based on the order of their discovery. We know five members, M1-M5, and the genes for the all subtypes were identified, cloned, and sequenced around 1990. They principally differ in their primary structure, localization, pharmacology, and signal transduction activity (**Table 1**) (Aronstam and Patil, 2009; Caulfield and Birdsall, 1998).

Muscarinic receptors proteins are single polypeptides of 460–590 amino acids, generically folded in seven transmembrane domains (TMD) and joined by alternating extracellular and intracellular loops, with the N-terminal end toward the extracellular side and the C-terminal end toward the intracellular side (Aronstam and Patil, 2009; Hulme et al., 1991). The amino acids sequences that form the membrane-spanning regions reveal 20-24 amino acids organized in  $\alpha$ -helical structures. Their composition in these domains is highly conserved among the five subtypes, with a 90% of similarity of the amino acid sequences. These receptors do not interact directly with their respective downstream effector, such as ionic channels do. They exert their intracellular effects controlling one or more systems through the activation of an intermediary GTP-binding (G-) protein.

	Subtype				
	M1	M2	M3	M4	M5
Molecular weight <sup>a</sup>	51240	51715	66127	53058	60186
Amino acids	460	466	590	479	532
G-proteins	G <sub>q</sub> , G <sub>11</sub>	G <sub>i</sub> , G <sub>o</sub>	G <sub>q</sub> , G <sub>11</sub>	G <sub>i</sub> , G <sub>o</sub>	G <sub>q</sub> , G <sub>11</sub>
Second messengers <sup>b</sup>	IP <sub>3</sub> /DAG, NO	CAMP (↓)	IP <sub>3</sub> /DAG, NO	cAMP (↓)	IP <sub>3</sub> /DAG, NO
Tissues <sup>c</sup>	brain, ANS ganglia, SNS ganglia, secretory glands, vas deferens	brain, heart, SNS ganglia, lung, ileum, uterus, smooth muscles	brain, secretory lands, smooth muscles	brain, lung	dilation of cerebral arteries and arterioles; dopamine release
Functions	agonist-induced seizures; learning, control of locomotor activity; indirect inhibition of N- and L-type calcium channels; M current inhibition in SNS ganglion neurons; MAPK pathway activation	agonist-induced akinesia central tremor; corticosterone release; analgesia; hypothermia; smooth muscle contraction; bradycardia; inhibition of N- and P/Q-type calcium channels	papillary and urinary bladder constriction; salivary secretion; smooth muscle contraction; control of dopamine release; maintenance of body mass and food intake	dopamine release; ACh release (hippocampus); depression of motor control; analgesia	dilation of cerebral arteries and arterioles; dopamine release

<sup>a</sup> Molecular weights are calculated only considering the polypeptide contribution. <sup>b</sup> IP<sub>3</sub> / DAG, stimulation of phospholipase C to release the second messenger inositol triphosphate (IP<sub>3</sub>) and diacylglycerol (DAG) from phosphatidylinositol; NO, increase in nitric oxide production. cAMP(↓): inhibition of adenylate cyclase, thereby lowering cellular content of the second messenger cAMP. <sup>c</sup> Only low levels of M5 receptor expression have been detected in tissues.

**Table 1. Properties of muscarinic receptor subtypes.** Table adapted from Aronstam and Patil, 2009; Caulfield and Birdsall, 1998.

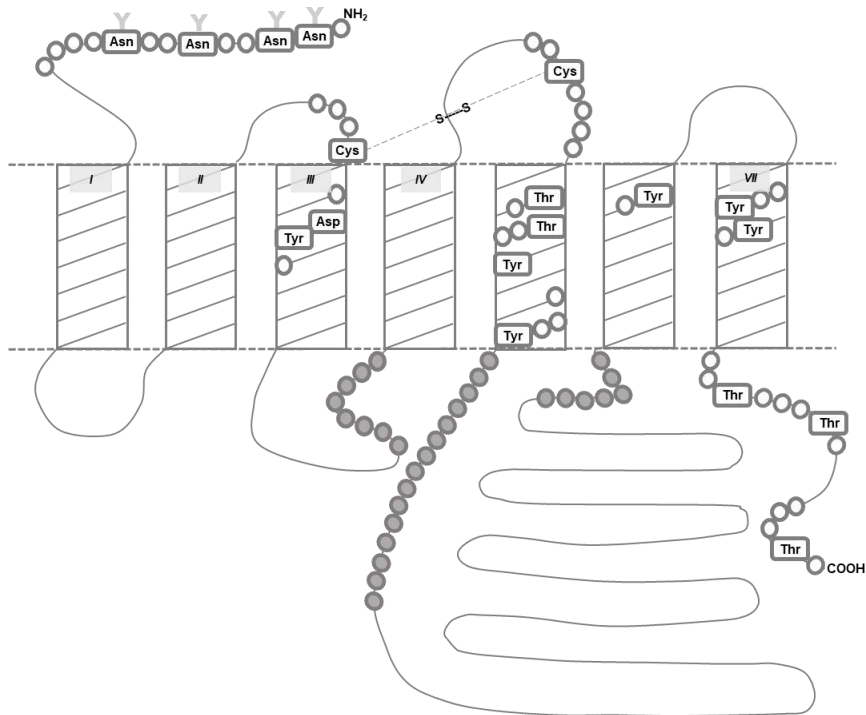


**Figure 4. Schematic Diagram of a Human mAChR.** Schematic diagram showing the primary amino acid sequence of an M2 mAChR. Four sites of glycosylation at Asparagine (Asn) residues are indicated in the extracellular N-terminal domain. In the membrane-spanning regions are indicated the aspartate (Asp), tyrosine (Tyr) and threonine (Thr) residues that are involved in the agonist binding. Regions of the third intracellular loop involved in G-protein recognition and coupling are indicated by gray circles. Possible sites of Thr phosphorylation in the C-terminal domain are also indicated. The Roman numerals indicate the transmembrane domains. Figure adapted from Aronstam and Patil, 2009.

These G-proteins are associated with the inner surface of the cell membrane. In synthesis, G-proteins work as signal transducers, linking extracellularly oriented receptors to inner membrane-bound effectors (Freissmuth et al., 1989). From chimeric receptors and mutational analysis, the regions of the mAChRs involved in the interaction with their respective G-proteins have been identified with the second intracellular loop plus the N- and C-terminal portions of the third intracellular loop (Aronstam and Patil, 2009). Practically, the intracellular signal transduction is the muscarinic receptors mode to alter the activity of receptive cells. This mode follows different pathways depending on the nature and the quantity of the receptor subtype, transducer proteins, effector molecules,

protein kinase substrates expressed in the tissue, and the potential for cross-talk between the various transduction pathways (Felder, 1995; Nathanson, 2000). Considering their intracellular signaling properties, mAChRs have been traditionally divided into two groups: M1, M3, and M5 are comprised in one and M2 and M4 in another (**Table 1, Table 2** and **Figure 5**).

### **1.1.2. M1, M3 and M5 receptor family**

By streamlining the intracellular traffic in "simpler" pathways, conventional wisdom holds that receptors classified using odd-numbers (M1, M3, and M5) efficiently couple through G-proteins of the G<sub>q</sub> family to the stimulation of the β subtype of phospholipase C (PLC), a class of membrane-associated enzymes. PLC is able to hydrolyze the membrane phospholipid phosphatidylinositol-4,5-bisphosphate (PIP<sub>2</sub>) just before the phosphate group, releasing the second messengers diacylglycerol (DAG) and inositol trisphosphate (IP<sub>3</sub>) (Felder, 1995). DAG remains on the membrane and mediates the association of protein kinase C (PKC) to the cellular membrane. This leads to a control of the function of other proteins, as PKC can phosphorylate hydroxyl groups of their serine (Ser) and threonine (Thr) amino acid residues, and participates to a multiplicity of cell functional responses. Differently, IP<sub>3</sub> is an intracellular cytoplasmic messenger, which interacts with the corresponding receptor on smooth endoplasmic reticulum with a subsequent release of Ca<sup>2+</sup> ions stored, increasing such intracellular ion concentration. Calcium is one of the main intracellular messengers and leads to several cellular responses, such as contraction of muscles and exocrine glandular secretion. M1, M3, and M5 also activate the pathway of mitogen-activated protein kinases (MAP kinase), as well as the pathway of the phospholipase D (PLD) (Costa et al., 2001). MAP kinase is a type of protein kinase that specifically phosphorylates the amino acids Ser and Thr of other proteins, regulating various cell functions including proliferation, gene expression, differentiation, mitosis, cell survival, and apoptosis (Kammer et al., 2000; Tobin and Budd, 2003). Phosphatidylcholine is the PLD's principal substrate. It is hydrolyzed to produce the signal molecule phosphatidic acid (PA), and soluble choline. The former can be further catalyzed by

phosphatidate phosphohydrolase (PAP) to form DAG. Then, DAG-lipase hydrolyzes DAG to generate free arachidonic acid (AA), a polyunsaturated fatty acid, which is an integral constituent of cell membrane phospholipids, conferring it with fluidity and flexibility. In particular, it is abundant in skeletal muscle, brain, liver, spleen and retina phospholipids (Hanna and Hafez, 2018; Ishimoto et al., 1994). AA presents in its chemical structure four double bonds, predisposing it to oxygenation. This reaction produces a plethora of important AA metabolites which are involved in the proper function of the immune system, as well as in the regulation of inflammation process, mood, and appetite. Moreover, M1 and M3 receptors can also inhibit an important type of voltage- and time-dependent potassium conductance, an outward  $K^+$  current known as M current. M channels are unique being open at rest and probably also during the cell depolarization, raising the threshold for firing an action potential. They are strongly involved in the slow depolarizations produced by mAChRs in many types of neurons. As voltage-dependent channels, initial depolarization of a neuron increases the probability that M-channels will open. These channels generate an outward  $K^+$  current which counteracts sodium influx in action potential. The result is the prevention of a full action potential. This is the typical function of M currents during the “phasic-firing”, situation characterized by a transient response with one or few action potentials at the onset of stimulus followed by accommodation. When M1 and M3 are activated, such potassium channels are more likely to be closed and neurons assume a “tonic-firing” behavior, situation characterized by a sustained response, which activates during the course of the stimulus (Brown and Adams, 1980). Other types of currents are activated by M1, M3, and M5 receptors. These are the calcium-dependent potassium, chloride, and cation conductances. The activation mechanism of these calcium-activated channels is probably the result of PLC activation by M1, M3 and M5, the resultant formation of  $IP_3$  and release of intracellular calcium ions (Neher et al., 1988).

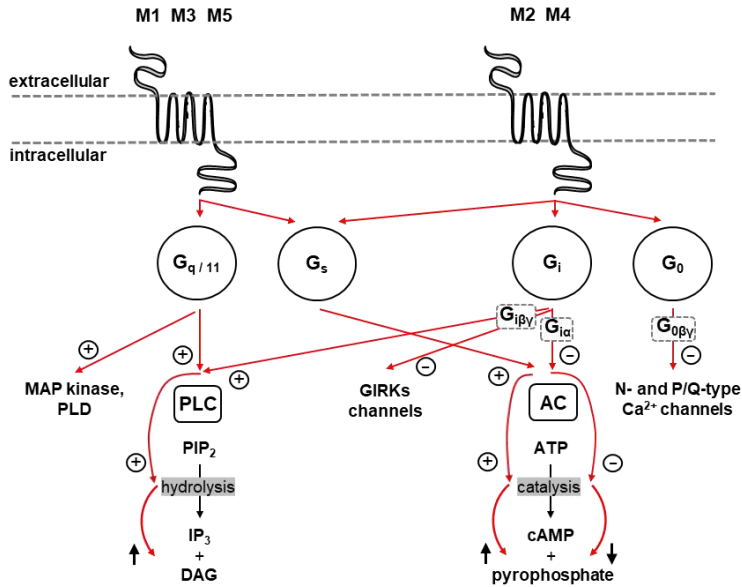


**Figure 5. Muscarinic Receptor Signaling Pathways.** The stages of the signal transduction after the mAChRs activation include the receptor, the transducer (G-protein), the effector (enzyme or ion channel), the second messenger production (cAMP, DAG, and IP<sub>3</sub>), and the protein kinase activation. M2 and M4 receptors inhibit adenylate cyclase (AC) through the activation of G<sub>i</sub>. M1, M3, and M5 receptors stimulate phospholipase C (PLC) through the activation of G<sub>q/11</sub>. mAChRs signaling involves an impressive variety of other pathways. For instance, under the right conditions all receptors can stimulate AC through the activation of G<sub>s</sub>. Other pathways are activated directly or secondarily.

### 1.1.3. M2 and M4 receptor family

On the other hand, receptors classified with even numbers (M2 and M4) prevalently couple through G protein of G<sub>i</sub> to inhibit adenylate cyclase (AC). Any of the three subtypes of G<sub>i</sub> proteins may be involved in such signaling pathway. AC plays a fundamental role in essentially all the cells (Hancock, 2010). This enzyme has six different classes, with unrelated gene families and unknown structural homology (Sadana and Dessauer, 2009), but all catalyzing the same reaction: the conversion of adenosine triphosphate (ATP) to 3',5'-cyclic adenosine monophosphate (cAMP) and pyrophosphate (Zhang et al., 1997). The cAMP is an important molecule in signal transduction. It is known as a second messenger and regulates other cAMP-binding proteins like protein kinase A (PKA) either transcription

factors, or ion transporters. For example, when two cAMP molecules bind to PKA, such kinase phosphorylates various substrate proteins at specific Ser or Thr sites, using the conversion of ATP to adenosine diphosphate (ADP), and causing a variety of cell functional responses, such as regulation of glycogen, sugar, and lipid metabolism (Byrne et al., 2016). One of the PKA substrates is the phosphodiesterase (PDE), which once gets phosphorylated, catalyzes the hydrolysis of cAMP to adenosine monophosphate (AMP) and play a negative feedback control role lead to the reduction of PKA activity. However, the molecular basis for the AC inhibition is not well known and clear.  $G_i$  proteins, as well as all the  $G$  proteins, consist of three subunits, called alpha, beta, and gamma subunits, or,  $G_\alpha$ ,  $G_\beta$ , and  $G_\gamma$ . GPCRs activation causes  $G_\alpha$  dissociation from the dimer  $G_\beta$ - $G_\gamma$  ( $G_{\beta\gamma}$ ), allowing both subunits to perform their respective effects. One of the major functions of  $G_{\beta\gamma}$  is the inhibition of the  $G_\alpha$  subunit (Clapham and Neer, 1997).  $G_i$  alpha subunit ( $G_{i\alpha}$ ) role is to inhibits AC, but not all the isoforms of this enzyme are inhibited by  $G_{i\alpha}$ , an even larger number of AC isoforms are inhibited by  $G_{\beta\gamma}$  dimers (Birnbaumer, 2007). In addition, the inactivation of  $G_i$  by pertussis toxin has revealed the activation of AC by all muscarinic receptor subtypes. In the case of M3, this activation seems to be mediated by an interaction between the muscarinic receptor to the G-protein of the  $G_s$  family. Therefore, the initial classification of muscarinic signaling paradigms in two groups (M1, M3, and M5 through  $G_q$ , and M2 and M4 through  $G_i$ ) has to be extended. It has been identified that mAChRs signaling pathways involve additional transducers. The presence of secondary effects and cross-talk between the different pathways exist and make the distinction between proximal and indirect signaling events problematic (Nathanson, 2000). Another effect related to muscarinic receptors stimulation is the activation of several depolarizing and hyperpolarizing currents through both direct and indirect mechanisms. In particular, M2 and M4 receptors activation were found to regulate and desensitize  $K^+$  channels, giving rise to the ion current known as  $I_{KACH}$ . This family of  $K^+$  channels has been found in cardiac and neuronal tissues. Here, they are classified as G protein-activated inwardly rectifying  $K^+$  channels (GIRKs) because of their direct activation upon binding to G protein subunits ( $G_{\beta\gamma}$  subunits). Such binding favors and serves to strengthen the required  $PIP_2$ -channel interaction, thereby

hyperpolarizing the cells (Bünemann et al., 2000). Since  $PIP_2$  seems to be required for the activity of such  $K^+$  channels (Huang et al., 1998), the M3 receptor activation, which stimulates PLC to hydrolyze  $PIP_2$ , limits the open state of GIRKs. From other studies, M2 and M4 have shown also to inhibit voltage-dependent calcium channels, known as L-type calcium channels. “L” stands for long-lasting, as it is referred to the length of its activation. L-type calcium channels are responsibly involved in the mechanism of excitation-contraction of skeletal, smooth, cardiac muscle, and in the aldosterone secretion in endocrine cells of the adrenal cortex (Felizola et al., 2014; Ortner and Striessnig, 2016; Striessnig et al., 2015). M2 and M4 receptors indirectly inhibit the L-type calcium conductance by a reduction in cAMP concentration. M1 receptors are as well able to inhibit the L-type calcium channel, via the activation of PKC (Pemberton and Jones, 1997). M2 and M4 receptors present also a direct inhibition mechanism for  $Ca^{2+}$  entrance through other voltage-dependent calcium channels, known as N- and P/Q-type calcium channels. N- and P-type calcium channels are distributed throughout the entire body and play a central role in the release of neurotransmitters. P-type and Q-type calcium channels are closely related as they are produced from the same gene via alternative splicing. Malfunctioning or mutated P/Q-type channels are related to several neurological diseases (Wakamori et al., 1998). The direct inhibition of such voltage-dependent calcium channels probably results from mAChRs activation of the G protein  $G_o$  and consequent direct interaction of the  $G_o$  protein subunit,  $G_{\beta\gamma}$ , with the channels (Allen and Brown, 1993).

<i>Intracellular messenger</i>					
	<b>IP<sub>3</sub></b>	<b>DAG</b>	<b>cAMP</b>	<b>MAP kinase</b>	<b>PLD</b>
<i>Action</i>	binding to smooth endoplasmic reticulum	staying on the cellular membranes (and hydrolyzed into AA)	activation of cAMP-binding proteins (PKC), transcription factors or ion transporters	phosphorylation of various proteins	generation of AA
<i>Effect</i>	↑ Ca <sup>2+</sup> intracellular	↑ PKC-cellular membrane association	↑ PKA	regulation of various cell functions	↑ AA
<i>Function</i>	contraction of muscles; exocrine glandular secretion; inhibition of M current; activation of Ca <sup>2+</sup> -dependent K <sup>+</sup> /Cl <sup>-</sup> /cation currents.	phosphorylation of proteins that regulate various cellular functions.	phosphorylation of proteins that regulate glycogen, sugar and lipidic metabolism; negative feedback by ↓cAMP → ↓PKA activity; ↓cAMP → inhibition of L-type Ca <sup>2+</sup> channels.	regulation of gene expression, proliferation, differentiation, mitosis, cell survival, and apoptosis	integral constituent of cell membranes; precursor of DAG; immune system proper function; regulation of inflammation, mood, and appetite.

Table 2. Actions and Effects of the Intracellular Messengers in the mAChRs Signaling.

#### **1.1.4. Conclusions about mAChRs intracellular signaling mechanisms**

In the present situation, a very large variety of biochemical effects of muscarinic receptor activation have been described and other novel effects have been evidenced and are under study. The activities of multiple kinases and phosphatases are affected by muscarinic receptors. It has been recently reported that the activity of nitric oxide synthetase (NOS) was found coupled to muscarinic receptor activation (Leirós et al., 2000; Rosignoli and Pérez Leirós, 2002), or also that muscarinic receptors have substantial mitogenic potency (De Angelis et al., 2012; Jiménez et al., 2002; Song et al., 2007) and activate small GTPases, such as Ras and Rho proteins. These GTPases are involved in turning on genes involved in cell growth, differentiation, and survival (Mattingly et al., 1994; Qian et al., 1995; De Sarno et al., 2005). These effects of muscarinic receptors are mediated by pathways that are not completely understood in detail. The heterogeneity and the unsuspected level of complexity of mAChR-mediated signal transduction grow increasingly complicated virtually every year and may reflect a mixture of factors. One of them is the identification of additional isoforms of signal transduction effectors. As an example, the AC family presents nine isoforms which specifically respond to different signals, including calcium and PKC and the subsequent activation of PKA (Ludwig and Seuwen, 2002). Another important factor is the frequent crosstalk between signaling pathways due to the lack of specificity, or vice versa the remarkably large combination of cell-type-specific differences in signaling produced by the same muscarinic receptor subtype, or the concomitance presence of direct and indirect/secondary effects, or also the expression of different varieties of signal transduction molecules (Nathanson, 2000). Other fundamental points are the agonist-induced downregulation of muscarinic receptor signaling, and the process of receptor desensitization and internalization. Prolonged stimulation of muscarinic receptors may evoke a rapid phosphorylation of conserved Thr residues on the C-terminal portion of the receptor, as well as other sites on the third intracellular loop. This process is associated with the reduction of the agonist affinity and the uncoupling from transducer G-proteins. It evolves in a phosphorylation-dependent internalization of muscarinic receptors. In this case, arrestins are the important small

protein family regulating this GPCRs signal transduction (Bermudez et al., 2017; Lohse and Hoffmann, 2014; Nuber et al., 2016). Arrestin binding to GPCRs can hinder the association of G-protein with receptors and recruit adaptor proteins, such as clathrin, for the receptor internalization (Lohse, 1995; Posor et al., 2015). Clathrins are proteins which play a major role in the formation of coated vesicles and regulate the Clathrin-mediated endocytosis (CME), involved in many cellular physiological processes such as the internalization of growth factors and receptors. Although muscarinic receptor domains located in the third intracellular loop are the ones prominently involved in receptor phosphorylation and subsequent downregulation, a large number of subtype dependent variations in arrestin association and internalization pathways have been described, confirming the high level of complexity involving the muscarinic-mediated signal transduction (Davis et al., 2010; Jung et al., 2017; Mosser et al., 2008). In conclusion, other recent studies reported how mAChRs induce a complex and sustained expression pattern of a variety of genes, which are in particular involved in the regulation of transcription factors, signaling factors, and in the control of cellular functions in post-synaptic target cells (Kammer et al., 2000). A deeper knowledge about the regulation of these genes' expression promises to increase our understanding of muscarinic receptors complex physiology and their intracellular signaling mechanisms (Aronstam and Patil, 2009).

## **1.2. ACh binding site and activation of mAChRs: the orthosteric site**

Despite the five mAChR subtypes share a high degree of sequence homology, they display marked differences in the G-protein-coupling preference and in the physiological responses they can mediate. Some general structural characteristics of these receptors can be identified because of conserved and semiconserved residues in all the five muscarinic subtypes. The TMDs are organized in  $\alpha$ -helical structures with a high percentage of similarity of the amino acid sequence (90%). Three domains are perpendicularly oriented to the membrane and the other four domains form an acute angle (Aronstam and Patil, 2009). These seven transmembrane helices are very tightly packed in a ring-like structure (**Figure 6**) (Wess, 1993). All the five subtypes have a conserved cysteine

adjacent to the third transmembrane segment and another Cys in the middle of the second extracellular loop. These two residues form a disulfide bridge. (**Figure 4**) Chemical modifications of these two Cys in the protein structure decrease the agonist binding affinity and the ability of the receptor to couple to G-proteins, as well as the elimination of such amino acids precludes receptor expression (Kurtenbach et al., 1990b, 1990a). The orthosteric site is defined as the acetylcholine-binding pocket of the muscarinic proteins. This site is formed by amino acid residues that are identical in all the five receptor subtypes. Such structural homologies are also shared with other functionally unrelated ACh-binding proteins, making the development of muscarinic subtype-specific agonists and antagonists very difficult.

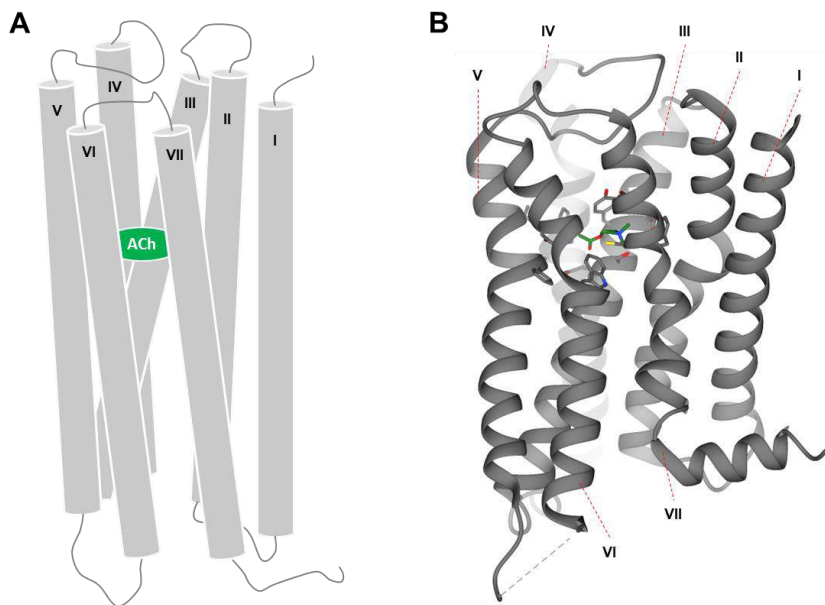


**Figure 6. Disposition of the Seven TMDs and the Orthosteric Binding Site of mAChRs. A)** Schematic view of the possible arrangement of muscarinic receptor transmembrane domains and the binding site of ACh (green). **B)** M2 muscarinic receptor side-view (PDB code 6OIK). ACh (green) is docked in the orthosteric binding site. The Roman numerals indicate the transmembrane domains. Figure adapted from Aronstam and Patil, 2009.

The ACh allocates within a pocket formed by the roughly circularly arranged seven TMDs. Some specific amino acids that reside on the internal surfaces of these different seven domains confers the ligand

binding specificity on the given receptor (**Figure 4** and **6**) (Maeda et al., 2019). Structure-function relationship studies of different muscarinic drugs demonstrated that a cationic head group, generally a quaternary ammonium moiety, is necessary to develop a compound with a strong muscarinic or antimuscarinic activity (Wess, 1993). In fact, looking at the structure of the ACh, it is immediately visible the presence of a positively charged ammonium group. The ACh cationic group is anchored to the muscarinic receptor orthosteric site through ionic interaction with the negatively charged carboxylate side chain of an aspartate (Asp) residue. This specific Asp residue is present in the third transmembrane region of the muscarinic receptor. (**Figure 4** and Asp103 in **Figure 7**) (Wess, 1993; Wess et al., 1995). As a confirmation of this essential interaction, the replacement of such Asp residue in third TMD of M1 receptor with another amino acid, like an asparagine (Asn), resulted in a mutant receptor with drastically reduced orthosteric ligand binding affinities (Fraser et al., 1989).

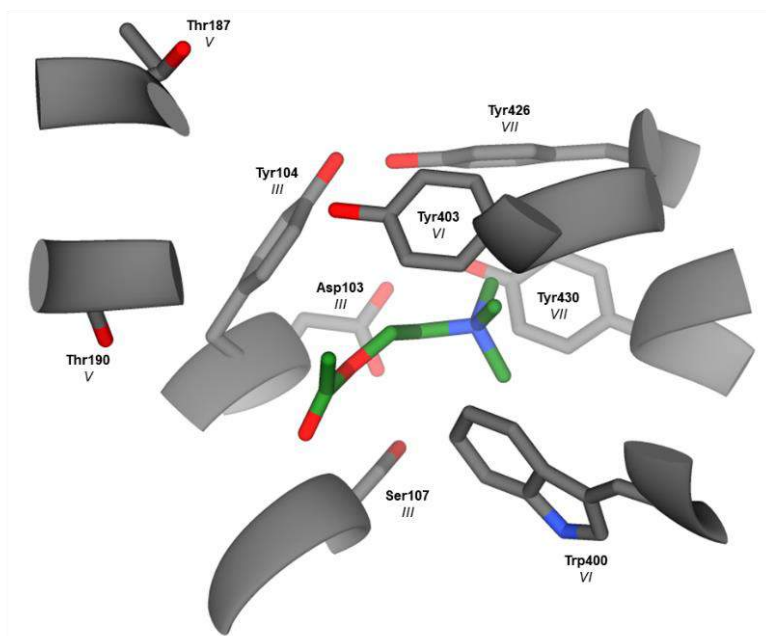


**Figure 7. Specific Amino Acid Residues Involved in the Binding of ACh and mAChRs.** A zoomed view of the orthosteric site of M2 muscarinic receptor (PDB code 6OIK). The amino acids involved in the high-affinity binding of the ACh (green) with mAChR are reported. The Roman numerals indicate the transmembrane domains.

However, the Asp located in the third TMD is not only an essential conserved amino acid among all the subtypes of muscarinic receptors. It appears likely that such specific residue has a fundamental similar role on the ligand-receptor binding affinity for all the endogenous biogenic amines, as it has been demonstrated for adrenaline with the  $\beta$ 2-adrenergic receptor (Strader et al., 1987, 1991). Thus, following these discoveries, the Asp in the third TMD should not be alone to confer the specific binding between ACh and mAChRs, and other important amino acids must be necessarily involved in this interaction. Characteristically, the TMDs of all the muscarinic receptors conserve a series of Serine (Ser), Tyrosine (Tyr) and Threonine (Thr) residues. Most of these amino acids are not present in other GPCRs. In particular, these three amino acids contain a hydroxyl group (OH-group), which can be able to specifically interact with electron-rich groups of muscarinic ligands through hydrogen bonds (Wess et al., 1991). Analyzing the chemical structure of the ACh and other potent muscarinic agonists, it is clear the presence of a common electron-rich center just beside the quaternary ammonium group. The ACh has an ester moiety, the renowned muscarinic agonist carbachol (CCh) has a carbamoyl group and the muscarine has a cyclic ether function. To understand if such conserved muscarinic transmembrane residues containing hydroxyl groups (Ser, Thr, and Tyr) are important to confer binding specificity between orthosteric ligands and mAChRs, specific single mutations on M3 receptor have been studied. Ser, Thr, and Tyr have been individually replaced with Alanine (Ala) and Phenylalanine (Phe), which do not contain OH-groups, and the resulting mutant M3 receptors were pharmacologically characterized in binding studies using ACh and CCh as orthosteric ligands. From these studies emerged that ACh and CCh strongly reduced their binding affinity of 10-60-fold in comparison with the wild type receptor (Wess et al., 1991). In contrast, muscarinic antagonist binding properties are not affected by such M3 receptor aminoacidic mutations. Antagonists maintained similarity to their binding profile obtained with the wild type receptor. This difference between muscarinic agonists and antagonists indicates that different specific residues of mAChRs are involved for their specific binding (Haga et al., 2012; Wess, 1993; Wess et al., 1991). In summary, the critical amino acids involved in the high-affinity binding of ACh to mAChRs are four Tyrosine,

two Threonine, and that Aspartate involved in the ionic interaction with the quaternary nitrogen of ACh. These residues are highly conserved among all the muscarinic receptor subtypes. They are located in the “upper” portion of the third, fifth and seventh TMDs, at about 15 Å from the extracellular surface. The position of these seven amino acids faces the central “binding cavity” and suggests the plane in which ACh interacts with the receptor. They define the ACh binding pocket on the mAChRs and are important both for the expression and the function of such proteins (**Figure 4, 6 and 7**) (Wess et al., 1995). The need of Thr and Tyr residues for the high-affinity binding of ACh to mAChRs suggests the presence of a complex network of hydrogen bonds between the two entities. Other functional studies revealed that two of these Thr and Tyr residues are not only involved in the ACh-receptor binding, but also in the conformational changes of the receptors once they are activated by ACh. The replacement of such two specific amino acids with Ala and Phe, respectively, creates a mutant mAChR with impaired abilities on evoking intracellular responses through G-proteins after its activation. The Thr and Tyr that affect such G-proteins activation are located at a similar level on the fifth and the sixth TMDs (**Figure 4, 6 and 7**). As these two domains are connected between them through the third intracellular loop, this last one is of pivotal importance for the G-protein recognition and their activation (Wess et al., 1992). Taken together, all these studies can affirm that two particular Thr and Tyr residues are conserved among all the subtypes of the mAChRs and play two key roles. The first is the mediation of high-affinity binding between ACh and muscarinic receptors. The second is the change of the geometry of the mAChR once it is activated by ACh through the movement of fifth and sixth TMDs. Such movements are transmitted to the third intracellular loop and result in the activation of the specific G proteins (**Figure 4, 6 and 7**). Therefore, the development of therapeutic agents that can selectively act through an only one subtype of the mAChRs remains an unmet challenge for the field of pharmacology. This is mainly hampered by the high homology of the amino acid sequence in the orthosteric site across all the mAChRs. The most common pharmacological strategy for studying the different profiles of the mAChR subtypes and which activity they govern, is the use of subtype-selective antagonists as they can bind different sites of the receptor than agonists (Wess, 1993). For example,

pirenzepine and 4-DAMP are antagonists with high affinity for binding M1, and low affinity for M2. Differently, methoctramine, himbacine and AFDX-384 have high specificity for M2 and very low for M1. M3 receptor pharmacological involvement was suggested by a high affinity with 4-DAMP, and a low affinity for the ligands pirenzepine, methoctramine, and himbacine. The M4 presence was determined by using PD-102,807 and a natural active peptide toxin, the muscarinic toxin 3 (MT3). The M5 receptor is the most difficult to identify pharmacologically, however, both the ligands AFDX-384 and AQ-RA 741 have the lowest affinity (at least 10-fold lower) for this subtype than any other (**Figure 8**) (Gregory et al., 2007).

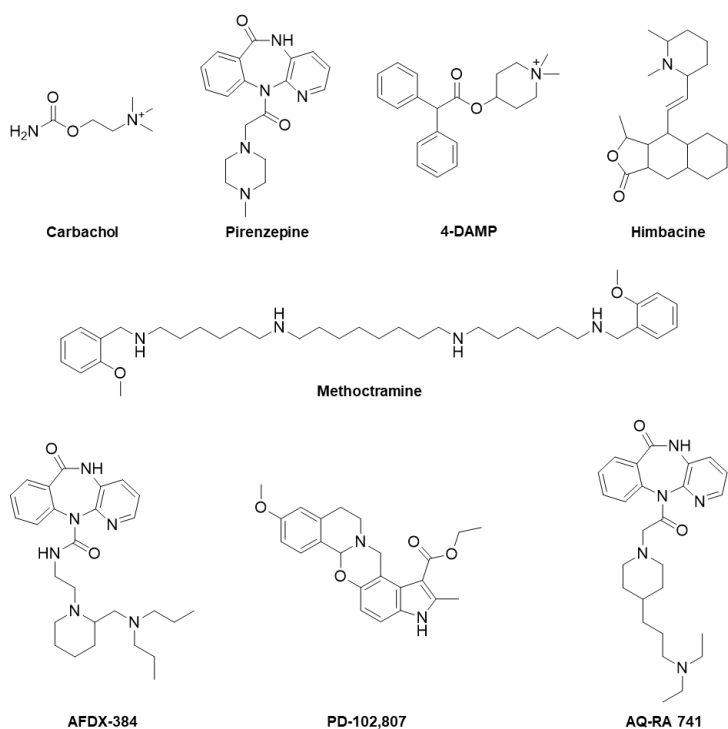
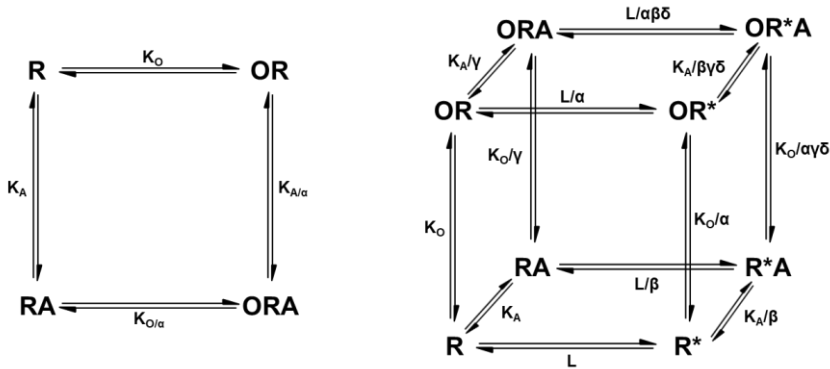


Fig. 8. Widely Used Orthosteric Ligands of mAChRs.

### 1.3. The Allosteric Site of mAChRs

Muscarinic receptors, as other GPCRs, can present one or more allosteric binding sites besides the orthosteric one (Ellis et al., 1991; Lazareno et al., 1998). In the last decades, significant efforts have been underway to study these allosteric sites. They topographically differ from the orthosteric site and are genetically less conserved among the five subtypes of mAChRs. For these peculiarities, the allosteric binding sites represent an interesting target for the development of muscarinic ligands. Various allosteric modulators have been discovered, studied, and reported, and are characterized by different chemical nature (Christopoulos, 2002). When an allosteric modulator is bound to a mAChRs, the receptor conformation can generally change. These conformational changes are transmitted from the allosteric site to the orthosteric site, directly affecting the coupling of the intracellular effectors to the protein. In this situation, it is possible to distinguish between two possible allosteric modulations. A positive allosteric modulation can drive to an increase of the binding affinity and/or the activity of the orthosteric ligand, conversely, a negative allosteric modulation generally decreases the binding affinity and/or the action of the orthosteric ligand (Christopoulos, 2002). To pharmacologically simplify the concept of the allosteric modulation with the theoretical model called “allosteric ternary complex model” (ATCM), it is generally assumed that an allosteric modulator can affect only the binding affinity of the orthosteric ligand to its receptor (**Figure 9**). In the ATCM model, the allosteric modulation mechanism is governed by three variables: 1) the concentration of each orthosteric (O) and allosteric (A) ligands; 2) the equilibrium dissociation constants of the orthosteric and allosteric ligands ( $K_O$  and  $K_A$ , respectively); and, 3) a factor, known as “cooperativity factor” ( $\alpha$ ) (Ehlert, 1988; Stockton et al., 1983).



**Figure 9. Allosteric GPCR models.** On the left, the allosteric ternary complex model (ATCM). This describes the interaction between the orthosteric ligand, O, and the allosteric modulator, A, in terms of their equilibrium dissociation constants ( $K_A$ ,  $K_O$ ) and the cooperativity factor,  $\alpha$ , which describes the magnitude and direction of the allosteric effect on ligand binding affinity. On the right, the allosteric two state model (ATSM). This describes allosteric modulator effects on affinity, efficacy and the distribution of the receptor between active ( $R^*$ ) and inactive ( $R$ ) states, in terms of distinct conformations selected by ligands according to their cooperativity factors for the different states (Gregory et al., 2007).

This  $\alpha$  is a value to indicate the type of cooperativity between orthosteric and allosteric ligands, once they are both interacting with the same receptor ( $R$ ). A negative cooperativity ( $\alpha < 1$ , but greater than 0) is presented when the binding of the allosteric ligand reduces the binding affinity of the orthosteric ligand. Conversely, a positive cooperativity ( $\alpha > 1$ ) exists when the allosteric modulator improves the binding affinity of the orthosteric ligand. A situation of neutral cooperativity ( $\alpha = 1$ ) can indicate a situation without net changes in the binding affinity at equilibrium. Moreover, since the allosteric and orthosteric sites are mechanically linked in the structure of the receptor, also the orthosteric ligand can modulate the binding affinity of the allosteric modulator in the same manner. Thus, the ATCM is a simplified description of the allosteric/orthosteric ligands cooperativity by considering only their binding affinities with a particular receptor. However, there are situations where the allosteric modulator does not affect the binding properties of the orthosteric ligand, but the effects are directly extended to the intracellular signaling efficacy. In these cases, the ATCM cannot successfully describe the allosteric modulation mechanisms. In fact, allosteric ligands can affect the intracellular signaling activities of orthosteric agonists, or also directly act as agonists in their

own right (Langmead et al., 2006; May et al., 2005). As a consequence, the allosteric effects on GPCR activities must be extended to situations that are not considered with the ATCM, such as: 1) the ability of the receptor to constitutively isomerize between an active ( $R^*$ ) and inactive ( $R$ ) states, represented by the isomerization constant ( $L$ ); 2) the capability of the orthosteric and allosteric ligands to modify such isomerization between states, which is governed by the parameters  $\alpha$  and  $\beta$ ; 3) the ability of each ligand to modulate the binding affinity of the other, represented by the “binding cooperativity” parameter ( $\gamma$ ); and 4) the ability of either ligand to modulate the transition to a particular active receptor state, represented by the “activation cooperativity” parameter ( $\delta$ ). All these situations are taken into account by another extended model, known as the “allosteric two-state model” (ATSM) (**Figure 9**), which can be considered as a completion of the previous ATCM (Hall, 2000). However, also the ATSM still remains a simplified mechanistic framework to describe the various allosteric modulatory effects, as GPCRs can adopt multiple active and inactive conformations beyond the simple active ( $R^*$ ) and inactive ( $R$ ) states (Urban et al., 2007). Therefore, an allosteric modulator can be classified as an “allosteric enhancer”, “allosteric inhibitor”, “allosteric agonist” or “allosteric antagonist” in terms of both affinity and efficacy. Moreover, an allosteric ligand can concomitantly express more than one of these profiles (May et al., 2005; Schwartz and Holst, 2006). In comparison to the use of classical orthosteric agonists, the use of allosteric modulators in pharmacology can have multiple advantages. In general, the allosteric sites of GPCRs did not face the same evolutionary pressure as the orthosteric sites did for accommodating an endogenous ligand. For this reason, the allosteric sites are less genetically conserved among the different subtypes of the same receptor family. The different evolution of the allosteric sites than the orthosteric ones opens the door on the potential development of allosteric ligands with higher subtype selectivity for the GPCR families (Kenakin, 2007). A second pharmacological advantage is the possibility of using an allosteric modulator to manipulate a physiological effect only when and where the endogenous ligand is present, without affecting the normal spatiotemporal functions of a receptor. In this case, it is necessary an allosteric modulator that does not have any activity in the absence of the orthosteric ligand, like the

"allosteric enhancers" class. The consequence is to use allosteric drugs with a safer profile than orthosteric ligands, as the pharmacological effect will reach a maximum that cannot be exceeded by the administration of large doses, but only depends by the physical presence of the endogenous ligand (Kenakin, 2007).

Gallamine (**Figure 10**) was the first allosteric modulator that was discovered and reported. This molecule first showed to inhibit ACh and CCh actions on the heart atrium (Clark and Mitchelson, 1976), then induced a right-shifting of dose-response curves of ACh and CCh, with the magnitude of the progressive shifts diminished even if the dose of gallamine was increased. Finally, the allosteric profile of gallamine was confirmed by binding studies, where it was evaluated its ability to slow down the dissociation of the radiolabeled orthosteric antagonist N-methylscopolamine (NMS) from muscarinic receptors (Stockton et al., 1983). Moreover, gallamine was discovered to be also active as a neuromuscular blocker, which is generally an effect of nicotinic acetylcholine receptors antagonists. Consequently, it has been discovered that many of nAChRs antagonists can have high affinities for the M2 receptor allosteric site. Two of these bivalent ligands are pancuronium and alcuronium (**Figure 10**) (Nedoma et al., 1985, 1986).

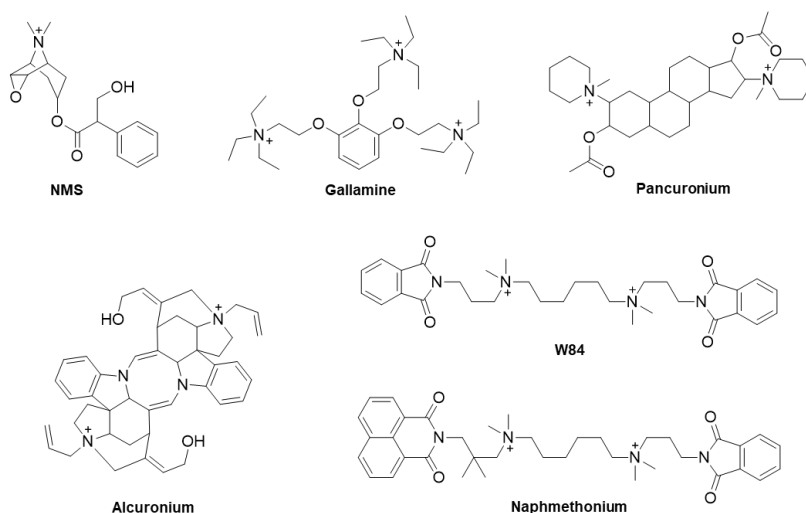
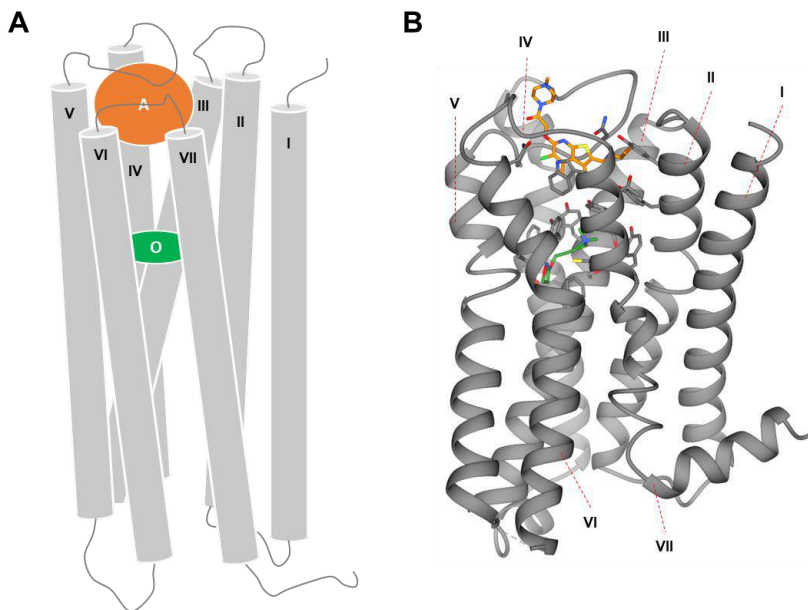


Figure 10. Ligands of mAChRs that led to the discovery of the muscarinic allosterism.

In the last decades, many efforts have been invested in the individuation of the allosteric binding sites of mAChRs. In particular, the extracellular part of the receptors rapidly became of prime focus for the discovery of allosteric sites (**Figure 11**). This was driven from the observation that gallamine, after supra-saturating concentrations, cannot change anymore the binding affinity of the orthosteric antagonist NMS, but it is able to slow down its velocity of association/dissociation to the receptor in a dose-dependent manner. Thus, it suggested that allosteric ligands may induce a steric hindrance to the access of NMS in its mAChR orthosteric binding site, which is located transmembrane (Proška and Tuček, 1994). M2 receptor subtype is the prototype for studying the GPCR allosterism, as the first-discovered allosteric ligands gallamine and alcuronium have the highest affinity for such receptor (Ellis et al., 1991; Jakubik et al., 1995). By replacing some specific amino acids in the extracellular domains, the second extracellular loop of the M2 receptor was found fundamental for the high-affinity binding profile of gallamine and other alkane-bisammonium allosteric modulators like alcuronium and W84 (**Figure 11** and **12**). In particular, the specific residues of this second extracellular loop that were found involved in the M2 allosteric binding site were nine amino acids between a Valine (Val) and a Tyr (Val168 and Tyr177, **Figure 12**) (Huang et al., 2005).



**Figure 11. Disposition of the Seven TMDs, the Allosteric and the Orthosteric Binding Site of mAChRs.** **A)** Schematic view of the possible arrangement of muscarinic receptor transmembrane domains, and the allosteric (A, orange) and orthosteric (O, green) binding cavities. **B)** M2 muscarinic receptor side-view (PDB code 4MQT) bound to the orthosteric agonist iperoxo (green) and to the allosteric modulator LY2119620 (orange).

However, the second extracellular loop is not the only one involved in the binding of the allosteric ligands to M2. The amino acids that link the third extracellular loop to the seventh TMD and the second extracellular loop to the fourth and fifth TMDs were found important for the high-affinity binding of alkane-bisammonium allosteric modulators. In particular, a cluster of tryptophan (Trp) and Thr residues at the top of the M2 seventh TMD plays a critical role in affinity and subtype selectivity of W84, Naphmethonium, and gallamine (**Figure 11** and **12**) Such important family of alkane-bisammonium allosteric compounds seem to be fixed in a “sandwich” like manner by  $\pi$ - $\pi$  interactions between a Trp (Trp422, **Figure 12**) at the top of the seventh TMD and a Tyr (Tyr177 **Figure 12**) in the middle of the second extracellular loop (**Figure 12**). Thus, a lot of extracellular residues of M2 receptor are involved in the binding of the allosteric modulators (Prilla et al., 2006; Voigtländer et al., 2003). Gallamine can bind all the five subtypes of mAChRs and it was used to study also the M1 allosteric binding site. Using M1 mutant receptors, two

Trp residues of the third extracellular loop were found fundamental for M1-gallamine binding (Matsui et al., 1995). As the orthosteric ligands mostly interact with the third and sixth TMDs of muscarinic receptors (Jöhren and Höltje, 2002), recent studies revealed that allosteric modulators may act by changing the spatial orientation of these two TMDs (**Figure 11**) (Huang and Ellis, 2007; Jakubík and Tuček, 1995). In this way, allosteric ligands can modify the dimension of the orthosteric binding site, favoring or complicating the placement of orthosteric agonists and antagonists. Obviously, the ortho-allosteric binding cooperativity is complicated and not only dictated by the rearrangement of two TMDs, but also other factors come into to play. Of high interest, some recent studies have been focused on the identification of an additional mAChRs allosteric site to the one already known (Lazareno et al., 2000, 2002). The receptor region of this “second” allosteric site has not been identified yet. Moreover, it has been demonstrated that the “common” mAChRs allosteric site can accommodate two allosteric ligand(s) molecules. This peculiarity makes the study of the second allosteric binding site even more complicated (Tränkle et al., 2005).

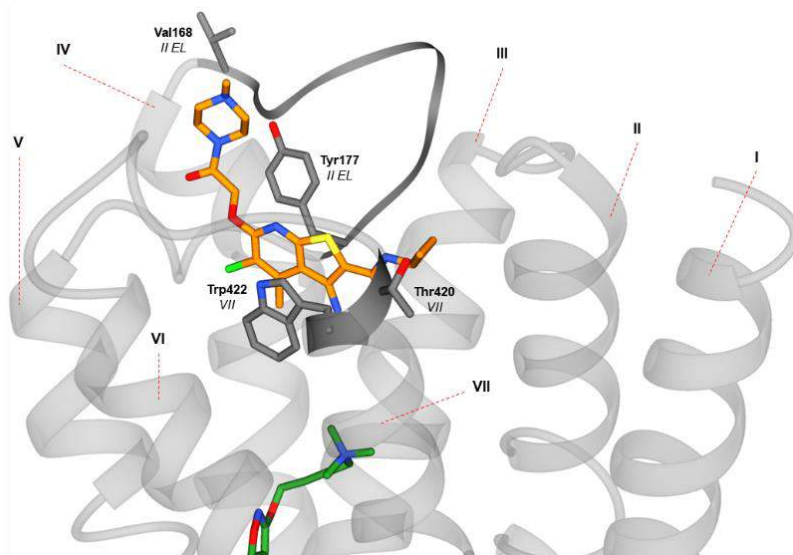


**Figure 12. Specific Amino Acid Residues Involved in the Binding of Allosteric Ligands and mAChRs.** A zoomed view of the allosteric site of M2 muscarinic receptor (PDB code 4MQT). The amino acids involved in the binding of the allosteric modulator LY2119620 (orange) with mAChR are highlighted. The Roman numerals indicate the transmembrane domains and the extracellular loops (EL). The orthosteric ligand iperoxo (green) stays in the orthosteric site.

In conclusion, it is more appropriate to consider an entire domain on the mAChRs where the allosteric molecules can interact with the receptor in different ways than a specific allosteric binding site. The allosterism is very complex and depends on a combination of factors regarding the receptor, the orthosteric ligand, and the allosteric modulator. A change of only one of these factors can lead to a completely different cooperativity and situation (Gregory et al., 2007; Jakubík and El-Fakahany, 2010). The first allosteric modulator of the muscarinic receptor was discovered 40 years ago. Since this discovery, the general knowledge about the binding, the mechanism of action and the structure-activity relationship (SAR) of muscarinic allosteric ligands has undergone huge progress. Today, allosteric modulators are considered as new potential candidates for the treatment of debilitating cholinergic-related disorders, such as Alzheimer's disease or schizophrenia, as their first pharmacological results are encouraging (Chan et al., 2008; Shirey et al., 2009).

#### **1.4. Classification of the mAChRs, physiological functions and pharmacology**

Muscarinic receptors can be subdivided into five subtypes, known as M1–M5. They principally differ in the tissue distribution and in the specific G protein-coupling. Each subtype of such class of receptors has key physiological roles. Various natural products have been found to be selective for muscarinic receptors. For example, some agonists like muscarine (*amanita muscaria*, *Fungi*) and pilocarpine (*Pilocarpus*, *Plantae*) or other well-known antagonists like atropine (*Atropa belladonna*, *Plantae*) and hyoscine (*Solanaceae*, *Plantae*) (**Figure 13**). These natural muscarinic ligands have been tested for the treatment of mAChRs-related diseases in the central and peripheral nervous system, but with limited clinical benefits (Eglen et al., 1999, 2001; Felder et al., 2000). Subsequently, synthetic derivatives of natural muscarinic ligands have been developed and pharmacologically studied. Despite their selectivity for the muscarinic receptors, the lack of subtype selectivity hampered the therapeutic application of these compounds due to their several side effects (Eglen and Watson, 1996). It is worth noting that during the screening of the activity of potential synthetic muscarinic drugs, the

compound known as tremorine was able to induce marked parasympathetic effects, such as tremor, hypokinesia, and rigidity (Everett et al., 1956). Only later it was elucidated that these effects were evoked by oxotremorine, the biologically active metabolite of tremorine. Oxotremorine is a specific muscarinic agonist without subtype selectivity but with the same potency of ACh (Cho et al., 1961). This fact was found surprising as its chemical structure differs in comparison to other muscarinic agonists. Moreover, oxotremorine was also found moderately selective for the CNS. Important derivatives of this compound have been rationally designed and developed, such as oxotremorine-M, which is still used as a research tool for studying anti-parkinsonian drugs (Conti et al., 1997). Another important synthetic derivative of oxotremorine is iperoxo. It was created by De Amici and coll. (Dallanoce et al., 1999) by replacing the pyrrolidin-2-one ring of oxotremorine with a  $\Delta^2$ -isoxazoline and the introduction of a permanent charge on the nitrogen. Iperoxo is still one of the most powerful muscarinic agonists reported in literature, but without muscarinic subtype-selectivity (Dallanoce et al., 1999; Schrage et al., 2013).

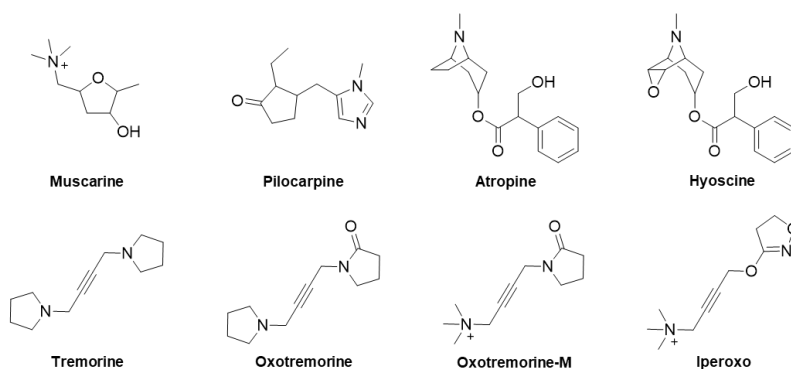


Figure 13. Natural and Synthetic Muscarinic Ligands.

#### 1.4.1. Muscarinic acetylcholine receptor M1

Muscarinic acetylcholine receptor M1 is present in different tissues. It was found in the brain, autonomic ganglia, sympathetic ganglia, exocrine glands, and vas deferens. In the brain, M1 is particularly abundant in the cerebral cortex, hippocampus and dentate gyrus, striatum, olfactory bulb

and tubercle, amygdala (Levey et al., 1995; Oki et al., 2005). This receptor has been also found in the esophageal smooth muscle (Preiksaitis et al., 2000) and in the bladder tissue (Tyagi et al., 2006). However, its tissue distribution largely overlaps with the distribution of the M3 and M4 subtypes. The M1 receptor is mostly involved in mediating higher cognitive processes, such as learning and memory (Fisher et al., 2003; Wein, 2005). It also plays important roles in the regulation of locomotor activity (Nathaniel et al., 2008), salivation (Gautam et al., 2004), indirect inhibition of N- and L-type calcium channels, M current inhibition in sympathetic ganglion neurons and MAP kinase pathway activation (Aronstam and Patil, 2009). Selective agonists of M1 receptor have been considered as a therapeutic approach to retard dementia, age-associated memory impairments, and the cognitive decline related to Alzheimer's diseases and schizophrenia (Anagnostaras et al., 2003; Bartus et al., 1982; Doggrell and Evans, 2003). Pharmacological studies with M1 agonists like alvameline, milameline, sabcomeline, RS 86, talsaclidine, xanomeline, SDZ 210-086, and YM-796, (**Figure 14**) have strongly confirmed their potential for the treatment of Alzheimer's disease. For this pathology, M1 activation has two main benefits: the moderate reversal of cognitive impairment and the decreased amyloid plaque formation (Fisher et al., 2002, 2003; Hock et al., 2003). Moreover, xanomeline showed an interesting potential for the treatment of schizophrenia in clinical studies. However, its mixed M1/M4 agonism hampered its use in medicine (Felder et al., 2000). Despite their pharmacological potential, only cevimeline (Evoxac) and pilocarpine (Salagen) are the M1 agonists currently approved in medicine as drugs for the autoimmune Sjögren syndrome. The failure of all these agonists for the treatment of dementia is mostly related to their still marginal subtype-selective profile. This lack of intra-selectivity for the mAChRs is considered very problematic for development of medical therapies (Felder et al., 2000; Longo and Massa, 2004). Differently, the M1 antagonists pirenzepine and telenzepine have been massively used for the treatment of chronic peptic ulcers until some years ago, when the discovery of their parasympathetic side effects has limited their medical application (Lazzaroni et al., 1986; Subudhi and Sahoo, 2016). In conclusion, the alternative to act on M1 receptors with high selectivity may be the development of allosteric ligands as they bind regions of the

receptor that are less conserved among all the subtypes (Lazareno et al., 2002). A large number of M1 allosteric ligands have been synthesized. For example, AC-42 showed high functional subtype selectivity for M1 (Gregory et al., 2007), and benzyl quinolone carboxylic acid (BQCA) is a compound that can improve learning and memory function after brain trauma without CNS side effects (Holschneider et al., 2019). However, the pharmacological profile of allosteric modulators must be better known before their medical applications will be real.

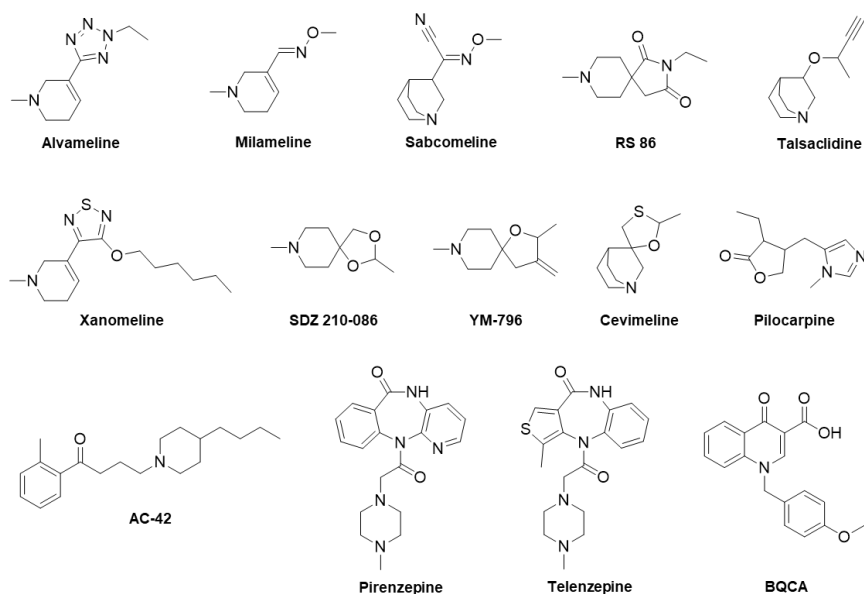


Figure 14. Ligands of M1 mAChR.

### 1.4.2. Muscarinic acetylcholine receptor M2

M2 muscarinic acetylcholine receptors are highly expressed in the brain, heart, sympathetic ganglia, lung, ileum, uterus and other smooth muscles. In the CNS, M2 is present in lower concentrations than M1 and is distributed in the cerebellum, medulla, pons, basal forebrain, olfactory bulb, and diencephalon (Cortés et al., 1986). The M2 receptor has an important role in the control of myocyte contraction, reducing the frequency of the heart beating (Brodde and Michel, 1999; Caulfield, 1993; Wein, 2005). This subtype has also a minor role in the control of smooth muscle contractile responses. In the smooth muscles, it is generally co-

expressed with M3 receptors (Wein, 2005). Moreover, M2 receptors are expressed in the thermo-regulatory centers of the hypothalamus and are likely to be involved in the regulation of the body temperature (Gomez et al., 1999). There are also other biological functions that are controlled by M2 receptors, like the corticosterone release and the mechanisms of analgesia (Aronstam and Patil, 2009). The M2 antagonists are able to improve cognitive performance and, in combination with M1 agonists, can be a potential treatment for Alzheimer's disease when the physiological cholinergic tone is not completely lost (Longo and Massa, 2004). For example, the M2 antagonists SCH 57790 and BIBN-99 showed to improve cognitive functions in preclinical studies (Rowe et al., 2003). The M2 receptors blockade is also considered as a potential therapy for schizophrenia. This disease is characterized by an excessive dopamine transmission. The M2 partial agonist BuTAC seems to reduce dopamine cell firing in the CNS, exhibiting antipsychotic behavior. Its mechanism of action is probably a competition with the endogenous full agonist ACh, reducing the activity of M2 (Bymaster et al., 1998; Rasmussen et al., 2001). Interestingly, the M2 receptor is the model for the study of both negative and positive allosterism. Gallamine and alcuronium were the firsts M2 allosteric modulators discovered. They pave the way to the development of other important synthetic M2 allosteric ligands, such as the alkylbisammonium derivatives W84 and Naphmethonium (Holzgrabe et al., 2000; Jöhren and Höltje, 2002; Tränkle et al., 2003; Zlotos et al., 2006). However, the potential of M2 allosteric compounds for therapeutic applications remains not fully investigated.

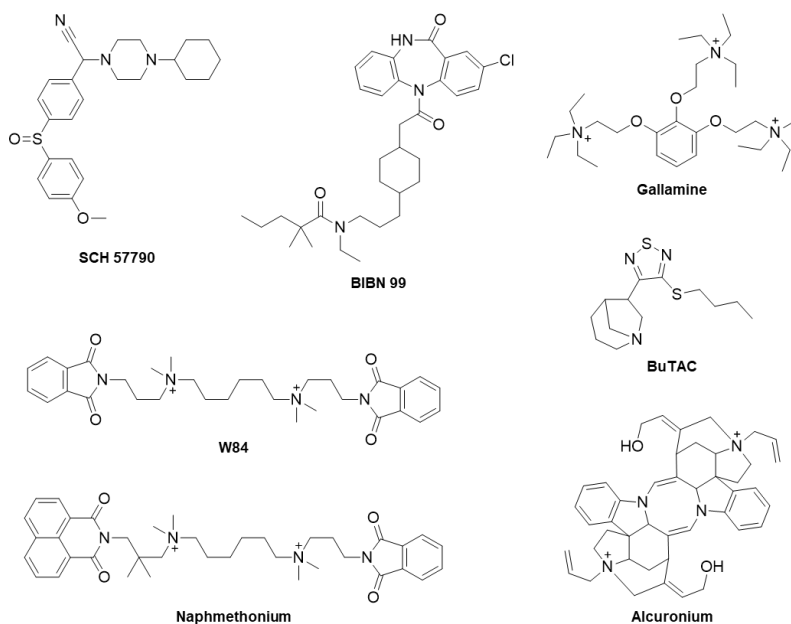


Figure 15. Ligands of M2 mAChR.

### 1.4.3. Muscarinic acetylcholine receptor M3

The M3 subtype of muscarinic acetylcholine receptors is mostly distributed in the smooth muscles, exocrine glands, pancreas, and brain (Lin et al., 1997; Post et al., 1991; Preiksaitis et al., 2000; Renuka et al., 2006; Vilaró et al., 1994). It is expressed in high levels in different regions of the CNS, in particular in the cerebral cortex, thalamus, piriform cortex, olfactory bulb, brain stem nuclei. The distribution of M3 largely overlaps with the distribution of the other subtypes M1 and M4. M3 has a main role in the contraction of smooth muscles in the airway, ileum, iris, and bladder (Caulfield, 1993; Eglen et al., 1996; Kruse et al., 2012). Moreover, this subtype seems to be strongly involved in the mechanisms of type 2 of diabetes mellitus, as it is largely expressed in pancreatic beta-cells and in areas of the brain that control insulin secretion (Gautam et al., 2006; Weston-Green et al., 2012). Other functions that are mediated by M3 are the exocrine secretion (particularly of saliva) (Gautam et al., 2004; Matsui et al., 2000), the dopamine release, the maintenance of body mass and the control of food intake (Aronstam and Patil, 2009). In pharmacology,

the M3 antagonists have been extensively studied for the treatment of urinary tract disorders. In particular, the very potent antagonists tolterodine, darifenacin (Enblex) and solifenacin (Vesicare) were developed for the overactive bladder disease and are characterized by very reduced side effects *in vivo* (Chapple and Nilvebrant, 2002; Chapple et al., 2004; Miyamae et al., 2003). Other studies showed that the concurrent blockade of M2 and M3 receptors is a potential strategy for the treatment of gastrointestinal motility disorders (Matsui et al., 2000; Stengel et al., 2002). In the treatment of the chronic obstructive pulmonary disease, the anticholinergic agent tiotropium (Spiriva) is interesting. This drug binds preferentially M1 and M3 and is considered a possible therapeutic approach with an effective once-a-day dose and reduced side effects (Faulkner and Hilleman, 2003; Hvizdos and Goa, 2002).

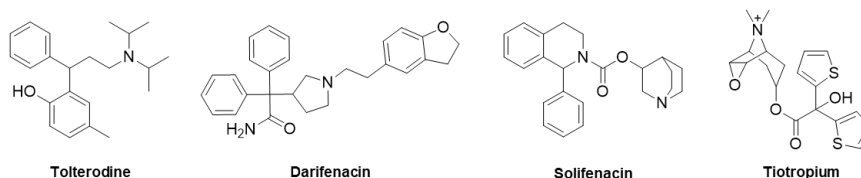


Figure 16. Ligands of M3 mAChR.

#### 1.4.4. Muscarinic acetylcholine receptor M4

M4 muscarinic acetylcholine receptors are present in the brain and lung tissue. The regions of the brain expressing such subtype are the occipital cortex, caudate and putamen, visual nuclei, olfactory tubercle, and hippocampus. M4 can induce the depression of motor control as its activation is able to inhibit the dopamine-induced locomotor stimulation in mice (Onali and Olanas, 2002). In fact, the alterations of the activity of the M4 receptor seem to be involved with Parkinson's disease (Guo et al., 2010; Langmead et al., 2008; Stein and Hell, 2010). The M4 antagonists have been largely studied for this pathology. In particular, the benzoxazine PD-0298029 showed to combine a good efficacy with favorable pharmacokinetic profile and bioavailability (Eglen, 2005). M4, together with M2, also control the release of ACh in the hippocampus. Here, the release of ACh has an important role in the mechanisms of analgesia, as it

has been demonstrated with the M4 agonists CMI-936 and CMI-1145 (Ellis et al., 1999; Iwamoto and Marion, 1993). As much as concern the allosterism of M4, the compound thiochrome recently showed to be an M4 selective allosteric modulator (Lazareno et al., 2004). However, M4 allosteric ligands have not been exploited yet for the development of novel potential therapies.

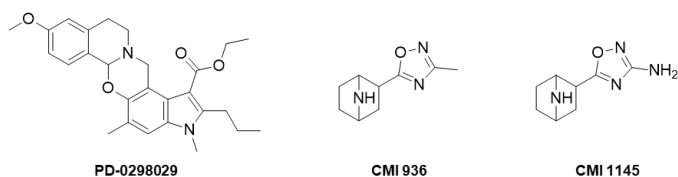


Figure 17. Ligands of M4 mAChR.

#### 1.4.5. Muscarinic acetylcholine receptor M5

M5 muscarinic acetylcholine receptor is known to be prevalently expressed in the CNS, in the midbrain (Vilaró et al., 1994; Weiner et al., 1990; Yasuda et al., 1993), in the esophageal smooth muscle (Preiksaitis et al., 2000) and in the heart (Wang et al., 2001). The activation of M5 can trigger different cellular responses. For example, it can cause the adenylate cyclase inhibition (Yamada et al., 2003), the phosphoinositide degradation (Bonner et al., 1988), and the potassium channel modulation (Jones, 1993). The M5 receptor can also stimulate gastric acid secretion (Aihara et al., 2005), be involved in the mechanism of the dopamine release, and change the dilatation of cerebral arteries and arterioles. M5 selective antagonism may be an important potential treatment of both schizophrenia and narcotic addiction (Eglen and Nahorski, 2000).

#### 1.5. Conclusions about mAChRs

The vast and various effects of the ACh in humans are the result of the activation of the nicotinic (ionotropic) and muscarinic (metabotropic) receptors. The complex roles of muscarinic receptors need further studies to be completely understood, but the cholinergic networks and their actions are getting clearer thanks to the last decades of research. The

peripheral muscarinic activation can modulate the smooth muscle contraction, the glandular secretion, and the frequency of the heartbeat. In the CNS the muscarinic receptors are strongly involved in the memory and the cognitive functions and also manage the motor control, the cardiovascular system regulation, and the body temperature regulation. The muscarinic receptors can be pharmacologically classified into five subtypes (M1-M5) on the basis of their different aminoacidic sequences and localization in the human body. This classification is of high interest due to the important therapeutic applications that muscarinic subtype-selective bioactive compounds can potentially have. Their development may be very effective for innovative therapies against Alzheimer's and Parkinson's disease, asthma, pain, intestinal motility disorders, heart disease, and urinary function disorders. Despite several decades of efforts on identifying novel muscarinic agonists and antagonists, their full therapeutic potential is not yet in our hands. The cause is mainly the lack of subtype selectivity of these drugs. The high homology of the amino acids at the M1-M5 orthosteric sites hampers the development of suitable agents. Recent studies allowed the discovery of more subtype-selective muscarinic ligands but of different nature. Such compounds bind an allosteric site, which is in a distinct receptor region from the orthosteric one and genetically less conserved among the five subtypes. The intracellular mechanisms activated through the allosteric compounds are not well known compared to the classical orthosteric ligands. Today, some partially selective orthosteric agonists for the M1, antagonists specific for M2 and other M1 selective allosteric modulators are under the clinical studies for the treatment of Alzheimer's disease. Other M3 selective antagonists are also under clinical studies for therapies against the overactive bladder and chronic obstructive pulmonary disease. Despite particular attention is focused on the development of allosteric regulators that may potentially target muscarinic receptors with high subtype selectivity, other alternative approaches to achieve such specificity are necessary. The success of this challenge can provide a revolution of the pharmacology against a large variety of diseases and disorders, as well as advancing the current knowledge of the metabotropic role of the ACh.

## 2. Control of Protein Function using Light

The drug is defined as a natural or synthetic substance, usually a small molecule of known structure, which produces a biological effect when administered to a living organism. A pharmaceutical drug, commonly called medicine, is a substance used in the treatment, prevention, or diagnosis of a disease or to promote the welfare of an organism. Pharmacology is “the science of drugs” and includes their origin, preparation, composition and particularly their biological effects. Traditionally, a drug was obtained from nature, through extraction from plants. Despite nature and its molecular devices are incomparable in their beauty, efficiency, and ability to integrate into complex systems, the synthetic chemistry has obtained outstanding results over the last decades and a huge number of molecules have been designed and created to simulate nature beauty. “Drug discovery” is defined as the multidisciplinary process of discovering new pharmaceutical drugs. This process needs knowledge of medicine, chemistry, biology, and pharmacology. The drugs obtained through synthetic chemistry are conceptually beautiful, but still simple and pale in comparison with what nature’s devices can achieve (Raymo, 2003; Wegner, 2012). The knowledge of nature's tools is dramatically increased during the last years. This growth is connected to the method of study, which mixes different science’s branches such as physics, biology, biophysics, engineering, and chemistry. Today, humans are able to describe in atomic detail a lot of crucial nature’s molecular machines, like the ATP synthase (Yoshida et al., 2001), various molecular motors (Kardon and Vale, 2009), or ion channels that control neuronal activity (Choe, 2002). The majority of these natural devices can be simplified in intuitive mechanical models. The possibility of understanding such machines at a molecular level can open the door to controlling them through man-made synthetic tools. In the last years, humans are able to manipulate natural nanomachines until a high genetic specific level by engineering endogenous protein or modifying them by attaching/adding synthetic moieties. The most recent pharmacological approach is not anymore only focused on the drug discovery and development. Today, pharmacology combines the potential of synthetic chemistry directly with the tools that nature can offer. For example, transmembrane proteins play key roles in human neurophysiology and can

be combined with synthetic chemistry creations, integrated into complex biological systems in order to be finally controlled by a very useful external stimulus: the light. Light emerged amongst all the methods that can modulate a transmembrane receptor activity for a lot of crucial reasons. Light normally does not influence the living system under study, it can be used remotely and in a non-invasive manner, it can be modulated both spatially (micrometers) and temporally (femtoseconds) with very high resolution and it can be controlled in a qualitative and quantitative manner through adjusting its wavelength and intensity until it carries enough energies to trigger molecular devices activity (Gorostiza and Isacoff, 2008; Lehár et al., 2009; Velema et al., 2014). Nature gave the idea of controlling protein activity using light. Rhodopsins are an important family of GPCRs strongly involved in animal vision. They belong to the class of opsins and are made light-sensitive by the compound retinal, also called vitamin A aldehyde, which is one of the many forms of vitamin A. In particular, retinal is a natural polyene chromophore bound as a Schiff base to opsins. This class of proteins mediates the first step in the visual transduction cascade. In the human eye, retinal is conjugated as 11-*cis*-retinal configuration to the opsins and isomerizes to all-*trans*-retinal by capturing a photon of the correct wavelength. Such a change of configuration triggers the electrochemical signal cascade and the result is the perception of light and images by the brain. In 2004, Retinal was also found bound to light-gated cation channels called “channelrhodopsins” (ChRs), which are excitatory protein channels isolated from the alga *Chlamydomonas reinhardtii* (Nagel et al., 2003). In this case, the chromophore is covalently linked as all-*trans*-retinal configuration to ChRs and upon absorption of a photon of the correct wavelength (ChR1 around 500 nm and ChR2 around 460 nm) isomerizes to 13-*cis*-retinal. Then, retinal relaxes back to all-*trans*-retinal rapidly once the light is gone (Banghart et al., 2006; Zhang et al., 2006). Thus, opsins naturally use the molecular photoswitch retinal and it is endogenously produced in many tissues. This natural system gave rise to a new research field called “optogenetics”, which aims to control neurons, or other cells of interest, with genetically targeted photoreceptors. ChRs have been largely used for genetically encoding “blind” neurons and triggering action potentials through light and its high spatio-temporal precision (Boyden et al., 2005).

Since its inception, optogenetics has found many applications in dissecting neuronal circuits and has helped to answer fundamental questions in neuroscience, being so deemed “Method of the Year” in 2010. Optogenetic molecular tools are mostly derived from bacteria and protozoa. The overexpression of such tools in mammalian tissues using genetic manipulation raises safety and regulatory concerns when therapeutic applications are considered. However, mammalian tissues express various transmembrane receptors on their own that are easily accessible but not inherently light-sensitive. The challenge of making endogenous receptors of living organisms sensitive to light is the main goal of “photopharmacology”. Photopharmacology combines synthetic chemistry and optics techniques to control endogenous protein functions with the use of light. In this case, the bioactive agent carries a photo-reversible switch that can be switched between two different configurations (Lerch et al., 2016; Velema et al., 2014). The photosensitive drug can change its efficacy at its target receptor in a reversible fashion because of the photoswitch can toggle between two different states and trigger the desired biological effect light-dependently. Upon photoswitching, these photosensitive drugs can dramatically change their efficacy. They could even act as agonist in one configuration and as antagonist in the other. These light-sensitive agents have all the advantages of small-molecules drugs such as their easiness of application and fast tissue distribution. Independently from the route of administration, when a common drug is released in the body the control of this substance is lost and the compound can bind the target receptor without caring about its cell, tissue, or system localization (Kramer et al., 2013). The poor selectivity of classical drugs is the main reason for their undesirable side effects and toxicity. This lack of specificity can often limit drug use in medicine in therapeutic applications (Lehár et al., 2009; Velema et al., 2014). Differently, photoexcitation of exogenous light-sensitive drugs can modulate the activity of the endogenous target protein with high spatiotemporal resolution and can control therapeutic interventions, drug dosing, duration of action and avoid most of the adverse effects of standard pharmacological treatments in use (Izquierdo-Serra et al., 2013, 2014, 2016; Lerch et al., 2016; Matera et al., 2018; Nevola et al., 2013; Pittolo et al., 2014). In combination with high-quality

devices that can deliver light in the human body with a certain specificity and intensity (Hamaoka et al., 2007; Kale et al., 2015), photopharmacology tools can create a more precise and less toxic approach than conventional pharmacological therapies.

## **2.1. The molecular photo-switches**

Light-sensitive moieties have the role of controlling protein functions using light. A fine and reversible modulation of protein activity is strictly related to the quality of the photoswitch that is directly linked to the target protein or inserted in the ligand structure that binds that target protein. The molecular photoswitch quality is evaluated by both its photochemical properties and, obviously, how such properties fit with the specific use that is needed. To achieve their function of controlling protein activity, these photochromic groups must behave as a reversible photoswitch. They have to isomerize under illumination with a specific wavelength in order to promote changes of geometry, polarity and flexibility which can directly affect protein function. Back-isomerization can be achieved by both illumination with a different specific wavelength and/or thermal relaxation and it mostly corresponds to the recovery of the initial activity of the target protein. Apart from the natural retinal, the most relevant synthetic classes of reversible photoswitches that have been used for controlling and modulating biological processes are diarylethenes, fulgimides, spiropyrans/merocyanines and azobenzenes (**Figure 18**), despite other classes of molecular photoswitches, such as stilbenes, fulgides, hemithioindigos, and chromenes, have also been studied and reported (Banghart et al., 2006; Szymański et al., 2013; Volgraf et al., 2011).

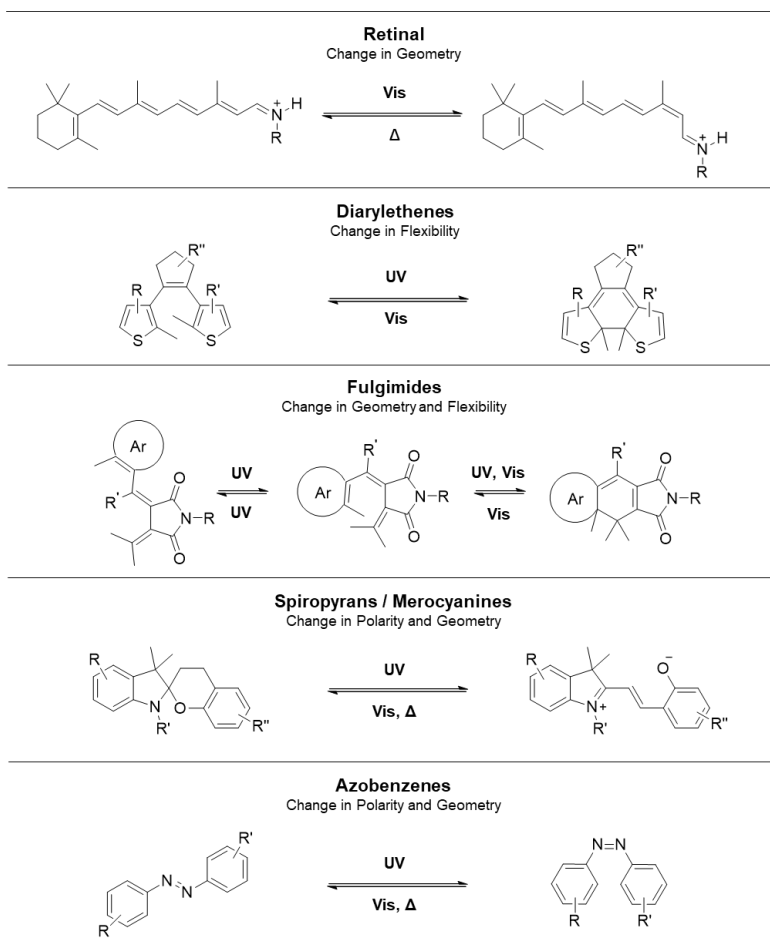


**Figure 18. Most Important Photoswitches Families.** Retinal, diarylethenes, fulgimides, spiroprans/merocyanones and azobenzenes general chemical structure and switching.

### 2.1.1. Diarylethenes

Dithienylethenes, or more generally called diarylethenes, are a type of photochromic molecular switches that undergo a reversible photoinduced cyclization through 6  $\pi$  electrons between a colorless open form, characterized by a hexatriene moiety, and a colored rigid closed form. The open isomer is very flexible and under irradiation with ultraviolet (UV) light (312 - 360 nm) cyclizes to afford the rigid closed isomer, which can be reverted to the open one with visible light (> 420 nm). Diarylethenes are mostly considered potential candidates for new material in optics and

optoelectronic devices because of their photochromic behavior (Bertarelli et al., 2011). They are mainly characterized by high fatigue resistance, short photoconversion time, high thermal stability in both isomeric forms and, depending on their substitutions, they can afford complete photoisomerization (Irie, 2000; Szymański et al., 2013; Tian and Wang, 2007). Despite they have been considered promising candidates as photochromic moieties for light-activated drugs, there are rare examples demonstrating their ability to efficiently controlling biological activities in living systems (Komarov et al., 2018).

### 2.1.2 Fulgimides

Fulgimides are very promising photoswitches that have been only minimally explored in photopharmacology, probably due to their challenging synthesis (Lachmann et al., 2019; Rustler et al., 2020). Similarly to the photochromism of diarylethenes, fulgimides undergo a photoinduced 6  $\pi$  electrons-cyclic rearrangement from a colorless open (O-)isomer to a colored closed (C-)isomer (Lachmann et al., 2019). The O-form can exist in its *E* and *Z* isomers. The *E/Z* isomerization is affected by the substitutions that are present in the 1,3,5-hexatriene system. In particular, the introduction of a sterically demanding group, such as isopropyl, in the alpha bridge position of the fulgimide (*R'* in **Figure 18**) suppress the  $O_{E/Z}$  isomerization, allowing exclusively the switching between the two observed  $O_E$ - and C-isomers (Schönborn and Hartke, 2014). Upon photoisomerization, not only the flexibility and the electronic properties of fulgimides change but also the geometry, which is mostly planar in the C- form, and twisted in the  $O_E$ -isomer (Lachmann et al., 2019). Absorption wavelengths and photostationary states of fulgimides depend on the heteroaromatic portion that dials their chemical structure: furan, thiophene, or indole remarkably separate the absorption bands of the  $O_{E/Z}$ - and C-isomers, consequently, high photostationary states can be observed. The photoisomerization of fulgimides from the O- to the C-form can be achieved with UV or visible wavelengths (270-481 nm). The back C- to O- isomerization can be obtained using visible light (> 470 nm) (Lachmann et al., 2019). Recently, an interesting pharmacological application of this class of photoswitches was reported with Fulgazepam,

a fulgimide derivative of benzodiazepine that is a light-sensitive potentiator of ionotropic  $\gamma$ -aminobutyric acid receptors (GABA<sub>A</sub>Rs) (Rustler et al., 2020).

### **2.1.3. Spiroprans/Merocyanines**

Spiroprans photochemical behavior is based on a 6  $\pi$  electrons ring-closing reaction through the rupture of the C-O bond. This class of photoswitches can undergo a reversible light-induced isomerization between the colorless and non-planar closed form ("spiropyran" form) to the colored, planar and zwitterionic conjugated open form ("merocyanine" form) under illumination with UV-light (360 – 380 nm). The merocyanine forms can back-isomerize thermally or under irradiation with visible light (> 460 nm). This type of isomerization principally creates a very strong change in the dipole and in the polarity of the molecule (8-15 Debyes) among the two forms. Despite spiroprans/merocyanines photochemical properties have several limitations, like their low thermal stability of the merocyanine form (Zhang et al., 1994), their thermochromic behavior and their photochemical degradation (Baillet et al., 1995; Day, 1963), some interesting photopharmacological applications have been successfully investigated. Due to the ability to change polarity upon photoisomerization, these compounds have been used for controlling changes of surface energy. The introduction of spiroprans/merocyanines units to a large-conductance mechanosensitive channel (MscL) is able to open and close the valve with light in a reversible manner. This system is promising for potentially controlling drug delivery with light in the future (Koçer et al., 2005). Interestingly, this switch has been found useful to drive hydrophobic/hydrophilic environmental changes in protein and cell membranes with light, which may influence the function of transmembrane proteins and cell arrangement/sorting on various surfaces (Izuta et al., 2019; Schild, 2010). Moreover, tethering a photochromic benzospiropyrane group inside the lipase active center allows the control of its hydrolytic activity and enantioselectivity with light (Bautista-Barrufet et al., 2014).

#### 2.1.4. Azobenzenes

Azobenzenes are among the first class of molecular switches reported (Hartley, 1937; Rau, 2002; Sekkat and Wolfgang, 2002) and have so far proven to be the most versatile and reliable ones for biological applications (Banghart et al., 2006). They were discovered in the middle of the XIX century and were initially used as synthetic coloring agents by the dye industries (Griffiths, 1972; Szymański et al., 2013). Azobenzene structure is based on a diazene (NH=NH) derivative with two phenyl rings instead of the two hydrogens. The -N=N- group is called azo-bond or azo-bridge. The two azobenzene isomers, *trans* and *cis*, have well-defined geometries and well-known conformational spaces that have relatively little overlap between them. The *trans* form is characterized by a planar geometry with a dihedral angle of 180° and a  $\pi$  electrons delocalization over the two aromatic rings and the azo-bridge. The dipolar moment of *trans* azobenzene is negligible. Differently, the azobenzene isomer *cis* has a shorter bent geometry of 3 Å in comparison to the *trans* one and has the aromatic rings twisted of 55° out of the plane with the dihedral angle of the azo-bond of 11°. The dipolar moment of the *cis* form is 3.7 Debye. This change in geometry of the *cis* azobenzene causes the rupture of the  $\pi$  electrons delocalization over the azo-bond, which was characteristic for the *trans* azobenzene. Generally, such different electronic properties with the rupture of the  $\pi$  electrons delocalization between the two azobenzene isomers can be easily determined through <sup>1</sup>H-NMR analysis. Here, the ortho-oriented protons of the *trans* isomer are located in the aromatic cone around 7.90 ppm (CDCl<sub>3</sub>, 600 MHz) which shift to around 6.83 ppm (CDCl<sub>3</sub>, 600 MHz) for the *cis* one, similarly to the typical chemical shift of the aniline protons (6.70 ppm, CDCl<sub>3</sub>, 400 MHz) (Chiba et al., 2010; Wagner et al., 2009). The two para-oriented substituents (4 and 4' positions) are closer in the *cis* configuration than in the *trans* one. This effect can be further amplified by additional/different appropriate substitutions as an azobenzene offers high possibilities of chemical functionalization (up to 10 different points). Commonly, the photoisomerization reaction of an azobenzene can be easily defined by UV-visible (UV-vis) absorbance measurements (Hartley, 1937). The absorption spectra of the *trans* and *cis* isomers of a simple azobenzene are overlapped but distinct. The *trans* form shows a strong  $\pi$ - $\pi^*$  band around 320 nm and a very weak n- $\pi^*$

band near 440 nm, due to its symmetric geometry. Differently, the *cis* form displays a less intense  $\pi$ - $\pi^*$  bands around 300 nm and a stronger  $n$ - $\pi^*$  band near 440 nm than the *trans* one. The *trans* to *cis* isomerization is obtained under illumination with ultraviolet light (320-370 nm). The back isomerization to the *trans* form can be obtained thermally or under irradiation using visible light (> 450 nm). Generally, azobenzenes have high extinction coefficients and quantum yields, meaning that light of relatively low intensity can be used for their photoisomerization. Thus, azobenzenes are photoswitchable molecules characterized by photostationary states that are a function of the wavelength. They can exist 100% in the *trans* form, as it is 10-12 kcal/mol more stable than the *cis* one, but it is not practically possible to convert them 100% into the *cis* state through irradiation (Szymański et al., 2013). Despite the impossibility to obtain a full *cis* state, the dependence of the photostationary ratio on the light wavelength offers the advantage to tune the biological activity of the photoswitchable azobenzene-based drug by gradually tuning the color and/or the intensity of the light. Moreover, azobenzenes undergo fast photoisomerization, preventing the formation of dangerous triplet diradicals. These radicals can generate highly reactive single oxygens (in the presence of triplet oxygen) which are cytotoxic and harmful for the chromophore itself (Szymański et al., 2013). Consequently, they offer a good stability under physiological conditions and a good photostability, as they can be switched over many cycles. Finally, azobenzene synthesis is relatively easy (Merino, 2011) and several synthetic strategies are reported, like diazonium coupling, Mills reactions or metal-catalyzed cross-coupling strategies (Hamon et al., 2009). Potential disadvantages for the use of azobenzenes into biological applications can be: a) their solubility in water, which is easily overcome with the addition of appropriate soluble functional groups, and b) the conditions to photoisomerize from *trans* to *cis* form, since UV-A or deeply violet light (315-380 nm) is harmful and not suitable for tissues and cells (Dong et al., 2007; Forman et al., 2007). However, appropriate substitutions in the aromatic rings of an azobenzene can easily influence the wavelength of its switching to red-shifted ranges, which are less dangerous and more biocompatible upon prolonged application on tissues, also modifying its thermal relaxing time (Beharry et al., 2011). The various azobenzenes can

be classified into different main groups, depending on the chemical nature of their substitutions and, consequently, the photochemical properties they have. These main families are azobenzenes derivatives, aminoazobenzenes, push-pull azobenzenes, tetra-ortho substituted azobenzenes and diazocines (Bandara and Burdette, 2012).

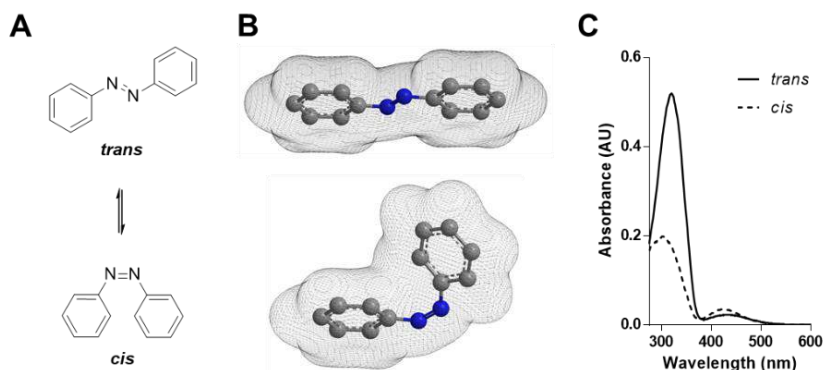
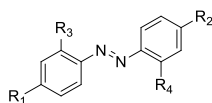


**Figure 19. General Structure and UV-Vis Absorption Spectrum of the *Trans* and *Cis* Isomers of an Azobenzene.** A) Azobenzene 2D structure; B) Azobenzene 3D structure in balls with a surface of charge density as a wire mesh, after minimizing the energy of both isomers to minimum RMS gradient of 0.010; C) UV-Vis absorption spectrum of both azobenzene isomers.

### ***Azobenzene derivatives family (ABn)***

This family includes azobenzenes with alkyl (Gegiou et al., 1968; Tamai and Miyasaka, 2000), aryl (Brode et al., 1952), halide (Brode et al., 1952), carbonyl (Tang et al., 2007), amide (Banghart et al., 2004; Lednev et al., 1998), nitrile (Tang et al., 2007), ester (Zacharias et al., 1998), carboxylic acid (Ohtani et al., 2004), nitro (Gegiou et al., 1968; Tang et al., 2007), 3-amino (Asanuma et al., 2000), 3-alkoxy substitutions and also azopyridines and phenylazopyridines. All these azobenzene derivatives are grouped together as they have similar absorption spectra to unsubstituted azobenzenes (Brown and Granneman, 1975). The thermal relaxation time of the *cis* isomer changes depending on the type and the number of substituents (**Table 3**), but they are relatively slow. For this reason, they are used for scientific applications, such as protein probes or molecular machines, where a fast thermal relaxation is undesired. Similarly to the

unsubstituted azobenzene, these derivatives in the *trans* form display a strong  $\pi$ - $\pi^*$  band and a weaker  $n$ - $\pi^*$  band. *Trans* to *cis* isomerization and vice versa are necessarily driven using both ultraviolet and visible light. Azobenzenes of this class with strong electron-withdrawing substituents, such as nitro and carboxylic acid groups, undergo faster thermal isomerization (Dokić et al., 2009).

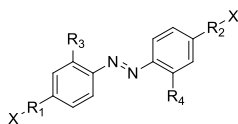


Group	R <sub>1</sub>	R <sub>2</sub>	R <sub>3</sub>	R <sub>4</sub>	$\lambda_{\max}$ (nm)	$t_{1/2}$ (min)
<b>ABn</b>	H	H	H	H	315	-
	Me	Me	H	H	330	401
	Cl	Cl	H	H	331	431
	NO <sub>2</sub>	H	H	H	330	94
	NO <sub>2</sub>	H	Me	H	336	60
	NO <sub>2</sub>	NO <sub>2</sub>	H	H	336	29
<b>aAB</b>	OMe	H	H	H	342	357
	OMe	OMe	H	H	353	221
	NMe <sub>2</sub>	H	H	H	390	103
	NMe <sub>2</sub>	Me	H	H	400	70
	NMe <sub>2</sub>	Me	Me	Me	399	24
	NMe <sub>2</sub>	NMe <sub>2</sub>	H	H	410	14.8
	NEt <sub>2</sub>	H	H	H	407	70
	NEt <sub>2</sub>	NEt <sub>2</sub>	H	H	431	7.4
<b>ppAB</b>	NMe <sub>2</sub>	NO <sub>2</sub>	H	H	440	1.7
	NMe <sub>2</sub>	NO <sub>2</sub>	Me	H	450	1
	NMe <sub>2</sub>	NO <sub>2</sub>	H	Cl	459	0.2

**Table 3. Chemical and Photochemical Properties of Different Azobenzene Derivatives.** Maximum of absorbance,  $\lambda_{\max}$  (nm), corresponding to the  $\pi$ - $\pi^*$  band and thermal relaxing half-time life,  $t_{1/2}$  (min), of different azobenzene derivatives. Measures of compounds ABn and aAB are in cyclohexane at temperature 35 °C and for compounds ppAB in hexane at the same temperature. Table adapted from Bandara and Burdette, 2012.

### Aminoazobenzene family (*aAB*)

Aminoazobenzenes class comprises all the azobenzenes displaying one or more amine, methoxy or hydroxyl groups in positions 2 or 4 (**Table 3**). These substitutions with electron-donating groups shift the strong  $\pi$ - $\pi^*$  transition band to higher wavelengths, overlapping it with the weaker  $n$ - $\pi^*$  band. In particular, this shift of the strong band is increased with amino groups substitutions and depends on the degree of amine alkylation (**Table 3**) (Blevins and Blanchard, 2004). Azobenenes having N-amides, N-carbamates and ureas groups as substitutions show a shift to higher wavelengths of the  $\pi$ - $\pi^*$  band in comparison to the unsubstituted azobenzene and can be included in this family (**Figure 20**) (Pozhidaeva et al., 2004). This class of aminoazobenzenes generally has a thermal relaxation time of the *cis* isomer that is relatively faster compared to the azobenzene derivatives class (ABn), in particular in polar solvents. However, bulky groups in ortho positions can stabilize the *cis* configuration and conferring a slower relaxation to the *trans* form (Sadovski et al., 2009).



Group	R <sub>1</sub>	R <sub>2</sub>	R <sub>3</sub>	R <sub>4</sub>	$\lambda_{\max}$ (nm)
<i>aAB</i>	-CH <sub>2</sub> -	-CH <sub>2</sub> -	H	H	342
	-NHCO-	-NHCO-	H	H	366
	-NHCOO-	-NHCOO-	H	H	372
	-NHCONH-	NHCONH	H	H	382

Figure 20. Red-shift of the  $\pi$ - $\pi^*$  Band of Azobenzenes with Pseudo-amine Groups. Azobenzenes with methyl, amide, carbamate and urea groups in para positions.

Moreover, if the azobenzenes of this class have an amino or hydroxyl substituent deprived of alkylation, they can create intermolecular hydrogen bonds between both the chromophore and the solvent molecules and undergo azo-hydrazone tautomeric equilibrium. This mechanism can remarkably decrease the thermal relaxation time of the *cis* isomers (**Figure 21**) (García-Amorós and Velasco, 2012). This effect is stronger in polar solvents. The majority of the aminoazobenzenes are intensely colored and used as industrial dyes (Bandara and Burdette, 2012), but also as pH and metal ion indicators (Momotake and Arai, 2003) or in photoelectric (Fujiwara and Yonezawa, 1991), in information storage devices (Iwamoto et al., 1991) and in photoresponsive polymers (Bandara and Burdette, 2012).

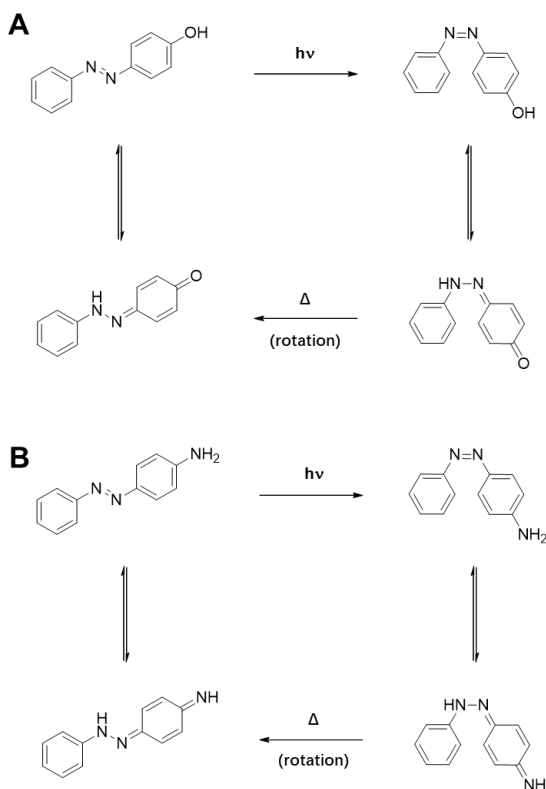
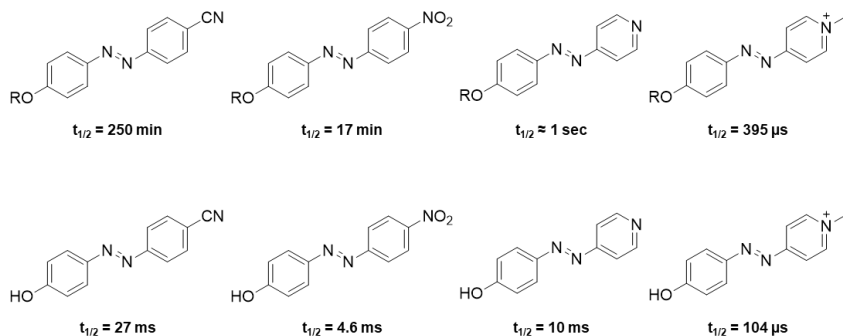


Figure 21. Proposed Azo-hydrazone Tautomeric Equilibrium and *cis*-to-*trans* Isomerization for Non-*N*-substituted Aminoazobenzenes or Non-*O*-substituted Hydroxyazobenzenes. Figure adapted from Bandara and Burdette, 2012.

### ***Push-pull azobenzene family (ppAB)***

Push-pull azobenzenes are generally characterized by the presence of both a strong electron-donor and a strong electron-acceptor group, which are oriented in the 4 and 4' positions of the aromatic rings of the azobenzene (**Table 3**). However, also electron-donor and -acceptor groups in 2 and 2' positions can create a "push-pull". This push-pull effect displays a decrease of the  $\pi$ - $\pi^*$  state energy, allowing a strong shift of the corresponding band to red-shifted wavelengths. This family of azobenzenes also display a very short thermal relaxation time of the *cis* isomer, from milliseconds to seconds, depending on the polarity of the solvent (Bandara and Burdette, 2012). The push-pull effect can be improved by using 2- or 4-pyridine as donor or 2- or 4-methylpyridinium salts as acceptor. In these cases, the  $\pi$ - $\pi^*$  band can be strongly shifted to red wavelengths (600 nm) and the relaxation time of the *cis* isomer is particularly reduced (Mourot et al., 2011). The relaxation time of the *cis* isomer can be also radically decreased if the electron-donor/acceptor groups allow tautomeric equilibrium (García-Amorós and Velasco, 2012) (**Figure 22**). The fast isomerization in both directions, high polarizability and large dipole moment of this family of azobenzenes make them very useful for non-linear optical and photo-refractive materials (Marder et al., 1997; Meerholz et al., 1994), optical poling, holographic memory storage devices (Berg et al., 1996; Kawano et al., 1999; Tsutsumi et al., 1995) or as fast information-transmitting light-sensitive switches (García-Amorós and Velasco, 2012). Of particular interest, nonlinear optical materials with push-pull azobenzenes are studied to generate high-frequency lasers from low-frequency radiation sources. As the aminoazobenzenes, lots of push-pull azobenzenes have an intense color, and so largely used in industry as dyes (Bandara and Burdette, 2012).



**Figure 22. Examples of Push-pull Azobenzenes.** Comparison of the *cis*-isomer relaxation half-life time ( $t_{1/2}$ ) for push-pull azobenzenes without and with azo-hydrazone tautomeric equilibrium.

### ***Tetra-ortho substituted azobenzene family (toAB)***

This class shows tetra-ortho substitutions (2,2',6 and 6' positions) in the two aromatic rings with methoxy or halide groups. They have a very characteristic photochemical behavior as the weaker  $n-\pi^*$  band of the *trans* isomer is shifted to higher wavelengths and is not overlapped with the same band of its *cis* isomer (**Figure 23**). Consequently, photoisomerization of these azobenzenes can be exclusively achieved through their  $n-\pi^*$  bands. *Trans* to *cis* isomerization can be obtained with green light (500-540 nm) and back isomerization to *trans* with blue light (420-450 nm). Moreover, such tetra-ortho functionalization strongly stabilizes the thermal relaxation time of the *cis* isomers, with half-times ranging from hours to days in water (Beharry et al., 2011; Samanta et al., 2013). Tetra-ortho-methoxy-substituted azobenzene derivatives, despite their well-separated  $n-\pi^*$  transitions, are often sterically too demanding for fitting into small receptors binding pockets, thus limiting their photobiological applications. Differently, tetra-ortho-functionalizations with chlorine and fluorine are less bulky and, even if they show less red-shifted *trans*  $n-\pi^*$  transitions than ortho-methoxylated-azobenzenes, have been remarkably employed in biology (Konrad et al., 2016; Rullo et al., 2014; Wegener et al., 2017). Interestingly the ortho-fluorinated azobenzenes, which are also sterically less demanding in comparison to the chlorinated ones, show a high two-photon absorption cross section. This property permits their photoisomerization using near-Infrared lights,

which can get the highest penetration into biological tissues with the lowest photodamages (Cabr  et al., 2019a).

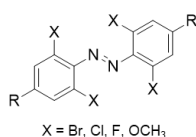


Figure 23. General Chemical Structure of Tetra-*ortho* Substituted Azobenzenes.

### ***Diazocines or “bridged azobenzene” family (bAB)***

Diazocines are “bridged” azobenzenes with superior photochemical properties as the *cis* is the thermodynamically stable isomer which can 100% exist, and also display high photochemical conversion rates to the *trans* isomer (> 90%) (Figure 24). The unsubstituted diazocine photoisomerizes from *cis* to *trans* configuration using 370-400 nm light and back isomerize to *cis* thermally in 5 hours (25  C) or using red-shifted light (450-500 nm) (Siewertsen et al., 2009, 2011). Recently, also nitrogen bridged diazocines (N-diazocines) derivatives have been reported (Lentes et al., 2019). Despite this class of photoswitches has the potential to be remarkably important in photopharmacology due to their structural similarity with many mainstream drugs (Lentes et al., 2019), their limited synthetic accessibility has so far limited the biological applications (Eljabu et al., 2015; Samanta et al., 2012). However, attempts to produce diazocines with larger yields have been reported during the development of photochromic ligands to control the neural receptors responding to glutamate (GluK1 and GluK2) (Cabr  et al., 2019b).

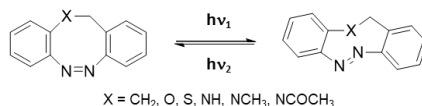


Figure 24. General Chemical Structure of Diazocines.

## 2.2. Methods to photocontrol biological systems

The control of protein function or a signaling path through the use of light is considered a potential innovative treatment for different pathologies and a useful tool for studying the complexity of various biological networks. This technology field assembles different techniques, that can be classified in optogenetic, optogenetic pharmacology, photopharmacology using caged compounds and photopharmacology using photoisomerisable compounds.

### 2.2.1. Optogenetic

Optogenetic takes advantage of the natural photoswitchable chromophores that are present in some class of proteins in order to control their activity using light in a fast and precise manner. Light-sensitive proteins are genetically expressed in cultured cells, generally in neurons, or even *in vivo*, in order to control the function of biological networks with light. Retinal is the most used natural photoswitchable chromophore for optogenetic applications, as it is naturally bound to opsin proteins. Opsins are GPCRs that regulate the visual transduction cascade (rhodopsins), the proton pumps as a source of energy (bacteriorhodopsins), and there are also transmembrane ionic channels (channelrhodopsins) and pumps (halorhodopsins) which permit the flow of ions when a photon is absorbed (**Figure 25**) (Boyden et al., 2005; Fenno et al., 2011; Kleinlogel et al., 2011; Wietek et al., 2014; Zhang et al., 2014).

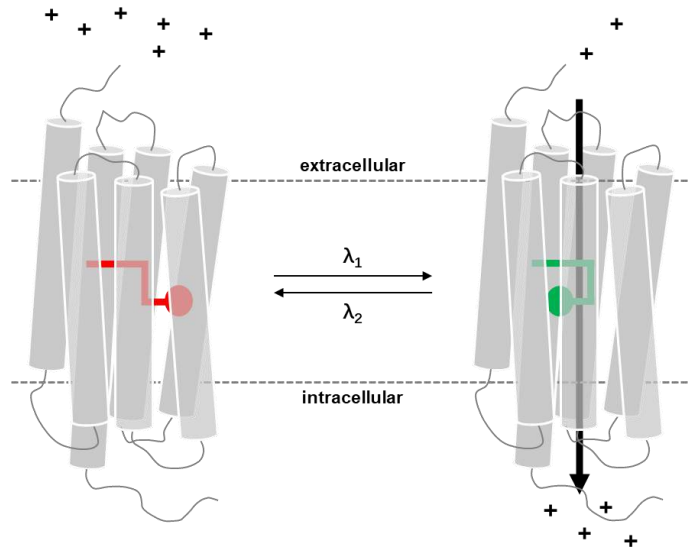


**Figure 25. Schematic View of the Optogenetic Approach for Controlling Protein Activity with Light.** Schematic view of the channelrhodopsin activity. All-*trans*-retinal is shown in red, *cis*-retinal is shown in green, cations (mostly Na<sup>+</sup>) permeating through the pore upon photoactivation are shown as positive charges. They enter the cell due to the concentration gradient and cause a membrane depolarization.

### 2.2.2. Photoswitchable tethered ligands (PTLs)

A photoswitchable-tethered ligand (PTL) is a particular type of light-sensitive drug as it is covalently attached to its target receptor through a tether that contains a photoswitch. In particular, it consists of a bioactive molecule for a specific receptor combined with one side of a photoswitchable moiety. The opposite side of the photoswitch is attached to a terminal cysteine-reactive group of the target receptor (**Figure 26**). Thus, the PTL must have a particular reactive group that can attach to the sulfhydryl groups of the protein. The most common reactive groups of PTLs are maleimides, activated carboxylic acids, and halides. The bioactive moiety of a PTL can be an agonist, an antagonist or a blocker. In the use of PTLs resides important pharmacological benefits. In fact, such activatable drugs are not able to diffuse away from their target receptors. This allows to obtain fast, reproducible, and spatially define protein responses upon illumination during long-lasting experiments (Ricart-Ortega et al., 2019). The PTLs can be bioconjugated to a target endogenous protein. Such light-

based technology is known as “tethered photopharmacology”. It includes the coupling of PTLs to genetically modified receptors which has been named “optogenetic pharmacology” (Kramer et al., 2013).

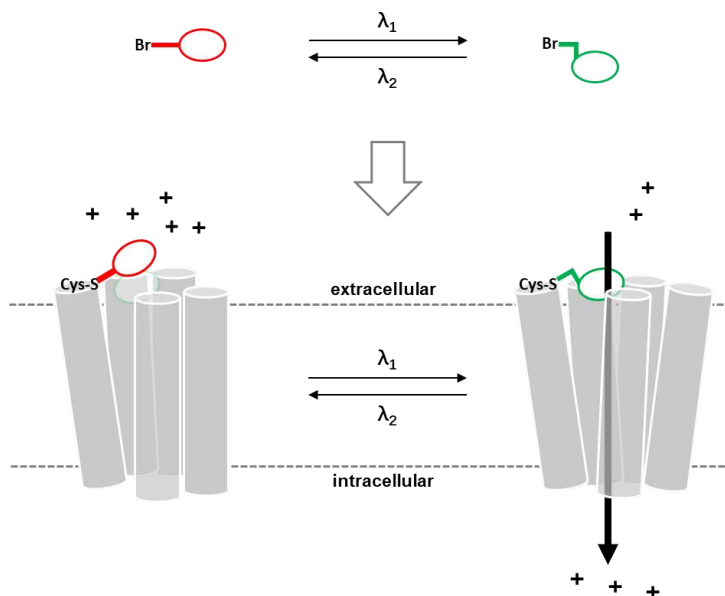


Figure 26. Schematic View of the Optogenetic Pharmacology Method for Controlling Protein Activity with Light.

The free cysteines are not generally abundant on the surface of an endogenous protein. For this reason, such residues are often introduced by mutagenesis near the binding site of the receptor, in an appropriate location that does not affect its physiological function. However, the position of a Cys residue in the target protein cannot be always optimized to facilitate the PTL-receptor binding site contacts. To help this interaction, a molecular chain of variable length can be introduced in the designed PTL to obtain a *cis* or *trans* active compound (Ricart-Ortega et al., 2019). Since the PTL is covalently attached to its target receptor, the affinity of the ligand is not a major concern as its concentration at the tethered site is very high in its active form. As a consequence, low-affinity ligands are usually preferred to guarantee that the photoswitching removes the ligand from the binding site.

Nicotinic Acetylcholine receptors (nAChRs) were the first coupled with PTLs. These receptors natively display a cysteine-rich loop near the orthosteric binding site. After reduction with dithiothreitol, the sulfhydryl

groups of these residues were made accessible for the conjugation with QBr (**Figure 27**), the specific PTL that can activate nAChRs in its *trans* configuration and leave the binding site in *cis* (Bartels et al., 1971). In combination with fine amino acidic mutations of the target protein, other PTLs have been developed. Of particular interest, a widely used class of PTLs are the MAQ family of K<sup>+</sup> channels blockers (Banghart et al., 2004; Chambers et al., 2006; Fortin et al., 2011; Sandoz et al., 2012), and the MAG family as agonists for glutamate ionotropic receptor kainate type subunit 2 (GluK2) and metabotropic glutamate receptors (mGluRs) (**Figure 27**) (Izquierdo-Serra et al., 2014; Volgraf et al., 2006).

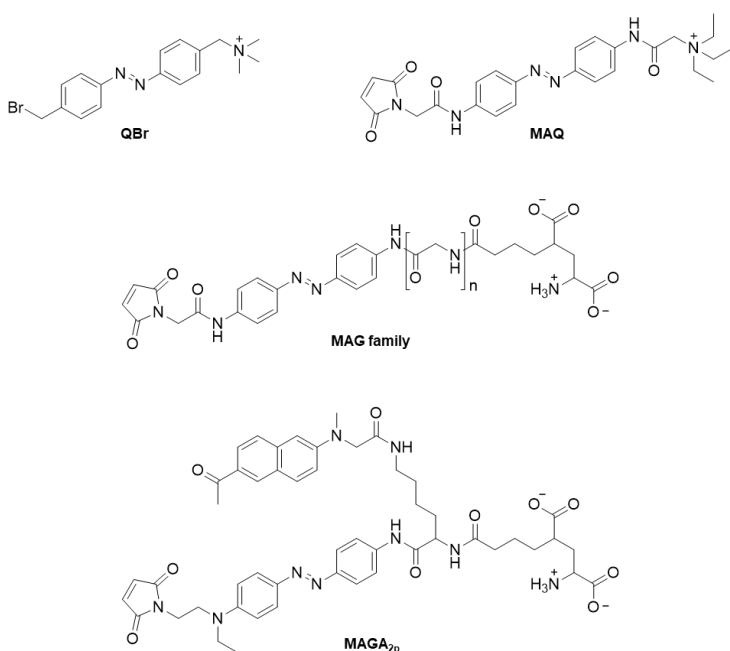


Figure 27. Representative examples of PTLs.

Despite the interesting results obtained with optogenetic pharmacology on controlling protein activity with light, the need of genetic manipulation hampers the therapeutic applications because of safety and regulatory concerns. This limitation was recently overcome by the development of targeted covalent photoswitches (TCPs) conjugated to native kainate receptor channel GluK1. Such TCPs (**Figure 28**) allow the photocontrol of the target protein activity in GluK1-expressing neurons (Izquierdo-Serra et

al., 2016). However, the tethered photopharmacology strategy has not yet been investigated on endogenous G-Protein Coupled Receptors.

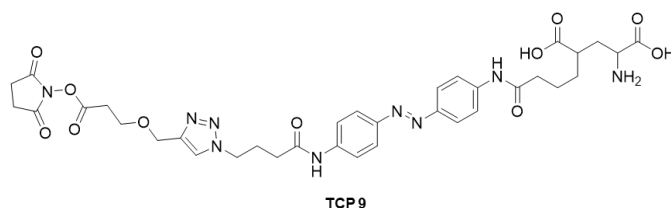


Figure 28. Chemical structure of TCP 9.

### 2.2.3. Photopharmacology using caged compounds

Photopharmacology with caged compounds stands as a potential therapeutic alternative in order to overcome the limitation of genetic manipulation, which is necessary for optogenetic techniques. Caged compounds can behave as drug-like compounds, a peculiarity that can make them interesting for human therapies. They are based on protecting groups that enclose, or “cage”, the bioactive agent and render this last one ineffective. These protecting groups are covalently linked to the drugs, avoiding the performance of their biological activity by masking a functional group crucial for the ligand-receptor interaction. The bond between the “cage” and the ligand is photolabile. Upon irradiation, with the right wavelength, the bond is broken in order to release the bioactive agent (**Figure 29**). Caged compounds have found important applications in cell biology and biochemistry as it is possible to control the drug release timing and to generate abrupt or localized changes of the active ligand concentration by controlling light wavelengths. This peculiarity makes caged ligands fundamentals for studying the fast kinetics or spatial heterogeneity of biochemical responses when rapid mechanical mixing is difficult, such as in intact cell, tissue, or protein crystal, or when microscopic spatial resolution is desired (Adams and Tsien, 1993). Recently, photocleavable ruthenium complexes have been designed to respond to widely separated wavelengths of light in order to achieve the sequential release of different bioactive compounds (Rapp and Dmochowski, 2019).

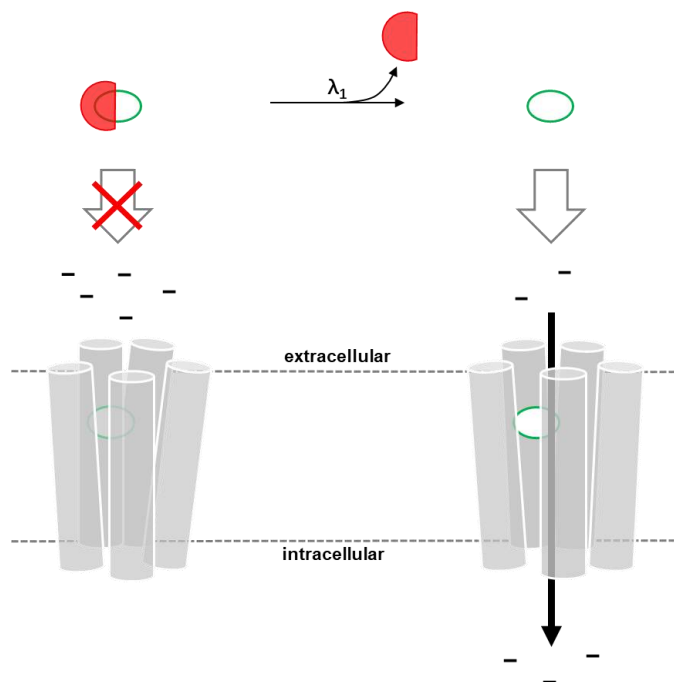


Figure 29. Schematic Representation of the concept of “Photopharmacology using Caged Compounds”.

Despite the use of caged compounds can avoid genetic modifications, this technique preserves some limitations. First, the release of the bioactive compound is not reversible. Of course, the caged compounds can effectively release the drug with high spatio-temporal precision. However, once the active compound is released, its control in the body is completely lost as it happens for conventional drugs. In this case, the only hope is that the ligand leaves the active zone as faster as possible or is cleared by either a reuptake pump or a deactivating enzyme. Second, the light-dependent cleavage can produce some by-products, such as the remnants of the protecting group, that can have secondary effects or be toxic. Other limitations may be the unwanted release of the ligand through thermal hydrolysis, and the fact that some caged ligands have off-target effects, such as antagonists on other receptors. (Figure 30) However, different caged compounds have been successfully designed to light-control the release of endogenous neurotransmitters (Klán et al., 2013), in particular for glutamate, that has been very useful for unraveling neural systems (Callaway and Katz, 1993; Canepari et al., 2001; Fino et al., 2009), for GABA

(Canepari et al., 2001; Donato et al., 2012; Verde et al., 2008), and for cage endogenous opioid neuropeptides L-enkephalin and dynorphin (**Figure 30**) (Banghart and Sabatini, 2012).

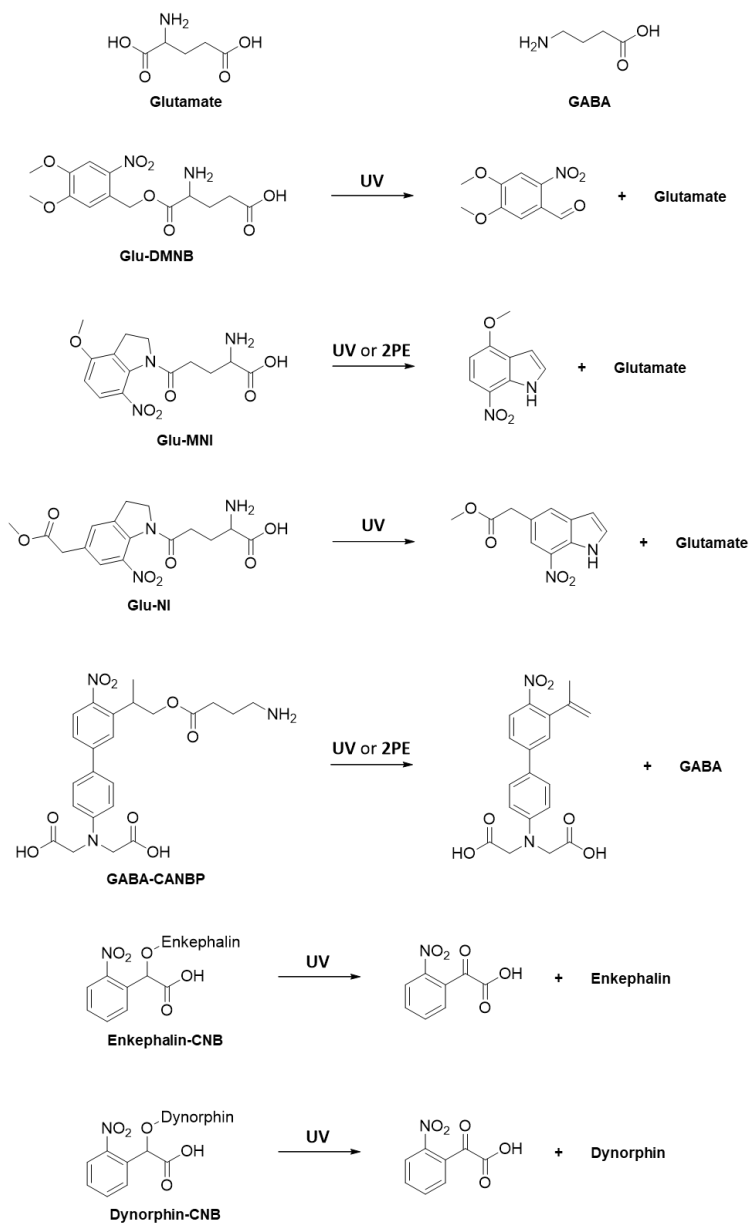


Figure 30. Examples of Caged Compounds to Precisely Control the CNS Activity.

Other applications of this technique are caged ATP for purinergic receptors P2X<sub>2</sub>, proteins involved in the synaptic transmission between neurons and from neurons to smooth muscle cells, and caged capsaicin for TRPV1 channels, capsaicin receptors involved in the regulation of body temperature. These two were the first approaches that showed to work in living animals (Zemelman et al., 2003).

#### **2.2.4. Photopharmacology using photoisomerisable free ligands**

Photoisomerisable compounds or photochromic ligands (PCLs) are based on the design and development of bioactive agents that have in their scaffold a photoswitchable moiety. This photoswitch is able to reversibly change the spatial disposition of the chemical groups of the bioactive molecule (Lerch et al., 2016). The configurations changes can strongly affect the efficacy of the compound to its specific target protein, allowing the modulation of its biological effect in a light-dependent manner. The control of both activation and inactivation of an endogenous protein, which is characteristic for photoisomerisable compounds, stands as an interesting evolution of the caged compounds, where the biological activity is triggered in an irreversible manner and the control of the drug is lost after its release. Moreover, using caged compounds other than glutamate is quite challenging, and their applications *in vivo* (e.g. in the brain) are rarely reported. Photoswitchable ligands preserve most advantages of caged compounds (**Figure 31**). They have the small molecule drug-like profile with the potential easiness of administration and fast tissue distribution, and the ability to control protein function with light without the need of genetic manipulation. Therefore, the ideal application of these tools for human therapies may be possible. However, the potential fast and passive tissue distribution could hamper the high selectivity of photoswitchable drugs, evoking undesired secondary effects.

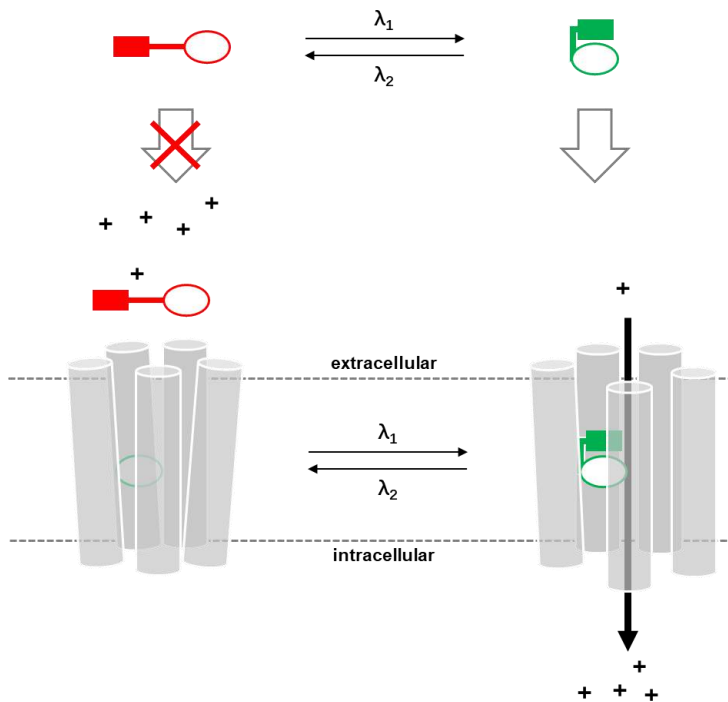


Figure 31. Schematic Representation of the concept of “Photopharmacology using Photoisomerisable Free Ligands”.

Accordingly, the ideal photoisomerisable compound should be inactive in its thermodynamically stable state in the absence of light. In this way, it is possible to spatiotemporally control its activation only through the spot of illumination. The most used reversible photochromic moieties for the development of bioactive photoswitchable ligands are azobenzenes. An azobenzene is able to isomerise from the thermodynamically stable *trans* to the *cis* isomer upon illumination with a specific wavelength, and can back isomerize to *trans* through irradiation with a different specific light or thermally. Exceptions are the “bridged” azobenzenes (diazocines) which have the *cis* configuration as the thermodynamically stable one. The transition between the two isomers strongly affects the length and the three-dimensional geometry of the ligand. These conformational changes create the existence of two possible approaches for an azobenzene-based drug: the “*trans*-active” or the “*cis*-active” compound. *Trans*-active compounds can bind the target receptor in their *trans* conformation and the *cis* one remains unbound, instead, the *cis*-active compounds behave

in the opposite way. The first photoswitchable compound with biological activity to be reported was BisQ (**Figure 32**). As an evolution of previous light-dependent pharmacological techniques, BisQ is the symmetric non-tethered derivative of QBr. (**Figure 27**) This ligand has a quaternary ammonium ion (Q) on both sides of the chromophore. Such a simple symmetric molecule is a photoswitchable version of the ACh and is able to open the nAChRs channels in its *trans* configuration (Bartels et al., 1971). Other interesting derivatives of tethered ligands have been designed and developed to have bioactive photoswitchable compounds. For example, a library of active MAQ-related K<sup>+</sup> channels blockers (**Figure 31**) have been studied and reported. These derivatives can exert their activity as *trans*- or *cis*-active compounds, depending on their chemical structure (Banghart et al., 2009; Fortin et al., 2008; Mourot et al., 2012). Another important example is Gluazo, (**Figure 32**) a photoisomerisable *trans*-active agonist of the ionotropic glutamate receptor GluK1. However, the design of new photoswitchable compounds is not only restricted on evolving the structure of previous reported PTLs. Through the study of the structure-activity relationship (SAR) of known drugs or drug-like bioactive agents, very fine structural modifications have been designed and applied to different compounds. This process created a large library of innovative drug-like photoisomerisable molecules.

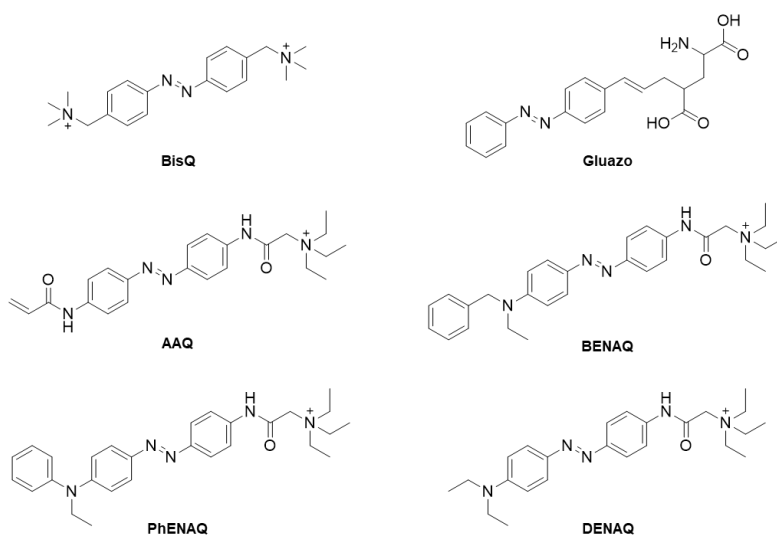


Figure 32. Examples of Photoisomerisable Compounds Which Are Active in the CNS.

The chemical modifications used to obtain new photoswitchable ligands can be classified into two types of approaches: the “azo-extension” and the “azologization” (Broichhagen et al., 2015). The azo-extension approach is based on “extending” a pre-existing aromatic ring of a bioactive agent into an azobenzene. In this way, a photoisomerisable derivative can be obtained and can maintain the activity of the original compound only in one configuration (*trans* or *cis*). Following this approach, various interesting tools have been developed. **(Figure 33)** Azopropofol is a *trans*-active derivative of the GABA<sub>A</sub> channel potentiator propofol, which is used for inducing or maintaining general anesthesia (Stein et al., 2012). Other interesting azo-extensions were applied to the antibiotic drug ciprofloxacin, obtaining the *cis*-active derivative quinolone-2 (Velema et al., 2013), and to the  $\mu$  opioid GPCR agonist fentanyl, which is used as a pain medication, creating the *trans*-active derivative Photofentanyl **(Figure 33)** (Schönberger and Trauner, 2014).

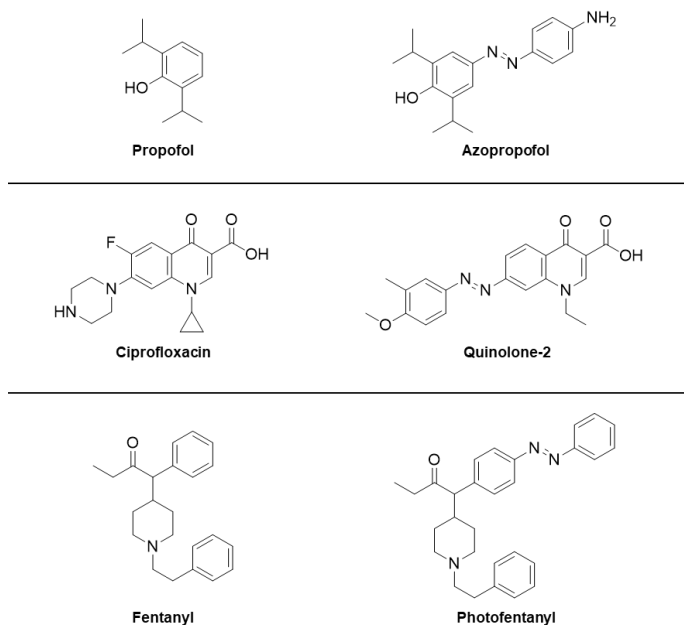


Figure 33. Examples of the Azo-extension Method to Afford Photoisomerisable Bioactive Compounds.

Differently, the azologization approach, or azo-replacement, is obtained by looking for a bridge between two aromatic rings into the chemical structure of the reference drug and replacing it with an azo-bond. The

bridge can be of different chemical nature, such as an ethylene, an amide or a methylene ether. This azologization design is the most used for building up new photoswitchable ligands libraries. The success of this strategy needs a fine study of the SAR and the three-dimensional orientation into the receptor binding site of the original molecule in order to bioisosterically introduce the molecular photoswitch. The anesthetic drug fomocaine has been successfully azologized in its *trans*-active derivative fotocaine (**Figure 33**) (Schönberger et al., 2014). Other important examples are the development of the *cis*-active azolog of glimepiride, a medication used for the treatment of diabetes mellitus type 2 (Broichhagen et al., 2014), and the *cis*-active azolog of the arvanil lipid, a derivative of the capsaicin, which activates the capsaicin channel receptors TRPV1 that are involved in the regulation of body temperature (**Figure 33**) (Frank et al., 2015). The allosteric site of endogenous GPCRs was targeted for the first time with photochromic ligands by the development of alloswitch-1, a photoswitchable negative allosteric modulator selective for the metabotropic glutamate receptor mGlu5 (**Figure 34**) (Pittolo et al., 2014). Another interesting application of the azologization is the development of the light-sensitive derivative of combretastatin A-4, called PST-1, which is able to inhibit the microtubule polymerization in its *cis* isomer and has antimitotic and pro-apoptotic properties (Borowiak et al., 2015). However, the presence of crystallographic poses of the bound target ligand into its receptor, combined with the performance of molecular docking simulations, facilitate the design of azolog derivatives and the success rate of this strategy. A clear example of the importance of these auxiliary details is demonstrated during the development of phototrexate, a putative photochromic dihydrofolate reductase (DHFR) inhibitor in its *cis* form obtained by bioisosteric azologization of the well-known chemotherapy agent Methotrexate (Matera et al., 2018).

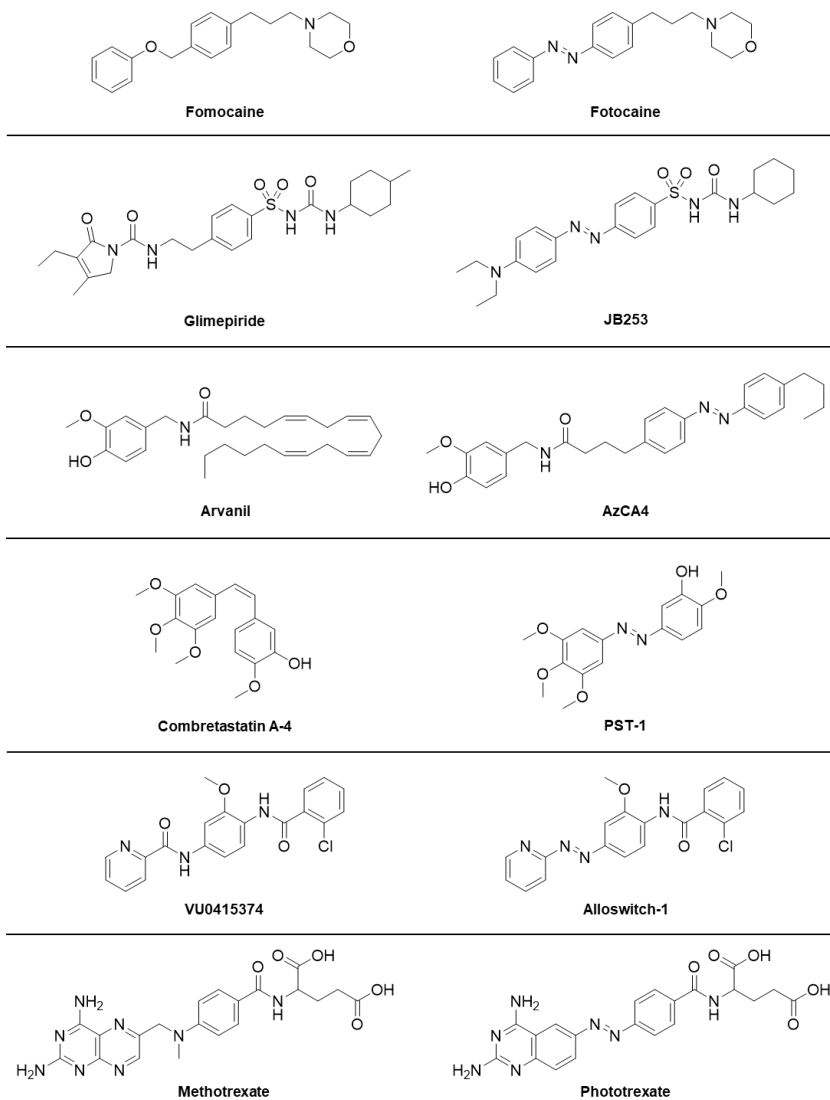


Figure 34. Examples of the Azologization Method to Afford Photoisomerisable Bioactive Compounds

### 2.3 Conclusions about photopharmacology

In conclusion, caged compounds, photoswitchable-tethered ligands, and photochromic ligands are advanced techniques to control the activity of any biological network with light. Some of their features allow overcoming the limits of optogenetics, which depends on genetic manipulation.

However, the targeted expression of proteins can be as well a very powerful technique, depending on the specific application that is needed. Indeed, in the last decades, genetics and pharmacology have been complementary techniques and often mixed with each other in order to understand physiology and manipulate the heterogeneity of its biochemical events.

Photopharmacology stands as a unique and innovative therapeutic approach that takes advantage of light. Patterned illumination can provide a highly precise spatiotemporal control of the action of photoswitchable drugs. This peculiarity can improve the selectivity of a drug, not only regarding a single receptor subtype, but also a very specific location of the human body where the target proteins are expressed. Such specificity cannot be achieved by the classical medicaments in use. Therefore, it may lead to a revolution in standard pharmacology. Photopharmacology is not only restricted to chemistry, biology and medicine studies in order to develop innovative photoswitchable drugs. Progress in this field occurs in parallel and in collaboration with physics, engineering and optics for the development of innovative optoelectronic devices that can be used for the photostimulation applied to human therapies.

### **3. Objectives of the Thesis**

Muscarinic acetylcholine receptors (mAChRs) are class A G-Protein Coupled Receptors (GPCRs) characterized by a widespread tissue distribution and involved in the control of numerous central and peripheral physiological responses. From the preceding sections, there are many potential therapeutic applications for drugs controlling the mAChRs activity. However, the high sequence homology among the different subtypes (M1–M5) of the transmembrane region hampers the development of subtype-selective ligands. Numerous muscarinic drugs have been created in the past decades, but their medical use is very limited due to their unwanted effects in the organism.

Classical pharmacology alone was not able to overcome the natural obstacles posed by this family of receptors for their therapeutic exploitation. In addition to the poor selective profile common to nearly all the muscarinic ligands, pharmacological agents are often widely distributed once administered into the body, further complicating their applications.

Photopharmacology offers the possibility of controlling muscarinic receptor pathways at different locations and times in order to disentangle their networks and to further understand their physiological functions.

Photopharmacology also promises several potential benefits for new pharmacological treatments. Using suitable illumination, the activity of a reversible photoisomerisable drug can be controlled with light in space and time over the body after administration, to improve its selectivity for a single target expressed in a specific location. Overall, this light-based approach presents novel perspectives in drug discovery and therapeutics and aims to improve the specificity and the control of drugs' action and minimize their side effects.

Recognizing both the need of new tools to control metabotropic cholinergic actions and better study their pathophysiological roles, and the opportunities offered by photoswitches, the grand aim of this thesis is the development of new and versatile light-regulated ligands that can enable the optical modulation of endogenous mAChRs and the physiological processes in which they are involved.

In order to achieve that aim, different objectives have been set in this thesis:

- 1) The design and synthesis of a series of photoswitchable muscarinic agonists, taking advantage of both the outstanding agonism activity of iperoxo and the application of the azo-extension approach to this mAChRs superagonist (Chapter II);
- 2) The design and synthesis of new photoswitchable muscarinic agonists using the molecular hybridization strategy, which allows combining in a single molecular structure the fundamental chemical and pharmacological elements of an allosteric modulator and a potent agonist (Iperoxo), in order to obtain a drug with improved affinity, efficacy, selectivity or safety in comparison to the parent agonist (Chapter III);
- 3) The design and synthesis of new photoswitchable muscarinic antagonists through the development of an innovative azologization strategy that is able to mimic the geometry of the tricyclic scaffold of the M1 antagonist pirenzepine (Chapter IV);
- 4) The complete photochemical characterization of all the new synthesized compounds, which must be photoisomerizable in aqueous solution compatible with pharmacological studies (Chapters II, III and IV);
- 5) The pharmacological characterization of the new compounds, which must affect mAChR-mediated functions and must photoisomerize in different biological contexts such as cell cultures, intact tissues, and wild-type animals (Chapter II, III, IV);
- 6) To devise strategies to overcome the use of ultra-violet wavelengths to photostimulate the new muscarinic ligands, in order to improve the light penetration deep into the tissues and reduce its potential cell damage (Chapter II, III, IV).

## **CHAPTER II**

### **Development of Orthosteric Photoswitchable Agonists to Control Muscarinic Receptors**



## General Introduction

### Chapter II

Iperoxo is recognized as a very appealing ligand for muscarinic receptors. Despite its 3-oxy- $\Delta^2$ -isoxazoline scaffold, which is atypical compared to acetylcholine (ACh) or carbachol (CCh), this quaternary ammonium salt is one of the most potent agonists at all the three investigated muscarinic receptor subtypes (M1, M2, and M3). However, its pharmacological profile is lacking subtype selectivity (Barocelli et al., 2000; Dallanocce et al., 1999).

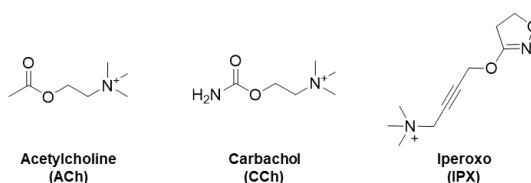


Figure 35. Chemical structures of acetylcholine (ACh), carbachol (CCh) and Iperoxo (IPX)

With the aim of developing innovative muscarinic agonists, we designed, synthesized and characterized the pharmacological profile of photoswitchable derivatives of iperoxo. These agents might have not only important applications in research and expand the knowledge about the mAChRs role in the pathophysiology of various diseases, but also clinical applications in medicine.

We elongated the quaternary ammonium nitrogen of iperoxo with unsubstituted and tetra-ortho-fluorinated azobenzenes and produced a set of monovalent and bivalent photoswitchable agonists. The synthesis work was followed by the photochemical characterization of the new compounds, to prove their behavior as reversible photoswitches. Their pharmacology on mAChRs was tested with specific competition binding experiments in rat brain membranes. Afterward, a more advanced biological *in vitro* assay was used to demonstrate their light-dependent activity on M1 receptors. The action of the new iperoxo derivatives was studied with the split-luciferase complementation technique in living

human embryonic kidney (HEK) cells expressing the human M1 mAChR. Lastly, we attempted to explain our pharmacological results with computational binding simulations using the active conformational model of M1 receptor.

*This project has been realized initially in parallel and later in collaboration with the laboratories of Professor Michael Decker and Professor Ulrike Holzgrabe from the University of Wuerzburg (Germany). I personally carried out the design of the compounds, the chemical synthesis of iperoxo and all its unsubstituted azobenzene-based derivatives with their photochemical characterizations, the development and the performance of all the competition binding experiments on mAChRs that are present in this work and I took part on writing the draft of the final paper. This full study has been published in the following article:*

“Fluorination of Photoswitchable Muscarinic Agonists Tunes Receptor Pharmacology and Photochromic Properties”

Luca Agnetta, Marcel Bermúdez, **Fabio Riefolo**, Carlo Matera, Enrique Claro, Regina Messerer, Timo Littmann, Gerhard Wolber, Ulrike Holzgrabe, and Michael Decker

*Journal of Medicinal Chemistry* 2019 62 (6), 3009-3020.

DOI: 10.1021/acs.jmedchem.8b01822

# Fluorination of Photoswitchable Muscarinic Agonists Tunes Receptor Pharmacology and Photochromic Properties

Luca Agnetta,<sup>†</sup> Marcel Bermudez,<sup>‡</sup> Fabio Riefolo,<sup>§,||</sup> Carlo Matera,<sup>§,||</sup> Enrique Claro,<sup>⊥</sup> Regina Messerer,<sup>†</sup> Timo Littmann,<sup>#</sup> Gerhard Wolber,<sup>‡</sup> Ulrike Holzgrabe,<sup>†</sup> and Michael Decker<sup>\*,†</sup>

<sup>†</sup>Pharmaceutical and Medicinal Chemistry, Institute of Pharmacy and Food Chemistry, Julius Maximilian University of Würzburg, Am Hubland, 97074 Würzburg, Germany

<sup>‡</sup>Institute of Pharmacy, Freie Universität Berlin, Königin-Luise-Straße 2 - 4, 14195 Berlin, Germany

<sup>§</sup>Institute for Bioengineering of Catalonia (IBEC), Barcelona Institute for Science and Technology, Carrer Baldori Reixac 15-21, 08028 Barcelona, Spain

<sup>||</sup>Network Biomedical Research Center in Bioengineering, Biomaterials, and Nanomedicine (CIBER-BBN), 50018 Zaragoza, Spain

<sup>⊥</sup>Institut de Neurociències (INc) and Departament de Bioquímica i Biologia Molecular, Unitat de Bioquímica de Medicina, Universitat Autònoma de Barcelona (UAB), Bellaterra, 08193 Barcelona, Spain

<sup>#</sup>Institute of Pharmacy, University of Regensburg, Universitätsstraße 31, 93053 Regensburg, Germany

**ABSTRACT:** Red-shifted azobenzene scaffolds have emerged as useful molecular photoswitches to expand potential applications of photopharmacological tool compounds. As one of them, tetra-ortho-fluoro azobenzene is well compatible for the design of visible-light-responsive systems, providing stable and bidirectional photoconversions and tissue-compatible characteristics. Using the unsubstituted azobenzene core and its tetra-ortho-fluorinated analogue, we have developed a set of uni- and bivalent photoswitchable toolbox derivatives of the highly potent muscarinic acetylcholine receptor agonist iperoxo. We investigated the impact of the substitution pattern on receptor activity and evaluated the different binding modes. Compounds **9b** and **15b** show excellent photochemical properties and biological activity as fluorination of the azobenzene core alters not only the photochromic behavior but also

the pharmacological profile at the muscarinic M1 receptor. These findings demonstrate that incorporation of fluorinated azobenzenes not just may alter photophysical properties but can exhibit a considerably different biological profile that has to be carefully investigated.

## INTRODUCTION

In recent years, many different biochemical targets, including ion channels, enzymes, and lipids, have been effectively modulated in a light-controlled fashion using photoswitchable ligands, expanding the vibrant field of photopharmacology.<sup>1</sup> Now, the potential of the application of photopharmacological tool compounds to G protein-coupled receptors (GPCRs) is being steadily investigated.<sup>2</sup> The rapid light-induced isomerization of photochromic ligands can be directly translated into a change in affinity or activity. This can give important new insights into the binding mode and time course of activation processes, enabling precise spatial and temporal resolution of the complex signaling pathway of GPCRs.<sup>3</sup> The muscarinic acetylcholine (ACh) receptors (mAChRs), which belong to class A GPCRs, have received special attention in this regard due to their role as a prototypic pharmacological system<sup>4</sup> and their therapeutic potential.<sup>5</sup> The muscarinic receptors mediate the excitatory and inhibitory effects of the neurotransmitter acetylcholine (ACh),<sup>6</sup> thus regulating diverse important biological processes. Muscarinic receptors are widely expressed in the human body including the central nervous system (M1/M4/M5) related to neurological processes of memory and learning. In the peripheral nervous system (M2/M3), they are related to the so-called “rest and digest” biological functions.<sup>7</sup> In this work, we present an optimized approach for the application of photochromic ligands to GPCRs by using the M1 receptor as a prototypic model system, outlining the advantages and challenges of using red-shifted molecular photoswitches.

Accordingly, we focused on the highly potent orthosteric agonist iperoxo in the design of bidirectional pharmacological tool compounds with tuned photochemical properties. Iperoxo (iper) is a muscarinic ACh receptor agonist with outstanding potency that is known to tolerate bulky substituents without compromising agonist efficacy.<sup>8</sup> Recently, we

reported on photoiperoxo (**9a**), a compound that consists of iperoxo extended with a molecular photoswitch and a dualsteric photochromic ligand BQCAAI.<sup>2c</sup> We made use of azobenzene as a molecular photoswitch to change intrinsically the geometry and polarity of the linking unit and to control its activation by light.<sup>1a,b,d</sup> Upon irradiation with UV- and blue light, and thus triggering a switch from the *trans*- to the *cis*- form, we were able to control the efficacy and to investigate the time course of receptor activation processes.<sup>2c</sup>

Despite this remarkable progress in the development of photopharmacological tool compounds, the poor photostationary states (PSSs) of our azobenzene-based systems resulted in an unclear correlation between the ratio of the *cis/trans* concentration to the actual activity at the receptor. The PSS strongly depends on the electronic environment of the system and the overlap of transitions of the *cis/trans* photoisomers and can be influenced by changing the substitution pattern of the azobenzene moiety. Additionally, the operational wavelengths to trigger photoisomerization can interfere to a significant degree with the fluorescent readout methods that are commonly used in GPCR research. To investigate the complex nature of M1 activation, photopharmacological tool compounds should ideally show superior photochemical properties, such as quantitative and stable bidirectional photoswitching, and be responsive to visible rather than high-energy light.<sup>1a,b,d</sup> A convincing approach to optimize the photochemical properties of azobenzenes involving the tetra-ortho-substitution of azobenzene has been described previously by the groups of Woolley<sup>9</sup> and Hecht.<sup>10</sup> By choosing the suitable moieties, tetra-ortho-substitution leads to a separation of the  $n \rightarrow \pi^*$  transitions of *trans* and *cis* isomers and ultimately to almost complete *trans/cis* photoconversions. Importantly, the desired isomer can be selectively formed with wavelengths in the visible-light window. Despite their promising application in photobiology due to the well-separated  $n \rightarrow \pi^*$  transitions,<sup>11</sup> ortho-methoxylated azobenzenes are sterically demanding and strongly twisted about the N–N double bond. This makes them unlikely to fit into the narrow receptor binding pocket. Ortho-chlorinated and fluorinated azobenzenes show comparable red-shifted *trans*  $n\text{-}\pi^*$  transitions, albeit somewhat less than ortho-methoxylated, and have been successfully employed in biological

applications.<sup>12</sup> However, tetra-ortho-fluoro substituted azobenzenes stand out in their slow thermal *cis*-to-*trans* relaxation rate, representing a truly bistable molecular switch on the biological time scale. Moreover, the fluorine substituents are sterically less demanding compared to the chlorine ones.<sup>10a</sup> Based on these results, we further investigated the effect of iperoxo-derived photoswitchable ligands by developing a set of tool compounds, containing the iperoxo motif and the tetra-ortho-fluoro azobenzene or unsubstituted azobenzene, separately.

In modern medicinal chemistry, the bivalent strategy has been extensively applied to GPCR ligands.<sup>13</sup> Appropriately designed bivalent ligands can exhibit higher affinity, potency, and selectivity compared with the parent ligand, with potential therapeutic application.<sup>14</sup> Successful examples of the application of this approach to GPCRs include the human cannabinoid receptor 2,<sup>15</sup> opioid receptor,<sup>16</sup> dopamine 2,<sup>17</sup> and muscarinic receptors.<sup>18</sup> To this end, we extended the photoiperoxo structure with another iperoxo moiety, creating a homobivalent ligand, to improve and investigate binding at the M1 receptor.

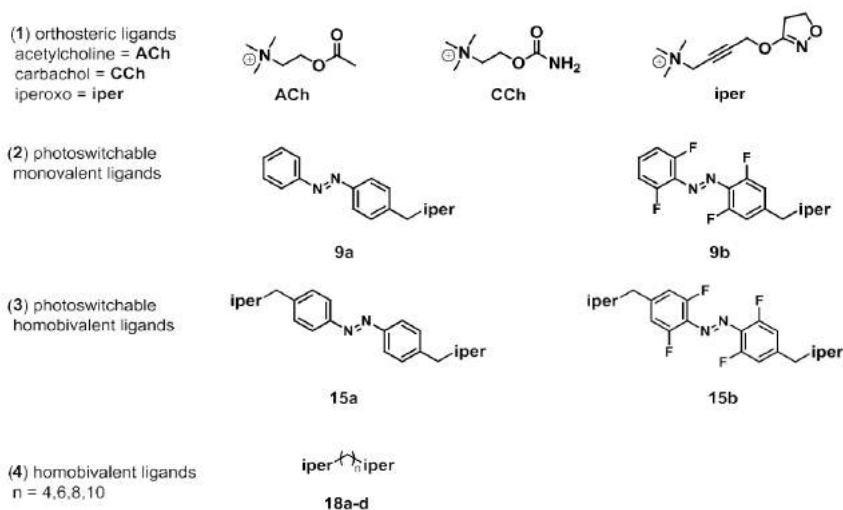
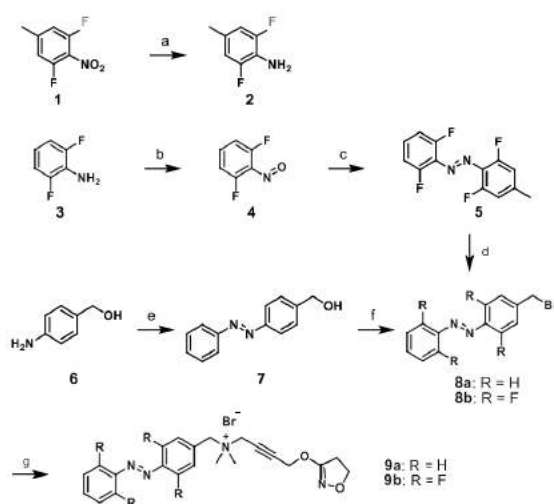


**Figure 1.** Structures of (1) reference agonists acetylcholine (ACh), carbachol (CCh), and iperoxo (iper); (2) univalent; and (3) homobivalent photoswitchable derivatives with azobenzene- and tetra-ortho-fluoro azobenzene scaffolds and homobivalent ligands linked by polymethylene linkers.

## RESULTS AND DISCUSSION

We now report the design and synthesis of photoswitchable homobivalent iperoxo (**15a**), tetra-ortho-fluoro-photoiperoxo (**9b**), and homobivalent tetra-ortho-fluoro-photoiperoxo (**15b**), being the corresponding tetra-ortho-fluorinated analogues of the azobenzene iperoxo derivatives (**Figure 1**). In addition, we synthesized homobivalent iperoxo derivatives (**18a-d**) connected by aliphatic chains as reference compounds to identify the optimal distance between the two orthosteric moieties for dualsteric binding.

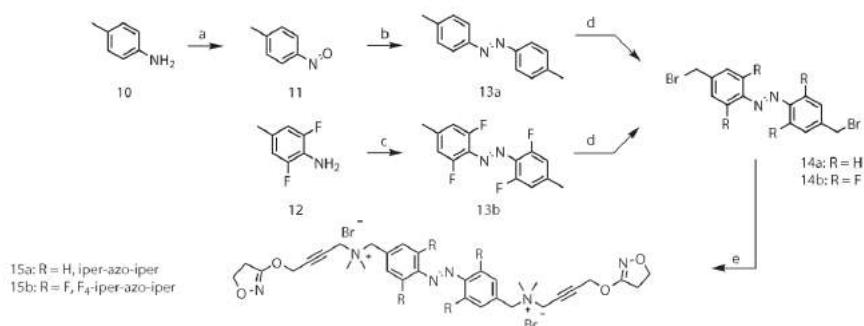


Scheme 1. Synthesis of Photoiperoxo and F4-Photoiperoxo<sup>a</sup>

<sup>a</sup>Reagents and conditions: (a) Pd/C, EtOH (87%); (b) oxone, CH<sub>2</sub>Cl<sub>2</sub>, water; (c) 2, AcOH/trifluoroacetyl (TFA), toluene (43%); (d) N-bromosuccinimide (NBS), azobisisobutyronitrile (AIBN), CCl<sub>4</sub>, 80 °C (50%); (e) nitrosobenzene, AcOH (75%); (f) CBr<sub>4</sub>, PPh<sub>3</sub>, CH<sub>2</sub>Cl<sub>2</sub> (60%); (g) 4((4,5-dihydroisoxazol-3-yl)oxy)-N,N-dimethylbut-2-yn-1-amine 16, EtOAc/MeCN (39% for **9a**, 92% for **9b**).

**Chemistry.** The synthetic routes for the uni- and homobivalent ligands are summarized in **Schemes 1** and **2**, respectively. Azobenzene moieties **5** and **7** were accessed starting from the corresponding anilines **2**, obtained from reduction of 1,3-difluoro-5-methyl-2-nitrobenzene **1**, and commercially available (4-aminophenyl)methanol **6**. Anilines were used in Baeyer–Mills reactions with 1,3-difluoro-2-nitrosobenzene **4** and nitrosobenzene,

respectively, to afford precursors for bromination, which took place under either radical (for **8b**) or nucleophilic substitution conditions (for **8a**).



Scheme 2. Synthesis of Iper-azo-iper and F4-Iper-azo-iper<sup>a</sup>

<sup>a</sup>**Reagents and conditions:** (a) oxone, CH<sub>2</sub>Cl<sub>2</sub>, water; (b) 10, AcOH (36%); (c) KMnO<sub>4</sub>, FeSO<sub>4</sub>·7H<sub>2</sub>O, CH<sub>2</sub>Cl<sub>2</sub> (29%); (d) NBS, AIBN, CCl<sub>4</sub>, 80 °C (76% for **14a**, 24% for **14b**); (e) 4((4,5-dihydroisoxazol-3-yl)oxy)-N,N-dimethylbut-2-yn-1-amine, EtOAc, 60 °C (83% for **15a**, 32% for **15b**).

Lastly, 4((4,5-dihydroisoxazol-3-yl)oxy)-N,N-dimethyl-but-2-yn-1-amine, prepared using the standard convergent procedure as described previously,<sup>19</sup> was connected to the photoswitches to afford photoiperoxo **9a** and F4-photoiperoxo **9b**. The synthesis of the homobivalent ligands started from commercially available p-toluidine **10**, which was condensed to compound **13a** by means of a Baeyer–Mills reaction. Tetra-ortho-fluorinated analogue **13b** was obtained by oxidative coupling of **12** with potassium permanganate and iron sulfate heptahydrate as oxidizing reagents.

compd.	trans		trans		cis		$\Delta\lambda$ (nm)	PSS <sub>trans</sub> (%)	PSS <sub>cis</sub> (%)
	$\lambda_{\max}$ ( $\pi-\pi^*$ )	$\epsilon$ ( $\pi-\pi^*$ ) (*10 <sup>3</sup> M <sup>-1</sup> cm <sup>-1</sup> )	$\lambda_{\max}$ ( $n-\pi^*$ ) (nm)	$\epsilon$ ( $n-\pi^*$ ) (M <sup>-1</sup> cm <sup>-1</sup> )	$\lambda_{\max}$ ( $n-\pi^*$ ) (nm)	$\epsilon$ ( $n-\pi^*$ ) (*10 <sup>3</sup> M <sup>-1</sup> cm <sup>-1</sup> )			
9a	320	12.2	418	680	418	1.04	<10	90	62
15a	320	22.0	426	920	426	1.42	<10	99	60
9b	307	16.7	443	1440	412	1.80	31	94	86
15b	311	14.8	447	1180	412	1.38	35	93	98

Table 1. UV–Vis Spectroscopic Data of Compounds **9a**, **9b**, **15a**, and **15b**<sup>a</sup>

<sup>a</sup> $\lambda_{\max}$  ( $\pi-\pi^*$ ,  $n-\pi^*$ ) represents the wavelength at the maximal absorption of the  $\pi-\pi^*$  and  $n-\pi^*$  transition bands, respectively. The molar extinction coefficients  $\epsilon$  ( $\pi-\pi^*$ ,  $n-\pi^*$ ) were calculated according to the Lambert–Beer formula.  $\Delta\lambda$  ( $n-\pi^*$ ) is the difference between *trans* and *cis* regarding  $\lambda_{\max}$  of the  $n-\pi^*$  band. PSS percentages after irradiation with operational wavelengths determined by liquid chromatography using the wavelength at the isosbestic point as the detecting wavelength.

Again, radical bromination and substitution with 4((4,5-dihydroisoxazol-3-yl)oxy)-N,N-dimethylbut-2-yn-1-amine resulted in formation of target compounds **15a** and **15b**. Aliphatic derivatives (**18a-d**) were synthesized reacting the corresponding double brominated aliphatic chains with 2 equiv of 4((4,5-dihydroisoxazol-3-yl)oxy)-N,N-dimethylbut-2-yn-1-amine (Suppl. Scheme 5).

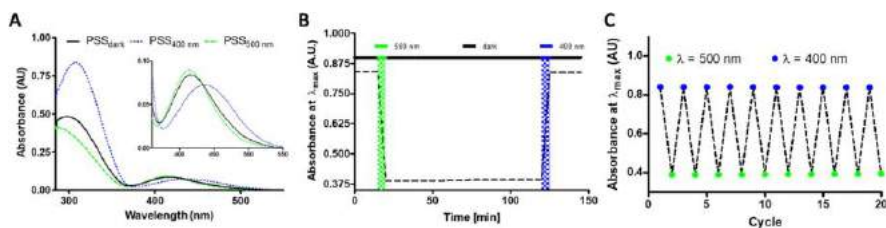


**Figure 2.** Representative (A) absorption spectra of PSS at the dark-adapted state and after illumination with 400 nm (to *trans*) and 500 nm (to *cis*), (B) stability measurement and (C) multiple *cis/trans* isomerization cycles of compound **9b** in dimethyl sulfoxide at 25 °C. Spectra of compounds **9a**, **15a**, and **15b** are displayed in the Supporting Information section.

**UV-Vis Spectroscopic Characterization.** The UV-vis absorption spectra of the set of compounds **9a**, **9b**, **15a**, and **15b** were measured at a concentration of 50  $\mu$ M in dimethyl sulfoxide (DMSO). For compounds **9a** and **15a** (with unsubstituted azobenzene scaffold), we observed a strong  $\pi$ - $\pi^*$  transition band at short wavelength ( $\lambda_{\pi-\pi^*} \approx 320$  nm) and a weaker  $n$ - $\pi^*$  ( $\lambda_{n-\pi^*} \approx 422$  nm) upon irradiation with blue light (400 nm, *trans* isomer). Irradiation with UV light (365 nm), and thus photoconversion to the *cis*-isomer, leads to a decrease in absorbance intensity of the  $\pi$ - $\pi^*$  and increase of the  $n$ - $\pi^*$  band without affecting the wavelengths of the respective transition bands. Spectra of fluorinated compounds **9b** and **15b** were measured using 400 nm for *cis*  $\rightarrow$  *trans* and 500 nm for *trans*  $\rightarrow$  *cis* photoconversions. Due to the n-orbital stabilization of electron-withdrawing groups in the *cis*-state, tetra-ortho-fluoro substitution of the azobenzene core causes a separation of the transitions of the  $n$ - $\pi^*$  band, in our case of around 33 nm on average, which makes it possible to address both isomers selectively with light in the visible region (Figure 1A).<sup>20</sup> As a direct consequence, the PSSs (measured by means of liquid chromatography at the isosbestic point wavelength) are substantially higher than for nonfluorinated analogues (Table 1), which is beneficial for the application of photoswitchable ligands in biological systems and allows

a clear correlation between the distinct photoisomer and its biological effect. Moreover, multiple *cis/trans* switching cycles did not cause noticeable degradation, highlighting the reliability and robustness of the photochromic conversion of both the tetra-ortho-fluoro and unsubstituted azobenzene scaffolds. This is confirmed by stability measurements in which the compounds were kept in the dark for at least 120 min after switching to the less stable *cis*-isomer, without significant changes in absorbance and hence in the PSS. Importantly, this information is required when considering eventual incubation times required in biological assays, making sure that the photoswitchable ligands do not relax to the *trans*-isoform during the readout (**Figure 1B, C**). From the physicochemical point of view, this set of compounds shows ideal characteristics for stable and bidirectional photoswitching (**Figure 2**).

**Binding Experiments.** First, **9a**, **9b**, **15a**, and **15b** were tested for affinity to the M receptors. This was achieved in competition experiments with the photoswitchable ligands in rat brain membrane preparations. These were conducted as described previously<sup>21</sup> and contained a high density of all the five mAChR subtypes. [<sup>3</sup>H]Quinuclidinyl benzilate ([<sup>3</sup>H]QNB) is a nonselective muscarinic ligand, which allows the identification of muscarinic receptors,<sup>22</sup> and displays an equilibrium dissociation constant of about 40 pM,<sup>23</sup> making it suitable for these experiments. Specific binding was defined with test compounds at total nominal concentrations in the range of 1–100  $\mu$ M and elaborating the raw dpm data from the scintillation counter,<sup>21</sup> representing total radioactivity. In general, compounds **9a**, **9b**, **15a**, and **15b** were found to show good affinity for the M receptors (**Figure 3**). In particular, the azobenzene-elongated iperexo **9a** and **9b** showed a binding affinity in the low-micromolar range, although no significant changes could be observed upon irradiation ( $pIC_{50} \approx 5$  for both photoisomers, **Figure 3A, C**). The affinity increased significantly for the homobivalent ligands **15a** and **15b**. In good agreement with results from the split-luciferase interaction assay, *trans*-**15a** showed an affinity in the high-nanomolar range, with a significant difference between the two photo isoforms ( $pIC_{50} = 6.32$  in the dark vs 5.88 under illumination with 365 nm light, **Figure 3B**). Thus, we observed that despite the introduction of an azobenzene molecular photoswitch, a good affinity could be preserved. Moreover, the presence of a second moiety of iperexo, as in

the homobivalent ligands **15a** and **15b**, improved binding affinity and created an appreciable difference between *trans* and *cis* isomers.

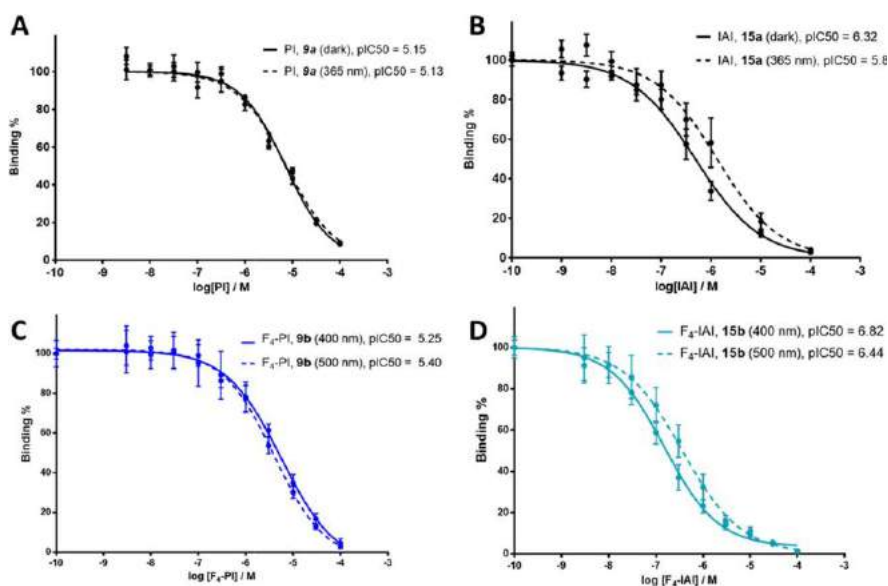


**Figure 3.** Competition for specific binding of 200 pM  $[^3\text{H}]\text{QNB}$  to rat brain membranes containing high density of all the five mAChRs by **9a**, **9b**, **15a**, and **15b**. Data points were fitted using the “log(inhibitor) vs normalized response – variable slope” function in GraphPad Prism 6.

**Biological in Vitro Assay.** Our goal was to assess the extent to which the pharmacological profiles of these compounds change after fluoro substitution of the azobenzene core. For this purpose, we used a novel split-luciferase complementation technique detecting the interaction between the  $G\alpha_q$  subunit and phospholipase C- $\beta 3$  (PLC- $\beta 3$ ) and thus reflecting G protein activation in living HEK 293T cells expressing the human M1 receptor.<sup>24</sup> The split-luciferase complementation technique is particularly suitable to detect protein–protein interactions and associated signaling in living cells.<sup>25</sup> Since it is not fluorescence-based, no excitement irradiation is needed and, consequently, its readout does not interfere with the operational wavelengths for photoswitching, providing clear-cut and distinguishable concentration–response curves for each photoisomer, which makes it highly suitable for photopharmacological investigations into GPCRs. Technically, HEK 293T cells were engineered to express a fragment of the luciferase at the  $G\alpha_q$  subunit of the heterotrimeric G protein and the complementary fragment at the N-

terminus of the PLC- $\beta$ 3. Upon binding of the endogenous or synthetic agonists, both fragments are brought in close proximity, leading to a reconstitution of the functional luciferase protein and emission of bioluminescence, in the presence of the substrate luciferin.<sup>24</sup> Also advantageous is the fact that the receptor itself, in this case M1, remains unengineered in contrast to, for example, fluorescence resonance energy transfer (FRET) sensors, where often large constructs at intracellular loops could act as anchors and may affect changes in conformations. Pharmacological data are depicted in **Figure 4** and summarized in **Table 2** and show the recorded potencies and efficacies of compounds **9a**, **9b**, **15a**, and **15b**, reflected by the pEC<sub>50</sub>, and maximal response E<sub>max</sub> for each isomer. The data are normalized to the maximum response of the synthetic agonist carbachol (CCh) at a concentration of 100  $\mu$ M. Measurements of the endogenous agonists acetylcholine (ACh) and the synthetic parent compound iperoxo as references were not affected by illumination with operational wavelengths. First, bivalent alkyl-substituted iperoxo compounds were screened to identify the correlation between the distance of the orthosteric moieties and their corresponding biological activity. For this purpose, homobivalent ligands **18a–d** with different chain lengths were employed. All compounds were characterized as full agonists, and longer spacer proved advantageous for the M1 affinity, suggesting a dualsteric binding.<sup>26</sup> The C10-spacer, which is comparable to the azobenzene scaffold, shows the highest effect and suggests this distance as optimal for the design of photoswitchable ligands (Suppl. **Figure 1**).

As investigated in previous studies, photoiperoxo **9a** was unable to induce a conformational change at the M1 receptor in FRET studies, upon illumination with either UV- or blue light. Instead, it exhibited antagonist behavior in competition experiments.<sup>2c</sup> Using the split-luciferase complementation assay, **9a** shows two distinct curves for each photoisomer, differing in their efficacy. The maximal response E<sub>max</sub> was 48% for the *trans* and 34% for the *cis* photoisomer, indicating partial agonism at the M1 receptor. Surprisingly, substitution of azobenzene with the tetra-ortho-fluorinated scaffold resulted in full agonist **9b** with a significant potency enhancement and pEC<sub>50</sub> values almost two log units higher (comparable to endogenous agonist ACh). However, no significant

changes in efficacy or affinity could be observed for **9b** upon irradiation. The potency at the M1 receptor was modulated effectively by introducing an additional iperoxo moiety, resulting in the homobivalent ligand **15a**. By doing so, considerable improvement in the potency was gained and a difference between the two photoisomers was re-established. Again, replacement of the azo-core with tetra-ortho-fluoro scaffold (**15b**) resulted in a distinctive change toward higher potency, being almost 10-fold more pronounced for the *trans* isomer. Noteworthy, *trans*-**15b** shows a pEC<sub>50</sub> concentration in the one-digit nanomolar range, which is comparable to the agonist iperoxo itself.

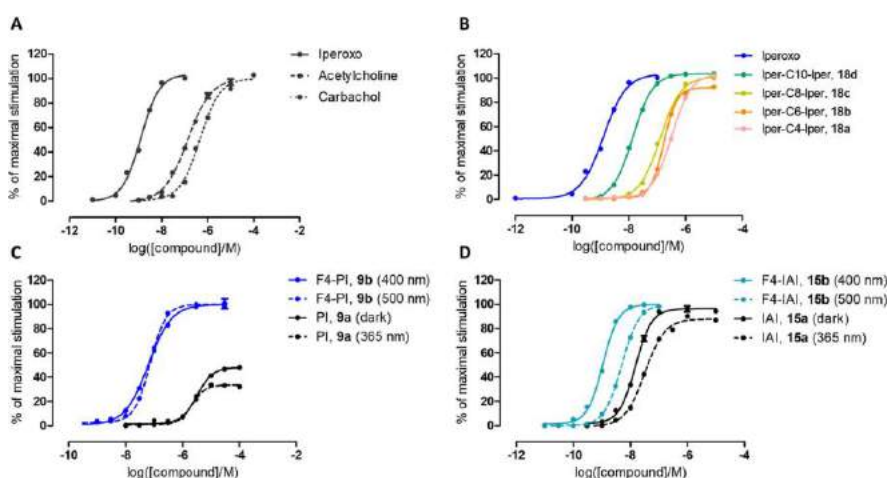


**Figure 4.** G $\alpha$ /PLC- $\beta$ 3 split-luciferase interaction assay in HEK 293T cells expressing the human muscarinic M1 receptors. Concentration–response curves for (A) reference compounds, (B) iper-linker-iper derivatives (**18a–d**), (C) **9a** and **9b**, and (D) **15a** and **15b** at operational wavelengths specific for the respective photoconversion. Data represent means  $\pm$  standard error of the mean of three to four experiments conducted at least in triplicate.

This is a remarkable observation, as the introduction of a molecular photoswitch generally causes an overall loss in activity at the receptor. A photoswitch-endowed compound showing an almost identical potency as the reference compound is hard to achieve. Taken together, these findings suggest that binding of *trans*-form of bivalent derivatives **15a**, **15b**, and **9b** stabilizes the M1 receptor in the active conformation to a greater extent than **9a**. Additionally, fluoro substitution leads to pronounced differences in biological activity and is beneficial for binding to the M1 receptor. As

such, we developed a set of photopharmacological GPCR tool compounds for a better understanding of M1 receptor binding modes.

**Molecular Modeling.** Docking studies using a previously reported homology model of the active M1 receptor conformation<sup>27</sup> reveal a dualsteric (bitopic) binding mode for all investigated photoswitchable iperoxo derivatives in their *trans* conformation (**Figure 5**). We surmise that the photoswitch primarily occurs in solution and that the pharmacological properties are mainly driven by binding of *trans* isomers. The active M1 receptor model indicates a narrow channel between the orthosteric and allosteric binding sites, rendering binding of *cis* conformations to the receptor unlikely due to steric interference with the tyrosine lid. Similar to other iperoxo-based dualsteric ligands,<sup>28</sup> the iperoxo moiety is located in the orthosteric binding pocket showing interactions with D84, N213, and the tyrosine lid consisting of Y85, Y212, and Y235 (**Figure 5**). For all compounds, a hydrogen bond between the azo group and the hydroxy group of Y235 is formed. The side chain of Y235 shows a reorientation toward the extracellular side, which allows binding of azobenzene scaffolds through  $\pi$ - $\pi$  interactions. This side-chain position allows full contraction of the orthosteric binding site without full closure of the tyrosine lid and thereby stabilizes active receptor conformations. Interestingly, fluorination of the azobenzene scaffold results in a higher potency of **9b** and **15b** compared to the nonfluorinated compounds **9a** and **15a**. This can be rationalized in our model by an optimal geometry of the aromatic ring in the M1 receptor. Whereas the phenyl ring opposite to Y235 is more flexible in **9a** and **15a**, it is restrained in an orientation optimal for parallel  $\pi$ - $\pi$  interaction. This is caused by the spatial requirements of the ortho-fluorine atoms in **9b** and **15b** and an additional hydrogen bond with the hydroxy group of Y85 (**Figure 5A**). In addition, fluorinated compounds show additional lipophilic contacts with the tyrosine lid as well as W231 (**Figure 5A, B**). Since the symmetric compounds **15a** and **15b** are larger, they show secondary interactions in the extracellular vestibule compared to **9a** and **9b**. In particular, a charge interaction of the ammonium group in the extracellular receptor domain with E228 can be observed (**Figure 5C**). Positive charges in the allosteric vestibule recognized by aromatic residues or the EDGE sequence have previously been found to be important for the M2 receptor.<sup>28b,29</sup>

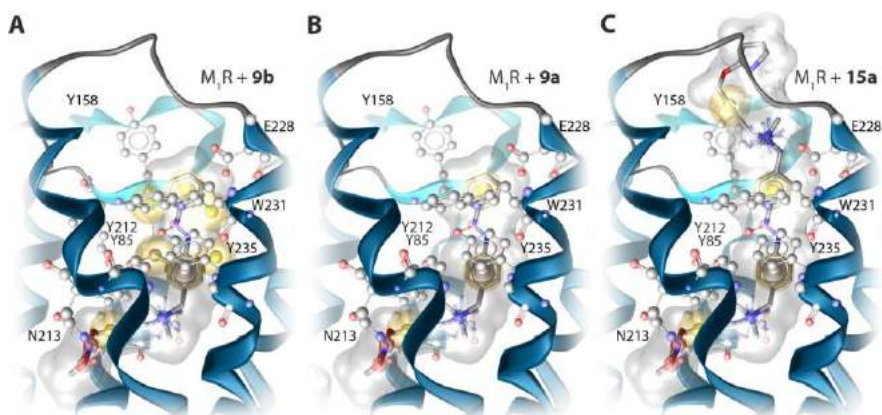


**Figure 5.** Proposed binding modes and interactions of *trans* isomers of photoswitchable dualsteric iperoxo derivatives (A) **9b**, (B) **9a**, and (C) **15a** in complex with the M1 receptor. Positive ionizable centers are shown as blue stars, yellow spheres indicate lipophilic contacts, purple disks show aromatic interactions, and red arrows indicate hydrogen bonds.

Interestingly, the M2 receptor lacks the presence of an acidic residue at the beginning of transmembrane domain 7, suggesting a specific role for E228 in the M1 receptor. This observation is in accordance with the higher potencies for **15a** and **15b** that can be explained by this specific charge interaction and additional lipophilic contacts with Y158, which were not observed for **9a** and **9b** due to the lack of an allosteric ammonium group (**Figure 5**). The absence of extensive allosteric interactions and less lipophilic contacts of **9a** compared with **9b** suggests a ligand–receptor complex in which **9a** is not able to fully stabilize the active receptor state. This is supported by previously reported FRET-based measurements indicating the insensitivity of the M1 receptor upon **9a** binding with regard to conformational changes.<sup>2c</sup> However, the here-applied G $\alpha$ /PLC- $\beta$ 3 split-luciferase interaction assay unveiled **9a** as a weak partial agonist ( $E_{\max}$  34–48%). At first sight, it may appear conflicting that the *cis* photoisomers bind to the receptor and induce a receptor response, whereas the docking data predict only the *trans* photoisomers to bind. On a closer look, even though the fluorinated azobenzene scaffold provides higher PSS, a distinct percentage of *trans* isomer remains (**Table 1**), which can still bind and activate the receptor. On a logarithmic scale, as used for the binding and functional studies, even a small *trans* percentage shows a pronounced effect. An alternative explanation can be rationalized by a second purely allosteric binding mode as shown for several other dualsteric ligands.<sup>26,28a</sup>

For such a binding pose, the *cis* orientation is compulsory, forming  $\pi$ - $\pi$  and cation- $\pi$  interactions, which can, to a certain extent, favor the active state of the receptor. In contrast, the linear nature of the *trans* photoisomer is not suitable to solely bind to the allosteric binding site. At this stage, this is still a subject of future investigations though.

## CONCLUSIONS

We successfully developed a set of photopharmacological tools that allowed detailed investigation of the distinct effects of fluorination and bivalency on binding properties at the M1 receptor. We designed photoswitchable iperoxo (**9a**) and bivalent iperoxo (**15a**) compounds, as well as the red-shifted congeners (**9b**, **15b**) by introduction of the tetra-ortho-fluoro scaffold. Bivalent compounds (**15a**, **15b**) show much higher affinity compared to the univalent compounds (**9a**, **9b**) due to additional interactions at allosteric binding sites. Remarkably, the fluorine compounds (**9b**, **15b**) not only show improved operational wavelengths as shown in a novel, light-independent luciferase complementation assay, but also increased potency at the M1 receptor. Bivalent and fluorinated photoiperoxo (**15b**) act as pronounced affinity switches, whereas the univalent photoiperoxo acts as an efficacy switch (**9a**). The work significantly enlarges the photopharmacological toolbox for mAChRs. We strongly recommend detailed pharmacological evaluation for red-shifted compounds since their biological properties might differ significantly from the parent compound. It will be interesting to investigate the potential for *in vivo* photopharmacological control of this series.

## EXPERIMENTAL SECTION

**General Information.** Common reagents and solvents were obtained from commercial suppliers (Aldrich, Steinheim, Germany; Merck, Darmstadt, Germany) and were used without any further purification. Tetrahydrofuran (THF) was distilled from sodium/benzophenone under an argon atmosphere. Microwave-assisted reactions were carried out on an MLS-rotaprep instrument (Milestone, Leutkirch, Germany) using 8–10 Weflon disks. Melting points were determined on a Stuart melting point apparatus SMP3 (Bibby Scientific, U.K.). Thin-layer chromatography was performed on silica gel 60 F254 plates

(Macherey-Nagel, Düren, Germany), and spots were detected under UV light ( $\lambda = 254$  nm) or by staining with iodine. Merck silica gel 60 (Merck, Darmstadt, Germany) was used for chromatography (230–400 mesh) columns or performed on an Interchim puriFlash 430 (Ultra Performance Flash Purification) instrument (Montluçon, France). Used columns are silica 25 g, 30  $\mu\text{m}$ , Alox-B 40 g, 32/63  $\mu\text{m}$ , and Alox-B 25 g, 32/63  $\mu\text{m}$  (Interchim, Montluçon, France). Nuclear magnetic resonance spectra were performed with a Bruker AV-400 NMR instrument (Bruker, Karlsruhe, Germany) in DMSO- $d_6$ ,  $\text{CDCl}_3$ ,  $(\text{CD}_3)_2\text{CO}$ . As internal standard, the signals of the deuterated solvents were used (DMSO- $d_6$ :  $^1\text{H}$  2.50 ppm,  $^{13}\text{C}$  39.52 ppm;  $\text{CDCl}_3$ :  $^1\text{H}$  7.26 ppm,  $^{13}\text{C}$  77.16 ppm;  $(\text{CD}_3)_2\text{CO}$ :  $^1\text{H}$  2.05 ppm,  $^{13}\text{C}$  39.52 ppm). Abbreviation for data quoted are as follows: s, singlet; d, doublet; t, triplet; q, quartet; m, multiplet; br, broad; dd, doublet of doublets; dt, doublet of triplets; tt, triplet of triplets; and tq, triplet of quartets. Coupling constants (J) are given in hertz. For purity and reaction monitoring, analytical high-performance liquid chromatography (HPLC) analysis was performed with a system from Shimadzu equipped with a DGU-20A3R controller, an LC20AB liquid chromatograph, and an SPD-20A UV-vis detector. Stationary phase was a Synergi 4  $\mu\text{m}$  fusion-RP (150  $\times$  4.6 mm $^2$ ) column (Phenomenex, Aschaffenburg, Germany). For the mobile phase, a gradient of MeOH/water with 0.1% formic acid was used. Parameters: A = water, B = MeOH,  $V(\text{B})/(V(\text{A}) + V(\text{B})) =$  from 5 to 90% over 10 min,  $V(\text{B})/(V(\text{A}) + V(\text{B})) = 90\%$  for 5 min,  $V(\text{B})/(V(\text{A}) + V(\text{B})) =$  from 90 to 5% over 3 min. The method was performed with a flow rate of 1.0 mL/min. Compounds were only used for biological evaluation if the purity was  $\geq 95\%$ . Electrospray ionization (ESI) mass spectral (MS) data were acquired with Shimadzu LCMS-2020. Data are reported as mass-to-charge ratio (m/z) of the corresponding positively charged molecular ions.

**2,6-Difluoro-4-methylaniline (2).** 1,3-Difluoro-5-methyl-2-nitrobenzene **1** (1.0 g, 5.78 mmol) and 10% Pd-C (190 mg) in EtOH (20 mL) were hydrogenated under atmospheric pressure for 3 h. The catalyst was filtered off, and the filtrate was evaporated to give **2** as a light reddish oil (0.686 g, 4.80 mmol, 87%).  $^1\text{H}$  NMR ( $\text{CDCl}_3$ , 400 MHz):  $\delta$  (ppm) = 6.63 (m, 2H), 3.49 (s, 2H), 2.23 (s, 3H).  $^{13}\text{C}$  NMR ( $\text{CDCl}_3$ , 400 MHz):  $\delta$  (ppm) = 153.3 (d, J = 8.3 Hz), 151.0 (d, J = 8.3 Hz), 127.4 (t, J = 8.5 Hz), 121.1 (t, J = 16.6 Hz), 111.9–111.3 (m), 20.7 (t, J = 1.7 Hz). ESI-MS: m/z calcd for  $\text{C}_7\text{H}_8\text{F}_4\text{N}_2^+ [\text{M} + \text{H}]^+$ : 144.1, found: 144.1.

**1-(2,6-Difluoro-4-methylphenyl)-2-(2,6-difluorophenyl)-diazene (5).** 2,6-Difluoroaniline **3** (641 mg, 4.96 mmol, 2.00 equiv) was dissolved in dichloromethane (DCM) (30 mL). To this solution, oxone (16.8g, 27.3 mmol, 20.00 equiv) dissolved in water (60 mL) was added. The solution was under argon at room temperature overnight. After separation of the layers, the aqueous layer was extracted with DCM twice. The combined organic layers were washed with 1 N HCl, saturated sodium bicarbonate solution, water, and brine, dried over  $\text{MgSO}_4$ , and evaporated to dryness. Afterward, toluene (10 mL) and 2,6-difluoro-4-methylaniline **2** (357 mg, 2.49 mmol, 1.00 equiv) were added. A mixture of acetic acid (20 mL) and TFA (50 mL) was prepared and added to the solution. The resulting mixture was stirred at room temperature for 24 h. Afterward, it was evaporated to dryness. Purification by column chromatography over silica gel (DCM/petrol ether (PE), 1:4, silica gel) yielded the desired product **5** as a deep orange solid (292 mg, 1.09 mmol, 43%).  $^1\text{H}$  NMR ( $\text{CDCl}_3$ , 400

MHz):  $\delta$  (ppm) = 7.40–7.29 (m, 1H), 7.05 (t,  $J$  = 8.6 Hz, 2H), 6.87 (d,  $J$  = 10.5 Hz, 2H), 2.41 (s, 3H). ESI-MS:  $m/z$  calcd for  $C_{13}H_9BF_4N_2^+ [M + H]^+$ : 269.1, found: 269.1.

**(4-(Phenyldiazenyl)phenyl)methanol (7).** Nitrosobenzene **4a** (1.28 g, 11.9 mmol, 3 equiv) was dissolved in ethanol (10 mL). To this solution, (4-aminophenyl)methanol **6** (491 mg, 4.00 mmol, 1 equiv) and acetic acid (20 mL) were added. The reaction mixture was stirred for 4 h at room temperature. Subsequently, the reaction mixture was poured into 30 mL of ice-cold water, and the precipitate was collected by filtration. Column chromatography (DCM/methanol = 50:1) provided compound **7** (659 mg, 2.99 mmol, 75%) as bright orange needles.  $^1H$  NMR (400 MHz, DMSO- $d_6$ ):  $\delta$  (ppm) = 7.88 (m,  $J$  = 6.9, 1.8 Hz, 4H), 7.65–7.50 (m, 5H), 5.40 (t,  $J$  = 5.7 Hz, 1H), 4.61 (d,  $J$  = 5.6 Hz, 2H).  $^{13}C$  NMR (101 MHz, DMSO- $d_6$ ):  $\delta$  (ppm) = 152.4, 151.3, 146.9, 131.8, 129.93, 127.6, 122.9, 62.9. ESI-MS:  $m/z$  calcd for  $C_{13}H_{12}N_2O^+ [M + H]^+$ : 213.1, found: 213.1.

**1-(4-(Bromomethyl)phenyl)-2-phenyldiazene (8a).** 4-(Phenyldiazenyl)phenyl)methanol **7** (300 mg, 1.41 mmol, 1 equiv) was dissolved in dry THF (15 mL) under argon atmosphere, tetrabromomethane (703 mg, 2.12 mmol, 1.5 equiv) and triphenylphosphine (556 mg, 2.12 mmol, 1.5 equiv) were added, and the reaction mixture was stirred for 4 h. The reaction mixture was filtered, and the filtrate was evaporated to dryness and purified by column chromatography (ethyl acetate (EA)/hex = 1:10) yielding compound **8a** as orange needles (232 mg, 0.84 mmol, 60%).  $^1H$  NMR (400 MHz, DMSO- $d_6$ ):  $\delta$  (ppm) = 7.89 (tt,  $J$  = 7.7, 2.0 Hz, 4H), 7.69–7.57 (m, 5H), 4.80 (s, 2H).  $^{13}C$  NMR (101 MHz, DMSO- $d_6$ ):  $\delta$  (ppm) = 151.9, 151.5, 141.5, 131.7, 130.5, 129.5, 122.9, 122.6, 33.6. ESI-MS:  $m/z$  calcd for  $C_{13}H_{11}BrN_2^+ [M + H]^+$ : 275.0, 277.0, found: 274.9, 276.9.

**1-(4-(Bromomethyl)-2,6-difluorophenyl)-2-(2,6-difluorophenyl)diazene (8b).** To a solution of 1,2-bis(2,6-difluoro-4-methylphenyl)diazene **5** (250 mg, 0.93 mmol) in 20 mL of  $CCl_4$  were added NBS (0.332 g, 1.86 mmol) and AIBN (11 mg, 0.076 mmol). The resultant solution was stirred overnight at 80 °C. After evaporation of the solvent, the product was purified by column chromatography over silica gel (DCM/PE,1:4, silica gel) yielding the desired product **8b** (163 mg, 0.47 mmol, 50%).  $^1H$  NMR ( $CDCl_3$ , 400 MHz):  $\delta$  (ppm) = 7.38 (t,  $J$  = 8.5 Hz, 4H), 7.21 (d,  $J$  = 8.5 Hz, 11H), 7.13–7.03 (m, 14H), 6.87 (dt,  $J$  = 14.8, 7.3 Hz, 42H), 6.65 (d,  $J$  = 8.8 Hz, 4H), 4.44 (s, 6H), 4.33 (s, 19H), 2.41 (s, 2H), 2.29 (s, 6H). ESI-MS:  $m/z$  calcd for  $C_{13}H_8BrF_4N_2^+ [M + H]^+$ : 347.0, 349.0 found: 347.0, 349.0.

**4-((4,5-Dihydroisoxazol-3-yl)oxy)-N,N-dimethyl-N-(4-(phenyldiazenyl)benzyl)but-2-yn-1-aminium (9a).** 1-(4-(Bromomethyl)phenyl)-2-phenyldiazene **8a** (100 mg, 0.36 mmol, 1 equiv) and 4-((4,5-dihydroisoxazol-3-yl)oxy)-N,N-dimethylbut-2-yn-1-amine **16** (132 mg, 0.73 mmol, 2 equiv) were dissolved in acetonitrile (10 mL) and stirred at room temperature for 12 h. The reaction was monitored by liquid chromatography (LC)–MS. The precipitate was filtered off, and the solvent was removed under reduced pressure. The crude product was purified by column chromatography (DCM/MA/NH $_3$  = 20:1:0.1) yielding compound **9a** as a dark red oil (54 mg, 0.14 mmol, 39%).  $^1H$  NMR (400 MHz,  $CDCl_3$ ):  $\delta$  (ppm) = 7.99–7.86 (m, 6H), 7.56–7.46 (m, 3H), 5.24 (s, 2H), 4.88 (d,  $J$  = 7.9 Hz, 4H), 4.42 (t,  $J$  = 9.6 Hz, 2H), 3.53–3.40 (m, 6H), 3.02 (t,  $J$  = 9.6 Hz, 2H).  $^{13}C$  NMR (101 MHz,  $CDCl_3$ ):  $\delta$  (ppm) = 166.9,

154.1, 152.6, 134.3, 131.9, 129.3, 129.0, 123.7, 123.3, 87.8, 75.9, 70.2, 66.2, 57.5, 54.8, 50.0, 33.1. ESI-MS:  $m/z$  calcd for  $C_{22}H_{25}BrN_4O_2^+$   $[M + H]^+$ : 377.2, found: 377.2.

***N*-(4-((2,6-Difluorophenyl)diazenyl)-3,5-difluorobenzyl)-4-((4,5-dihydroisoxazol-3-yl)oxy)-*N,N*-dimethylbut-2-yn-1-aminium Bromide (9b).** 1-(4-(Bromomethyl)-2,6-difluorophenyl)-2-(2,6-difluorophenyl)diazene **8b** (64 mg, 0.184 mmol) and 4-((4,5-dihydroisoxazol-3-yl)oxy)-*N,N*-dimethylbut-2-yn-1-amine (34 mg, 0.184 mmol, 1 equiv) in ethyl acetate (10 mL) were charged in a sealed reaction vessel and stirred for 4 h. The precipitate was collected and washed several times with ethyl acetate to afford the desired product **9b** as a bright yellow powder (90 mg, 0.170 mmol, 92%).  $^1H$  NMR (MeOD, 400 MHz):  $\delta$  (ppm) = 7.63–7.30 (m, 3H), 7.12 (dt,  $J = 17.0, 8.7$  Hz, 2H), 4.97 (d,  $J = 14.5$  Hz, 2H), 4.66 (d,  $J = 49.0$  Hz, 2H), 4.48–4.28 (m, 4H), 3.21 (d,  $J = 30.4$  Hz, 6H), 3.05 (dt,  $J = 15.1, 9.6$  Hz, 2H).  $^{13}C$  NMR (MeOD, 400 MHz):  $\delta$  (ppm) = 168.82, 154.23 (d,  $J = 5.1$  Hz), 151.71 (d,  $J = 5.5$  Hz), 132.40 (t,  $J = 9.7$  Hz), 131.22 (d,  $J = 9.0$  Hz), 118.4, 118.1, 113.5 (d,  $J = 19.1$  Hz), 89.1, 76.7, 71.2, 66.0, 58.3, 55.3, 51.1, 33.6. ESI-MS:  $m/z$  calcd for  $C_{22}H_{21}F_4N_4O_2^+$   $[M]^+$ : 449.16, found: 449.05.

**1-Methyl-4-nitrosobenzene (11).** *p*-Toluidine **10** (2.00 g, 18.7 mmol) was dissolved in DCM (60 mL), and a solution of oxone (11.5 g, 18.7 mmol) in water (60 mL) was added. The resulting biphasic mixture was stirred at room temperature for 30 min. The organic layer was separated, and the aqueous layer was extracted twice with DCM. The combined organic layers were washed with 1 M aqueous hydrochloric acid, saturated sodium hydrogen carbonate, and brine and dried over anhydrous sodium sulfate. Mixture **11** was concentrated to 10–15 mL volume, which was further used without purification.

**4,4'-Dimethylazobenzene (13a).** 1-Methyl-4-nitrosobenzene **11** and *p*-toluidine **10** (1.00 g, 9.33 mmol) were dissolved in glacial acetic acid (20 mL) and stirred overnight. The solution was diluted with water and extracted with ethyl acetate. The organic phase was washed four times with water and once with brine and dried over anhydrous sodium sulfate. The crude product was purified by flash chromatography (pentane/diethyl ether, 9:1) to obtain the desired product **13a** as an orange crystalline solid (695 mg, 3.31 mmol, 36%).  $^1H$  NMR (400 MHz,  $CDCl_3$ ):  $\delta$  (ppm) = 7.82 (d,  $J = 8.3$  Hz, 4H), 7.31 (d,  $J = 8.6$  Hz, 4H), 2.44 (s, 6H).  $^{13}C$  NMR (101 MHz,  $CDCl_3$ ):  $\delta$  (ppm) = 151.0, 141.3, 129.9, 122.9, 21.6. ESI-MS:  $m/z$  calcd for  $C_{14}H_{14}N_2^+$   $[M + H]^+$ : 211.1, found: 211.0.

**1,2-Bis(2,6-difluoro-4-methylphenyl)diazene (13b).** 2,6-Difluoro-4-methylaniline **12** (397 mg, 2.77 mmol) and a freshly ground mixture of potassium permanganate (1.17 g, 4.21 mmol) and iron(II) sulfate heptahydrate (1.17 g, 7.40 mmol) were dissolved in DCM (10 mL). The solution was refluxed overnight, filtered through celite, dried over anhydrous sodium sulfate, filtered, and concentrated under reduced pressure. The crude residue was purified by column chromatography (DCM/petrol ether 1:1) to give the desired product **13b** (110 mg, 0.39 mmol, 29%).  $^1H$  NMR ( $CDCl_3$ , 400 MHz):  $\delta$  (ppm) = 6.86 (d,  $J = 10.3$  Hz, 4H, arom. *trans*), 6.65 (d,  $J = 8.3$  Hz, 0.39H, arom. *cis*), 2.40 (s, 6 H,  $-CH_3$ , *trans*), 2.29 (s, 0.62H,  $-CH_3$ , *cis*).  $^{13}C$  NMR ( $CDCl_3$ , 400 MHz):  $\delta$  (ppm) = 156.8 (d,  $J = 5.0$  Hz), 154.3 (d,  $J = 5.2$  Hz), 143.2 (t,  $J = 10.3$  Hz), 113.2, 113.0, 21.7.

**4,4'-Bis(bromomethyl)azobenzene (14a).** To a solution of 4,4'-dimethylazobenzene **13a** (2.17 g, 10.3 mmol) in 20 mL of carbon tetrachloride (40 mL) were added N-bromosuccinimide (4.22 g, 23.7 mmol) and azobisisobutyronitrile (127 mg, 0.77 mmol). The resultant solution was stirred overnight at 70 °C, filtered, washed with chloroform and water, and dried under reduced pressure, which yielded **14a** as an orange crystalline powder (2.88 g, 7.81 mmol, 76%). <sup>1</sup>H NMR (400 MHz, CDCl<sub>3</sub>): δ (ppm) = 7.90 (d, J = 8.4 Hz, 4H), 7.54 (d, J = 8.5 Hz, 4H), 4.56 (s, 4H). <sup>13</sup>C NMR (101 MHz, CDCl<sub>3</sub>): δ (ppm) = 152.3, 140.8, 129.9, 32.7. ESI-MS: m/z calcd for C<sub>12</sub>H<sub>13</sub>Br<sub>2</sub>N<sub>2</sub><sup>+</sup> [M + H]<sup>+</sup>: 368.9, found: 368.8.

**1,2-Bis(4-(bromomethyl)-2,6-difluorophenyl)diazene (14b).** To a solution of 1,2-bis(2,6-difluoro-4-methylphenyl)diazene **13b** (226 mg, 0.801 mmol) in 17 mL of CCl<sub>4</sub> were added NBS (0.356 g, 2.02 mmol) and AIBN (10 mg, 0.060 mmol). The resultant solution was stirred overnight at 80 °C. After evaporation of the solvent, the product was recrystallized from methanol to afford the desired product **14b** as red needles (86 mg, 0.195 mmol, 24%). <sup>1</sup>H NMR (CDCl<sub>3</sub>, 400 MHz): δ (ppm) = 7.11 (d, J = 9.1 Hz, 4H), 4.43 (s, 4H). <sup>13</sup>C NMR (CDCl<sub>3</sub>, 400 MHz): δ (ppm) = 160.9 (d, J = 7.6 Hz), 158.8 (d, J = 6.7 Hz), 150.4 (t, J = 6.7 Hz), 125.2 (t, J = 27.2 Hz), 114.0 (dd, J = 26.7, 3.7 Hz), 30.6 (t, J = 3.7 Hz). ESI-MS: m/z calcd for C<sub>14</sub>H<sub>9</sub>Br<sub>2</sub>F<sub>4</sub>N<sub>2</sub><sup>+</sup> [M]<sup>+</sup>: 440.9, found: 440.7.

**4-((4,5-Dihydroisoxazol-3-yl)oxy)-N-(4-(((4-((4,5-dihydroisoxazol-3-yl)oxy)but-2-yn-1-yl)dimethyl-1*l*-azaneyl)-methyl)phenyl)diazeyl)benzyl)-N,N-dimethylbut-2-yn-1-aminium Bromide (15a).** 4,4'-Bis(bromomethyl)azobenzene **14a** (100 mg, 0.272 mmol) and 4-((4,5-dihydroisoxazol-3-yl)oxy)-N,N-dimethylbut-2-yn-1-amine **16** were dissolved in 30 mL of ethyl acetate and stirred at 60 °C for 16 h. The precipitate was filtered and washed with cold ethyl acetate to afford the desired product **15a** as a yellow powder (166 mg, 0.227 mmol, 83%). <sup>1</sup>H NMR (400 MHz, DMSO-d<sub>6</sub>): δ (ppm) = 8.03 (d, J = 8.4 Hz, 1H), 7.83 (d, J = 8.4 Hz, 1H), 4.99 (s, 1H), 4.75 (s, 1H), 4.47 (s, 1H), 4.33 (t, J = 9.6 Hz, 1H), 3.13 (s, 3H), 3.05 (t, J = 9.6 Hz, 1H). <sup>13</sup>C NMR (101 MHz, DMSO-d<sub>6</sub>): δ (ppm) = 166.8, 152.8, 134.2, 131.1, 123.0, 86.8, 76.3, 69.6, 64.9, 57.3, 53.3, 49.5, 32.3. ESI-MS: m/z calcd for C<sub>32</sub>H<sub>40</sub>N<sub>6</sub>O<sub>4</sub><sup>2+</sup> [M]<sup>2+</sup>: 286.2, found: 286.1.

**N,N'-((Diazene-1,2-diylbis(3,5-difluoro-4,1-phenylene))bis-(methylene))bis(4-((4,5-dihydroisoxazol-3-yl)oxy)-N,N-dimethylbut-2-yn-1-aminium) Bromide (15b).** 4-((4,5-Dihydroisoxazol-3-yl)oxy)-N,N-dimethylbut-2-yn-1-amine **16** (24.5 mg, 0.134 mmol) in ethyl acetate (40 mL) was slowly added to a stirred solution of 1,2-bis(4-(bromomethyl)-2,6-difluorophenyl)diazene **14b** (118 mg, 0.269 mmol, 2 equiv) in ethyl acetate (10 mL) at 60 °C. The reaction mixture was stirred for 18 h. The reaction mixture was evaporated to dryness and purified by reverse phase column chromatography (acetonitrile/water) yielding the desired product **15b** as a bright orange powder (35 mg, 0.043 mmol, 32%). <sup>1</sup>H NMR (MeOD, 400 MHz): δ (ppm) = 7.55 (dd, J = 60.3, 8.6 Hz, 4H), 5.03 (dd, J = 7.6, 6.1 Hz, 4H), 4.77 (d, J = 38.9 Hz, 4H), 4.51 (s, 2H), 4.44 (s, 2H), 3.29 (d, J = 24.8 Hz, 12H), 3.09 (dt, J = 19.3, 9.7 Hz, 4H). <sup>13</sup>C NMR (MeOD, 400 MHz): δ (ppm) = 176.6, 169.90, 168.9 (d, J = 2.4 Hz), 119.0, 118.4, 89.1, 76.7 (d, J = 7.4 Hz), 71.2, 58.4, 55.4 (d, J = 11.4 Hz), 51.2, 33.7. ESI-MS: m/z calcd for C<sub>32</sub>H<sub>36</sub>F<sub>4</sub>N<sub>6</sub>O<sub>4</sub><sup>2+</sup> [M]<sup>2+</sup>: 322.14, found: 322.25.

**General Procedure for the Synthesis of the Homobivalent Quaternary Iperoxo Dimers 18a–d.** To a solution of 2 equiv of 4-((4,5-dihydroisoxazol-3-yl)oxy)-N,N-dimethylbut-2-yn-1-amine **16** in 10 mL of acetonitrile, 1 equiv of the corresponding bromoalkane 17-C4, 17-C6, 17-C8, and 17-C10 and a catalytic amount of KI/K<sub>2</sub>CO<sub>3</sub> (1:1) were added. The reaction mixture was heated in the microwave (500 W, 70 °C) for 2–3 h. After cooling to room temperature, the surplus of KI/K<sub>2</sub>CO<sub>3</sub> was filtered off and the solvent was evaporated to half of the volume. The solution was kept in the fridge overnight. The precipitate obtained was filtered, washed with Et<sub>2</sub>O, and dried in vacuo.

**N1,N4-Bis(4-((4,5-dihydroisoxazol-3-yl)oxy)but-2-yn-1-yl)-N1,N1,N4,N4-tetramethylbutane-1,4-diaminium Bromide (18a).** Light, yellow solid; yield 69%. <sup>1</sup>H NMR (400 MHz, DMSO-d<sub>6</sub>): δ (ppm) = 2.73–2.77 (m, 4H), 3.03 (t, 4H, J = 9.6 Hz), 3.12 (s, 12H), 3.44–3.48 (m, 4H), 4.33 (t, 4H, J = 9.6 Hz), 4.53 (s, 4H), 4.95 (s, 4H). <sup>13</sup>C NMR (101 MHz, DMSO-d<sub>6</sub>): δ (ppm) = 19.1, 32.2, 49.7, 53.6, 57.2, 62.2, 69.6, 76.0, 86.1, 166.7. ESI-MS: m/z calcd for C<sub>22</sub>H<sub>36</sub>N<sub>4</sub>O<sub>4</sub><sup>2+</sup> [M]<sup>2+</sup>: 210.1, found: 210.1

**N1,N6-Bis(4-((4,5-dihydroisoxazol-3-yl)oxy)but-2-yn-1-yl)-N1,N1,N6,N6-tetramethylhexane-1,6-diaminium Bromide (18b).** Light, yellow solid; yield 49%. <sup>1</sup>H NMR (400 MHz, DMSO-d<sub>6</sub>): δ (ppm) = 1.32–1.37 (m, 4H), 1.69–1.78 (m, 4H), 3.03 (t, 4H, J = 9.6 Hz), 3.11 (s, 12H), 3.36–3.40 (m, 4H), 4.33 (t, 4H, J = 9.6 Hz), 4.50 (s, 4H), 4.94 (s, 4H). <sup>13</sup>C NMR (101 MHz, DMSO-d<sub>6</sub>): δ (ppm) = 21.6, 25.1, 32.2, 49.7, 53.3, 57.1, 62.9, 69.5, 76.1, 85.9, 166.6. ESI-MS: m/z calcd for C<sub>24</sub>H<sub>40</sub>N<sub>4</sub>O<sub>4</sub><sup>2+</sup> [M]<sup>2+</sup>: 224.2, found: 224.1.

**N1,N8-Bis(4-((4,5-dihydroisoxazol-3-yl)oxy)but-2-yn-1-yl)-N1,N1,N8,N8-tetramethyloctane-1,8-diaminium Bromide (18c).** Light, yellow solid; yield 15%. <sup>1</sup>H NMR (400 MHz, DMSO-d<sub>6</sub>): δ (ppm) = 1.29–1.32 (m, 8H), 1.64–1.72 (m, 4H), 3.02 (t, 4H, J = 9.6 Hz), 3.10 (s, 12H), 3.39–3.41 (m, 4H), 4.32 (t, 4H, J = 9.6 Hz), 4.51 (s, 4H), 4.93 (s, 4H). <sup>13</sup>C NMR (101 MHz, DMSO-d<sub>6</sub>): δ (ppm) = 21.7, 25.5, 28.1, 32.2, 49.7, 53.2, 57.2, 63.0, 69.5, 76.1, 85.9, 166.7. ESI-MS: m/z calcd for C<sub>26</sub>H<sub>44</sub>N<sub>4</sub>O<sub>4</sub><sup>2+</sup> [M]<sup>2+</sup>: 238.2, found: 238.1.

**N1,N10-Bis(4-((4,5-dihydroisoxazol-3-yl)oxy)but-2-yn-1-yl)-N1,N1,N10,N10-tetramethyldecane-1,10-diaminium Bromide (18d).** Light, yellow solid; yield 36%. <sup>1</sup>H NMR (400 MHz, DMSO-d<sub>6</sub>): δ (ppm) = 1.30 (s, 12H), 1.62–1.72 (m, 4H), 3.02 (t, 4H, J = 9.2 Hz), 3.09 (s, 12H), 3.36–3.38 (m, 4H), 4.32 (t, 4H, J = 9.2 Hz), 4.51 (s, 4H), 4.93 (s, 4H). <sup>13</sup>C NMR (101 MHz, DMSO-d<sub>6</sub>): δ (ppm) = 21.7, 25.6, 28.3, 28.6, 32.2, 49.7, 53.2, 57.1, 63.0, 69.5, 76.1, 85.8, 166.6. ESI-MS: m/z calcd for C<sub>28</sub>H<sub>48</sub>N<sub>4</sub>O<sub>4</sub><sup>2+</sup> [M]<sup>2+</sup>: 252.2, found: 252.2.

**Photochemical Characterization.** UV–vis spectra and experiments were recorded on a Varian Cary 50 Bio UV/vis spectrophotometer using Hellma (type 100-QS) cuvettes (10 mm light path). Data were plotted using GraphPad Prism 5.0. For irradiation, high-performance light-emitting diodes (LEDs, Mouser Electronics Inc. or Hartenstein) were used as the light source. A concentration of 50 μM was prepared for each compound and measured in its dark-adapted state. Next, the probe was illuminated with LEDs of different wavelengths (254, 365, 380, 400, 430, 500 nm, and white light) while gradually increasing the irradiation time until no change in the spectrum was detectable. Stability measurements were performed irradiating the probe with the light source, which provided the highest

photoconversion to the *cis*-isomer, and kept in dark for at least 120 min. During this time, the absorbance at  $\lambda_{\max}$  was recorded every 5 min. Lastly, the probe was irradiated with the light source, which provided the highest photoconversion to the *trans* isomer. Photostationary distributions were determined by HPLC analysis using a 50  $\mu\text{m}$  probe in physiological buffer. Absorption was measured at the respective isosbestic point wavelengths. Analysis was carried out with GraphPad Prism software (GraphPad Software Inc., San Diego, CA, [www.graphpad.com](http://www.graphpad.com)).

**Pharmacology. Cell Culture.** All experiments were performed with HEK 293T cells stably expressing the novel split-luciferase receptor sensor. Cells were incubated at 37 °C with 5% CO<sub>2</sub> and cultivated in DMEM with 4500 mg/L glucose, 10% (v/v) fetal calf serum, 100  $\mu\text{g}/\text{mL}$  penicillin, 100  $\mu\text{g}/\text{mL}$  streptomycin sulfate, 2 mM L-glutamine, and 600  $\mu\text{g}/\text{mL}$  G-418. Every 2–3 days the cell lines were routinely passaged.

**Split-Luciferase Complementation Assay.** The assay was performed as described previously,<sup>24</sup> except for the following modifications: a Berthold Mithras LB 940 plate reader was used to quantify the luminescence emitted by the cells, using white, flatbottomed nunc f96 microwell polystyrene plates.

**Molecular Modeling.** In brief, all receptor–ligand docking experiments reported in this study were carried out with CCDs software GOLD version 5.1.30 The active M1 receptor homology model used as protein was previously reported.<sup>27</sup> All residues of the extracellular domains and the receptor core region were defined as a potential binding pocket. Default settings were chosen for receptor–ligand docking, and GoldScore was used as the primary scoring function. All obtained docking poses and receptor–ligand interactions were analyzed with LigandScout 4.2 using 3D-pharmacophores.<sup>31</sup>

**Binding Experiments.** [<sup>3</sup>H]Quinuclidinyl benzilate ([<sup>3</sup>H]QNB), ethanol solution, was purchased from Amersham Biosciences (catalog number TRK 604, 42 Ci/mmol, 1 mCi/mL). The experiments were carried out in 10 mM Tris–HCl buffer, pH 7.0, containing 6 mM MgCl<sub>2</sub>. Rat brain cortices were used as a source of muscarinic receptors in the assay. After cleaning the meninges with buffer-soaked filter paper, cortices were dissected, and white matter was carefully trimmed off. This tissue was homogenized in 40 mL of buffer using a Potter homogenizer with a motor-driven Teflon pestle. The homogenate was centrifuged for 30 min at 50 000g, and the resulting pellet was homogenized and centrifuged again. After protein determination by the Bradford assay, the final pellet was resuspended at 1 mg of protein/mL, transferred to 1.5 mL microcentrifuge tubes, and centrifuged once more. After discarding the supernatant, membrane pellets were kept at –80 °C until use.<sup>23</sup> The general procedure consists of the incubation of 20  $\mu\text{g}$  of membrane protein with 200 pM [<sup>3</sup>H]QNB (200 pM), in a total volume of 2 mL and in the presence of varying concentrations of competing compounds. An excess (2  $\mu\text{M}$ ) of the unlabeled muscarinic antagonist atropine was used to define nonspecific binding. After 45 min at 25 °C to reach equilibrium, the reaction mixtures were quickly filtered through glass fiber disks using a semiautomated Brandel harvester allowing the simultaneous filtration of 24 samples.<sup>21</sup> Filters were washed twice with 4 mL of ice-cold Tris–HCl buffer (10 mM, pH 7.0) and counted for radioactivity. The final results were reported as % binding of [<sup>3</sup>H]QNB in each

condition. This analysis was carried out with GraphPad Prism software (GraphPad Software Inc., San Diego, CA, [www.graphpad.com](http://www.graphpad.com)).

**ASSOCIATED CONTENT. Supporting Information.** The Supporting Information is available free of charge on the ACS Publications website at DOI: 10.1021/acs.jmedchem.8b01822. UV-vis spectra, NMR data, HPLC traces, molecular modeling, binding experiments, Molecular formula strings.

**Accession Codes.** PDB code for the crystal structure of the human M2 receptor in complex with agonist iperovo is 4MQS. This crystal structure was used for the generation of the homology model for computational studies of the human M1 receptor in complex with compounds **9a**, **9b**, **15a**, **15b**, and **18a-d**.

**AUTHOR INFORMATION.** Corresponding Author \*E-mail: [michael.decker@uni-wuerzburg.de](mailto:michael.decker@uni-wuerzburg.de).

**Notes.** The authors declare no competing financial interest.

**ACKNOWLEDGMENTS.** L.A. and T.L. were supported by the International Doctoral Program “Receptor Dynamics: Emerging Paradigms for Novel Drugs” funded within the framework of the Elite Network of Bavaria (ENB). We kindly thank Prof. Klaus Mohr from the Institute of Pharmacy and Toxicology at Bonn University for fruitful discussions.

## REFERENCES

(1) (a) Lerch, M. M.; Hansen, M. J.; van Dam, G. M.; Szymanski, W.; Feringa, B. L. Emerging Targets in Photopharmacology. *Angew. Chem., Int. Ed.* 2016, 55, 10978–10999. (b) Velema, W. A.; Szymanski, W.; Feringa, B. L. Photopharmacology: Beyond Proof of Principle. *J. Am. Chem. Soc.* 2014, 136, 2178–2191. (c) Hüll, K.; Morstein, J.; Trauner, D. In Vivo Photopharmacology. *Chem. Rev.* 2018, 118, 10710–10747. (d) Broichhagen, J.; Frank, J. A.; Trauner, D. A Roadmap to Success in Photopharmacology. *Acc. Chem. Res.* 2015, 48, 1947–1960.

(2) (a) Pittolo, S.; Gómez-Santacana, X.; Eckelt, K.; Rovira, X.; Dalton, J.; Goudet, C.; Pin, J.-P.; Llobet, A.; Giraldo, J.; Llebaria, A.; Gorostiza, P. An Allosteric Modulator to Control Endogenous G protein-coupled Receptors with Light. *Nat. Chem. Biol.* 2014, 10, 813–815. (b) Schönberger, M.; Trauner, D. A Photochromic Agonist for  $\mu$ -Opioid Receptors. *Angew. Chem., Int. Ed.* 2014, 53, 3264–3267. (c) Agnetta, L.; Kauk, M.; Canizal, M. C. A.; Messerer, R.; Holzgrabe, U.; Hoffmann, C.; Decker, M. A Photoswitchable Dualsteric Ligand Controlling Receptor Efficacy. *Angew. Chem., Int. Ed.* 2017, 56, 7282–7287. (d) Bahamonde, M. I.; Taura, J.; Paoletta, S.; Gakh, A. A.; Chakraborty, S.; Hernando, J.; Fernández-Dueñas, V.; Jacobson, K. A.; Gorostiza, P.; Ciruela, F. Photomodulation of G Protein-Coupled Adenosine Receptors by a Novel Light-Switchable Ligand. *Bioconjugate Chem.* 2014, 25, 1847–1854. (e) Broichhagen, J.; Johnston, N. R.; von Ohlen, Y.; Meyer-Berg, H.; Jones, B. J.; Bloom, S. R.; Rutter, G. A.; Trauner, D.; Hodson, D. J. Allosteric Optical Control of a Class B G-Protein-Coupled Receptor. *Angew. Chem., Int. Ed.* 2016, 55, 5865–5868. (f) Hauwert, N. J.; Mocking, T. A. M.; Da Costa Pereira, D.; Kooistra, A. J.; Wijnen, L. M.; Vreeker, G. C. M.; Verweij, E. W. E.; De Boer, A. H.; Smit, M. J.; De Graaf, C.; Vischer, H. F.; de Esch, I. J. P.; Wijtmans, M.; Leurs, R. Synthesis and Characterization of a Bidirectional Photoswitchable Antagonist Toolbox for Real-Time GPCR Photopharmacology. *J. Am. Chem. Soc.* 2018, 140, 4232–4243. (g) Westphal, M. V.; Schafroth, M. A.; Sarott, R. C.; Imhof, M. A.; Bold, C. P.; Leippe, P.; Dhopeswarkar, A.; Grandner, J. M.; Katritch, V.; Mackie, K.; Trauner, D.; Carreira, E. M.; Frank, J. A. Synthesis of Photoswitchable  $\Delta^9$ -Tetrahydrocannabinol Derivatives Enables

- Optical Control of Cannabinoid Receptor 1 Signaling. *J. Am. Chem. Soc.* 2017, 139, 18206–18212. **(h)** Dolles, D.; Strasser, A.; Wittmann, H.-J.; Marinelli, O.; Nabissi, M.; Pertwee, R. G.; Decker, M. The First Photochromic Affinity Switch for the Human Cannabinoid Receptor 2. *Adv. Ther.* 2018, 1, No. 1700032.
- (3)** Lohse, M. J.; Hofmann, K. P. Spatial and Temporal Aspects of Signaling by G-Protein-Coupled Receptors. *Mol. Pharmacol.* 2015, 88, 572–578.
- (4)** Burger, W. A. C.; Sexton, P. M.; Christopoulos, A.; Thal, D. M. Toward an Understanding of the Structural Basis of Allostery in Muscarinic Acetylcholine Receptors. *J. Gen. Physiol.* 2018, 150, 1360–1372.
- (5)** **(a)** Kruse, A. C.; Kobilka, B. K.; Gautam, D.; Sexton, P. M.; Christopoulos, A.; Wess, J. Muscarinic Acetylcholine Receptors: Novel Opportunities for Drug Development. *Nat. Rev. Drug Discovery* 2014, 13, 549–560. **(b)** Svoboda, J.; Popelikova, A.; Stuchlik, A. Drugs Interfering with Muscarinic Acetylcholine Receptors and Their Effects on Place Navigation. *Front. Psychiatry* 2017, 8, No. 215. **(c)** van Koppen, C. J.; Kaiser, B. Regulation of Muscarinic Acetylcholine Receptor Signaling. *Pharmacol. Ther.* 2003, 98, 197–220. **(d)** Eglén, R. M. Muscarinic Receptor Subtypes in Neuronal and Non-neuronal Cholinergic Function. *Auton. Autacoid Pharmacol.* 2006, 26, 219–233.
- (6)** Wess, J.; Eglén, R. M.; Gautam, D. Muscarinic Acetylcholine Receptors: Mutant Mice Provide New Insights for Drug Development. *Nat. Rev. Drug Discovery* 2007, 6, 721–733.
- (7)** Caulfield, M. P. Muscarinic Receptors Characterization, Coupling and Function. *Pharmacol. Ther.* 1993, 58, 319–379.
- (8)** **(a)** Antony, J.; Kellershohn, K.; Mohr-Andrä, M.; Kebig, A.; Prilla, S.; Muth, M.; Heller, E.; Disingrini, T.; Dallanoce, C.; Bertoni, S.; Schrobang, J.; Tränkle, C.; Kostenis, E.; Christopoulos, A.; Hölting, H. D.; Barocelli, E.; De Amici, M.; Holzgrabe, U.; Mohr, K. Dualsteric GPCR Targeting: A Novel Route to Binding and Signaling Pathway Selectivity. *FASEB J.* 2009, 23, 442–450. **(b)** Disingrini, T.; Muth, M.; Dallanoce, C.; Barocelli, E.; Bertoni, S.; Kellershohn, K.; Mohr, K.; De Amici, M.; Holzgrabe, U. Design, Synthesis, and Action of Oxotremorine-Related Hybrid-Type Allosteric Modulators of Muscarinic Acetylcholine Receptors. *J. Med. Chem.* 2006, 49, 366–372.
- (9)** **(a)** Beharry, A. A.; Sadovski, O.; Woolley, G. A. Azobenzene Photoswitching without Ultraviolet Light. *J. Am. Chem. Soc.* 2011, 133, 19684–19687. **(b)** Samanta, S.; Beharry, A. A.; Sadovski, O.; McCormick, T. M.; Babalhavaeji, A.; Tropepe, V.; Woolley, G. A. Photoswitching Azo Compounds In Vivo with Red Light. *J. Am. Chem. Soc.* 2013, 135, 9777–9784.
- (10)** **(a)** Bléger, D.; Hecht, S. Visible-Light-Activated Molecular Switches. *Angew. Chem., Int. Ed.* 2015, 54, 11338–11349. **(b)** Bléger, D.; Schwarz, J.; Brouwer, A. M.; Hecht, S. o-Fluoroazobenzenes as Readily Synthesized Photoswitches Offering Nearly Quantitative Two-Way Isomerization with Visible Light. *J. Am. Chem. Soc.* 2012, 134, 20597–20600.
- (11)** Dong, M.; Babalhavaeji, A.; Samanta, S.; Beharry, A. A.; Woolley, G. A. Red-Shifting Azobenzene Photoswitches for in Vivo Use. *Acc. Chem. Res.* 2015, 48, 2662–2670.
- (12)** **(a)** Rullo, A.; Reiner, A.; Reiter, A.; Trauner, D.; Isacoff, E. Y.; Woolley, G. A. Long Wavelength Optical Control of Glutamate Receptor Ion Channels Using a Tetra-ortho-substituted Azobenzene Derivative. *Chem. Commun.* 2014, 50, 14613–14615. **(b)** Wegener, M.; Hansen, M. J.; Driessen, A. J. M.; Szymanski, W.; Feringa, B. L. Photocontrol of Antibacterial Activity: Shifting from UV to Red Light Activation. *J. Am. Chem. Soc.* 2017, 139, 17979–17986. **(c)** Konrad, D. B.; Frank, J. A.; Trauner, D. Synthesis of Redshifted Azobenzene Photoswitches by Late-Stage Functionalization. *Chem. – Eur. J.* 2016, 22, 4364–4368.

- (13) Shonberg, J.; Scammells, P. J.; Capuano, B. Design Strategies for Bivalent Ligands Targeting GPCRs. *ChemMedChem* 2011, 6, 963–974.
- (14) (a) Mohr, K.; Schmitz, J.; Schrage, R.; Tränkle, C.; Holzgrabe, U. Molecular Alliance-From Orthosteric and Allosteric Ligands to Dualsteric/Bitopic Agonists at G Protein Coupled Receptors. *Angew. Chem., Int. Ed.* 2013, 52, 508–516. (b) Halazy, S. G Protein-coupled Receptors Bivalent Ligands and Drug Design. *Expert Opin. Ther. Pat.* 1999, 9, 431–446.
- (15) Nimczick, M.; Pemp, D.; Darras, F. H.; Chen, X.; Heilmann, J.; Decker, M. Synthesis and Biological Evaluation of Bivalent Cannabinoid Receptor Ligands Based on hCB(2)R Selective Benzimidazoles Reveal Unexpected Intrinsic Properties. *Bioorg. Med. Chem.* 2014, 22, 3938–3946.
- (16) Decker, M.; Si, Y. G.; Knapp, B. I.; Bidlack, J. M.; Neumeyer, J. L. Synthesis and Opioid receptor Binding Affinities of 2-substituted and 3-Aminomorphinans: Ligands for Mu, Kappa, and Delta Opioid Receptors. *J. Med. Chem.* 2010, 53, 402–418.
- (17) Kühhorn, J.; Hübner, H.; Gmeiner, P. Bivalent Dopamine D2 Receptor Ligands: Synthesis and Binding Properties. *J. Med. Chem.* 2011, 54, 4896–4903.
- (18) (a) Piergentili, A.; Quaglia, W.; Tayebati, S. K.; Paparelli, F.; Malmusi, L.; Brasili, L. Synthesis and Muscarinic Receptors affinity of a Series of Antagonist Bivalent Ligands. *Farmaco* 1994, 49, 83–87. (b) Messer, W. S., Jr. Bivalent Ligands for G Protein-Coupled Receptors. *Curr. Pharm. Des.* 2004, 10, 2015–2020.
- (19) Kloeckner, J.; Schmitz, J.; Holzgrabe, U. Convergent, Short Synthesis of the Muscarinic Superagonist Iperoxo. *Tetrahedron Lett.* 2010, 51, 3470–3472.
- (20) Knie, C.; Utecht, M.; Zhao, F.; Kulla, H.; Kovalenko, S.; Brouwer, A. M.; Saalfrank, P.; Hecht, S.; Bléger, D. Ortho- Fluoroazobenzenes: Visible Light Switches with Very Long-Lived Z Isomers. *Chem. – Eur. J.* 2014, 20, 16492–16501.
- (21) Claro, E. Analyzing Ligand Depletion in a Saturation Equilibrium Binding Experiment. *Biochem. Mol. Biol. Educ.* 2006, 34, 428–431. (22) (a) Yamamura, H. I.; Snyder, S. H. Muscarinic Cholinergic Binding in Rat Brain. *Proc. Natl. Acad. Sci. U.S.A.* 1974, 71, 1725– 1729. (b) Yamamura, H. I.; Kuhar, M. J.; Snyder, S. H. In Vivo Identification of Muscarinic Cholinergic Receptor Binding in Rat brain. *Brain Res.* 1974, 80, 170–176.
- (23) Sallés, J.; Wallace, M. A.; Fain, J. N. Differential Effects of Alkylating Agents on the Multiple Muscarinic Receptor Subtypes Linked to Activation of Phospholipase C by Carbachol in Rat Brain Cortical Membranes. *J. Pharmacol. Exp. Ther.* 1993, 264, 521–529.
- (24) Littmann, T.; Ozawa, T.; Hoffmann, C.; Buschauer, A.; Bernhardt, G. A Split Luciferase-based Probe for Quantitative Proximal Determination of Gαq Signalling in Live Cells. *Sci. Rep.* 2018, 8, No. 17179.
- (25) Hattori, M.; Ozawa, T. Split Luciferase Complementation for Analysis of Intracellular Signaling. *Anal. Sci.* 2014, 30, 539–544.
- (26) Chen, X.; Klöckner, J.; Holze, J.; Zimmermann, C.; Seemann, W. K.; Schrage, R.; Bock, A.; Mohr, K.; Tränkle, C.; Holzgrabe, U.; Decker, M. Rational Design of Partial Agonists for the Muscarinic M1 Acetylcholine Receptor. *J. Med. Chem.* 2015, 58, 560–576.
- (27) Bermudez, M.; Rakers, C.; Wolber, G. Structural Characteristics of the Allosteric Binding Site Represent a Key to Subtype Selective Modulators of Muscarinic Acetylcholine Receptors. *Mol. Inf.* 2015, 34, 526–530.

- (28) (a) Bock, A.; Bermudez, M.; Krebs, F.; Matera, C.; Chirinda, B.; Sydow, D.; Dallanoce, C.; Holzgrabe, U.; De Amici, M.; Lohse, M. J.; Wolber, G.; Mohr, K. Ligand Binding Ensembles Determine Graded Agonist Efficacies at a G Protein-coupled Receptor. *J. Biol. Chem.* 2016, 291, 16375–16389. (b) Bermudez, M.; Bock, A.; Krebs, F.; Holzgrabe, U.; Mohr, K.; Lohse, M. J.; Wolber, G. Ligand-Specific Restriction of Extracellular Conformational Dynamics Constrains Signaling of the M2 Muscarinic Receptor. *ACS Chem. Biol.* 2017, 12, 1743–1748.
- (29) Dror, R. O.; Green, H. F.; Valant, C.; Borhani, D. W.; Valcourt, J. R.; Pan, A. C.; Arlow, D. H.; Canals, M.; Lane, J. R.; Rahmani, R.; Baell, J. B.; Sexton, P. M.; Christopoulos, A.; Shaw, D. E. Structural Basis for Modulation of a G-Protein-coupled Receptor by Allosteric Drugs. *Nature* 2013, 503, 295–299.
- (30) Jones, G.; Willett, P.; Glen, R. C.; Leach, A. R.; Taylor, R. Development and Validation of a Genetic Algorithm for Flexible Docking. *J. Mol. Biol.* 1997, 267, 727–748.
- (31) Wolber, G.; Seidel, T.; Bendix, F.; Langer, T. Molecule pharmacophore Superpositioning and Pattern Matching in Computational Drug Design. *Drug Discov. Today* 2008, 13, 23–29.

## Supporting Information

### Fluorination of Photoswitchable Muscarinic Agonists Tunes Receptor Pharmacology and Photochromic Properties

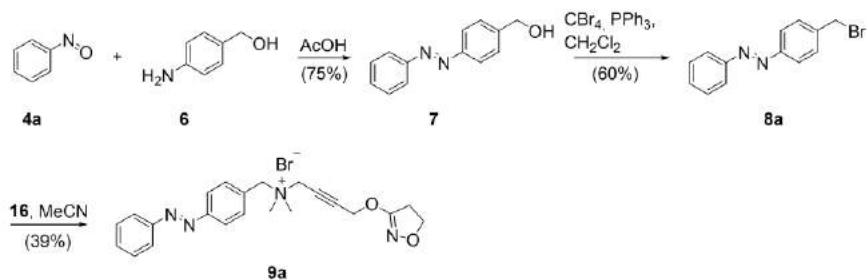
Luca Agnetta, Marcel Bermudez, Fabio Riefolo, Carlo Matera, Enrique Claro, Regina Messerer, Timo Littmann, Gerhard Wolber, Ulrike Holzgrabe, Michael Decker

#### Table of content

1. Syntheses
2. Photochemical characterization

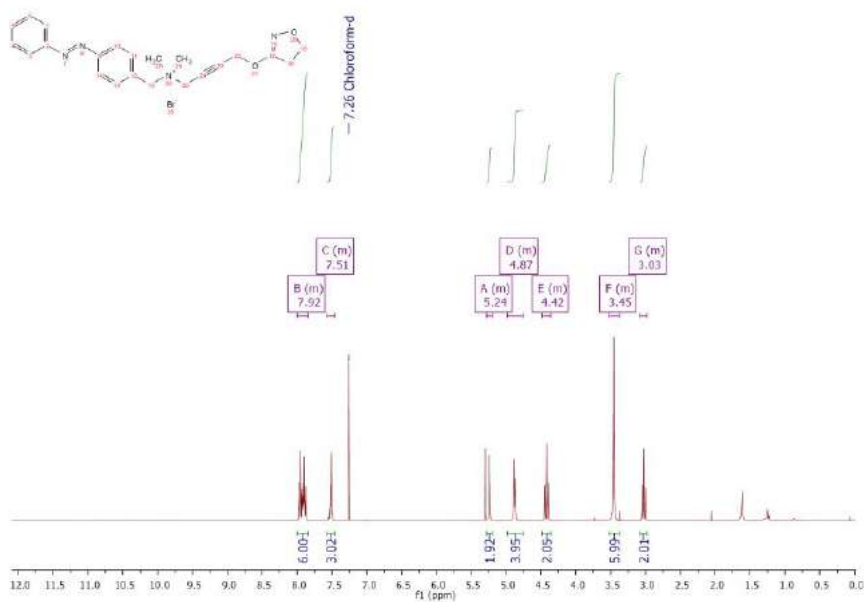
## 1. Syntheses

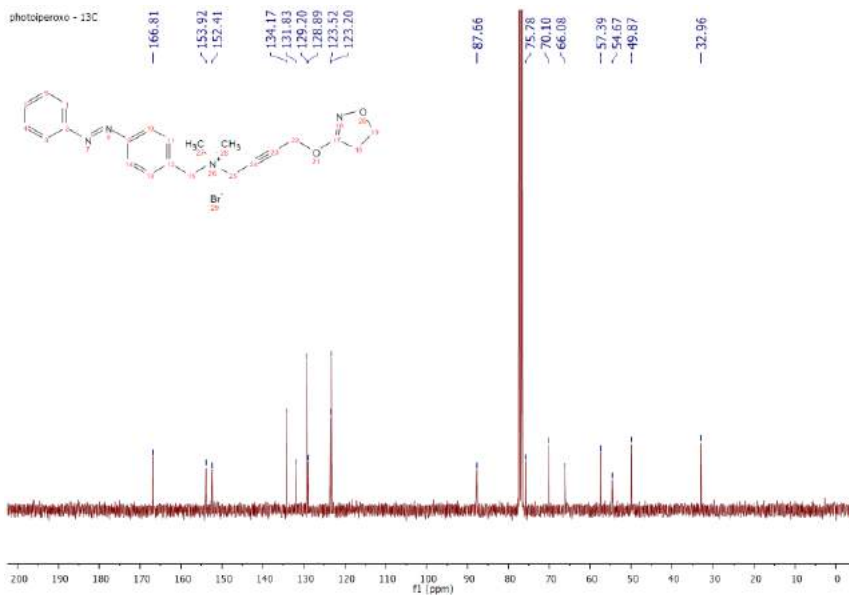
### 1.1 Photoiperoxo (PI, 9b)



Suppl. Scheme 1. Three-step synthesis of photoiperoxo 9a.

#### 1.1.1 <sup>1</sup>H-NMR and <sup>13</sup>C-NMR spectra of photoiperoxo (PI, 9b)

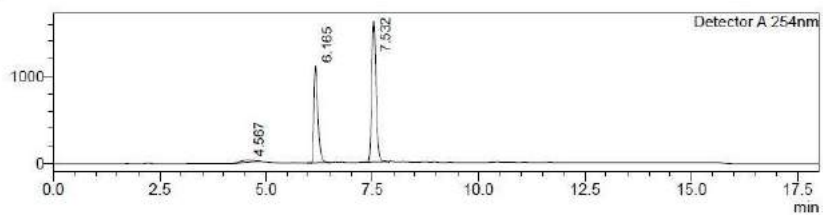




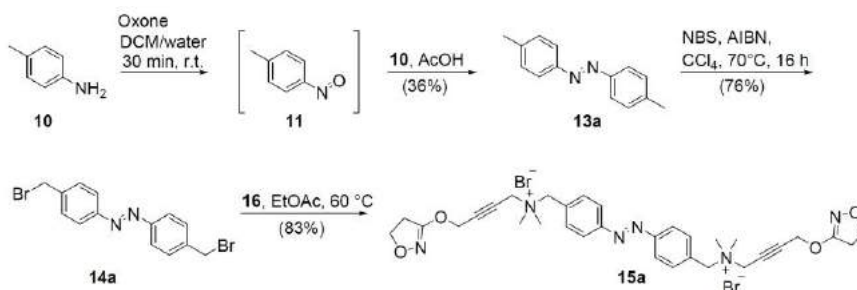
### 1.1.2 HPLC analysis of photoiperoxo (PI, 9b)

<Chromatogram>

mV

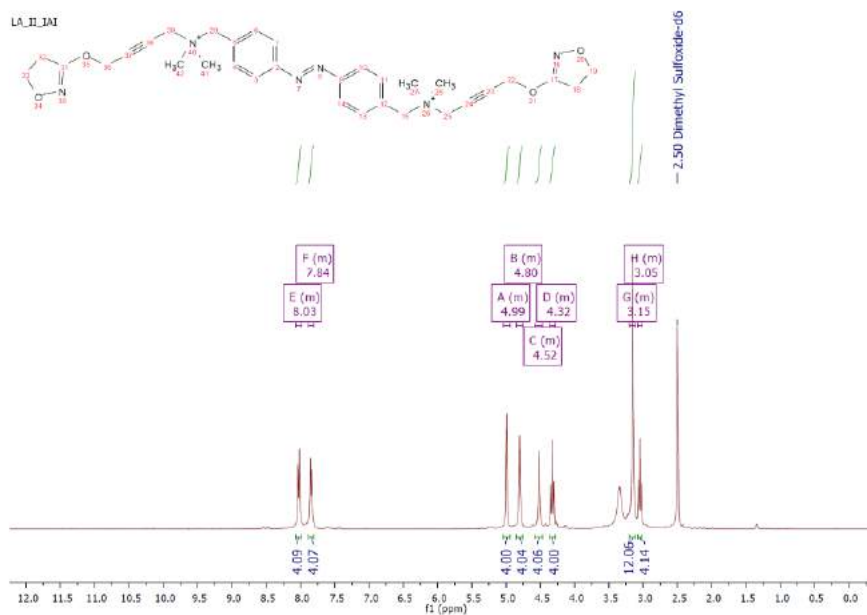


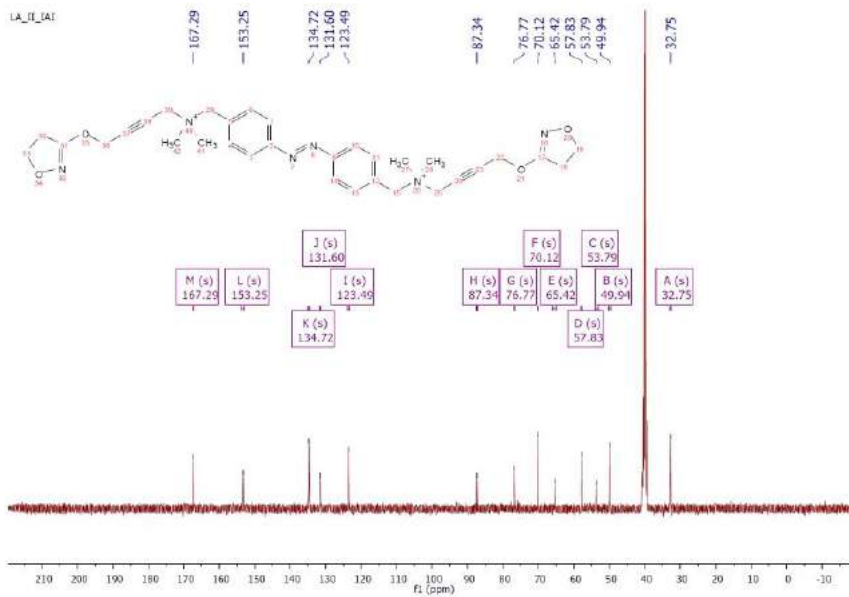
## 1.2 Iper-Azo-Iper (IAI, 15a)



Suppl. Scheme 2. Synthesis of Iper-azo-Iper 15a.

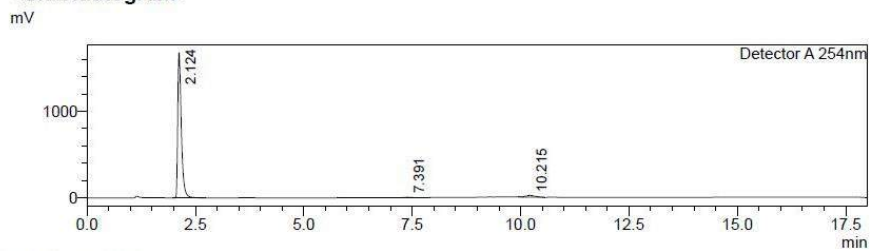
### 1.2.1 <sup>1</sup>H-NMR and <sup>13</sup>C-NMR spectra of iper-azo-iper (IAI, 15a)





### 1.2.2 HPLC analysis of iper-azo-iper (IAI, 15a)

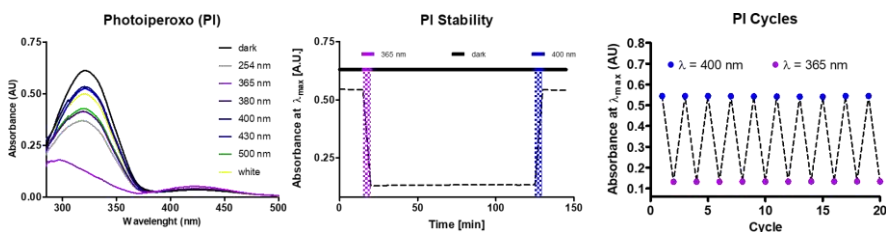
<Chromatogram>



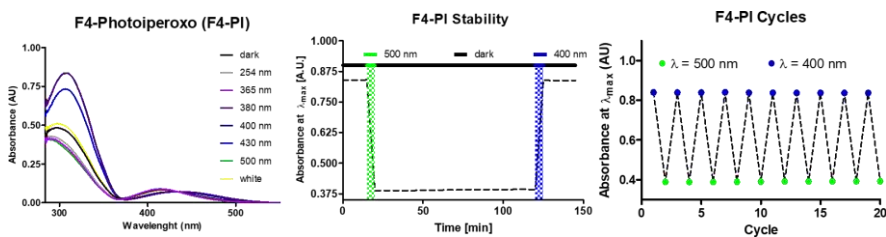
## 2. Photochemical characterization

### 2.1. UV-Vis spectra, stability measurements, multiple switching cycles

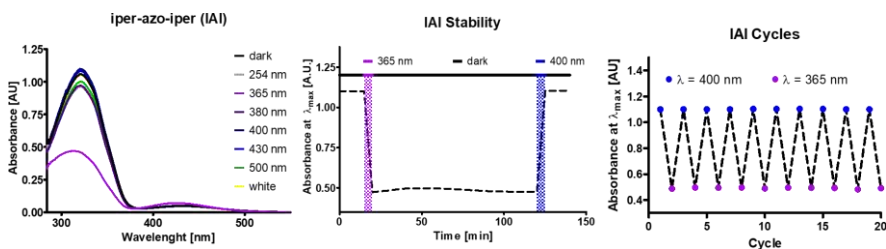
#### 2.1.1 Photoiperoxo (PI, 9a)



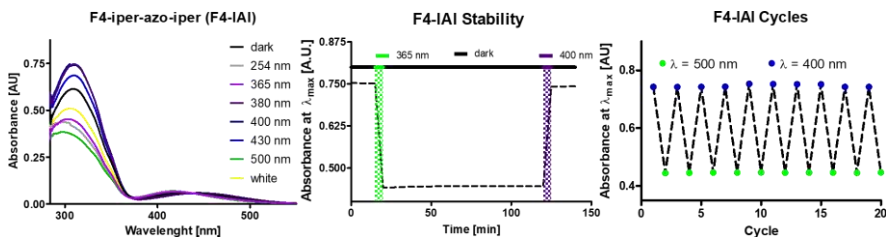
#### 2.1.2 F4-photoiperoxo (F4-PI, 9b)



#### 2.1.3 Iper-azo-iper (IAI, 15a)



#### 2.1.4 F4-iper-azo-iper (F4-IAI, 15b)



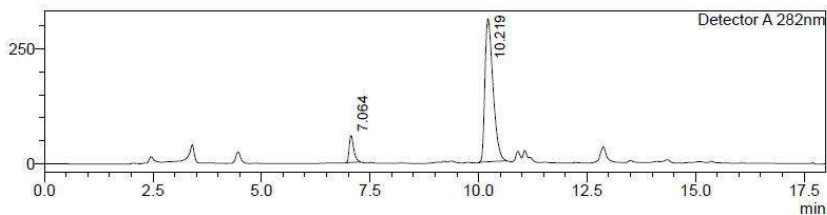
## 2.2 Photostationary states (PSS)

### 2.2.1 Photoiperoxo (PI, 9a)

#### 2.2.1.1 PSS *trans*

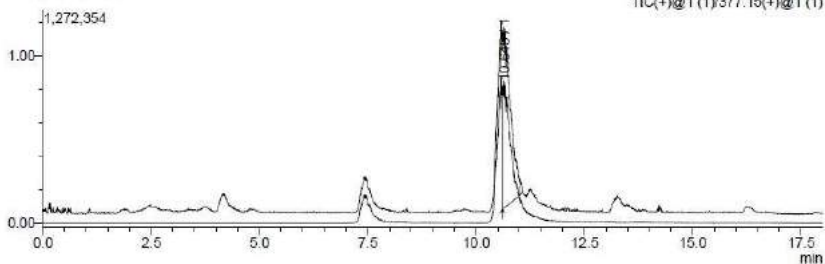
<Chromatogram>

mV



Peak#	Ret. Time	Area	Height	Area%
1	7.064	421894	58784	9.493
2	10.219	4022390	311159	90.507
Total		4444285	369942	100.000

Segment#1 (x1,000,000)

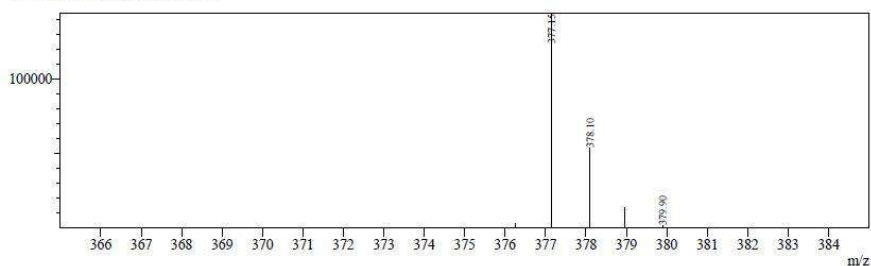


Line#: 1 R.Time: 10.646(Scan#: 7098)

MassPeaks: 5

Spectrum Mode: Averaged 10.644-10.647(7097-7099) Base Peak: 377.15(143946)

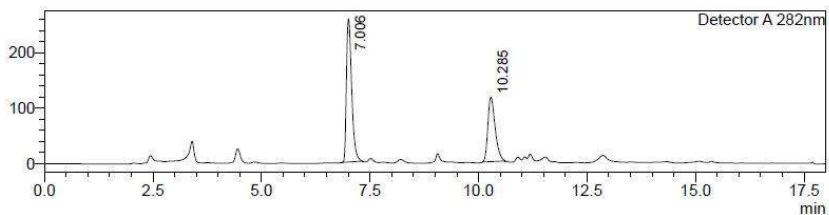
BG Mode: Calc Segment 1 - Event 1



### 2.2.1.2 PSS *cis*

<Chromatogram>

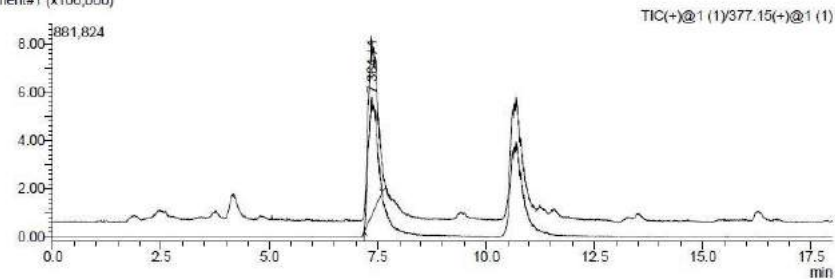
mV



Detector A 282nm

Peak#	Ret. Time	Area	Height	Area%
1	7.006	2160372	257748	61.484
2	10.285	1353319	115789	38.516
Total		3513691	373537	100.000

Segment#1 (x100,000)

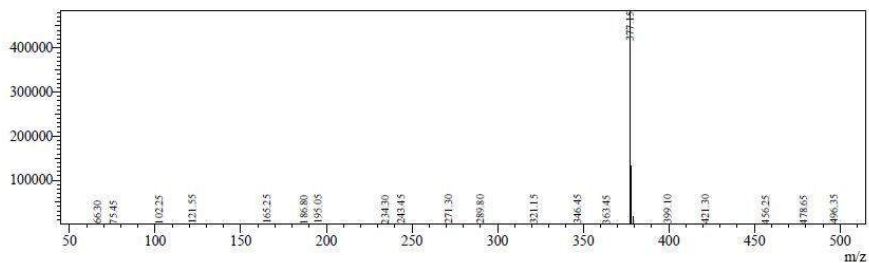


Line# 1 R. Time: 7.364 (Scan#: 4910)

Mass Peaks: 206

Spectrum Mode: Averaged 7.362-7.365(4909-4911) Base Peak: 377.15(484099)

EG Mode Calc Segment 1 - Event 1

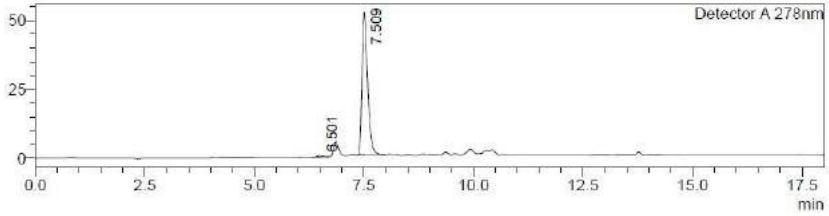


## 2.2.2 Iper-azo-iper (IAI, 15a)

### 2.2.2.1 PSS *trans*

<Chromatogram>

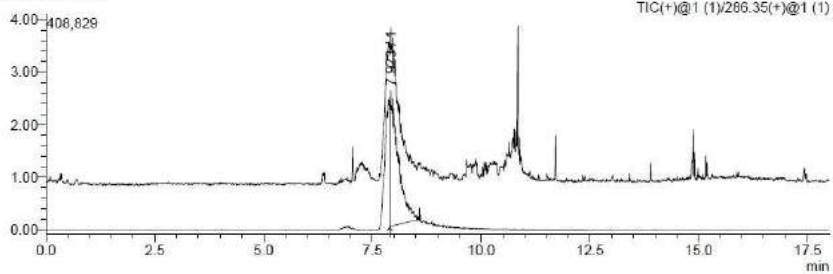
mV



Detector A 278nm

Peak#	Ret. Time	Area	Height	Area%
1	6.501	4524	427	0.969
2	7.509	462176	51581	99.031
Total		466700	52008	100.000

Segment#1 (x100,000)

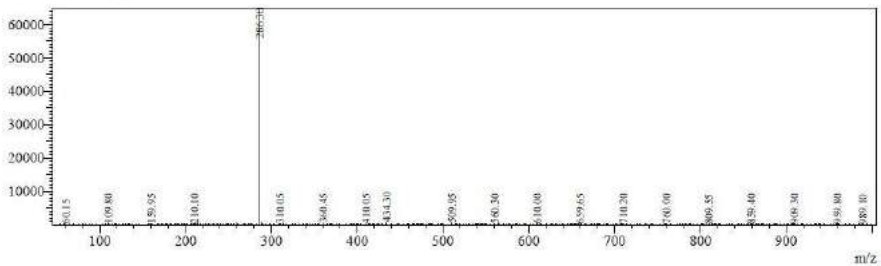


Line#:1 R.Time:7.923(Scan#:2378)

MassPeaks:553

Spectrum Mode:Averaged 7.920-7.927(2377-2379) Base Peak:266.30(64991)

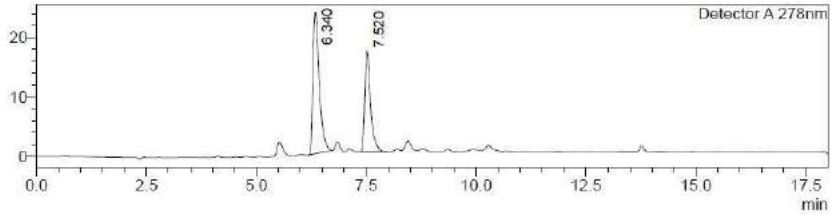
BG-Mode:Calc Segment 1 - Event 1



### 2.2.2.2 PSS cis

<Chromatogram>

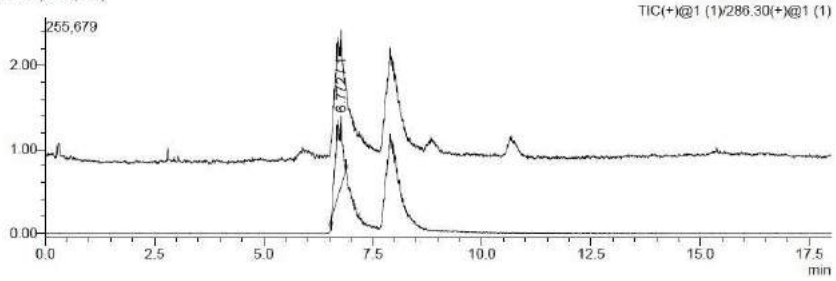
mV



Detector A 278nm

Peak#	Ret. Time	Area	Height	Area%
1	6.340	236211	23707	60.426
2	7.520	154697	16863	39.574
Total		390908	40570	100.000

Segment#1 (x100,000)

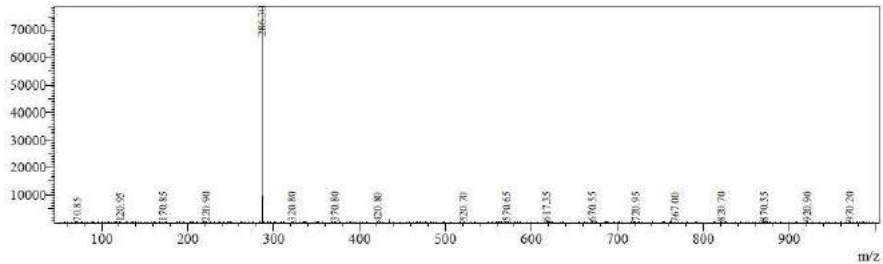


Line#:1 R.Time:6.773(Scan#:2033)

MassPeaks:487

Spectrum Mode: Averaged 6.770-6.777(2032-2034) Base Peak:286.30(78792)

BG-Mode:Calc Segment 1 - Event 1



## General Discussion

### Chapter II

In this first work, we demonstrated the potential of the photopharmacological strategy to modulate the activity of muscarinic receptors with light.

We designed, synthesized and pharmacologically characterized light-sensitive monovalent (PI and F4-PI) and bivalent (IAI and F4-IAI) derivatives of iperoxo, which is a potent agonist of mAChRs. Among other possibilities, we chose azobenzenes as molecular switches because these scaffolds display many favorable properties, such as design flexibility, large changes in geometry upon isomerization, high and efficient photoisomerization, chemical stability, and a proven safety profile in humans. In particular, we coupled the quaternary ammonium nitrogen of iperoxo with unsubstituted and tetra-ortho-fluorinated azobenzenes.

The first important information we obtained from our studies was that the extension of the relatively small chemical structure of iperoxo with bulky moieties, such as azobenzenes, does not compromise the agonist activity. This result could not be taken for granted and is of fundamental importance to develop light-sensitive ligands of muscarinic receptors.

Other conclusions that can be drawn from our *in vitro* studies concern the behavior of the new compounds as M1 agonists. Only the monovalent derivative PI showed significantly lower efficacy and potency compared to iperoxo, whereas all the other ligands maintained a pharmacological behavior comparable to the parent drug. In particular, the bivalent and fluorinated compound F4-IAI has a dose-response curve that is almost identical to iperoxo.

After evaluating the pharmacological properties, we focused on the photoswitchable activity of our light-sensitive agonists. Our work suggests that ligands with bivalent nature have come up with more promising

agonist properties for mAChRs than their corresponding monovalent derivatives. IAI and F4-IAI displayed higher binding affinity, higher potency, and better photoswitchable performances than PI and F4-PI. In fact, the split-luciferase complementation assays detected a potency shift between *trans* and *cis* configurations for the two bivalent agonists, with the *trans*-enriched form being more potent than the *cis* in both cases. These significant shifts strongly suggest the possibility of photocontrolling the activity of muscarinic receptors reversibly and in real-time in animal models.

In order to account for these results and to rationally improve the photopharmacological activity of the ligands, we simulated their binding modality into the active M1 receptor model with computational studies. The superior photoswitchable activity of bivalent iperoxo derivatives seems to be caused by additional interactions at the muscarinic allosteric site that monovalent ligands are not in a position to do because of the reduced size of their chemical structure. Thus, the next design of iperoxo derivatives should include the improvement of allosteric contacts as it might optimize their light-dependent activity on muscarinic receptors.

## CHAPTER III

### Novel Photoswitchable Muscarinic Agonists Obtained by Molecular Hybridization of Orthosteric and Allosteric Ligands



## General Introduction

### Chapter III

The primary aim of this work is to develop new synthetic tools to control endogenous muscarinic receptors with light that display improved performance. We studied different strategies to develop new agonists, such as the full involvement of the muscarinic allosteric site into the drug design. This approach was expected to improve light-dependent behavior of iperoxo derivatives, as suggested by our previous work.

Molecular hybridization is an emerging concept to discover novel biological agents, based on combining the pharmacophores of different bioactive molecules in a single chemical structure. The new hybrid compound can show a "hybrid" pharmacological profile, which can result in an enhanced affinity, efficacy, selectivity or safety than the parent drugs (Claudio Viegas-Junior et al., 2007; Decker, 2017; Matera et al., 2019; Mohr et al., 2010). This design emerged as a promising option to develop new muscarinic ligands with potential clinical applications. The conventional hybrid agents designed for mAChRs merge in the same molecular skeleton the fundamental elements of both a potent orthosteric agonist and a subtype-selective allosteric ligand (De Amici et al., 2010; Antony et al., 2009). Such hybrids are named "dualsteric" (or "bitopic") because they interact with both the allosteric and orthosteric sites of the same receptor (Antony et al., 2009). The presence of an allosteric portion into the chemical structure of orthosteric agonists confers distinctive features to the resulting hybrids, such as a certain subtype selectivity. Moreover, some of them showed functional selectivity and/or enhanced tolerability for *in vivo* applications compared to the agonists alone (Bock et al., 2012, 2016; Cristofaro et al., 2018; De Min et al., 2017).

Among the five subtypes, the M2 receptor is recognized as a fundamental prototype for the study of GPCR allosterism, and the allosteric agents W84 and Naphmethonium have been extensively combined with iperoxo to

develop various M2 dualsteric agonists (Matera et al., 2014; Messerer et al., 2017). In this work, we focused on the best-performing hybrid compounds of these series, Phthalimide-8-Iperoxo (P-8-Iper) and Naphthalimide-8-Iperoxo (N-8-Iper), and developed the corresponding non-canonical azologized derivatives. Their octane chains that separate the ortho/allosteric moieties were replaced with unsubstituted azobenzenes. The syntheses and the photochemical characterizations of the obtained novel compounds, named Phthalimide-Azobenzene-Iperoxo (PAI) and Naphthalimide-Azobenzene-Iperoxo (NAI), were performed. In our hands, PAI was the only one that photoswitched reversibly, and we moved on to study its pharmacological properties.

PAI activity was studied with real-time calcium imaging assays. We overexpressed human M2 receptors in cultured cells and quantified receptor activation by measuring cytosolic calcium oscillations in response to the application of our compound and illumination. Once we demonstrated that PAI can effectively photocontrol M2 activation *in vitro*, we developed different assays to test its potential applications in research and future clinical therapies.

M2 receptors are highly expressed in the heart and their activation can decrease the heart rate. Such activity makes them a potential pharmacological target to modulate cardiac function (Brodde et al., 2001; Dhein et al., 2001). The spatio-temporal and reversible photoregulation technique is of fundamental interest in the cardiovascular field, in particular for arrhythmia diseases, where the classical therapies like the electrical stimulation of cardiac muscles display several limitations (Bingen et al., 2014; Boyle et al., 2015; Bruegmann et al., 2016; Pianca et al., 2017; Yu et al., 2017).

Thus, we first applied PAI to control cardiac function with light in two wildtype animal models.

*This project was carried out at IBEC with several collaborations. I personally performed the design, chemical synthesis, and photochemical characterizations of all the compounds shown in this work. I contributed to the development of the experimental set-up to pharmacologically*

*characterize the compounds and in the performance of all the in vitro and in vivo experiments that are described in this work. I gave central contributions to the final paper realization. This study has been published in the following article:*

*“Optical Control of Cardiac Function with a Photoswitchable Muscarinic Agonist”*

*Fabio Riefolo, Carlo Matera, Aida Garrido-Charles, Alexandre M. J. Gomila, Rosalba Sortino, Luca Agnetta, Enrique Claro, Roser Masgrau, Ulrike Holzgrabe, Montserrat Batlle, Michael Decker, Eduard Guasch, and Pau Gorostiza*

*Journal of the American Chemical Society 2019 141 (18), 7628-7636.*

*DOI: 10.1021/jacs.9b03505*

At a second stage, we converged on the important brain functions that are controlled by the cholinergic system (Scarr, 2012). The distribution of M1, M2, and M3 receptors is abundant in brain tissues. Acetylcholine neuromodulation is complex and can be directly associated with characteristic patterns of neural activity, called brainwaves or brain states (Ruiz-Mejias et al., 2011; Sanchez-Vives and Mattia, 2014). In general, neurons have an incessant oscillatory activity that is a marker of various human behaviors and mental states. The cholinergic system cooperates with other endogenous neurotransmitter pathways to control the transition between different neural oscillatory patterns, that is, between different behaviors (Hasselmo and Sarter, 2011; Lee and Dan, 2012; Pinto et al., 2013; Ramaswamy et al., 2018). The manipulation of such brainwaves is not only important for neuroscience research purposes but also has the potential to stand as an innovative therapy against several neurological disorders (Lefaucheur, 2009; Lefaucheur et al., 2014; Paulus, 2014; Pereira et al., 2016). In this study, we enabled the direct control of brain state transitions with light in wildtype animals using our photoswitchable muscarinic ligand PAI in isolated cortical slices and anesthetized mice.

*This project has been realized in collaboration between the laboratories of María Victoria Sánchez-Vives (IDIBAPS) and Pau Gorostiza (IBEC). I personally carried out the chemical synthesis and the photochemical characterizations in the new experimental conditions of PAI, the competition binding experiments on mAChRs, the development of the light-sensitive experimental set-up for achieving the final pharmacological results, the design and the co-performance of all the in vitro and in vivo experiments. I made major contributions to prepare the manuscript.*

*The results of this research have been recently submitted for publication and are currently under review. The preprint version of the article has been deposited here and published with the following reference:*

*“Control of brain state transitions with light”*

*Almudena Barbero-Castillo\*, Fabio Riefole\*, Carlo Matera, Sara Caldas-Martínez, Pedro Mateos-Aparicio, Julia F. Weinert, Enrique Claro, Maria Victoria Sánchez-Vives, and Pau Gorostiza. \*co-first authors.*

*DOI: <https://doi.org/10.1101/793927>*

# Optical Control of Cardiac Function with a Photoswitchable Muscarinic Agonist

Fabio Riefolo,<sup>†,‡,¶</sup> Carlo Matera,<sup>†,‡,¶</sup> Aida Garrido-Charles,<sup>†,‡</sup> Alexandre M. J. Gomila,<sup>†,‡</sup> Rosalba Sortino,<sup>†,‡</sup> Luca Agnetta,<sup>§</sup> Enrique Claro,<sup>||</sup> Roser Masgrau,<sup>||</sup> Ulrike Holzgrabe,<sup>§</sup> Montserrat Batlle,<sup>⊥</sup> Michael Decker,<sup>§</sup> Eduard Guasch,<sup>⊥,#</sup> and Pau Gorostiza<sup>\*,†,‡,∇</sup>

<sup>†</sup>Institute for Bioengineering of Catalonia (IBEC), Barcelona Institute for Science and Technology (BIST).

<sup>‡</sup>Network Biomedical Research Center in Bioengineering, Biomaterials, and Nanomedicine (CIBER-BBN).

<sup>§</sup>Pharmaceutical and Medicinal chemistry, Institute of Pharmacy and Food Chemistry, Julius Maximilian University of Würzburg, Am Hubland, D-97074 Würzburg, Germany.

<sup>||</sup>Institut de Neurociències (INc), and, Dept. Bioquímica i Biologia Molecular, Unitat de Bioquímica de Medicina, Universitat Autònoma de Barcelona (UAB).

<sup>⊥</sup>Cardiovascular Institute, Hospital Clinic; University of Barcelona (UB); IDIBAPS.

<sup>#</sup> Network Biomedical Research Center in Cardiovascular Diseases (CIBER-CV).

<sup>∇</sup>Catalan Institution for Research and Advanced Studies (ICREA).

<sup>¶</sup>Contributed equally to this work.

**ABSTRACT:** Light-triggered reversible modulation of physiological functions offers the promise of enabling on-demand spatiotemporally controlled therapeutic interventions. Optogenetics has been successfully implemented in the heart, but significant barriers to its use in the clinic remain, such as the need for genetic transfection. Herein, we present a method to modulate cardiac function with light through a photoswitchable compound and without genetic manipulation. The molecule, named PAI, was designed by introduction of a photoswitch into the molecular structure of an M2 mAChR agonist. *In vitro* assays revealed that PAI enables light-dependent activation of M2 mAChRs. To validate the method, we show that PAI photoisomers display different cardiac effects

in a mammalian animal model, and demonstrate reversible, real-time photocontrol of cardiac function in translucent wildtype tadpoles. PAI can also effectively activate M2 receptors using two-photon excitation with near-infrared light, which overcomes the scattering and low penetration of short-wavelength illumination, and offers new opportunities for intravital imaging and control of cardiac function.

## **INTRODUCTION**

Remote spatiotemporal control of physiological processes may provide novel treatment opportunities. Cardiopathies are paradigmatic in this regard because of the rapid time course and complex integration of electrophysiological and molecular events in very specific areas of the heart. For instance, most cardiac rhythm control strategies rely on antiarrhythmic drugs (AADs) targeting ionic currents, whose effects cannot be regulated spatiotemporally. As a result, AADs often give rise to intolerable side effects, including ventricular pro-arrhythmogenicity, and are only partially effective. Overcoming the high failure and complication rates of current therapeutic strategies to treat these diseases will require both patient-personalized determination of the specific physiopathological mechanism and qualitative pharmacological breakthroughs.<sup>1</sup>

The application of light and optical techniques in medicine has had a profound impact over the last several decades, in diagnostics, surgery and therapy.<sup>2</sup> In particular, photoexcitation of intrinsic molecules or exogenous light-sensitive agents introduced in the body can affect the tissues and cells within in various ways, via the generation of heat (photothermal), chemical reactions (photochemical), and biological processes (photobiological/photopharmacological or optogenetic).<sup>2</sup> The potential of light as a therapeutic tool with high spatiotemporal resolution has been recently investigated in the cardiovascular field, particularly for arrhythmias, through optogenetics.<sup>3-7</sup> However, the application of such genetic techniques to human subjects with therapeutic purposes is still hampered by safety, regulatory and economic hurdles. Unlike optogenetics, photopharmacology rely on the use of exogenous light-

regulated small molecules that can photocontrol native targets and that could be tested and approved using standard drug development procedures.<sup>8–15</sup> These molecules can be used in combination with devices that deliver light to specific locations in the body<sup>7,16–18</sup> in order to remotely control drug dosing and duration of action. Since the activity of drugs is structure-dependent, reversible photoresponsive drugs are obtained by the rational introduction of a molecular photoswitch into the structure of a bioactive compound.<sup>8,14</sup>

Cardiac function is controlled by the autonomic sympathetic and parasympathetic nervous systems, which act via adrenoceptors and muscarinic acetylcholine receptors (mAChRs), respectively.<sup>19</sup> In particular, stimulation of  $\beta$ 1 and  $\beta$ 2 adrenergic receptors increases the heart rate (positive chronotropy) and contractility (positive inotropy), whilst stimulation of M2 mAChRs decreases heart rate and prolongs the atrioventricular conduction time.<sup>20,21</sup> Thus, adrenergic and muscarinic receptors constitute suitable target candidates to control cardiac function with light. Muscarinic acetylcholine receptors (mAChRs) belong to class A G protein-coupled receptors (GPCRs) and are divided in five different subtypes (M1-M5).<sup>22</sup> M2 receptor is extensively expressed in the heart. All five mAChRs are characterized by a high sequence homology in the orthosteric site located in the transmembrane region. This fact limits the development of subtype-selective orthosteric agonists. On the other hand, the allosteric site located in the extracellular loop is less conserved, thus muscarinic allosteric agents are commonly endowed with a more pronounced subtype-selectivity.<sup>23</sup> A chemical strategy commonly applied to overcome such limitation is the incorporation, within the same molecular structure, of two distinct pharmacophore elements belonging to (a) high-affinity orthosteric agonists and (b) highly selective allosteric ligands.<sup>24–28</sup> These hybrid compounds, termed “dualsteric” or “bitopic”, are capable to bind simultaneously to both the orthosteric and the allosteric sites of mAChRs and usually display valuable properties,<sup>29</sup> such as receptor subtype selectivity, functional selectivity,<sup>26,30</sup> and higher tolerability *in vivo*.<sup>31</sup> Moreover, such ligands bear in their structure two permanently charged nitrogen atoms, which likely prevent them from crossing the blood-brain barrier, confining their effects to the periphery, which is advantageous for cardiovascular agents. Herein, we describe the

first non-genetic method for the optical control of cardiac function with a photoswitchable agonist. The design and synthesis of this molecule and its pharmacological characterization under one-photon (1P) and two-photon (2P) excitation are reported.

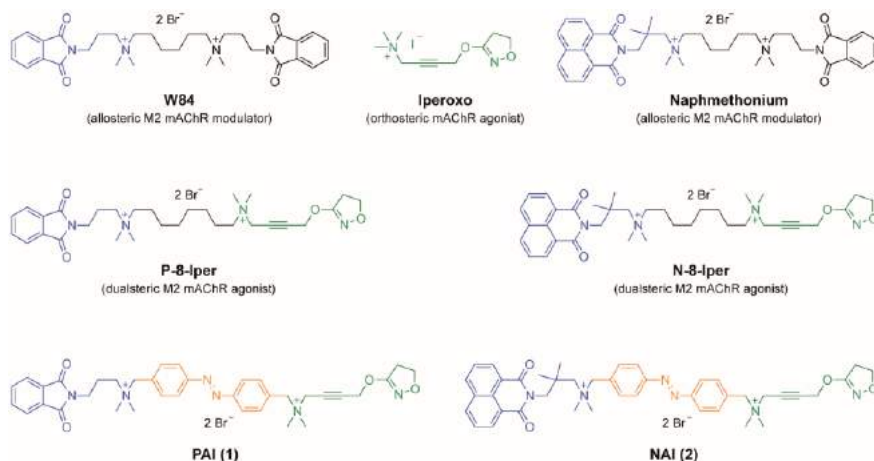


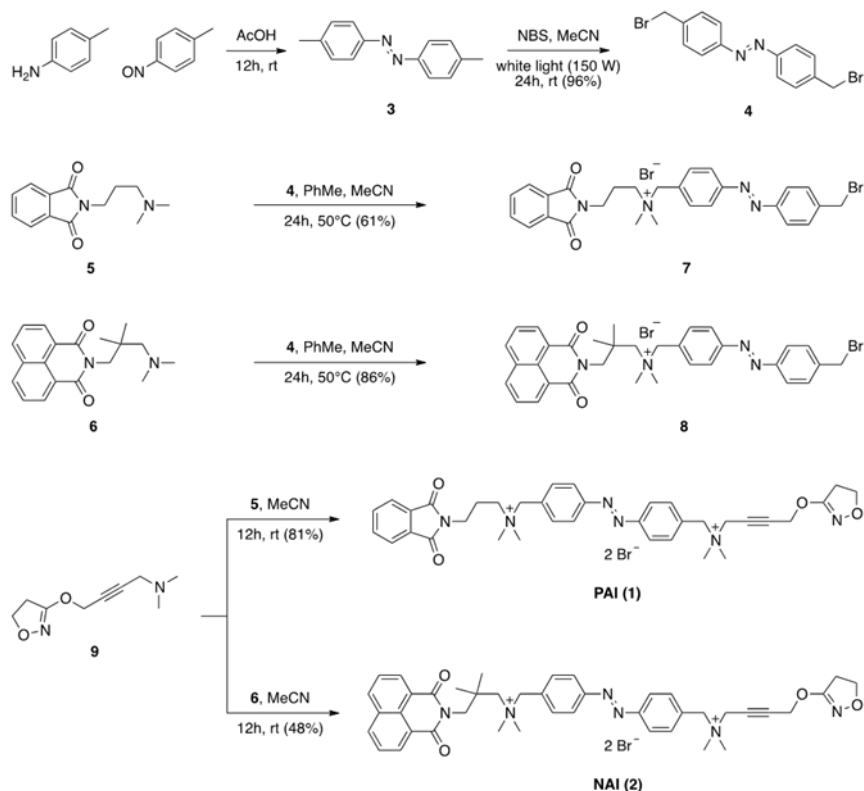
**Figure 1.** Chemical structures of the muscarinic ligands discussed in this work: the allosteric modulators W84 and Naphmethonium, the orthosteric agonist Iperoxo, the dualistic agonists P-8-Iper and N-8-Iper, and the photoswitchable dualistic ligands PAI and NAI.

## RESULT AND DISCUSSION

### ***Rational design, chemical synthesis and photochemical characterization.***

Two novel putative photoresponsive muscarinic agents, named Phthalimide-Azo-Iperoxo (PAI) and Naphthalimide-Azo-Iperoxo (NAI), were designed by replacing the polymethylene spacer chain of known M2 dualistic agonists (P-8-Iper and N-8-Iper)<sup>30–32</sup> with a molecular photoswitch, while conserving (a) the Iperoxo-like orthosteric agonist moiety, and (b) the M2-selective allosteric fragments derived from W84 and Naphmethonium (**Figure 1**). The incorporation of a photoisomerizable unit into the structure of a dualistic agonist should enable controlling with light the mutual position of the orthosteric and the allosteric moieties, presumably leading to differences between the two isomers in receptor affinity and efficacy. We chose an azobenzene core as photoresponsive component because of the favourable characteristics that azobenzene-based photoswitches normally display for biological

purposes in comparison to other photoswitches, such as design flexibility, large changes in geometry upon isomerization, high photostationary states and fatigue resistance, fast photoisomerization rates, and chemical stability, among others.<sup>33</sup> Moreover, the use of arylazo compounds has been proven safe in humans for some approved drugs and food colorants.<sup>33</sup>



**Scheme 1.** Chemical synthesis of PAI and NAI.

PAI (**1**) and NAI (**2**) were prepared via two subsequent Menshutkin reactions between the azobenzene linker (**4**) and the corresponding allo- and orthosteric intermediates (**5** and **6**, **9**) (**Scheme 1**). Compound **3** was synthesized via the typical Mills reaction and successively brominated photochemically to afford the desired linker **4**. Notably, this photochemical reaction exempted us from using a radical initiator<sup>34</sup> and gave an excellent yield (96%), proving for the first time that light-induced benzylic halogenations can be conveniently used also for the preparation of such versatile photoswitchable linkers. Compounds **5**, **6** and **9** were

prepared as previously reported from commercially available starting materials (**Scheme 1** and SI).<sup>24–26,31</sup>

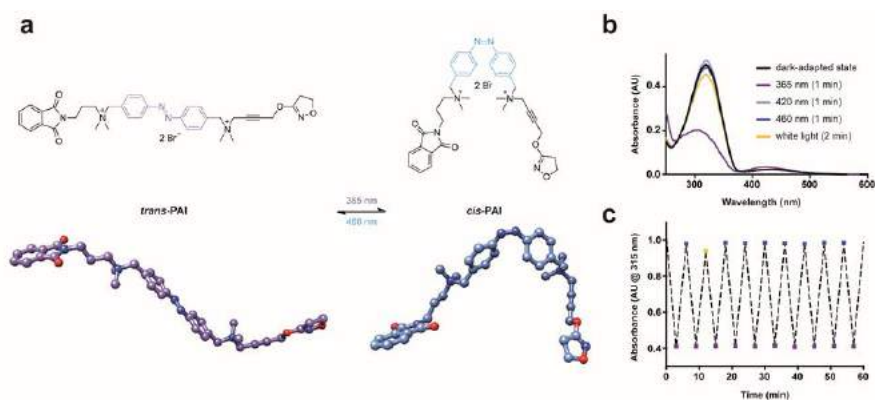


**Figure 2. Photochemical characterization.** a) 2D and 3D representation of the chemical structures of *trans*- and *cis*-PAI. b) Absorption spectra of PAI showing distinct photochromic behaviour. c) The photoswitching process can be repeated over several cycles without noticeable photofatigue.

As a prerequisite for a reversible light-dependent control of their biological activity, PAI and NAI need to effectively behave as reversible photoswitches, which means that the photoisomerization should be relatively fast and quantitatively significant in both directions. UV/Vis spectroscopy experiments showed that PAI and NAI have the typical absorption bands of conventional azobenzenes. PAI can be isomerized to the *cis* form (about 73% conversion) by applying 365 nm light, while it thermally relaxes back to the *trans* form in several hours at room temperature. It can be also effectively back-isomerized to the *trans* form by applying white or blue (460 nm) light (83% *trans*) (**Figure 2** and SI, **Figure S2**). Surprisingly, NAI resulted refractory to photoisomerization (only 23% *cis* after 10 min at 365 nm, SI, **Figure S2.1CD**), which shows that rational design of azobenzene-containing ligands does not always afford the expected results. We hypothesized that the absorption and emission properties of the naphthalimide moiety<sup>35</sup> could interfere with its photochromism. Given the unsatisfactorily photochromic behaviour of NAI, we selected only PAI for further studies.

**PAI allows reversible photo-activation of M2 mAChRs in calcium imaging experiments and molecular docking simulations.** The photopharmacological properties of PAI were first assessed *in vitro* with real-time calcium imaging assays in transiently transfected HEK cells under 1P-illumination (**Figure 3** and SI). We tested also the non-photoswitchable muscarinic agonist Iperoxo (IPX)<sup>36</sup> as a control (**Figure 3a**). The application of *trans*-PAI (dark-adapted state) induced cytosolic calcium oscillations indicative of M2 agonism, which were reduced by converting PAI to its *cis* form upon illumination with UV light (365 nm) (**Figure 3bc**).

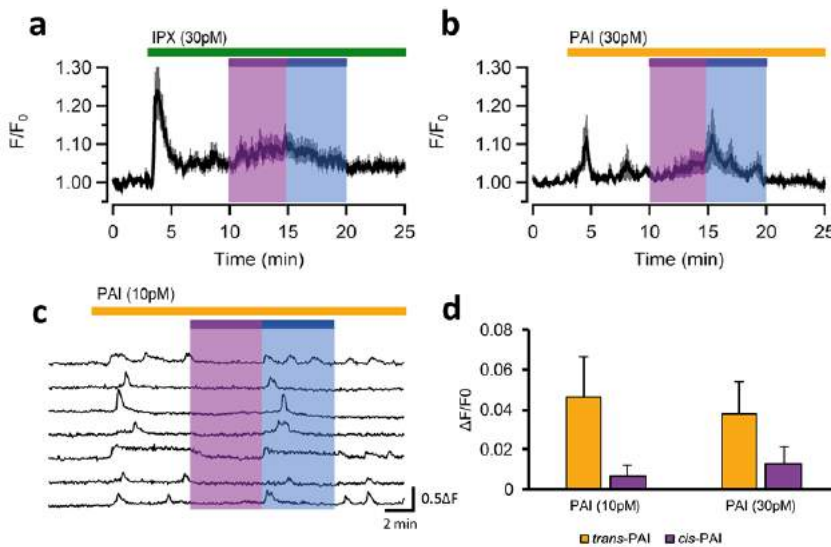


**Figure 3. PAI reversibly activates M2 mAChRs with light in calcium imaging assays.** Real-time calcium imaging traces from HEK cells co-expressing M2mAChR and GqTOP loaded with 10  $\mu$ M of the calcium indicator OGB1AM. **a**) Average trace of cell responses to 30 pM of non-photoswitchable muscarinic agonist IPX (n=130). Cells gave a sharp response to the application of IPX but, as expected, the concomitant application of pulses of UV or blue light did not alter calcium responses. **b**) Average trace of cell responses to 30 pM of *trans*-PAI (n=8). **c**) Single cell calcium responses induced by the direct application of 10 pM of *trans*-PAI (yellow bar). Purple bars indicate illumination at 365 nm, blue bars indicate illumination at 460 nm. Gray shadow in the recordings represents  $\pm$ SEM. **d**) Quantification of photoresponses to the application of PAI (yellow bar) at 10 pM (n = 356 cells from 5 different experiments) and 30 pM (n = 293 cells from 6 different experiments), and recovery after 365 nm illumination (purple bar). Error bars are  $\pm$  SEM.

Calcium oscillations could be restored after back-isomerizing PAI to the *trans* configuration using blue light (460 nm). The time course of calcium

responses during activation with *trans*-PAI displayed a diversity of behaviours in individual cells (**Figure 3c**), including oscillatory waves, transient peaks, and step responses as previously observed with PLC-activating GPCRs.<sup>12</sup> Quantification of photoresponses ( $\Delta F/F_0$ ) to PAI application and 365 nm illumination shows a reduction in the calcium signal induced by UV light pulses (**Figure 3d**). Intriguingly, PAI activated M2 mAChRs in the range of picomolar concentrations, similarly to the super-agonist Iperoxo.<sup>36</sup> Thus, we demonstrated that PAI can effectively activate M2 mAChRs *in vitro* in its dark-adapted (*trans*) form and its activity can be reversibly switched off and on with light. In order to account for the observed photoswitchable activity of PAI in M2 mAChR, we looked for putative differences on the receptor level regarding binding efficacy of *cis*- and *trans*-PAI using molecular docking simulations (see SI for details). PAI isomers were docked into their theoretical binding site at the human M2 mAChR (PDB 4MQT). Our results suggested that *trans*-PAI can bind to the M2 mAChR in a typical dualsteric pose compatible with receptor activation (SI, **Figure S5.1a**).<sup>37</sup> In contrast, a flipped orientation is favoured in the case of the *cis*-isomer (SI, **Figure S5.1b**). This binding pose is likely incompatible with receptor activation and provides a possible explanation for the light-dependent efficacy of PAI.

***Trans-PAI is more effective than cis-PAI at inducing bradycardia and PR lengthening in rats.*** Once established that PAI allows light-dependent reversible activation of M2 mAChRs, we aimed at testing it as an agent to photocontrol cardiac function *in vivo*. We initially used Wistar rats for our experiments. The intraperitoneal administration of PAI induced progressive bradycardia and PR lengthening in a dose-dependent manner in both configurations (**Figure 4** and SI, **Figure S6.1**). These effects were accompanied with variable degrees of systemic parasympathetic effects, such as salivation, urination and defecation. At low doses ( $\leq 3 \mu\text{M}/\text{kg}$ ), both isomers yielded a similar small effect, but remarkably differed at intermediate and high doses. At  $10 \mu\text{M}/\text{kg}$  PAI and higher doses, the PR interval was significantly more prolonged in *trans*; at  $30 \mu\text{M}$  and higher doses, heart rate was also lower in *trans*. The effects of PAI could not be photoswitched either with blue or with UV light, showing that the ability of light to penetrate murine cardiac tissue at those wavelengths is likely not sufficient to reach M2 mAChR location. Only the administration of

atropine (2 mg) completely reverted bradycardia, PR lengthening and systemic parasympathetic effects in both groups (SI, **Figure S6.1**). These results demonstrated an enhanced parasympathetic activity for the *trans*-isomer, and confirmed in mammals the previous findings observed in cells.

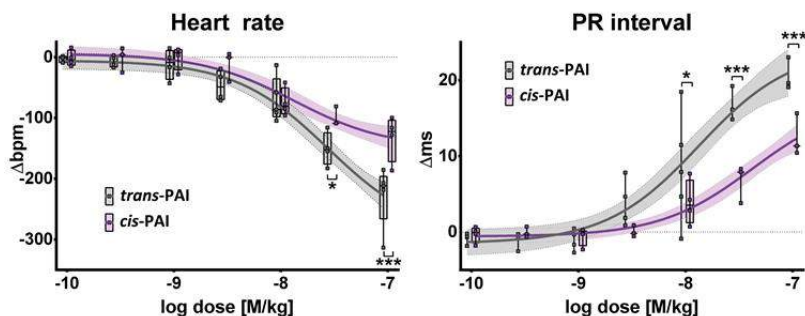


**Figure 4.** *In vivo* effect of *trans*- and *cis*-PAI on the cardiac activity of rats. The activity of dark-relaxed (*trans*, grey plots) and UV-illuminated PAI (*cis*, purple plots) administered intraperitoneally in anesthetized rats was tested by means of electrocardiography. The heart rate (left panel) and PR interval (right panel) are plotted as a function of increasing doses of both isomers, which induced progressive bradycardia and PR lengthening in a dose-dependent manner. Significant differences between the dark-relaxed and UV-treated PAI were found in the heart rate and PR interval at the higher doses (\* $p < 0.05$ ; \*\*\* $p < 0.001$  *trans* vs *cis*), in agreement with the higher agonist activity of the *trans* form observed *in vitro* and in tadpoles. Three rats in the *trans*-group died because of extreme bradycardia after the 100  $\mu\text{M}/\text{kg}$  dose. The effects of PAI were reversible only upon administration of the muscarinic antagonist Atropine.

***PAI enables reversible photocontrol of cardiac activity in *Xenopus tropicalis* tadpoles.*** As an alternative to demonstrate reversible control of cardiac function *in vivo*, we turned to an animal model in which light scattering is known to be low thus allowing better light penetration. We selected *Xenopus tropicalis* tadpoles for this purpose since they are translucent and are recognized as an excellent model for studying the human cardiovascular system (**Figure 5**).<sup>38,39</sup> Moreover, we had already successfully used video light microscopy to acquire real-time images of the developing beating heart by digitizing the expanding and contracting blood pool in early translucent hearts (**Figure 5a**).<sup>38,40</sup>

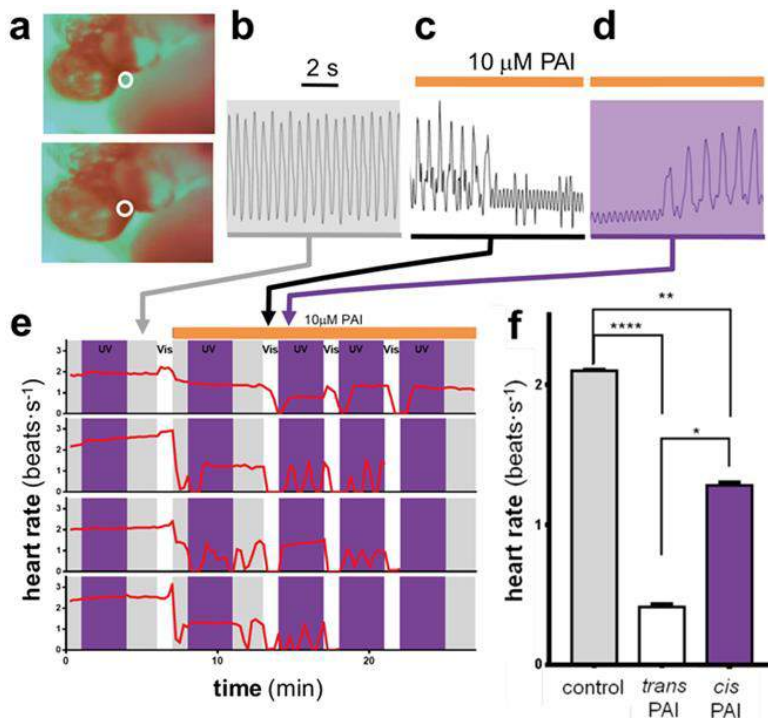


**Figure 5. Photoregulation of heart rate with PAI in frog tadpoles.** **a)** Two video frames of a paralyzed tadpole heart indicating a region of interest (white circle) used to obtain the time course of heart beating movements (average of intensity versus time). **b)** Normal heartbeat recording obtained in control conditions (dim red light, indicated by a grey shade). Time scale: 2 s. **c)** Adding 10  $\mu\text{M}$  *trans*-PAI under white light illumination reduces the heartbeat frequency, eventually causing cardiac arrest. **d)** Under UV illumination (purple shade), *trans*-PAI is isomerized to *cis*-PAI and heartbeat is recovered. **e)** Red traces indicate the heart rate (in  $\text{beats}\cdot\text{s}^{-1}$ , calculated every 15 s interval) as a function of time in 4 independent experiments with different animals. White, purple, and grey backgrounds indicate illumination with white, UV and dim red light, respectively. Heart rate is not altered by illumination under control conditions (SI Appendix, **Figure S6.2**). Adding 10  $\mu\text{M}$  *trans*-PAI under dim light reduces the heart rate in animals 2, 3 and 4. UV illumination isomerizes PAI to the *cis* form and the heart rate is partially recovered. Dim red light does not isomerize PAI (SI Appendix, **Figure S6.1**) and heart rate is relatively stable. White light converts PAI to the *trans* isomer, causing cardiac arrest in all 4 animals. UV light restores heartbeat in all animals, some displaying an unstable rate. Several white/UV light cycles were repeated in some animals, showing similar effects. **f)** Quantification of heart rate during the last minute of each period ( $\text{beats}\cdot\text{s}^{-1}$ ,  $n=4$  tadpoles) in control conditions, under white light (*trans*-PAI) and under UV light (*cis*-PAI). Two-way for repeated measures ANOVA was performed with uncorrected Fisher's LSD test, significance values were established with a  $p$ -value = 0.05. Error bars represent standard error of the mean (SEM). The heart rate was significantly higher under UV illumination compared to visible light ( $p$ -value < 0.05). Both isomers produced a significant reduction of heart rate in comparison to controls ( $p$ -value < 0.001).

In the absence of PAI, the cardiac rate of tadpoles remained nearly constant at  $2.3 \pm 0.1$  beats·s<sup>-1</sup> during control illumination with UV light and at  $2.10 \pm 0.01$  beats·s<sup>-1</sup> in the dark. The variability score (V.S.) was  $7.97 \pm 0.07$ . Upon administration of 10 μM *trans*-PAI, heart rate decreased dramatically ( $0.41 \pm 0.02$  beats·s<sup>-1</sup> in the trace of **Figure 5e**) leading in some cases to cardiac arrest (**Figure 5c**). Heart beating recovered progressively upon UV illumination (*cis*-isomerisation,  $1.28 \pm 0.02$  beats·s<sup>-1</sup>, **Figure 5f**), and was not altered in the dark since thermal relaxation is slow. Some animals displayed less stable cardiac rate during UV periods compared to controls (V.S. of  $17.4 \pm 0.2$  and  $8.30 \pm 0.02$ , respectively; SI, **Figure S7.3**). Subsequent illumination of the animals with visible light (*cis*-to-*trans* isomerization) again reduced cardiac rate and eventually interrupted heart beating (V.S. of  $374 \pm 47.7$ , SI, **Figure S7.3**). Cardiac activity was restored by later exposition to UV light, and further UV/visible light cycles confirmed the reversibility of the pharmacological effects. (see example **Supporting Movie S1**). Overall, these experiments demonstrated that PAI allows remote and reversible control of heart rate with light in living animals.

**Activation of PAI with near infrared (NIR) light.** In order to overcome the scattering and low penetration of violet and visible illumination, we tested whether PAI could be used to activate M2 mAChRs at longer wavelengths. In fact, a critical aspect that must be addressed to unleash the full potential of light-regulated drugs and favour their translation into clinic is their responsiveness to red or NIR radiation,<sup>44,41</sup> which enables higher penetration through tissue, abolishes photodamage and, in the case of 2P excitation, allows three-dimensional subcellular resolution.<sup>42-46</sup> PAI has an excellent thermal stability in both configurations (**Figure S2.3**) and is photochemically suited for *cis*-to-*trans* photoisomerization with NIR light under 2P-excitation, which encouraged us to test its effects in living cells in real-time calcium imaging assays using a confocal microscope equipped with a pulsed laser. (**Figure 6**). PAI was initially applied in its *cis* (off) state, which as expected did not produce cytosolic calcium oscillations. Subsequent illumination at 840 nm induced robust calcium responses, as previously observed in calcium imaging experiments for *cis*-to-*trans* photoisomerization under 1P-excitation (**Figure 6a**). These results are quantified in **Figure 6c**. The responses ( $\Delta F/F_0$ ) obtained for *cis*-PAI (1P pre-

irradiation at 365 nm) are comparable to controls, and 2P-induced isomerization to *trans*-PAI achieves calcium responses nearly as high as perfusion of iperoxo. It is worth noting that even under NIR excitation PAI maintains an outstanding potency (picomolar) to activate M2 mAChRs, which is rarely observed in photoswitches.<sup>11,44,47,48</sup> Interestingly, 2P microscopy is extensively used for intravital imaging including cardiovascular imaging at subcellular resolution.<sup>49,50</sup> Thus, PAI has a bright future to control cardiac function with light.

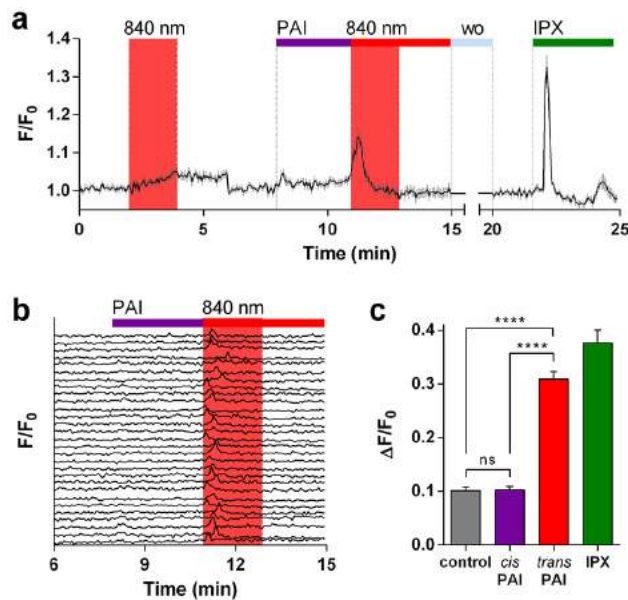


**Figure 6. Activation of PAI with NIR light under 2P excitation.** Real-time calcium imaging traces from HEK cells co-expressing M2 mAChR and GqTOP loaded with 10  $\mu$ M of the calcium indicator OGB1AM. **a**) Average trace of cell responses to 30 pM *cis*-PAI pre-irradiated at 365 nm (purple bar), *trans*-enriched PAI obtained under 2P excitation at 840 nm (red bar), and the muscarinic agonist IPX (green bar) after wash-out (wo, light blue bar) (n=29 cells). Neither 2P excitation alone (red panel) nor *cis*-PAI elicited calcium responses. Cells gave a sharp response upon application of pulsed NIR light (840 nm) in the presence of PAI as a consequence of its photoisomerization to the *trans*- active form. IPX was applied as a positive control. Gray shadow in the recordings represents  $\pm$ SEM. **b**) Single cell calcium responses induced by PAI under 2P-excitation at 840 nm (red panel) (29 cells). Purple bar indicates application of pre-irradiated PAI (365 nm), red bar indicates illumination at 840 nm. **c**) Quantification of photoresponses of 29 cells to the application of *cis*-PAI (purple bar) at 30 pM, after switching to *trans*-PAI using 2P-excitation at 840 nm (red bar), control under 2P-excitation at 840 nm (grey bar) and IPX (green bar). Error bars are  $\pm$  SEM. Data were analyzed by using one-way ANOVA with Sidak post hoc test for multiple comparisons for statistical significance (p-value (\*\*\*\*) < 0.0001; GraphPad Prism 6).

## CONCLUSIONS

The rapid and reversible control of cardiac activity is of particular interest in medicine, including the spatiotemporal manipulation of close anatomic structures bearing different electrophysiological functions in the heart. Light-activated cardiac drugs could be selectively enhanced in certain regions of the heart (e.g., preventing undesired pro-arrhythmogenic ventricular effects when atria are targeted), or at certain times (on-demand, i.e., active only during atrial fibrillation or bradycardia). For that purpose, cardiac patches with integrated electronics and electric stimulation<sup>46</sup> could be further equipped with optoelectronic devices for photostimulation. Drug-based cardiac photoregulation techniques offer potential advantages compared to electric stimulation of cardiac muscle, which produces inhomogeneous areas of de- and hyperpolarization, causes faradaic reactions that alter pH, and produce toxic gases (H<sub>2</sub>, O<sub>2</sub>, Cl<sub>2</sub>), all of which would be prevented by light-stimulation.

To this end, we have developed the first photoswitchable compound that enables control of cardiac activity with light in wildtype animals without genetic manipulation. To the best of our knowledge, PAI is also the first photoswitchable M2 mAChR agonist to be reported. Despite the changes introduced in the ligand structure in order to photoregulate its activity, PAI retains the high potency of its parent compounds Iperoxo and P-8-Iper.<sup>31,36</sup> PAI activates M2 receptors in its *trans* configuration and can be reversibly photoswitched with different wavelengths including NIR light under 2P excitation. Future experiments will be addressed to demonstrate that PAI enables precise spatio-temporal control of cardiac function in mammals in combination with 2P cardiovascular imaging.

**ASSOCIATED CONTENT. Supporting Information.** The Supporting Information is available free of charge on the ACS Publications website at DOI: 10.1021/jacs.9b03505. Detailed materials and methods, synthetic procedures, chemical analyses, and any additional data and figures as noted in the text. Movie S1 (AVI).

**AUTHOR INFORMATION.** Corresponding Author \*E-mail: pau@icrea.cat.

**Author Contributions.** †Fabio Riefolo and Carlo Matera contributed equally. Notes The authors declare no competing financial interest.

**ACKNOWLEDGMENTS.** The authors are grateful to Jean-Philippe Pin for providing the chimeric Gi/Gq protein clone and to Núria Camarero for helping during preliminary in vitro experiments. CM and FR are grateful to Prof. Marco De Amici for helpful discussion and continuous support. Molecular graphics and analyses were performed with the UCSF Chimera package. Chimera is developed by the Resource for Biocomputing, Visualization, and Informatics at the University of California, San Francisco (supported by NIGMS P41-GM103311). Mass spectrometry was performed at the IRB Barcelona Mass Spectrometry Core Facility, which actively participates in the BMBS European COST Action BM 1403 and is a member of Proteored, PRB2- ISCIII, supported by grant PRB2 (IPT13/0001 – ISCIIISGEFI/FEDER). This project has received funding from the EU Horizon 2020 Framework Programme for Research and Innovation under the Specific Grant Agreement 2 (Human Brain Project WaveScaleS SGA2 No. 785907), AGAUR/ Generalitat de Catalunya (CERCA Programme, 2017-SGR- 1442 and 2017-SGR-1548), FEDER funds, ERANET SynBio MODULIGHTOR, Fundaluce foundation, Ramón Areces foundation, MINECO (FPI fellowship BES-2014-068169 and project CTQ2016-80066R), and CATCH-ME (grant agreement no. 633196). CM was supported by the Ermenegildo Zegna Founder’s Scholarship. LA was supported by the graduate program “Receptor Dynamics Emerging paradigms for novel drugs” funded by the Elite Network of Bavaria. All animal procedures were authorized by the local ethics review boards (IDIBAPS-Hospital Clínic de Barcelona, no. 92117, 02/03/2017; Comitè Ètic d’Experimentació Animal de la Universitat de Barcelona, no. 306/18, 25/06/2018).

## REFERENCES

- (1) Fabritz, L.; Guasch, E.; Antoniades, C.; Bardinnet, I.; Benninger, G.; Betts, T. R.; Brand, E.; Breithardt, G.; Bucklar-Suchankova, G.; Camm, A. J.; et al. Expert Consensus Document: Defining the Major Health Modifiers Causing Atrial Fibrillation: A Roadmap to Underpin Personalized Prevention and Treatment. *Nat. Rev. Cardiol.* 2016, 13 (4), 230–237.
- (2) Yun, S. H.; Kwok, S. J. J. Light in Diagnosis, Therapy and Surgery. *Nat. Biomed. Eng.* 2017, 1 (1), 8.
- (3) Pianca, N.; Zaglia, T.; Mongillo, M. Will Cardiac Optogenetics Find the Way through the Obscure Angles of Heart Physiology? *Biochem. Biophys. Res. Commun.* 2017, 482 (4), 515–523.
- (4) Yu, L.; Zhou, L.; Cao, G.; Po, S. S.; Huang, B.; Zhou, X.; Wang, M.; Yuan, S.; Wang, Z.; Wang, S.; et al. Optogenetic Modulation of Cardiac Sympathetic Nerve Activity to Prevent Ventricular Arrhythmias. *J. Am. Coll. Cardiol.* 2017, 70 (22), 2778–2790.
- (5) Bingen, B. O.; Engels, M. C.; Schalij, M. J.; Jangsangthong, W.; Neshati, Z.; Feola, I.; Ypey, D. L.; Askar, S. F. A.; Panfilov, A. V.; Pijnappels, D. A.; et al. Light-Induced Termination of Spiral Wave Arrhythmias by Optogenetic Engineering of Atrial Cardiomyocytes. *Cardiovasc. Res.* 2014, 104 (1), 194–205.
- (6) Bruegmann, T.; Boyle, P. M.; Vogt, C. C.; Karathanos, T. V.; Arevalo, H. J.; Fleischmann, B. K.; Trayanova, N. A.; Sasse, P. Optogenetic Defibrillation Terminates Ventricular Arrhythmia in Mouse Hearts and Human Simulations. *J. Clin. Invest.* 2016, 126 (10), 3894–3904.
- (7) Boyle, P. M.; Karathanos, T. V.; Trayanova, N. A. “Beauty Is a Light in the Heart”: The Transformative Potential of Optogenetics for Clinical Applications in Cardiovascular Medicine. *Trends Cardiovasc. Med.* 2015, 25 (2), 73–81.

- (8) Lerch, M. M.; Hansen, M. J.; van Dam, G. M.; Szymanski, W.; Feringa, B. L. Emerging Targets in Photopharmacology. *Angew. Chem. Int. Ed. Engl.* 2016, 55 (37), 10978–10999.
- (9) Izquierdo-Serra, M.; Trauner, D.; Llobet, A.; Gorostiza, P. Optical Modulation of Neurotransmission Using Calcium Photocurrents through the Ion Channel LiGluR. *Front. Mol. Neurosci.* 2013, 6, 3.
- (10) Nevola, L.; Martín-Quirós, A.; Eckelt, K.; Camarero, N.; Tosi, S.; Llobet, A.; Giral, E.; Gorostiza, P. Light-Regulated Stapled Peptides to Inhibit Protein-Protein Interactions Involved in Clathrin-Mediated Endocytosis. *Angew. Chemie Int. Ed.* 2013, 52 (30), 7704–7708.
- (11) Izquierdo-Serra, M.; Gascón-Moya, M.; Hirtz, J. J.; Pittolo, S.; Poskanzer, K. E.; Ferrer, È.; Alibés, R.; Busqué, F.; Yuste, R.; Hernando, J.; et al. Two-Photon Neuronal and Astrocytic Stimulation with Azobenzene-Based Photoswitches. *J. Am. Chem. Soc.* 2014, 136 (24), 8693–8701.
- (12) Pittolo, S.; Gómez-Santacana, X.; Eckelt, K.; Rovira, X.; Dalton, J.; Goudet, C.; Pin, J.-P.; Llobet, A.; Giraldo, J.; Llebaria, A.; et al. An Allosteric Modulator to Control Endogenous G Protein-Coupled Receptors with Light. *Nat. Chem. Biol.* 2014, 10 (10), 813–815.
- (13) Izquierdo-Serra, M.; Bautista-Barrufet, A.; Trapero, A.; Garrido-Charles, A.; Díaz-Tahoces, A.; Camarero, N.; Pittolo, S.; Valbuena, S.; Pérez-Jiménez, A.; Gay, M.; et al. Optical Control of Endogenous Receptors and Cellular Excitability Using Targeted Covalent Photoswitches. *Nat. Commun.* 2016, 7, 12221.
- (14) Velema, W. A.; Szymanski, W.; Feringa, B. L. Photopharmacology: Beyond Proof of Principle. *J. Am. Chem. Soc.* 2014, 136 (6), 2178–2191.
- (15) Matera, C.; Gomila, A. M. J.; Camarero, N.; Libergoli, M.; Soler, C.; Gorostiza, P. Photoswitchable Antimetabolite for Targeted Photoactivated Chemotherapy. *J. Am. Chem. Soc.* 2018, 140 (46), 15764–15773.
- (16) Hamaoka, T.; McCully, K. K.; Quaresima, V.; Yamamoto, K.; Chance, B. Near-Infrared Spectroscopy/imaging for Monitoring Muscle Oxygenation and Oxidative Metabolism in Healthy and Diseased Humans. *J. Biomed. Opt.* 2007, 12 (6), 62105.
- (17) Taub, A. F. Photodynamic Therapy in Dermatology: History and Horizons. *J. Drugs Dermatol.* 3 (1 Suppl), S8-25.
- (18) Kale, R. P.; Kouzani, A. Z.; Walder, K.; Berk, M.; Tye, S. J. Evolution of Optogenetic Microdevices. *Neurophotonics* 2015, 2 (3), 31206.
- (19) Brodde, O. E.; Michel, M. C. Adrenergic and Muscarinic Receptors in the Human Heart. *Pharmacol. Rev.* 1999, 51 (4), 651–690.
- (20) Brodde, O.-E.; Bruck, H.; Leineweber, K.; Seyfarth, T. Presence, Distribution and Physiological Function of Adrenergic and Muscarinic Receptor Subtypes in the Human Heart. *Basic Res. Cardiol.* 2001, 96 (6), 528–538.
- (21) Dhein, S.; van Koppen, C. J.; Brodde, O. E. Muscarinic Receptors in the Mammalian Heart. *Pharmacol. Res.* 2001, 44 (3), 161–182.
- (22) Caulfield, M. P.; Birdsall, N. J. International Union of Pharmacology. XVII. Classification of Muscarinic Acetylcholine Receptors. *Pharmacol. Rev.* 1998, 50 (2), 279–290.

- (23) De Amici, M.; Dallanoce, C.; Holzgrabe, U.; Tränkle, C.; Mohr, K. Allosteric Ligands for G Protein-Coupled Receptors: A Novel Strategy with Attractive Therapeutic Opportunities. *Med. Res. Rev.* 2009, 30 (3), 463–549.
- (24) Mohr, K.; Tränkle, C.; Kostenis, E.; Barocelli, E.; De Amici, M.; Holzgrabe, U. Rational Design of Dualsteric GPCR Ligands: Quests and Promise. *Br. J. Pharmacol.* 2010, 159 (5), 997–1008.
- (25) Disingrini, T.; Muth, M.; Dallanoce, C.; Barocelli, E.; Bertoni, S.; Kellershohn, K.; Mohr, K.; De Amici, M.; Holzgrabe, U. Design, Synthesis, and Action of Oxotremorine-Related Hybrid-Type Allosteric Modulators of Muscarinic Acetylcholine Receptors. *J. Med. Chem.* 2006, 49 (1), 366–372.
- (26) Antony, J.; Kellershohn, K.; Mohr-Andrä, M.; Kebig, A.; Prilla, S.; Muth, M.; Heller, E.; Disingrini, T.; Dallanoce, C.; Bertoni, S.; et al. Dualsteric GPCR Targeting: A Novel Route to Binding and Signaling Pathway Selectivity. *FASEB J.* 2009, 23 (2), 442–450.
- (27) Matera, C.; Tata, A. M. Pharmacological Approaches to Targeting Muscarinic Acetylcholine Receptors. *Recent Pat. CNS Drug Discov.* 2014, 9 (2), 85–100.
- (28) Agnetta, L.; Kauk, M.; Canizal, M. C. A.; Messerer, R.; Holzgrabe, U.; Hoffmann, C.; Decker, M. A Photoswitchable Dualsteric Ligand Controlling Receptor Efficacy. *Angew. Chem. Int. Ed. Engl.* 2017, 56 (25), 7282–7287.
- (29) De Min, A.; Matera, C.; Bock, A.; Holze, J.; Kloeckner, J.; Muth, M.; Traenkle, C.; De Amici, M.; Kenakin, T.; Holzgrabe, U.; et al. A New Molecular Mechanism To Engineer Protean Agonism at a G Protein-Coupled Receptor. *Mol. Pharmacol.* 2017, 91 (4), 348–356.
- (30) Bock, A.; Merten, N.; Schrage, R.; Dallanoce, C.; Bätz, J.; Klöckner, J.; Schmitz, J.; Matera, C.; Simon, K.; Kebig, A.; et al. The Allosteric Vestibule of a Seven Transmembrane Helical Receptor Controls G-Protein Coupling. *Nat. Commun.* 2012, 3, 1044.
- (31) Matera, C.; Flammini, L.; Quadri, M.; Vivo, V.; Ballabeni, V.; Holzgrabe, U.; Mohr, K.; De Amici, M.; Barocelli, E.; Bertoni, S.; et al. Bis(ammonio)alkane-Type Agonists of Muscarinic Acetylcholine Receptors: Synthesis, in Vitro Functional Characterization, and in Vivo Evaluation of Their Analgesic Activity. *Eur. J. Med. Chem.* 2014, 75, 222–232.
- (32) Cristofaro, I.; Spinello, Z.; Matera, C.; Fiore, M.; Conti, L.; De Amici, M.; Dallanoce, C.; Tata, A. M. Activation of M2 Muscarinic Acetylcholine Receptors by a Hybrid Agonist Enhances Cytotoxic Effects in GB7 Glioblastoma Cancer Stem Cells. *Neurochem. Int.* 2018, 118, 52–60.
- (33) Broichhagen, J.; Frank, J. A.; Trauner, D. A Roadmap to Success in Photopharmacology. *Acc. Chem. Res.* 2015, 48 (7), 1947–1960.
- (34) Tolosa, J.; Kub, C.; Bunz, U. H. F. Hyperbranched: A Universal Conjugated Polymer Platform. *Angew. Chemie Int. Ed.* 2009, 48 (25), 4610–4612.
- (35) Jacquemin, D.; Perpète, E. A.; Scalmani, G.; Ciofini, I.; Peltier, C.; Adamo, C. Absorption and Emission Spectra of 1,8-Naphthalimide Fluorophores: A PCM-TD-DFT Investigation. *Chem. Phys.* 2010, 372 (1–3), 61–66.
- (36) Schrage, R.; Seemann, W. K.; Klöckner, J.; Dallanoce, C.; Racké, K.; Kostenis, E.; De Amici, M.; Holzgrabe, U.; Mohr, K. Agonists with Supraphysiological Efficacy at the Muscarinic M2 ACh Receptor. *Br. J. Pharmacol.* 2013, 169 (2), 357–370.

- (37) Bock, A.; Bermudez, M.; Krebs, F.; Matera, C.; Chirinda, B.; Sydow, D.; Dallanoce, C.; Holzgrabe, U.; De Amici, M.; Lohse, M. J.; et al. Ligand Binding Ensembles Determine Graded Agonist Efficacies at a G Protein-Coupled Receptor. *J. Biol. Chem.* 2016, 291 (31), 16375–16389.
- (38) Bartlett, H. L.; Scholz, T. D.; Lamb, F. S.; Weeks, D. L. Characterization of Embryonic Cardiac Pacemaker and Atrioventricular Conduction Physiology in *Xenopus Laevis* Using Noninvasive Imaging. *Am. J. Physiol. Heart Circ. Physiol.* 2004, 286 (6), H2035-41.
- (39) Nieuwkoop P., F. J. Normal Table of *Xenopus Laevis* (Daudin): A Systematical & Chronological Survey of the Development from the Fertilized Egg till the End of Metamorphosis; 1994.
- (40) Eckelt, K.; Masanas, H.; Llobet, A.; Gorostiza, P. Automated High-Throughput Measurement of Body Movements and Cardiac Activity of *Xenopus Tropicalis* Tadpoles. *J. Biol. Methods* 2014, 1 (2), 9.
- (41) Dong, M.; Babalhavaeji, A.; Samanta, S.; Beharry, A. A.; Woolley, G. A. Red-Shifting Azobenzene Photoswitches for in Vivo Use. *Acc. Chem. Res.* 2015, 48 (10), 2662–2670.
- (42) Pawlicki, M.; Collins, H. A.; Denning, R. G.; Anderson, H. L. Two-Photon Absorption and the Design of Two-Photon Dyes. *Angew. Chem. Int. Ed. Engl.* 2009, 48 (18), 3244–3266.
- (43) Bort, G.; Gallavardin, T.; Ogden, D.; Dalko, P. I. From One-Photon to Two-Photon Probes: “caged” Compounds, Actuators, and Photoswitches. *Angew. Chem. Int. Ed. Engl.* 2013, 52 (17), 4526–4537.
- (44) Cabré, G.; Garrido-Charles, A.; Moreno, M.; Bosch, M.; Porta-de-la-Riva, M.; Krieg, M.; Gascón-Moya, M.; Camarero, N.; Gelabert, R.; Lluch, J. M.; et al. Rationally Designed Azobenzene Photoswitches for Efficient Two-Photon Neuronal Excitation. *Nat. Commun.* 2019, 10 (1), 907.
- (45) Pittolo, S.; Lee, H.; Lladó, A.; Tosi, S.; Bosch, M.; Bardia, L.; Gómez-Santacana, X.; Llebaria, A.; Soriano, E.; Colombelli, J.; et al. Reversible Silencing of Endogenous Receptors in Intact Brain Tissue Using Two-Photon Pharmacology. *bioRxiv* 2019, 515288.
- (46) Feiner, R.; Engel, L.; Fleischer, S.; Malki, M.; Gal, I.; Shapira, A.; Shacham-Diamand, Y.; Dvir, T. Engineered Hybrid Cardiac Patches with Multifunctional Electronics for Online Monitoring and Regulation of Tissue Function. *Nat. Mater.* 2016, 15 (6), 679–685.
- (47) Passlick, S.; Richers, M. T.; Ellis-Davies, G. C. R. Thermodynamically Stable, Photoreversible Pharmacology in Neurons with One- and Two-Photon Excitation. *Angew. Chem. Int. Ed. Engl.* 2018, 57 (38), 12554–12557.
- (48) Bartels, E.; Wassermann, N. H.; Erlanger, B. F.; Kienzler, M. A.; Yuan, Z.; Madsen, D.; Larsen, D. S.; Isacoff, E. Y. Photochromic Activators of the Acetylcholine Receptor. *Proc. Natl. Acad. Sci. U. S. A.* 1971, 68 (8), 1820–1823.
- (49) Scherschel, J. A.; Rubart, M. Cardiovascular Imaging Using Two-Photon Microscopy. *Microsc. Microanal.* 2008, 14 (6), 492–506.
- (50) Matsuura, R.; Miyagawa, S.; Fukushima, S.; Goto, T.; Harada, A.; Shimozaki, Y.; Yamaki, K.; Sanami, S.; Kikuta, J.; Ishii, M.; et al. Intravital Imaging with Two-Photon Microscopy Reveals Cellular Dynamics in the Ischemia-Reperfused Rat Heart. *Sci. Rep.* 2018, 8 (1), 15991.



## Supporting Information

### Optical Control of Cardiac Function with a Photoswitchable Muscarinic Agonist

Fabio Riefolo, Carlo Matera, Aida Garrido-Charles, Alexandre M. J. Gomila, Rosalba Sortino, Luca Agnetta, Enrique Claro, Roser Masgrau, Ulrike Holzgrabe, Montserrat Batlle, Michael Decker, Eduard Guasch, and Pau Gorostiza

#### Table of content

1. Chemical synthesis
2. Photochemical characterization
3. NMR spectroscopy and mass spectrometry
4. In vitro calcium imaging experiments
5. Molecular docking simulations
6. *In vivo* experiments in rats
7. *In vivo* experiments in *X. tropicalis* tadpoles
8. Additional references

## 1. Chemical synthesis

### 1.1 Materials and methods

All reagents and solvents were purchased from Sigma-Aldrich and Serviquimia and were used without any further purification. All reactions were performed under inert atmosphere of argon or nitrogen, unless differently stated. TLC analyses were performed on commercial silica gel 60 F<sub>254</sub> aluminium foils (Merck); spots were further evidenced by spraying with a dilute alkaline potassium permanganate solution or a phosphomolybdic acid solution 5% in ethanol and, for tertiary amines and quaternary ammonium compounds, with the Dragendorff reagent. Flash chromatography was performed on PanReac AppliChem silica gel 60 (40-63 microns) as stationary phase; mobile phases are specified for each compound. UV/Vis spectra and experiments were recorded with a Shimadzu UV-1800 UV-VIS Spectrophotometer with standard quartz cuvettes (10 mm light path). <sup>1</sup>H-NMR, <sup>13</sup>C-NMR, COSY and HSQC spectra were registered with a Varian Mercury 400 MHz instrument (400 MHz for <sup>1</sup>H-NMR and 101 MHz for <sup>13</sup>C-NMR) in DMSO-*d*<sub>6</sub>, CDCl<sub>3</sub>, CD<sub>3</sub>OD. Residual signals of the deuterated solvents were used as an internal standard (DMSO-*d*<sub>6</sub>: <sup>1</sup>H 2.50 ppm, <sup>13</sup>C 39.52 ppm; CDCl<sub>3</sub>: <sup>1</sup>H 7.26 ppm, <sup>13</sup>C 77.16 ppm; CD<sub>3</sub>OD: <sup>1</sup>H 3.31 ppm, <sup>13</sup>C 49.00 ppm). Chemical shifts ( $\delta$ ) are expressed as parts-per-million (ppm) and coupling constants (*J*) as hertz (Hz). HPLC analyses and purification were performed with a Waters Alliance e2695 Separations Module, equipped with a Waters 2998 UV/Vis Photodiode Array Detector and a Waters ACQUITY QDa Mass Detector for detecting the analytes and a XSelect CSH C18 OBD Prep Column (130Å, 5  $\mu$ m, 10 mm X 150 mm, 1/pkg, Waters). Water with 0.1% formic acid (v/v) and acetonitrile with 0.1% formic acid (v/v) were used as mobile phases (named A and B, respectively) with the following gradient: concentration phase B: 5→25% from 0 to 4 min; 25% from 4 to 7 min; 25→100% from 7 to 9 min; 100→5% from 9 to 11 min; 5% from 11 to 12 min. The flow rate was of 3 mL min<sup>-1</sup>. The purity of PAI compound was found to be  $\geq$ 95%. High resolution mass spectroscopy measurements (ionization: NanoESI, positive ionization) were performed at the mass spectrometry core facility of the IRB (Barcelona, Spain) with a LTQ-FT Ultra (Thermo Scientific) for direct infusion (Automated Nanoelectrospray) of the sample. The NanoMate (AdvionBioSciences, Ithaca, NY, USA) aspirated the samples from a 384-well plate (protein Lobind) with disposable, conductive pipette tips, and infused the samples through the nanoESI Chip (which consists of 400 nozzles in a 20 x20 array) towards the mass spectrometer. Spray voltage was 1.70 kV and delivery pressure was 0.50 psi. Data are reported as mass-to-charge ratio (*m/z*) of the corresponding positively charged molecular ions.

### 1.2 Abbreviations

**Solvents:** AcOEt: ethyl acetate; DCM: dichloromethane; MeCN: acetonitrile; MeOH: methanol; EtOH: ethanol; THF: tetrahydrofuran; Et<sub>2</sub>O: diethyl ether; iPr<sub>2</sub>O: diisopropyl ether; DMSO: dimethylsulfoxide.

**Analytical characterizations:** NMR: d: doublet; dd: double doublet; ddd: double double doublet; dt: double triplet; m: multiplet; q: quartet; quin: quintet; s: singlet; t: triplet; m.p.: melting point;  $R_f$ : retention factor; r.t.: room temperature; RT: retention time.

### 1.3 Synthetic procedures

**4,4'-Bis(bromomethyl)azobenzene (4).** A solution 4,4'-dimethylazobenzene **3** (1.10 g, 5.23 mmol), prepared as reported by Velema et al.,<sup>4</sup> and N-bromosuccinimide (2.33 g, 13.08 mmol) in MeCN (200 mL) was stirred at room temperature under white light illumination (Dolan-Jenner Fiber-Lite Mi-150 Fiber Optic Illuminator, 150 W) for 24 hours. Then, the mixture was concentrated, and the obtained orange solid was filtered and washed several times with MeOH. The resulting solid was dried under vacuum to afford **4** as an orange solid (1.34 g, 96% yield). M.p.: 228-230 °C. <sup>1</sup>H NMR (400 MHz, CDCl<sub>3</sub>): δ 7.90 (d, J = 8.4 Hz, 4H), 7.54 (d, J = 8.3 Hz, 4H), 4.56 (s, 4H). <sup>13</sup>C NMR (101 MHz, CDCl<sub>3</sub>): δ 152.42, 140.93, 130.06, 123.51, 32.83.

**N-(4-((4-(bromomethyl)phenyl)diazenyl)benzyl)-3-(1,3-dioxoisindolin-2-yl)-N,N-dimethylpropan-1-aminium bromide (7).** Azobenzene **4** (713 mg, 1.94 mmol) was completely dissolved in toluene (200 mL) at 70 °C, and the resulting solution was left under stirring at 50 °C. Then a solution of phthalimide **5** (50 mg, 0.22 mmol) in MeCN (50 mL) was slowly added dropwise. The reaction was left under stirring for 24 hours at 50 °C. Reaction progress was controlled by silica gel TLC to monitor the disappearance of the starting material **5** (eluent: DCM/MeOH, 95:5). At the end, the mixture was concentrated under reduced pressure and the resulting solid was washed several times with toluene in order to completely remove the excess azobenzene **4** and finally dried under reduced pressure to afford **7** as an orange solid (79 mg, 61%). <sup>1</sup>H NMR (400 MHz, CD<sub>3</sub>OD): δ 7.98 – 7.89 (m, J = 8.8 Hz, 4H), 7.87 (dd, J = 5.5, 3.1 Hz, 2H), 7.80 (dd, J = 5.5, 3.1 Hz, 2H), 7.74 (d, J = 8.5 Hz, 2H), 7.64 (d, J = 8.4 Hz, 2H), 4.68 (s, 2H), 4.67 (s, 2H), 3.83 (t, J = 6.3 Hz, 2H), 3.48 – 3.40 (m, 2H), 3.14 (s, 6H), 2.37 – 2.25 (m, 2H). <sup>13</sup>C NMR (101 MHz, CD<sub>3</sub>OD): δ 169.80, 154.98, 153.39, 143.78, 135.57, 135.15, 133.32, 131.29, 124.42, 124.35, 124.32, 68.52, 63.12, 50.81, 35.66, 33.00, 23.53. LC-MS (QMS, [M + H]<sup>+</sup>): calcd for C<sub>27</sub>H<sub>28</sub>BrN<sub>4</sub>O<sub>2</sub><sup>+</sup>, 519.14 and 521.14; found 519.3 and 521.2.

**(E)-N-(4-((4-(bromomethyl)phenyl)diazenyl)benzyl)-3-(1,3-dioxo-1H-benzo[de]isoquinolin-2(3H)-yl)-N,N,2,2-tetramethylpropan-1-aminium bromide (8).** Azobenzene **4** (276 mg, 0.75 mmol) was completely dissolved in toluene (30 mL) at 70 °C, and the resulting solution was left under stirring at 50 °C. Then a solution of Naphthalimide **6** (25 mg, 0.08 mmol) in MeCN (20 mL) was slowly added dropwise. The reaction was left under stirring for 24 hours at 50 °C. Reaction progress was controlled by silica gel TLC to monitor the disappearance of the starting material **6** (eluent: DCM/MeOH, 95:5). At the end, the mixture was concentrated under reduced pressure and the resulting solid was washed several times with toluene in order to completely remove the excess azobenzene **4** and finally dried under reduced pressure to afford **8** as an orange solid (10 mg, 86%). <sup>1</sup>H NMR (400 MHz, CD<sub>3</sub>OD): δ 8.56 (dd, J = 7.3, 1.1 Hz, 2H), 8.35 (dd, J = 8.5, 1.0 Hz, 2H), 7.95 (dd, J = 8.4, 3.2 Hz, 4H), 7.85 – 7.74 (m, 4H), 7.66 (d, J = 8.7 Hz, 2H), 4.73 (s, 2H), 4.68 (s, 2H), 4.30 (s, 2H), 3.55 (s, 2H), 3.32 (s, 6H), 1.41 (s, 6H). <sup>13</sup>C NMR (101 MHz, CD<sub>3</sub>OD): δ

165.21, 153.44, 151.99, 142.34, 134.31, 134.23, 131.73, 131.23, 130.17, 129.89, 127.85, 126.81, 122.99, 122.84, 122.10, 72.62, 71.92, 51.06, 49.04, 39.16, 31.60, 25.31.

**Phthalimide-Azo-Iperoxo, PAI (1).** Compound **7** (50.4 mg, 0.08 mmol) and the isoxazoline **9** (30.6 mg, 0.17 mmol) were dissolved in MeCN (30 mL) and stirred at room temperature for 12 hours. Reaction progress was controlled by silica gel TLC to monitor the disappearance of the starting material **7** (eluent: DCM/MeOH, 9:1). PAI (**1**) was then isolated from the resulting solution by precipitation after adding a few drops of Et<sub>2</sub>O to the reaction mixture, filtered, further washed with Et<sub>2</sub>O (20 mL x 3), and dried under reduced pressure (53 mg, 81%). <sup>1</sup>H NMR (400 MHz, CD<sub>3</sub>OD) δ 8.10 (d, J = 8.5 Hz, 2H), 8.02 (d, J = 8.5 Hz, 2H), 7.90 (dd, J = 5.6, 3.0 Hz, 2H), 7.85 (d, J = 8.5 Hz, 2H), 7.82 (dd, J = 5.6, 3.0 Hz, 2H), 7.75 (d, J = 8.5 Hz, 2H), 4.99 (t, J = 1.6 Hz, 2H), 4.74 (s, 2H), 4.64 (s, 2H), 4.41 (t, J = 9.6 Hz, 2H), 4.35 (t, J = 1.7 Hz, 2H), 3.84 (t, J = 6.3 Hz, 2H), 3.47 – 3.38 (m, 2H), 3.22 (s, 6H), 3.11 (s, 6H), 3.07 (t, J = 9.6 Hz, 2H), 2.37 – 2.24 (m, 2H). <sup>13</sup>C NMR (101 MHz, CD<sub>3</sub>OD) δ 169.79, 168.80, 163.40, 163.05, 162.71, 154.99, 154.83, 135.56, 135.28, 124.70, 124.54, 124.31, 88.78, 76.82, 71.22, 68.47, 67.39, 63.24, 58.29, 54.94, 50.90, 50.76, 35.65, 33.66, 23.51. RT (HPLC-PDA) = 6.24 min (*cis* isomer), 6.67 min (*trans* isomer); purity ≥ 95% (**Figure S1.1**). HR-MS (ESI, [M + H]<sup>+</sup>): calcd for C<sub>36</sub>H<sub>42</sub>N<sub>6</sub>O<sub>4</sub><sup>2+</sup>, 311.16; found 311.1625 (**Figure S1.2**).

**Naphthalimide-Azo-Iperoxo, NAI (2).** Compound **8** (10 mg, 0.015 mmol) and the isoxazoline **9** (4.03 mg, 0.022 mmol) were dissolved in MeCN (10 mL) and stirred at room temperature for 12 hours. Reaction progress was controlled by silica gel TLC to monitor the disappearance of the starting material **8** (eluent: DCM/MeOH, 9:1). NAI (**2**) was then isolated from the resulting solution by precipitation after adding a few drops of Et<sub>2</sub>O to the reaction mixture, filtered, further washed with Et<sub>2</sub>O (20 mL x 3), and dried under reduced pressure (6.10 mg, 48%). <sup>1</sup>H NMR (400 MHz, CD<sub>3</sub>OD) δ 8.58 (dd, J = 7.3, 1.1 Hz, 2H), 8.37 (dd, J = 8.4, 1.1 Hz, 2H), 8.11 (d, J = 8.4 Hz, 2H), 8.01 (d, J = 8.4 Hz, 2H), 7.89 (d, J = 8.4 Hz, 2H), 7.86 – 7.77 (m, 4H), 4.99 (s, 2H), 4.79 (s, 2H), 4.76 (s, 2H), 4.48 – 4.38 (m, 4H), 4.31 (s, 2H), 3.58 (s, 2H), 3.33 (s, 6H), 3.25 (s, 6H), 3.07 (t, J = 9.6 Hz, 2H), 1.42 (s, 6H). <sup>13</sup>C NMR (101 MHz, CD<sub>3</sub>OD) δ 168.82, 166.66, 155.00, 154.76, 135.79, 135.75, 135.41, 133.18, 132.66, 132.20, 131.85, 129.31, 128.26, 124.68, 124.46, 123.57, 88.70, 76.94, 74.28, 73.17, 71.23, 67.39, 58.35, 55.01, 52.53, 50.96, 50.48, 40.63, 33.69, 26.73. HR-MS (ESI, [M + H]<sup>+</sup>): calcd for C<sub>36</sub>H<sub>42</sub>N<sub>6</sub>O<sub>4</sub><sup>2+</sup>, 350.18; found 350.18630.

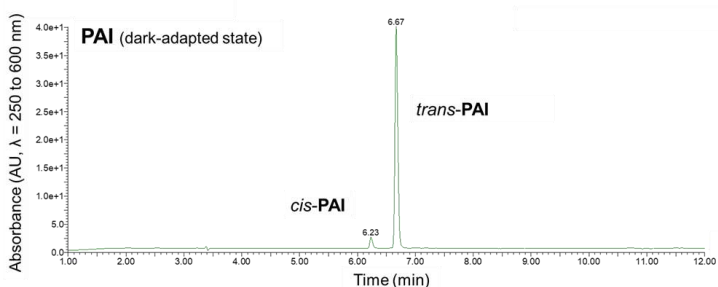


**Figure S1.1.** HPLC chromatogram of PAI as obtained under benchtop conditions (PDA detector from 250 to 600 nm; compound purity ≥ 95%).

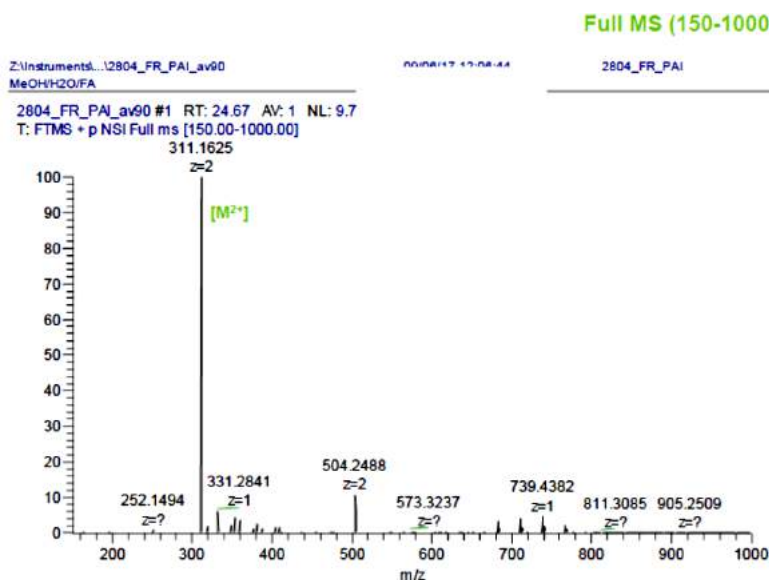
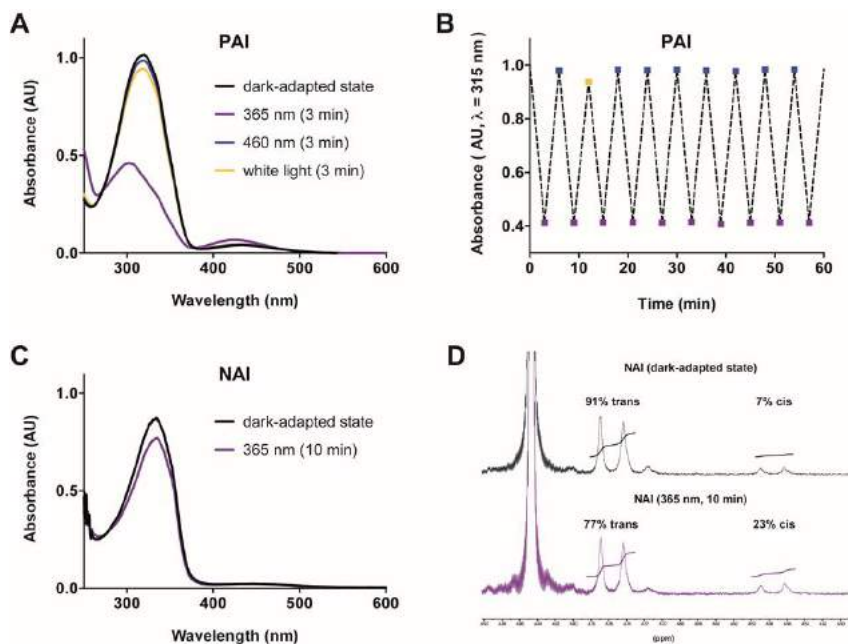


Figure S1.2. Full high-resolution mass spectrum of PAI (positive ionization).

## 2. Photochemical characterization

An essential requirement for using PAI and NAI as light-regulated M2 mAChRs agonists is that they effectively respond to light, which means that they can be quickly photoisomerized (from *trans* to *cis* and vice versa) between two different conformations with a relatively high degree of photoconversion (*trans/cis* ratio). To this end, we characterized PAI and NAI by UV/Vis spectroscopy. PAI revealed a clear photochromic behavior with the typical absorption bands of azobenzenes. Maximum absorption peaks in aqueous solution were observed at around 315 nm and 430 nm and are due to the  $\pi-\pi^*$  and  $n-\pi^*$  transitions, respectively, which allows for distinct photoswitching between the *trans* and *cis* isomers (Figure S2.1, panel A). PAI can be effectively isomerized from *trans* to *cis* with ultraviolet light (365 nm), and back-isomerized from *cis* to *trans* with white or blue (460 nm) light. The process is reversible and can be repeated several times without any noticeable loss of photochromic behavior (Figure S2.1, panel B). Annoyingly, NAI resulted unusually refractory to photoisomerization than other azobenzene-containing compounds. We hypothesized that the absorption and emission properties of the naphthalimide moiety could interfere with the photoisomerization of the azobenzene unit (Figure S2.1, panels C and D).



**Figure S2.1.** Photochemical characterization of PAI and NAI. **A)** Absorption spectra of PAI in H<sub>2</sub>O (30 μM). **B)** Reversibility and stability of the photochromic behavior of PAI over several cycles of isomerization. **C)** Absorption spectra of NAI in H<sub>2</sub>O (30 μM). **D)** Quantification of NAI photostationary state by <sup>1</sup>H-NMR analysis (800 μM in CD<sub>3</sub>OD), showing the ratio between the two isomers in the dark-adapted state and after illumination with 365 nm light (10 min).

We next quantified by <sup>1</sup>H-NMR and HPLC analysis the extent of photoisomerization for PAI (**Figure S2.2**). The amount of the thermodynamically less stable *cis* isomer shifted from an initial value of 13% (as obtained under benchtop conditions) to 73% upon irradiation with 365 nm light for 10 minutes. Finally, we analyzed the thermal stability of the photostationary state (PSS) achieved after ultraviolet illumination. The PSS was relatively stable for at least 2 hours in aqueous solution at 37 °C in the dark. PAI could be rapidly reconverted to the *trans* state after illumination with white light. Such thermal stability allowed us to conveniently study the two different photostationary states of PAI in a relatively large timescale (**Figure S2.3**).

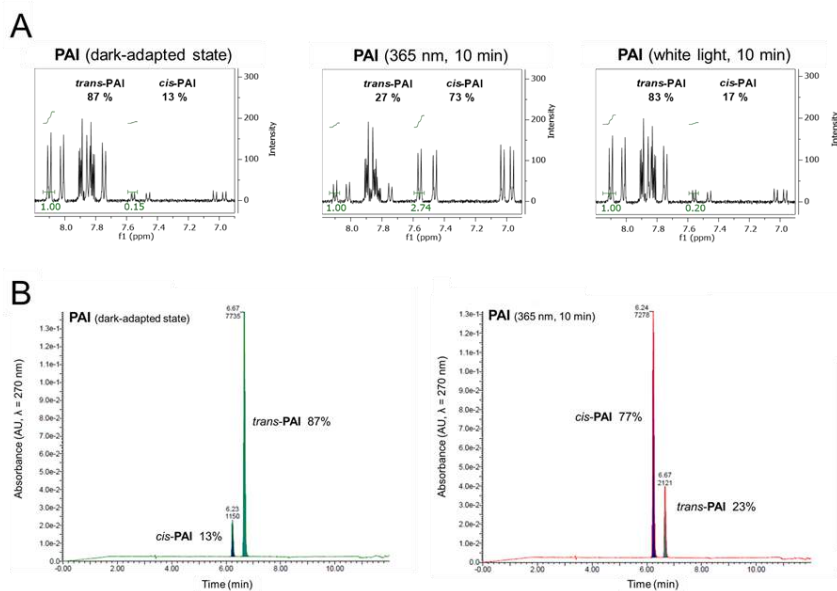


**Figure S2.2.** Quantification of PAI photostationary state by  $^1\text{H-NMR}$  ( $800\ \mu\text{M}$  in  $\text{CD}_3\text{OD}$ , panel **A**) and HPLC (panel **B**) analysis, showing the ratio between the two isomers as obtained under benchtop conditions and after 10 minutes of irradiation with 365 nm light and white light.

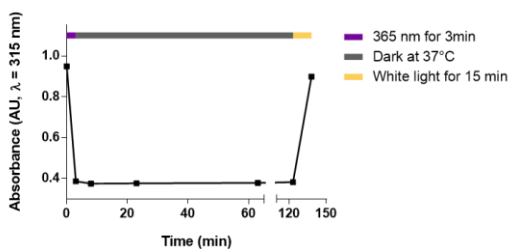


**Figure S2.3.** Thermal stability of PAI. The photostationary state achieved after irradiation with 365 nm light in aqueous solution ( $30\ \mu\text{M}$ ) is stable for more than 2 hours at  $37\ ^\circ\text{C}$  in the dark. Irradiation with white light allows to rapidly regain a PSS in favor of the *trans* isomer.

### 3. NMR spectroscopy

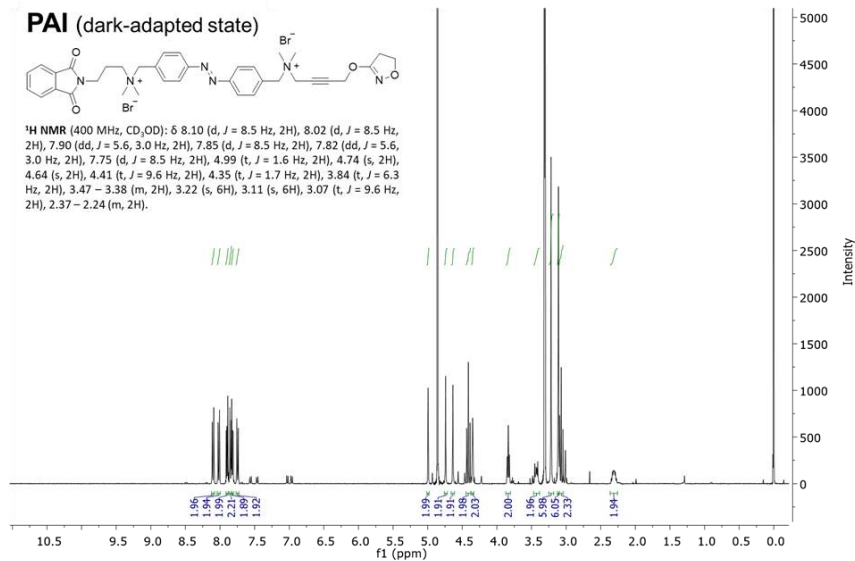


Figure S3.1. <sup>1</sup>H-NMR of PAI as obtained under benchtop conditions.

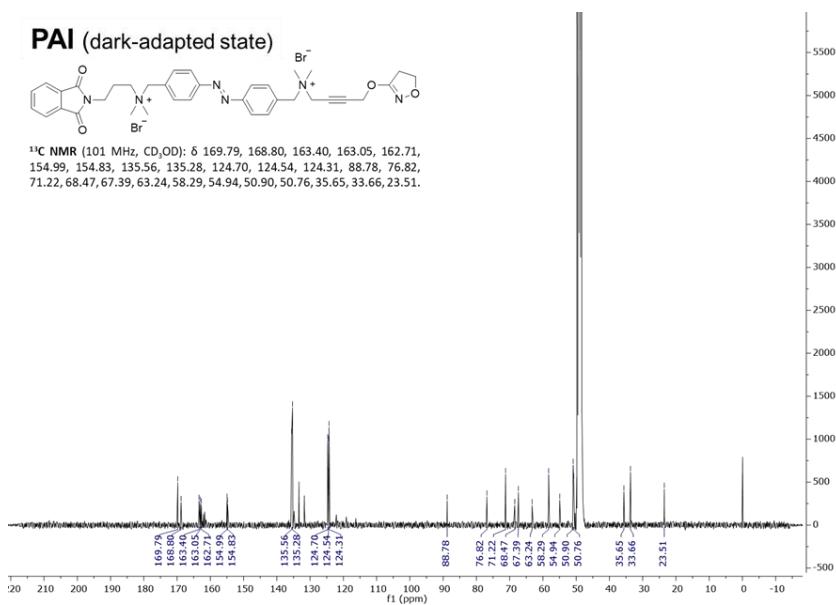
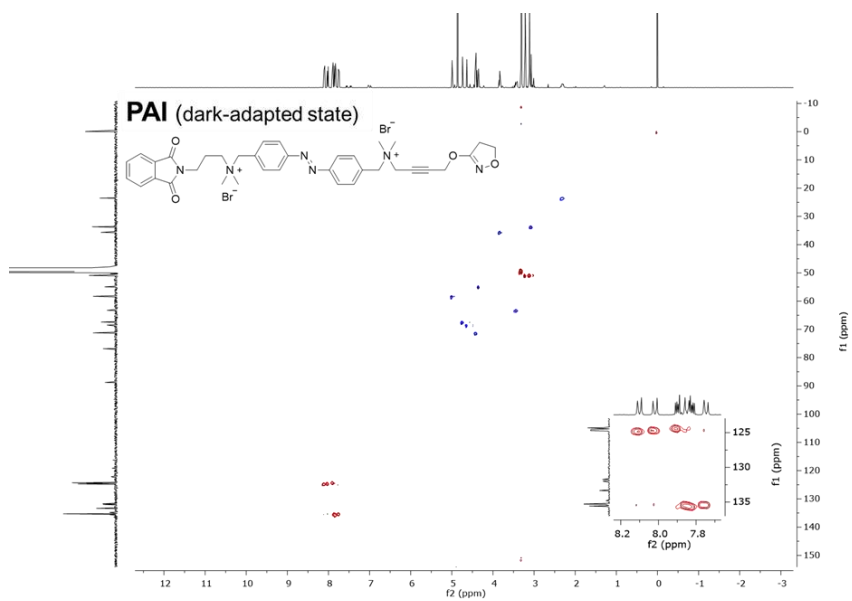
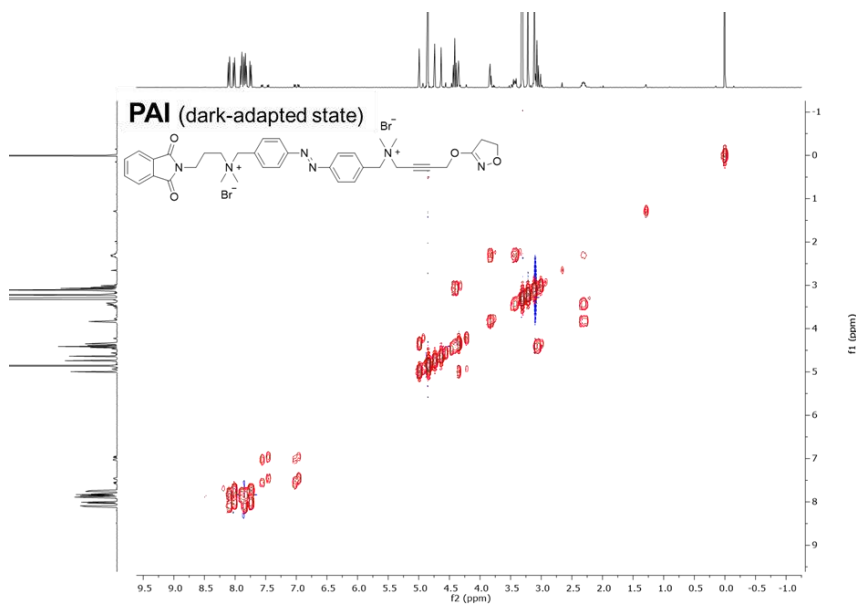


Figure S3.2. <sup>13</sup>C-NMR of PAI as obtained under benchtop conditions.



**Figure S3.3.** HSQC of PAI as obtained under benchtop conditions.



**Figure S3.4.** gCOSY of PAI as obtained under benchtop conditions.

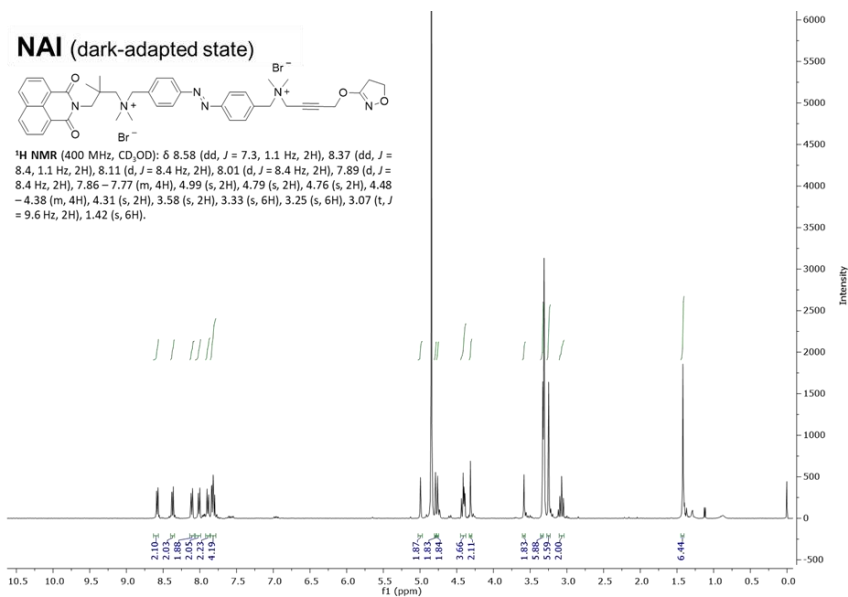


Figure S3.5. <sup>1</sup>H-NMR of NAI as obtained under benchtop conditions.

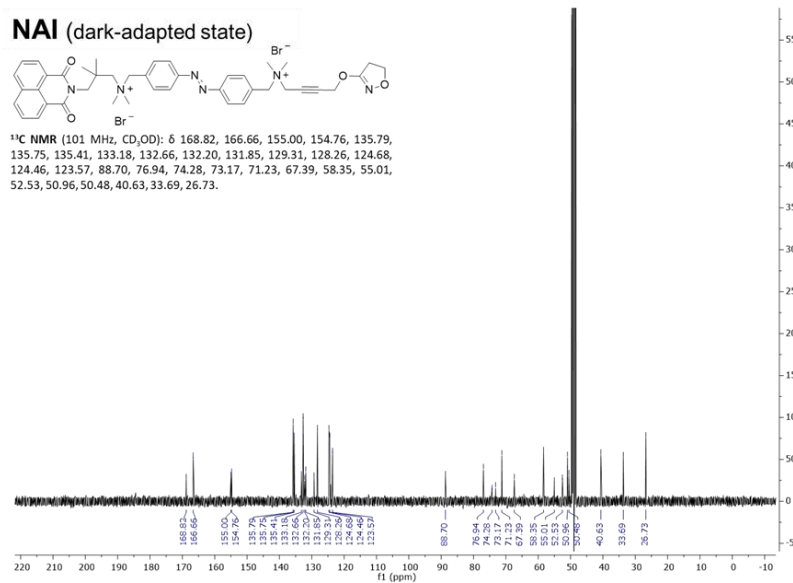


Figure S3.6. <sup>13</sup>C-NMR of NAI as obtained under benchtop conditions.

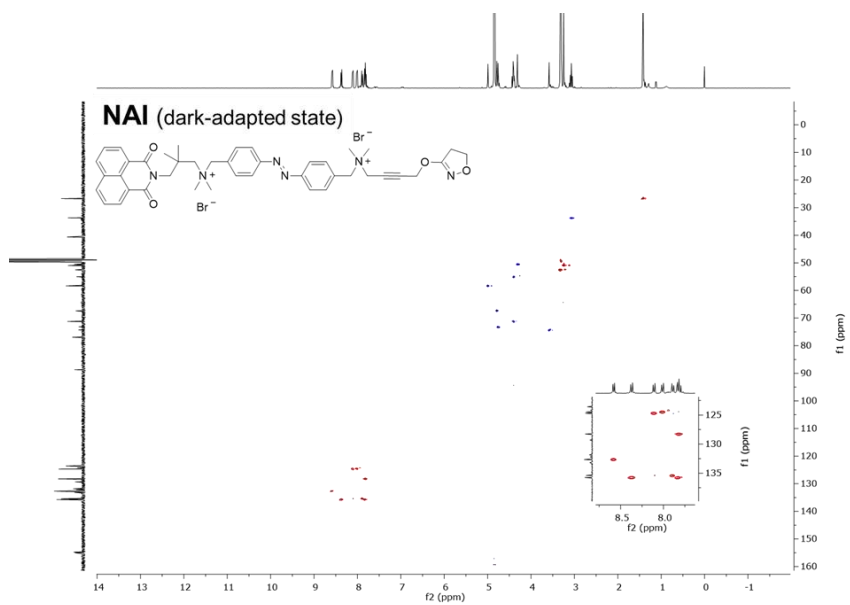


Figure S3.7. HSQC of NAI as obtained under benchtop conditions.

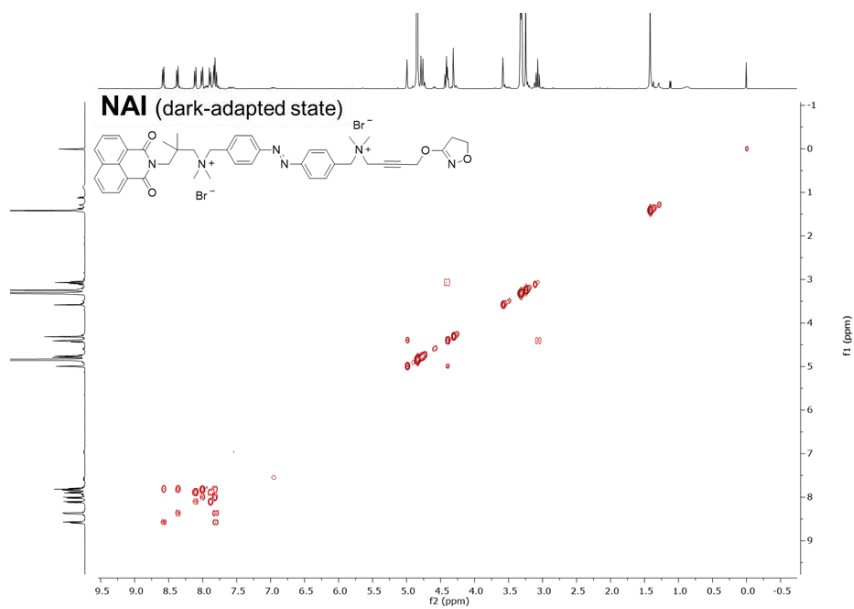


Figure S3.8. gCOSY of NAI as obtained under benchtop conditions.

## 4. *In vitro* calcium imaging experiments

### 4.1 Materials and methods

Since M2 mAChRs activate the  $G_i$  protein subfamily, we co-transfected a chimeric  $G_{q/i}$ -protein in order to couple M2 receptor activation to the phospholipase C pathway, thus inducing inositol 1,4,5-trisphosphate (IP3) production and subsequent intracellular calcium release from the endoplasmic reticulum.

**Cell culture and transfection.** HEK tsA201 cells were maintained at 37 °C in a humidified atmosphere with 5%CO<sub>2</sub> and grown in Dulbecco's Modified Eagle's Medium/Nutrient Mixture F-12 Ham (DMEM/F12 1:1, Life Technologies) medium, supplemented with 10% fetal bovine serum (FBS, Life Technologies) and antibiotics (1% penicillin/streptomycin, Sigma-Aldrich). Co-expression of human muscarinic acetylcholine receptor M2 (Addgene) and chimeric  $G_i/G_q$  protein (GqTOP) (ratio 1:1) was induced by plasmid transient transfection with X-tremeGENE 9 DNA Transfection Reagent (Roche Applied Science) following the manufacturer's instructions.<sup>5</sup> The day after transfection, cells were harvested with accutase (Sigma-Aldrich) and seeded onto 16-mm glass coverslips (Fisher Scientific) pretreated with collagen (Sigma-Aldrich) to allow cell adhesion. Preconfluent cultures were used for experiments between 48 h and 72 h after transfection.

***In vitro* single-cell calcium imaging.** The bath solution used for single cell intracellular calcium recordings contained: 140 mM NaCl, 5.4 mM KCl, 1 mM MgCl<sub>2</sub>, 10 mM HEPES, 10 mM glucose and 2 mM CaCl<sub>2</sub>, and was adjusted to pH 7.4 with NaOH. Before each experiment, cells were mounted on the recording chamber (Open Diamond Bath Imaging Chamber for Round Coverslips from Warner Instruments) and loaded with the calcium indicator Oregon Green BAPTA-1, AM (OGB-1AM) (Life Technologies) for 30 min at 37 °C and 5% CO<sub>2</sub>, at a final concentration of 10 μM in Ca<sup>2+</sup>-free bath solution. Cells were rinsed with fresh solution, and the recording chamber was filled with 1 mL recording solution. Calcium imaging was performed on an IX71 inverted microscope (Olympus) with a XLUMPLFN 20XW x20/1-NA water immersion objective (Olympus). OGB-1 AM was excited during 8 ms at 488 nm using a Polychrome V monochromic light source (Till Photonics) equipped with a Xenon Short Arc lamp (Ushio) and a 505 nm dichroic beam splitter (Chroma Technology). Emission at 526 nm was filtered by a D535/40nm emission filter (Chroma Technology) and finally collected by a C9100-13 EM-CCD camera (Hamamatsu). Images under 1P-illumination were acquired at room temperature with an imaging interval of 4 seconds with the SmartLux software (HEKA), and the imaging analysis was done with FIJI (ImageJ). Images under 2P-illumination were acquired at room temperature with an inverted laser-scanning confocal microscope (TCS SP5, Leica Microsystems) equipped with a HCX PL APO 40x/1.25-0.75-NA oil objective for imaging cultured cells, and a HC PL APO 20x/0.7-NA CS air objective (Leica Microsystems). The imaging interval was of 4 seconds. Acquired image sequences were stored in the Leica image format and stacks for offline analysis with FIJI (ImageJ).

**Drug application and photoswitching assays.** Addition of agonists was carried out by carefully pipetting 50 μL of the initial 200 pM solution of the compound directly into the

accessory pool of the recording chamber for a final dilution of approximately 1:20. Iperoxo, a previously described muscarinic selective superagonist,<sup>2</sup> was used as a positive control to stimulate mAChRs in HEK tsA201 cells (30 pM). Photostimulation under 1P-excitation during recordings was done by illumination of the entire focused field using the Polychrome V connected to a personal computer, and shutter and wavelength were controlled using Patchmaster software (HEKA). Light intervals lasted a total of 5 minutes for all the HEK cell experiments, with flashes of blue (460 nm, 3.5-seconds duration) and UV (365 nm, 3.5-seconds duration) light. The light power measured with a Newport 1916-C light meter placed after the objective was  $16.48 \text{ W}\cdot\text{m}^{-2}$  for 488 nm,  $4.94 \text{ W}\cdot\text{m}^{-2}$  for 365 nm, and  $15.92 \text{ W}\cdot\text{m}^{-2}$  for 460 nm. 2P-excitation experiments were performed in the Advanced Digital Microscopy Core Facility of IRB Barcelona with a confocal multiphoton microscope equipped with a pulsed broadband Ti:Sapphire laser (Mai Tai, Spectra-Physics, Santa-Clara, CA-USA) which can be tuned from 710-990 nm (80 MHz repetition rate, 80 fs pulse, light power  $2.8 \text{ mW } \mu\text{m}^{-2}$  at 720–840 nm).

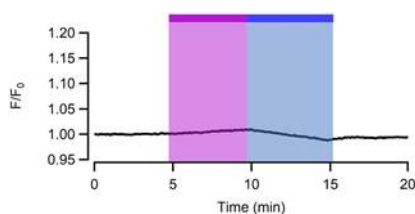


**Figure S4.1.** Real time calcium imaging traces from HEK cells incubated with  $10 \mu\text{M}$  of OGB-1AM for 30 min. The diagrams show **A**) the average trace of cells expressing M2-GqTOP in response to illumination at 365 nm (purple bar) and 460 nm (blue bar) ( $n = 34 \pm \text{SEM}$ ); **B**) the average trace of cells expressing M2-GqTOP in response to 2P-excitation at 840 nm (red bar) ( $n = 29 \pm \text{SEM}$ );

### 4.3 Receptor activation efficacy

Direct *cis*-PAI isomer application at 10 pM induce a response 50% lower than direct application of *trans*-PAI isomer. Application of the *cis* isomer at 30 pM induced a response 10-fold lower compared to the *trans* isomer response at the same concentration (**Figure S4.2**). Moreover, residual responses upon application of the *cis* isomer can be attributed to the incomplete photoisomerization of the *trans*-isomer (*trans/cis* = 23:77 after 10 min at 365 nm).

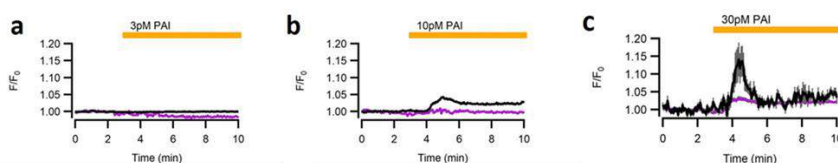


**Figure S4.2.** Real time calcium imaging traces from HEK cells expressing M2-GqTOP incubated with OGB-1AM (10  $\mu$ M for 30 min). A) Average trace of cell response induced by the direct application of 3 pM PAI (yellow bar) in its *trans* isoform (black line;  $n = 167$ ) or its *cis* isoform (purple line;  $n = 150$ ). B) Average trace of cell response induced by the direct application of 10 pM PAI in its *trans* isoform (black line;  $n = 296$ ) or its *cis* isoform (purple line;  $n = 150$ ). C) Average trace of cell response to 30 pM PAI in its *trans* isoform (black line;  $n = 8$ ) or its *cis* isoform (purple line;  $n = 230$ ). Gray shadow in the recording represents  $\pm$  SEM.

### 4.3 Receptor subtype selectivity

Receptor subtype-selectivity of PAI (M2 against M1 mAChRs) has been studied by comparing amplitude of calcium signal response of cells expressing M2-GqTOP or M1 mAChR in presence of *trans*-PAI (10 pM). Human M1 mAChR (Addgene) was transfected as described in the *Materials and methods* section of the main text. M2 mAChR transfected cells gave a significantly higher response than M1 mAChR expressing cells (8% for M1 against 33% for M2). Data were normalized over the maximum response obtained with the nonselective orthosteric superagonist IPX at 30 pM. (*t*-test of two samples assuming equal variances  $p = 0.00158$ ).

## 5. Molecular docking simulations

### 5.1 Materials and methods

Molecular docking simulations were performed using the crystal structure of the human M2 muscarinic acetylcholine receptor retrieved from the Protein Data Bank (PDB code: 4MQT, chain A).<sup>6</sup> To allow the docking of the dualsteric ligands into the active M2 AChR structure, the so called “tyrosine lid”<sup>7,8</sup> was remodeled using rotamer libraries (UCSF Chimera)<sup>9</sup> of the tyrosine residues involved (Tyr-104, Tyr-403, Tyr-426). The protein pdb file was then prepared for docking by removing co-crystallized ligands, non-complexed ions and water molecules, and finally applying the Dock Prep tool available in the free software package UCSF Chimera. This involved the addition of hydrogens and assigning partial charges (AMBER ff14SB method). The structures of *trans*- and *cis*-PAI were built with standard bond length and angles using ChemDraw and then energy minimized with Chem3D by the MM2 method. The minimized compounds were further prepared for docking studies with UCSF Chimera by adding hydrogens and assigning partial charges (AMBER ff14SB method). The necessary pdbqt files of ligands and receptor were prepared using AutoDock 4.2 software. The docking studies were carried out using the standard docking protocol applied for AutoDock Vina in PyRx 0.8 virtual screening software.

Autodock Vina has been reported to be an effective tool capable of quickly and accurately predicting bound conformations and binding energies of ligands with macromolecular targets.<sup>10,11</sup> A grid box of size 10.08 × 27.44 × 28.96 Å, with x, y and z coordinates of -2.98, -11.92 and -12.00, respectively, was fixed to cover the entire allosteric and orthosteric binding sites and accommodate the ligands to move freely. Docking studies were performed using an exhaustiveness value of 8 while all other parameters were maintained as defaults. All rotatable bonds within the ligands were allowed to rotate freely, and the receptor was considered rigid. The docking simulations were repeated three times for each ligand. The obtained poses were then ranked based on the predicted affinity docking scores (kcal/mol) and the best pose for each experiment was selected. The results were then analyzed using UCSF Chimera.

## 5.2 Results and discussion

We used molecular docking simulations in an attempt to rationalize the photoswitchable efficacy of PAI. Both isomers of the ligand were docked into their putative allosteric and orthosteric binding sites of the human M2 muscarinic acetylcholine receptor in its active conformation (PDB code: 4MQT, chain A). As previously reported,<sup>7</sup> molecular docking of dualsteric ligands into the M2 mAChR required remodeling of the tyrosine lid (formed by Tyr-104, Tyr-403 and Tyr-426) which separates the orthosteric binding site from the allosteric binding site in the active conformation of the protein. To open this lid and put the two binding sites in communication, we selected different allowed conformers of each side chains while keeping all the other residues in their original position. Therefore, the only differences between the crystal structure and the obtained active-like receptor model were the side chain conformations of Tyr-104, Tyr-403 and Tyr-426. *Trans*-PAI and *cis*-PAI were docked at this receptor model using a standard docking protocol with AutoDock Vina in the PyRx 0.8 software with a suitable grid box. We ran three simulations for each ligand and selected the best pose obtained in each experiment based on the predicted binding affinity scores (kcal/mol). Best poses were superimposed into the M2 receptor model in the presence of the reference agonist Iperoxo (in its receptor-bound conformation) and analyzed using UCSF Chimera. The results of our *in silico* studies are presented in **Table S1** and **Figure S5.1**. In Iperoxo, key binding elements for agonist activity are (a) the positively charged nitrogen, which interacts with Asp-103 and displays  $\pi$ -cation interactions with Tyr-104, Tyr-403 and Tyr-426, (b) the triple bond, which exhibits hydrophobic contacts with Tyr-104, Trp-155 and Trp-400, and additionally (c) the oxygen of the 4,5-dihydroisoxazole moiety, which forms a hydrogen bond with Asn-404.<sup>8</sup> Our simulations revealed a dualsteric binding topography of PAI in both configurations. The Iperoxo moiety of *trans*-PAI binds to the orthosteric binding site, with an orientation close to that observed for Iperoxo in the receptor-bound crystal structure and the key elements for agonist activity lying in proximity of those of the reference agonist, whereas the phthalimide moiety protrudes toward extracellular domains, likely engaging residues of the common allosteric binding site (**Figure S5.1a**). In agreement with our results, *trans*-PAI could therefore bind to the M2 mAChR in a dualsteric pose capable of inducing receptor activation. In contrast, *cis*-PAI appeared to bind preferentially in a flipped orientation, with the phthalimide group pointing out towards the orthosteric binding pocket and the 4,5-dihydroisoxazole moiety positioned in the allosteric binding site. Such a binding mode is not likely to form an active ligand-receptor complex and may justify the difference observed in terms of agonist efficacy between the two photo-isomers (**Figure S5.1b**).

experiment number	<i>trans</i> -PAI (best pose)	<i>cis</i> -PAI (best pose)
	<b>binding affinity (kcal/mol)</b>	
1	-11.6	-12.0
2	-11.6	-11.8
3	-11.3	-11.6

**Table S1.** Binding affinity scores of the best poses for each of the docking studies performed with *trans*- and *cis*-PAI.

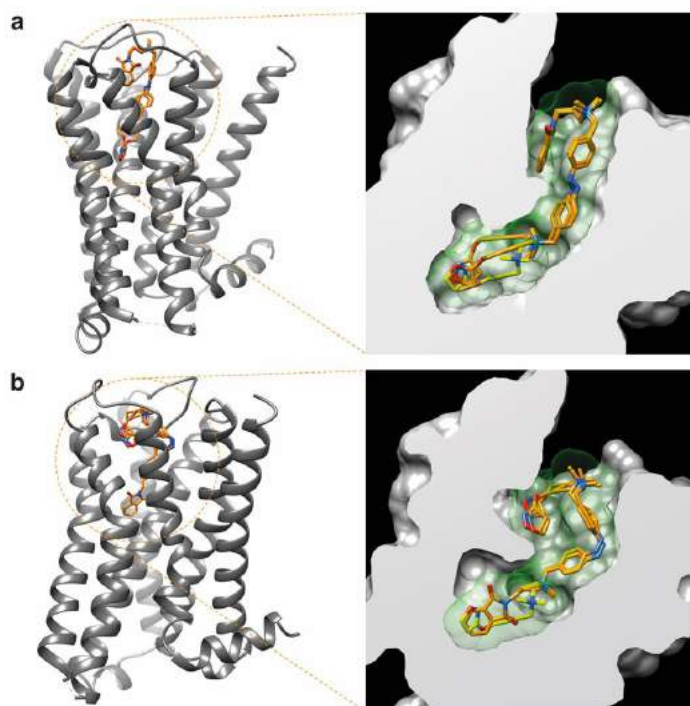


**Figure S5.1** Hypothetical binding mode of *trans*-PAI and *cis*-PAI to a M2 mAChR model in its active state. Panels (a) and (b) show a full view (left side, ribbon-style representation) and a zoomed view (right side, hydrophobicity surface representation with sectioning) of the simulated ligand-receptor complexes. The reference orthosteric agonist Iperoxo, in yellow, appears in its receptor-bound conformation. *Trans* and *cis*-PAI are represented in orange. Nitrogen and oxygen atoms of the ligands are colored in blue and red, respectively. Our simulations revealed a dualsteric binding topography of PAI for both configurations, but, while the *trans* isomer seems to bind preferentially in an Iperoxo-like binding pose (Panel a), which is likely able to trigger receptor activation, the *cis* isomer shows preference for a flipped orientation (Panel b), which might be not compatible with the formation of active ligand-receptor complexes.

## 6. *In vivo* experiments in rats

### 6.1 Materials and methods

*In vivo* effects of PAI in both configurations (*trans* and *cis*) were further tested in male Wistar rats (400-500 g) under inhaled anesthesia (isoflurane 1.5%) and maintained at  $37\pm 0.3$  °C with a homothermic pad (Kent Scientific, Torrington, CT, US). All animals had a continuous electrocardiogram (ECG) obtained (lead II) and recorded for later offline analyses (PowerLab and LabChart v.8.1.2, ADInstruments, Colorado Springs, CO, US). Analyses were performed in a blinded manner. Nine rats were randomly assigned to receive cumulative doses of either predominantly *trans*- (“*trans*” group, n = 5) or *cis*-isomer (“*cis*” group n = 4) PAI. A single stock solution was used for all experiments, and dilutions were prepared just prior to each experiment. In the “*cis*” group, a vial containing 1 mL of PAI solution was irradiated with UV-light lamp (365 nm) in a custom-made closed chamber for 5 minutes, and thereafter administered intraperitoneally in dark conditions. Two animals (one for each “*cis*” and “*trans*” groups) were initially used to delimitate the effective dose range, which was found to be in the range of 100 nM/kg – 100  $\mu$ M/kg (results not shown). Subsequently, the following PAI doses were intraperitoneally administered at 7-minute intervals in the remaining rats: 100 nM/kg; 300 nM/kg; 1  $\mu$ M/kg; 3  $\mu$ M/kg; 10  $\mu$ M/kg; 30  $\mu$ M/kg; 100  $\mu$ M/kg. The heart rate (beats·min<sup>-1</sup>) and the PR interval (ms) were measured offline to assess the parasympathetic effect of both PAI isomers (LabChart v.8.1.2, ADInstruments, Colorado Springs, CO, US). A one-minute recording (from minute 5’30” to minute 6’30” after each dose administration) of stable ECG was analyzed. Heart rate and the PR interval were automatically determined, manually reviewed for accuracy, and modified if needed. Second degree Wenckebach atrio-ventricular block and subsequent complete block occurred in one rat receiving the 30  $\mu$ M/kg dose and one rat receiving the 100  $\mu$ M/kg dose, and were excluded from PR interval measurements. Results are shown as difference to the baseline value ( $\Delta$ ). In order to test that parasympathetic activity was driving heart rate and PR-interval changes, and to assess its reversibility, atropine (two 1 mg doses separated by 5-7 minutes) was administered to one rat per group. A representative profile of a full experiment is shown in **Figure S6.1**.

**Data analysis and statistics.** *In vivo* data is shown in boxplots. Because some rats died after the administration of high doses of the active isomer *trans*-PAI, a maximum effect asymptotic value was not reached, and a formal dose-response curve could not be built. Therefore, analyses were carried out with a two-way ANOVA in which two main factors (Isomer, Dose) and their interaction (Isomer x Dose) were included. In the case of a significant interaction, pairwise comparisons (Isomer effect at each Dose) were performed with the LSD test.

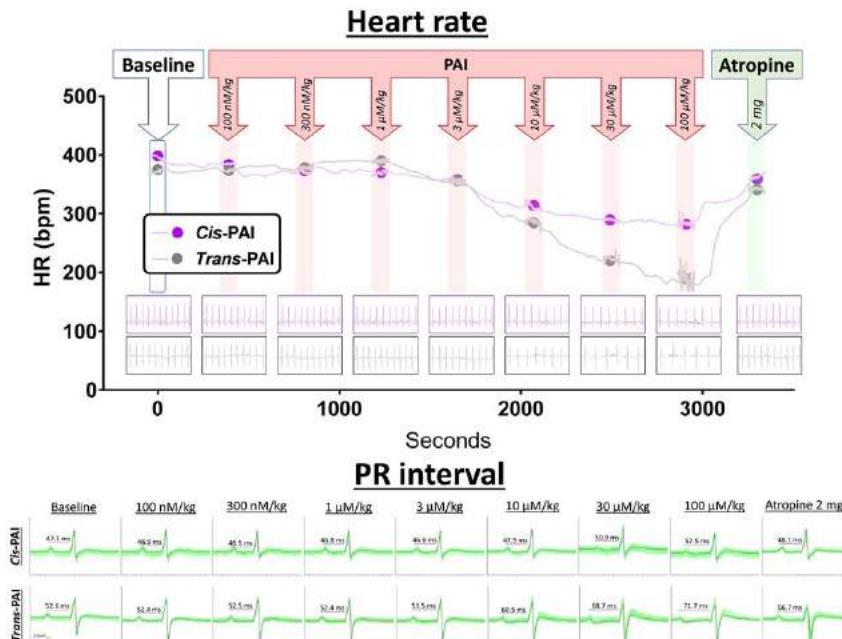


**Figure S6.1.** Representative profile of the heart rate (upper panel) and the PR interval (lower panel) in two rats receiving increasing doses of PAI (*trans* or *cis* form), and atropine. Heart rate is averaged every second in shadowed areas in the upper panel; in between doses, heart rate is averaged every 30 seconds.

## 7. In vivo experiments in *Xenopus tropicalis* tadpoles

### 7.1 Materials and methods

African clawed frogs constitute an excellent animal model for behavioral, genetic and electrophysiological studies,<sup>12,13</sup> and a powerful tool for drug discovery and preclinical animal testing.<sup>14</sup> In addition, they are especially suitable for heart monitoring since tadpoles are transparent until stage 48-50<sup>15</sup> and, in contrast to fish, their three-chamber heart is an excellent model for studying the human cardiovascular system.<sup>16,17</sup>

**Animal housing.** *Xenopus tropicalis* embryos (Nasco) were obtained by natural mating and maintained till 3-4 days post fertilization (dpf) in 0.1X Marc's modified Ringer's (MMR) solution in agarose coated Petri dishes (10-15 cm diameter) in a dark incubator (24 °C). Animals were transferred to tanks containing *Xenopus* water, which was prepared by adding 8 g of instant ocean salt (Instant Ocean) to 20 L of distilled water. Conductivity and pH were 700 μS and 7.4-7.5, respectively. Tadpoles were kept at a density of 30-50 animals L<sup>-1</sup>, at 24 °C and fed daily with spirulina. All procedures complied with the standards of the ethical commission of the University of Barcelona. *Xenopus tropicalis* tadpoles

(developmental stages 44-48 according to Nieuwkoop and Faber)<sup>15</sup> were paralyzed in 0.23 mM of Pancuronium dibromide solution (PCD) (Merck, Cat no. P1918) for 10 minutes and placed into a 48-well plate (Nunc<sup>TM</sup>Microwell<sup>TM</sup>) with 200 $\mu$ L of 0.1X solution of MMR-CaCl<sub>2</sub> (referred as BS from now on). PCD was preferred to tricaine because of its higher cardiac tolerability and non-UV dependent effects.<sup>17</sup>

**Cardiac activity measurements.** Video recordings of tadpole hearts were performed using a Nikon Eclipse TS100 microscope equipped with an OptixCam Summit Series OCS-D3K2-5 camera, which substantially improved the resolution of the previously reported setup.<sup>18</sup> In order to prevent unintended *cis*-to-*trans* isomerisation of photoswitchable compounds, the microscope top-down light pathway was dimmed with a red plastic filter, which could be placed or removed during experimentation. Video recordings were acquired using the ToupView software, enhancing visual contrast to improve cardiac imaging and video streams were converted to the AVI format. Recordings were briefly interrupted during compound addition and changes of illumination conditions. Video information and data analysis were extracted and executed with custom scripts based on ImageJ<sup>19</sup> for AVI files analysis and subsequently converted to the TXT format for R software analysis.<sup>20</sup> The illumination protocol established for control and treatment video recordings applied the following procedure: one minute dimmed red light (650 nm, 34.0 W·m<sup>-2</sup>), three minutes under UV (365nm, 2.3 W·m<sup>-2</sup>) due to the required exposure time for a complete *trans*-to-*cis* isomerisation, two minutes dimmed red light and one minute under visible light (455 nm, 169.8 W·m<sup>-2</sup>) for *cis*-to-*trans* back isomerisation. Tadpoles (n = 4) were firstly paralyzed with PCD as previously described, placed in the BS and video recorded under the established protocol of illumination in the absence of PAI to monitor the effect of the light on cardiac activity and verify control conditions. Afterwards, animals were placed into a 10  $\mu$ M PAI solution and underwent the same protocol of illumination to observe the light-dependent effects of the drug.

**Data analysis and statistics.** Heart beating movies were converted to a linear signal by selecting a region of interest displaying large periodic variations corresponding to heart movements, and calculating the corresponding grey scale level as a function of time (**Figure 5a-d**). The cardiac rate (beats·s<sup>-1</sup>) was calculated from this linear signal from the number of maxima every 15 s (red plots in **Figure 5e**). To statistically compare between different illumination periods and drug conditions, the cardiac rate was calculated from the last 30 s of every period. The stability of cardiac rhythm in each period was quantified with a unitless variability score as the number of video frames between heartbeats. High scores correspond to longer periods with asynchronous or arrested cardiac activity. Perfectly steady rate in the absence of PAI yields a variability score of 8 (**Figure S7.2**). Statistical analyses were carried out with a two-way repeated measures ANOVA with uncorrected Fisher's Least Significant Differences (LSD) test in which two main factors (heart beats per second, 10  $\mu$ M of PAI) and their interaction (heart beats per second x 10  $\mu$ M of PAI) were included (**Figure 5f**).

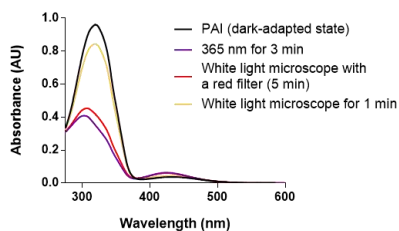


**Figure S7.1.** Validation of the photochromic behavior of PAI under the illumination conditions used for our *in vivo* experiments in *X. tropicalis* tadpoles. PAI could be effectively isomerized to *cis* under illumination with 365 nm light (external source) and back-isomerized to *trans* using unfiltered microscope white light (100% intensity), whereas the *cis*-enriched photostationary state could be satisfactorily maintained when the microscope light was filtered with a common red polycarbonate filter.

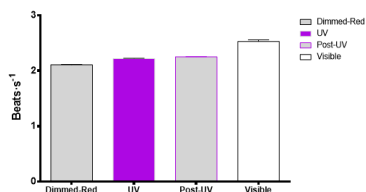


**Figure S7.2.** Cardiac activity (beats per second) recorded under different conditions of illumination in absence of PAI (control experiment). Error bars represent SEM ( $n = 4$ ).

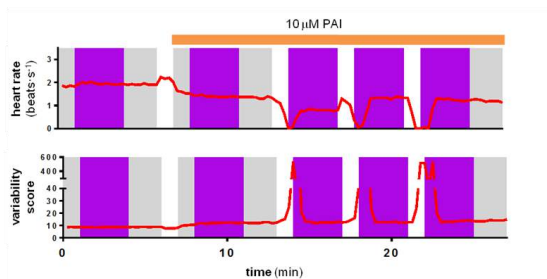


**Figure S7.3.** Example trace of cardiac rate from one animal (top) and corresponding variability score calculated as the number of video frames between heartbeats (averaged every 15 s). Although the first exposure to 10  $\mu\text{M}$  *trans*-PAI did not immediately reduce the heart rate of this animal, subsequent cycles of UV/white light in the presence of PAI reversibly switched the heartbeat on and off. Reduced heart rate was associated with longer periods displaying unstable, asynchronous cardiac activity and thus a higher variability score.

## 8. Additional references

- (1) Dallanoce, C.; Conti, P.; De Amici, M.; De Micheli, C.; Barocelli, E.; Chiavarini, M.; Ballabeni, V.; Bertoni, S.; Impicciatore, M. Synthesis and Functional Characterization of Novel Derivatives Related to Oxotremorine and Oxotremorine-M. *Bioorg. Med. Chem.* 1999, 7 (8), 1539–1547.
- (2) Kloeckner, J.; Schmitz, J.; Holzgrabe, U. Convergent, Short Synthesis of the Muscarinic Superagonist Iperoxo. *Tetrahedron Lett.* 2010, 51 (27), 3470–3472.
- (3) Disingrini, T.; Muth, M.; Dallanoce, C.; Barocelli, E.; Bertoni, S.; Kellershohn, K.; Mohr, K.; De Amici, M.; Holzgrabe, U. Design, Synthesis, and Action of Oxotremorine-Related Hybrid-Type Allosteric Modulators of Muscarinic Acetylcholine Receptors. *J. Med. Chem.* 2006, 49 (1), 366–372.
- (4) Velema, W. A.; van der Toorn, M.; Szymanski, W.; Feringa, B. L. Design, Synthesis, and Inhibitory Activity of Potent, Photoswitchable Mast Cell Activation Inhibitors. *J. Med. Chem.* 2013, 56 (11), 4456–4464.
- (5) Gomeza, J.; Mary, S.; Brabet, I.; Parmentier, M. L.; Restituito, S.; Bockaert, J.; Pin, J. P. Coupling of Metabotropic Glutamate Receptors 2 and 4 to G Alpha 15, G Alpha 16, and Chimeric G Alpha Q/i Proteins: Characterization of New Antagonists. *Mol. Pharmacol.* 1996, 50 (4).
- (6) Kruse, A. C.; Ring, A. M.; Manglik, A.; Hu, J.; Hu, K.; Eitel, K.; Hübner, H.; Pardon, E.; Valant, C.; Sexton, P. M.; et al. Activation and Allosteric Modulation of a Muscarinic Acetylcholine Receptor. *Nature* 2013, 504 (7478), 101–106.
- (7) Antony, J.; Kellershohn, K.; Mohr-Andrä, M.; Kebig, A.; Prilla, S.; Muth, M.; Heller, E.; Disingrini, T.; Dallanoce, C.; Bertoni, S.; et al. Dualsteric GPCR Targeting: A Novel Route to Binding and Signaling Pathway Selectivity. *FASEB J.* 2009, 23 (2), 442–450.
- (8) Bock, A.; Bermudez, M.; Krebs, F.; Matera, C.; Chirinda, B.; Sydow, D.; Dallanoce, C.; Holzgrabe, U.; De Amici, M.; Lohse, M. J.; et al. Ligand Binding Ensembles Determine Graded Agonist Efficacies at a G Protein-Coupled Receptor. *J. Biol. Chem.* 2016, 291 (31), 16375–16389.
- (9) Pettersen, E. F.; Goddard, T. D.; Huang, C. C.; Couch, G. S.; Greenblatt, D. M.; Meng, E. C.; Ferrin, T. E. UCSF Chimera—A Visualization System for Exploratory Research and Analysis. *J. Comput. Chem.* 2004, 25 (13), 1605–1612.
- (10) Morris, G. M.; Huey, R.; Lindstrom, W.; Sanner, M. F.; Belew, R. K.; Goodsell, D. S.; Olson, A. J. AutoDock4 and AutoDockTools4: Automated Docking with Selective Receptor Flexibility. *J. Comput. Chem.* 2009, 30 (16), 2785–2791.
- (11) Dallakyan, S.; Olson, A. J. Small-Molecule Library Screening by Docking with PyRx. In *Methods in molecular biology* (Clifton, N.J.); 2015; Vol. 1263, pp 243–250.
- (12) Grainger, R. M. *Xenopus Protocols*. 2012, 917, 1–11.
- (13) Burggren, W. W.; Warburton, S. Amphibians as Animal Models for Laboratory Research in Physiology. *ILAR J.* 2007, 48 (3), 260–269.
- (14) Schmitt, S. M.; Gull, M.; Brändli, A. W. Engineering *Xenopus* Embryos for Phenotypic Drug Discovery Screening. *Adv. Drug Deliv. Rev.* 2014, 69–70, 225–246.
- (15) Nieuwkoop P., F. J. Normal Table of *Xenopus laevis* (Daudin): A Systematical & Chronological Survey of the Development from the Fertilized Egg till the End of Metamorphosis; 1994.

- (16) Boppart, S. A.; Tearney, G. J.; Bouma, B. E.; Southern, J. F.; Brezinski, M. E.; Fujimoto, J. G. Noninvasive Assessment of the Developing *Xenopus* Cardiovascular System Using Optical Coherence Tomography. *Proc. Natl .Acad. Sci. USA* 1997, 94 (9), 4256–4261.
- (17) Bartlett, H. L.; Scholz, T. D.; Lamb, F. S.; Weeks, D. L. Characterization of Embryonic Cardiac Pacemaker and Atrioventricular Conduction Physiology in *Xenopus Laevis* Using Noninvasive Imaging. *Am. J. Physiol. Heart Circ. Physiol.* 2004, 286 (6), H2035-41.
- (18) Eckelt, K.; Masanas, H.; Llobet, A.; Gorostiza, P. Automated High-Throughput Measurement of Body Movements and Cardiac Activity of *Xenopus Tropicalis* Tadpoles. *J. Biol. Methods* 2014, 1 (2), 9.
- (19) Schindelin, J.; Arganda-Carreras, I.; Frise, E.; Kaynig, V.; Longair, M.; Pietzsch, T.; Preibisch, S.; Rueden, C.; Saalfeld, S.; Schmid, B.; et al. Fiji: An Open-Source Platform for Biological-Image Analysis. *Nature Methods*. 2012, pp 676–682.
- (20) R-Core Team. A Language and Environment for Statistical Computing. 2016.

# Control of brain state transitions with a photoswitchable muscarinic agonist

Almudena Barbero-Castillo,<sup>†,¶</sup> Fabio Riefolo,<sup>‡,§,¶</sup> Carlo Matera,<sup>‡,§</sup> Sara Caldas-Martínez,<sup>†</sup> Pedro Mateos-Aparicio,<sup>†</sup> Julia F. Weinert,<sup>†</sup> Enrique Claro,<sup>¶</sup> Maria V. Sanchez-Vives,<sup>†,⊥,\*</sup> and Pau Gorostiza<sup>‡,§,⊥,\*</sup>

<sup>†</sup>Institut d'Investigacions Biomèdiques August Pi i Sunyer (IDIBAPS), Barcelona, Spain

<sup>‡</sup>Institute for Bioengineering of Catalonia (IBEC), Barcelona Institute for Science and Technology (BIST), Barcelona, Spain.

<sup>§</sup>Network Biomedical Research Center in Bioengineering, Biomaterials, and Nanomedicine (CIBER-BBN), Madrid, Spain.

<sup>¶</sup>Institut de Neurociències and Departament de Bioquímica i Biologia Molecular, Unitat de Bioquímica de Medicina, Universitat Autònoma de Barcelona (UAB), Barcelona, Spain.

<sup>⊥</sup>Catalan Institution for Research and Advanced Studies (ICREA), Barcelona, Spain.

<sup>\*</sup>Contributed equally to this work.

**ABSTRACT:** The ability to control neural activity is essential for research in basic neuroscience, as it affects the mental state of an individual, but also in clinical neurology for brain therapies or stimulation. Available forms of spatiotemporally controlled neuromodulation include transcranial-magnetic or current (AC/DC) stimulation as well as light-mediated control. Among the latter, optogenetics has revolutionized neuroscience, yet its clinical translation is hampered by the need of gene therapy. As a drug-based alternative, the effect of a photoswitchable muscarinic agonist (PAI) on a brain network is evaluated in this work. First, the conditions to manipulate muscarinic receptors with light in the experimental setup are determined. Then, the emergent cortical activity consisting on synchronous slow oscillations –as in slow wave sleep– is transformed into a higher frequency pattern in the cerebral cortex both *in vitro* and *in vivo*. These results open the way to study cholinergic neuromodulation and to control spatiotemporal patterns of activity in different brain states, their

transitions, and their links to cognition and behavior. The approach can be applied to different organisms and does not require genetic manipulation, which makes it translational to humans.

## INTRODUCTION

All perceptions, memories and behaviors are based in the communication between the billions of neurons that constitute the brain.<sup>1-4</sup> Individual neurons transmit information using chemical and electrical signals, and are organized in groups or circuits involved in different functions.<sup>3,5,6</sup> The electrochemical interactions of neuronal ensembles result into the electrical activity emerging from the brain, which can show synchrony across populations in the form of brain rhythms and waves that propagate<sup>7-9</sup> or asynchronous discharges, depending on the brain states.<sup>10</sup> Brain rhythms, their frequency, synchronization, and underlying functional connectivity, are associated with internal brain states and result in specific behaviors.<sup>1</sup> Neural and network activity undergo significant changes during brain state transitions, which have been linked to substantial changes in electroencephalography (EEG) pattern activity.<sup>11</sup> For example, large and synchronous brain waves are mostly associated with deep sleep, whereas there is a shift towards more desynchronized and high frequencies during wakefulness.<sup>8,12,13</sup> These changes in brain and behavioral states and the concomitant alterations in electrophysiological activity, can be driven by the action of neuromodulators like acetylcholine (ACh).<sup>11,14</sup> However, it is not fully understood how the different cells expressing ACh receptors contribute to the alteration of the global cortical state. Cholinergic receptors include ionotropic nicotinic ion channels and muscarinic metabotropic G protein-coupled receptors. Together they modulate brain activity, and in particular, the activity of the cerebral cortex, and are involved in crucial neocortical functions such as attention,<sup>15-17</sup> learning,<sup>18-20</sup> memory,<sup>21</sup> as well as sensory and motor functions.<sup>22-24</sup> In the neocortex, ACh is released mostly at cholinergic terminals from neurons with somas in the basal forebrain nuclei. Electrical stimulation of the nucleus basalis can evoke the release of ACh in the neocortex but in an unselective manner, as ascending projections from basal forebrain nuclei not only comprise cholinergic axons, but also

GABAergic and glutamatergic axons.<sup>25</sup> Such a lack of selectivity complicates the study of cholinergic signaling in the neocortex and its effects on controlling brain states.

Selective stimulation of cholinergic projections in the neocortex from basal forebrain nuclei has been demonstrated with optogenetics and has enabled the disruption of neocortical synchronous activity during certain sleep states.<sup>12</sup> Optogenetic stimulation of basal forebrain cholinergic neurons also revealed their influence in awake cortical dynamics: cholinergic neuromodulation was found to be relevant for visual discrimination tasks, modulating the encoding properties of V1 neurons and activating cortical transitions faster than previously presumed.<sup>12</sup> However, the cell type specificity of optogenetics is limited by the availability of suitable promoters. In addition, it is based on the overexpression of microbial proteins using genetic manipulation, which can distort synaptic physiology<sup>26-28</sup> and raises safety and regulatory concerns regarding therapeutic applications.

The control of neuronal signaling with photopharmacology is based on synthetic ligands that target endogenous proteins, and thus its physiological relevance spans from circuit to sub-cellular levels. Since neuronal receptors are highly conserved, photoswitchable ligands can generally be used in multiple species, and their safety and regulation can be established in the same manner as other drugs. The cholinergic system is key to the modulation of a variety of CNS functions<sup>29</sup> and thus the use of selective and photoswitchable cholinergic drugs to spatiotemporally-control cortical activity might have relevant scientific and clinical implications. We recently developed a photoswitchable agonist of M2 muscarinic acetylcholine receptors (mAChRs), Phthalimide-Azo-Iper (PAI),<sup>30</sup> but its action on neuronal circuits and networks has never been explored. Herein, we report that the cholinergic-dependent brain state transitions in the neocortex can be directly controlled with light using PAI. In particular, we have found that PAI enables the modulation of spontaneous emerging slow oscillations (SO) in neuronal circuits. PAI *cis*-to-*trans* photoisomerization decreases the Down- and Up-state durations and increases oscillatory frequency (OF) in cortical slices. In addition, PAI allows the reversible manipulation of the cortical OF in anesthetized mice

using light. Two different species, ferret (*in vitro*) and mouse (*in vivo*) were used in this study, since ferret cortical slices are more suitable than rodents to spontaneously generate network activity under physiological conditions.<sup>31</sup> Thus, we demonstrate that photopharmacology allows to selectively control SO *in vitro* and *in vivo*, opening the way to analyze their spatiotemporal dynamics and their effects on brain and behavioral state transitions.

## RESULTS

***Non-specific activation of mAChRs evokes neuronal hyperexcitability in cortical slices.*** Changes in cortical rhythms underlie behavioral state transitions, and endogenous ACh actions play a central role in such variations.<sup>32-39</sup> However, a complete and unifying view regarding the cholinergic impact on neocortical network dynamics and underlying mechanisms does not yet exist.<sup>13</sup> It is known that ACh contributes to the shift of the neocortical network state from synchronous to asynchronous activity -associated to awake state- in a dose-dependent manner, but the activity of ACh in the majority of neocortical neurons and synapses is still poorly characterized. For this reason, photoswitchable cholinergic drugs allowing spatiotemporal control of their activation would be a most suitable tool. Neocortical activation of mAChRs *in vitro* facilitates synaptic transmission,<sup>40</sup> recurrent excitation,<sup>41</sup> and reversibly increases the power of fast-frequency oscillations.<sup>42-45</sup> On these basis, we first studied *in vitro* the effect of Iperoxo, a potent muscarinic agonist,<sup>46,47</sup> on cortical SO spontaneously generated in cortical slices. The goal was to evaluate the potential of mAChRs to selectively modulate the dynamics of the neocortical network, while avoiding the simultaneous activation of nicotinic cholinergic receptors (nAChRs), and to validate that Iperoxo-based photoswitches would be useful photopharmacological tools to control neuronal activity. Ferret cortical slices spontaneously generate cortical SO, a hallmark of activity during deep sleep or anesthesia.<sup>31</sup> We recorded this spontaneous oscillatory activity (control) and then the activity under different concentrations (1, 10, 100 nM) of Iperoxo. SO consists on the alternation between periods of activity or high neuronal firing (Up states) and periods of near silence (Down states). The activation

of mAChRs by Iperoxo resulted in a global change in the network's dynamics into a hyperexcitable state in a dose-dependent way (**Figure 1**). At 100 nM Iperoxo, the oscillatory frequency (OF) -or frequency of the Up/Down state cycle- increased (from  $0.89 \pm 0.12$  Hz in the control to  $1.34 \pm 0.18$  Hz with 100 nM Iperoxo), while the firing rate (FR; see Methods)<sup>48</sup> in the Up states decreased (from  $1.13 \pm 0.23$  a.u. to  $0.10 \pm 0.02$  a.u. with 100 nM Iperoxo) (**Figure 1B**). At concentrations equal or higher than 100 nM Iperoxo, the oscillatory activity evolved to periods of seizure-like discharges (**Figure 1C**)<sup>49-50</sup> characterized by a radically different spectrogram showing larger low (<1 Hz), delta (1-4 Hz) and alpha (7-12Hz) frequency components, and including enhancement of beta (12-30 Hz) and gamma frequencies (30-100 Hz) (**Figure 1D**). However, our interest was to avoid epileptiform discharges and to activate muscarinic receptors within the range of physiological activity, therefore with the activation achieved below 100 nM Iperoxo.

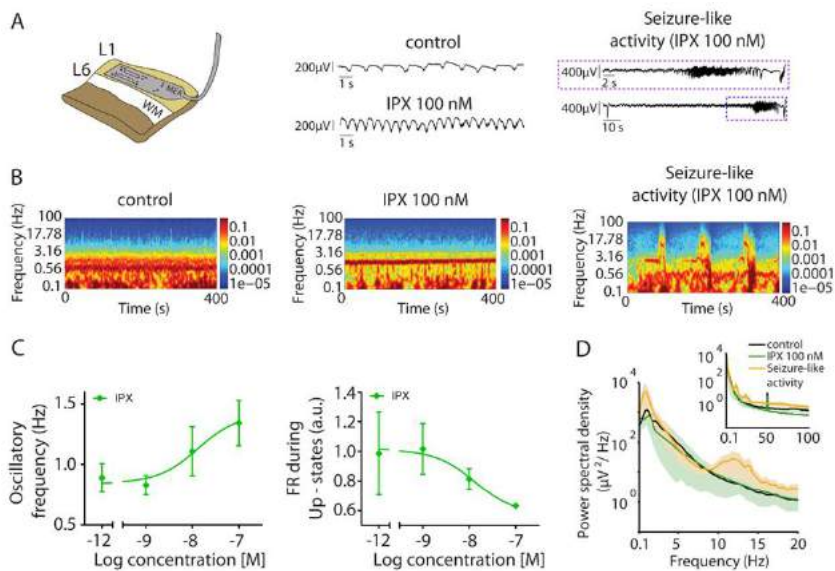


**Figure 1. Non-specific activation of mAChRs evokes neuronal hyperexcitability in cortical slices.** (A) On the left, the experimental setup: 16-channel multielectrode array (MEA); WM, white matter; L1-L6, layer 1-6. On the right, raw local field potential (LFP) traces illustrating network activity showing the increase in OF corresponding to the spectrogram of panel B. (B) Spectrogram from the same time recording of LFP traces on panel A: control, 100 nM Iperoxo (IPX) and periods of seizure-like discharges. (C) OF (Hz) and FR (a.u.) during the Up-states.

**Effect of PAI isomers on slow and fast oscillations in vitro.** The hyperexcitable network state induced with Iperoxo reflects the impact of mAChRs activation on cortical networks and brain states.<sup>13</sup> In order to remotely control these states, we aimed at the muscarinic neuromodulation using PAI, a novel photoswitchable Iperoxo-derivative that allows the reversible activation of M2 mAChRs with light.<sup>30</sup> The light-dependent behavior of PAI is achieved with a molecular switch in its structure that is based on azobenzene. PAI exists in two forms, *trans* and *cis*, that are in dynamic equilibrium with each other. A distribution of 87% in favor of the *trans* form (13% of the *cis*) is found in the dark or after illumination with visible light (white light (WL) for 2 minutes). After illumination with ultraviolet (UV) light (365 nm for 1 minute) the ratio between the two configurations rapidly changes to about 77% *cis* (13% *trans*). Both PAI isomeric mixtures (respectively termed “*trans*” and “*cis*” for simplicity) are thermally stable for hours and their biological effects have been characterized *in vitro* in cardiac cells. Despite the partial photoconversion (which is characteristic of azobenzene-based switches) the *trans*- and the *cis*-enriched forms of PAI display different pharmacological activity: the *trans* configuration is more potent to activate M2 receptors than the *cis*, allowing to reversibly manipulate muscarinic functions with light over many cycles.<sup>30</sup> M2 receptors play a relevant role in several CNS disorders<sup>29</sup> and controlled-spatiotemporal regulation of their activity and subsequent effects on cortical neuronal networks may provide new therapeutic opportunities for diseases involving the cholinergic system. We applied PAI to spontaneously active neocortical brain slices and recorded their oscillatory activity before and after photoactivating the drug. We first obtained dose-response curves of the two drug forms separately, *trans*- (dark-adapted state) and *cis*-PAI (after UV irradiation), in order to identify the most convenient concentration range to manipulate brain waves with light. The baseline activity (characterized by SO) was recorded as a control, prior to bath-application of artificial cerebrospinal fluid (ACSF) with increasing PAI concentrations (10 nM, 100 nM, 300 nM, and 1  $\mu$ M,  $n = 6$  for each PAI form, *trans* and *cis*) (**Figure 2A**). *Trans*-PAI significantly modulated the Up- and Down-state sequence already at 100 nM (**Figure 2**). It increased the OF from  $0.58 \pm 0.06$  Hz (control) to  $1.87 \pm 0.12$  Hz with 1  $\mu$ M *trans*-PAI

(**Figure 2B**) and it decreased the FR during the Up-states (from  $0.98 \pm 0.11$  a.u. in control to  $0.37 \pm 0.03$  a.u. with  $1 \mu\text{M}$  *trans*-PAI) (**Figure 2C**). In comparison, *cis*-PAI displayed weaker effects, in agreement with the reported PAI properties in cardiac cells.<sup>30</sup> At 100 nM and 300 nM, *cis*-PAI did not significantly alter the spontaneous activity observed in control experiments (control OF:  $0.48 \pm 0.037$  Hz; 100 nM *cis*-PAI OF:  $0.52 \pm 0.07$  Hz; 300 nM *cis*-PAI OF:  $0.87 \pm 0.20$  Hz), in contrast to the strong modulation in oscillatory activity obtained with 100 nM and 300 nM *trans*-PAI (**Figure 2**). Only at concentrations as high as  $1 \mu\text{M}$ , *cis*-PAI altered the Up- and Down-state sequence in comparison to the control, increasing the OF (to  $1.32 \pm 0.27$  Hz) and decreasing the FR of the Up-states (from  $0.86 \pm 0.04$  a.u. in control to  $0.74 \pm 0.27$  a.u. with  $1 \mu\text{M}$  *cis*-PAI) (**Figure 2**). In summary, the most compelling differences between *trans*- and *cis*-PAI emerged between 100 nM and 300 nM and were observed in the OF and in the Up-states' FR (**Figure 2**). Thus, we focused in this concentration range in order to photomodulate cortical SO using PAI.

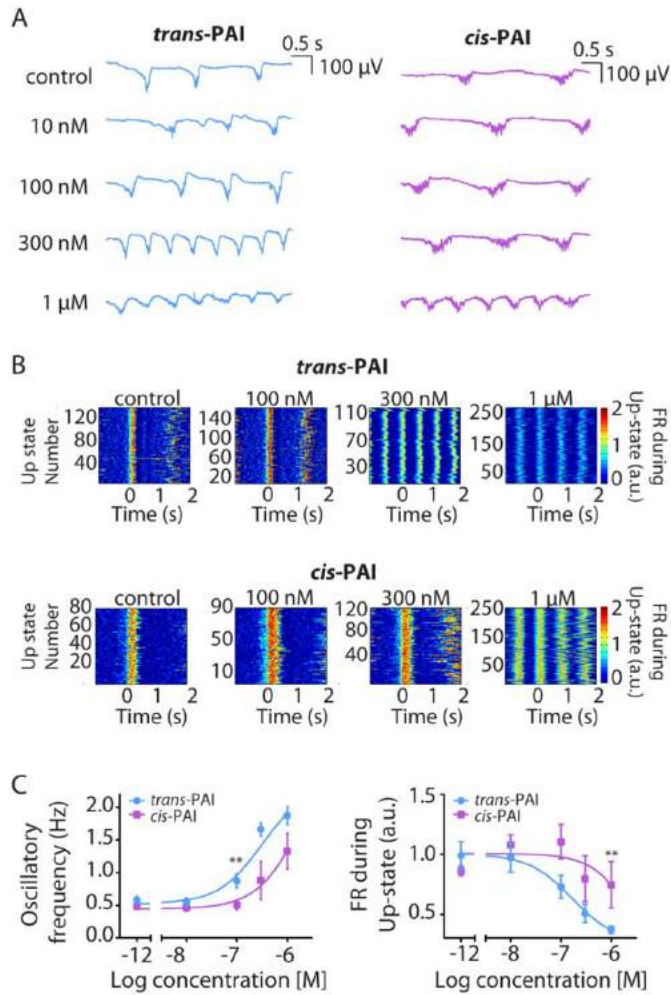


**Figure 2. Effect of mAChRs activation by *trans*-PAI and *cis*-PAI on SO.** (A) Raw Local Field Potential (LFP) example recordings showing the different ability of *trans*- and *cis*-PAI to increasing the OF. Note that *trans*-PAI is a stronger agonist of M2 mAChR than *cis*-PAI.<sup>30</sup> (B) Raster plots showing the FR during the Up-states (color coded) under control conditions and different *trans*- and *cis*-PAI concentrations. (C) OF (Hz) and FR during the Up-states (a.u.) of the two different PAI isomers, *trans*- (blue,  $n = 6$ ) and *cis*-PAI (pink,  $n = 6$ ) at different concentrations. \*\* $p$ -value  $< 10^{-2}$ .

**PAI effectively light-modulates cortical slow oscillations *in vitro*.** Once the concentration range of drug to obtain different oscillatory activity evoked by *cis*- and *trans*-PAI was quantified *in vitro* (Figure 2), we moved on to control the rhythmic activity with light in the same cortical slices (Figure

**3).** We took advantage of the thermal stability of both PAI forms to apply initially the less potent one (*cis*-PAI) at 200 nM in cortical slices ( $n = 15$ ), in the absence of WL to avoid photoconversion to *trans*-PAI during the recordings.<sup>30</sup> As shown in **Figure 3**, 200 nM *cis*-PAI evoked only a minor increment of the OF (from  $0.53 \pm 0.04$  Hz in the control to  $1.04 \pm 0.14$  Hz with *cis*-PAI,  $p$ -value =  $1.6 \cdot 10^{-3}$ ), and no significant effects in the FR of the Up-states (from  $0.98 \pm 0.09$  a.u. in the control to  $0.86 \pm 0.10$  a.u. with *cis*-PAI,  $p$ -value =  $2.9 \cdot 10^{-1}$ ) in comparison to the control situation (**Figure 3**). Subsequent illumination of the slices with WL produced a robust increase in OF (from  $0.53 \pm 0.04$  Hz in the control to  $1.68 \pm 0.13$  upon illumination,  $p$ -value =  $2.9 \cdot 10^{-4}$ ; from  $1.04 \pm 0.14$  Hz with *cis*-PAI to  $1.68 \pm 0.13$  upon illumination,  $p$ -value =  $3.5 \cdot 10^{-4}$ ), a significant decrease in FR of the Up-states (from control values of  $0.98 \pm 0.09$  a.u. to  $0.52 \pm 0.06$  a.u. upon illumination,  $p$ -value =  $2.9 \cdot 10^{-4}$ ; from  $0.86 \pm 0.10$  a.u. with *cis*-PAI to  $0.52 \pm 0.06$  a.u. upon illumination,  $p$ -value =  $2.9 \cdot 10^{-4}$ ), and a noticeable change in the activity regime of the network (**Figure 3**). The changes in the power spectrum in the population were incremental, as illustrated in the **Figure 3**. These changes are similar to the effects of adding Iperoxo to the bath (**Figure 1**), and in agreement with PAI photoconversion to the active form (*trans*). The modulation of cortical activity was not reversible with 365 nm light (to isomerize PAI to the *cis* form *in situ*), due to the reduced penetration and the potential neuronal damages that characterize the use of UV light in brain tissue.

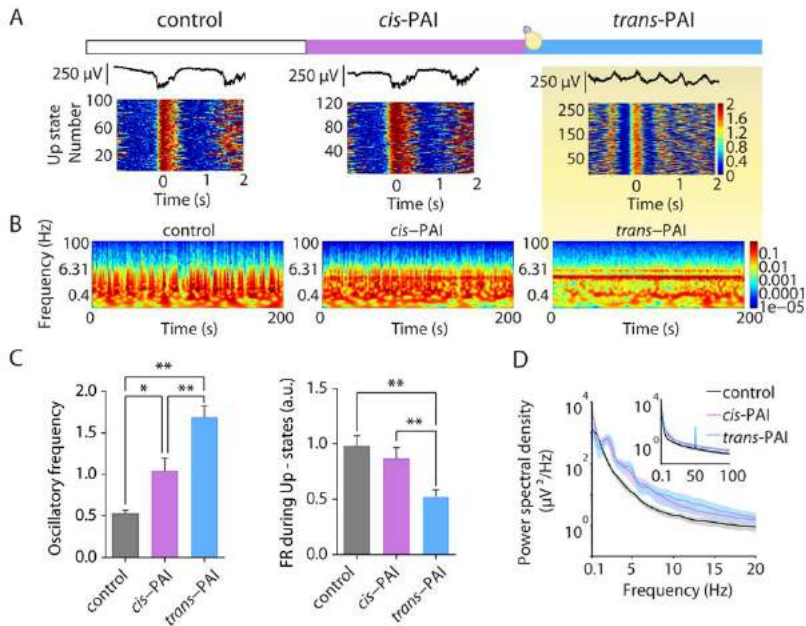


**Figure 3. Modulation of brain waves *in vitro* using PAI, a light-regulated ligand.** (A) Representative local field potential (LFP) traces (top) and raster plots of FR during the Up-states under control conditions, 200 nM of *cis*-PAI and 200 nM *trans*-PAI after light activation ( $n = 15$ ) (bottom). (B) Representative spectrogram under control condition, 200 nM of *cis*-PAI and 200 nM *trans*-PAI after light activation. (C) OF (Hz) and FR during the Up-states (a.u.) at 200 nM PAI after pre-irradiation with 365 nm (*cis*-PAI), and photoswitching with WL (*trans*-PAI). (D) Averaged power spectral density (PSD) of oscillatory activity under control conditions, 200 nM of *cis*-PAI and 200 nM *trans*-PAI after white light activation (color code). \* $p$ -value  $< 5 \cdot 10^{-3}$ ; \*\* $p$ -value  $< 10^{-3}$ .

***PAI can modulate brain wave activity with light in vivo.*** Having established the unique ability of PAI to alter cortical oscillatory activity with light in slices, we then aimed at obtaining a proof of concept of photocontrolling the cortical state *in vivo*. Cortical brain waves were recorded in C57BL6/JR mice ( $n = 3$ ) with an electrode inserted through a craniotomy across which we carried out the drug application and brain illumination (see Methods). Initially, we induced deep anesthesia in the animals, a state that is known to reproduce the slow wave sleep state,<sup>33,34,51</sup> and which is characterized by the generation of cortical SO similar to the slow frequency waves observed in our experiments in slices under control conditions (**Figure 1-3**).<sup>7</sup> Such SO activity in anesthetized

mice was recorded for 500 s under WL illumination of the brain, and the characteristic parameters obtained (OF  $0.64 \pm 0.06$  Hz, FR during the Up-states  $0.83 \pm 0.23$  a.u.) were taken as the control condition *in vivo*. Since the dose-response curves of *cis*- and *trans*-PAI could differ from *in vitro* conditions (**Figure 2**), we tested two different concentrations, 200 nM and 1  $\mu$ M (**Figure 4A**). A 100  $\mu$ L drop of 200 nM *cis*-PAI solution was initially applied to the brain surface, and the activity was recorded for another 500 s in the absence of WL, to avoid *cis* to *trans* photoisomerization of PAI. The OF and the frequency power (**Figure 4 BD**) of the cortical oscillatory activity were not significantly altered by *cis*-PAI ( $0.61 \pm 0.06$  Hz) and caused only a minor increase in the FR during the Up-states ( $1.02 \pm 0.31$  a.u.) (**Figure 4**). Subsequently, we illuminated the brain using WL in the proximity of the recording electrode in order to isomerize PAI to its more active form (*trans*) and recorded the activity for another 500 s. An increment in the OF to  $0.76 \pm 0.1$  Hz and in the power of the alpha (7-12 Hz) and gamma (30-100 Hz) frequency bands were observed under illumination (**Figure 4AD**), without concomitant changes in the FR during the Up-states ( $1.04 \pm 0.27$  a.u.). Similar effects were observed when a higher concentration of *cis*-PAI (1  $\mu$ M) was applied at the same brain surface site: it reduced the OF to  $0.61 \pm 0.1$  Hz, increased the power of the low frequency band (< 1 Hz) and decreased the power of alpha and gamma bands (**Figure 4 BD**), while the FR during the Up-states ( $0.99 \pm 0.27$  a.u.) (**Figure 4 C**) remained relatively elevated than the control. At this concentration, illumination significantly increased the OF (from  $0.64 \pm 0.06$  Hz in the control to  $0.83 \pm 0.06$  Hz upon illumination,  $p = 4.2 \cdot 10^{-2}$ ) (**Figure 4 B**), and again induced an increment of the alfa and gamma frequencies band (**Figure 4 D**), while the FR during Up states was decreased to the control values ( $0.86 \pm 0.19$  a.u., **Figure 4C**). This evidence is in agreement with *in vitro* results in this range of drug concentration. By using two concentrations of the drug, we observed that the effect on the OF is nearly saturated at 200  $\mu$ M, while the decrease of the FR during the Up-states occurs under 1  $\mu$ M. This strategy allowed us to repeat twice the photocontrol of cortical activity by subsequent application of 1  $\mu$ M *cis*-PAI and photoconversion to *trans*-PAI. The extent to which the drug diffuses and reaches adequate concentrations in deep layers of the cortex and to

which these regions can be effectively illuminated needs further studies, given that the “engine” of SO lies deep in layer 5 and layer 6.<sup>31,52-55</sup>

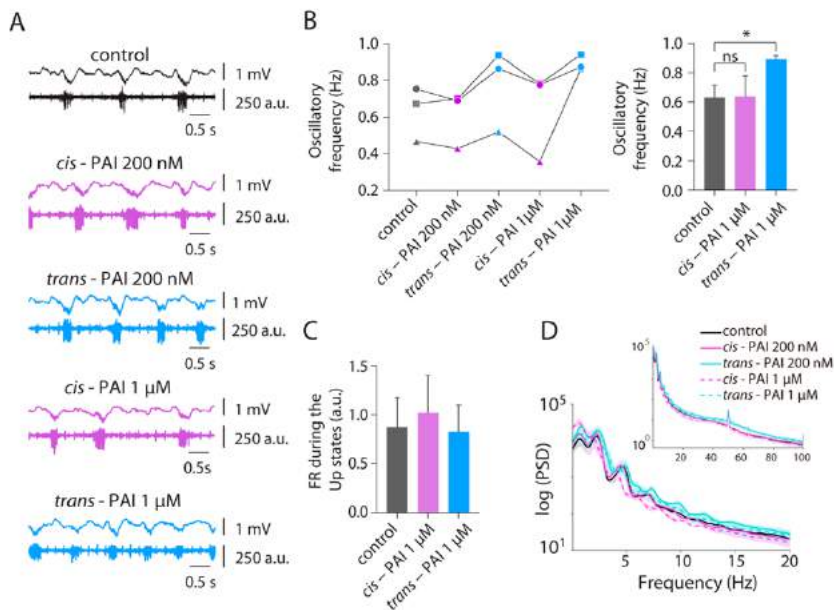


**Figure 4. *In vivo* photomodulation of brain waves.** (A) Representative raw traces of local field potential (LFP) (top, in mV) and multiunit activity (bottom, in arbitrary units), showing the differences in OF and FR during the Up-states between the control, 200 nM, and 1 μM *cis*-PAI (pre-irradiated with 365 nm), and after photoswitching with WL (*trans*-PAI). (B) Individual (left) and mean (right) quantification of OF (Hz) at different concentrations ( $n = 3$ ). (C) Mean quantification of FR during the Up-states (a.u.) at different concentrations ( $n = 3$ ). (D) Averaged power spectral density (PSD) of oscillatory activity at different concentrations displays an enhancement at high-frequency bands after WL activation. \* $p$ -value =  $5 \cdot 10^{-2}$ ; ns = not significant.

## DISCUSSION

Different brain states are associated with distinct behaviors. In order to investigate the causality between them, behavioral outcomes must be correlated with the spontaneous and evoked activity in the cortical network. Thus, understanding the mechanisms of brain and behavioral state transitions requires new techniques to manipulate neuronal activity<sup>1</sup> beyond the pharmacological approach, which affects brain waves in a systemic way.<sup>56</sup> New methods must enable the activation and inhibition of

specific brain regions and neuronal circuits defined by several complementary criteria, namely electrical stimulation with implanted microelectrodes, and photostimulation with cell-specific optogenetics<sup>57-60</sup> and with neurotransmitter-specific photopharmacology.<sup>61</sup> Electromagnetic stimulation pioneered the noninvasive modulation of brain waves and is used therapeutically to treat CNS diseases.<sup>62</sup> For example, transcranial alternating current stimulation has been applied to modulate alpha and beta waves in the motor cortex<sup>63</sup> and transcranial magnetic stimulation has been used to modulate gamma oscillations in the prefrontal cortex.<sup>64</sup> However, further improvements are required to enhance their spatiotemporal and spectral performance, both for fundamental research and therapeutic purposes.<sup>62</sup> Optogenetics<sup>57-60</sup> has emerged as an alternative to electromagnetic stimulation, allowing the activation or inhibition of specific cell populations. For example, photocontrolling the release of ACh, which modulates the transitions between different brain states,<sup>11,14</sup> can be achieved by overexpressing photosensitive proteins in cholinergic neurons of mice neocortex.<sup>12,65</sup> However, genetic manipulation is required in this approach, limiting so far its usability in humans. The photopharmacological approach presented here is, to date, the only way to directly photomodulate brain state transitions in intact tissue. We first studied the effect of the superagonist Iperoxo<sup>46</sup> on isolated cortical slices (**Figure 1**) in order to demonstrate that deep-sleep brain states can be controlled by selectively manipulating muscarinic receptors at their physiological location and context. The oscillatory frequency of the network was increased at 100 nM Iperoxo, leading to seizure-like discharges, in agreement with the outcome of muscarinic stimulation using knockout mice and pilocarpine.<sup>49,50</sup> Photocontrol of muscarinic signaling was subsequently achieved *in vitro* and *in vivo* with the photochromic Iperoxo derivative PAI,<sup>30</sup> which is targeted allosterically at M2 subtype receptors (**Figure 2-4**). Aspects of PAI that can be optimized include its activation wavelength, photosensitivity, pharmacological selectivity and reversibility, safety profile, and permeability to the blood-brain barrier. Still, as a small molecule, PAI is less likely to trigger immune reactions and mutagenesis than the overexpression of microbial opsins. M2 mAChRs are involved in several CNS diseases like major depressive<sup>29,66</sup> and bipolar disorders,<sup>29,67</sup>

Parkinson's<sup>29,68</sup> and Alzheimer's<sup>29,68</sup> diseases, but also in alcohol, smoking and drug dependence<sup>29,69</sup> These disorders are thus susceptible to drug-based photomodulation *in vivo* without requiring genetic manipulation.

In summary, the manipulation of brain state transitions, by means of photocontrolling the frequency of cortical oscillations, has been achieved with a photoswitchable dualsteric agonist of M2 mAChRs. This result opens the way to (a) dissecting the spatiotemporal distribution and pharmacology of brain states, namely mapping how they depend on agonists, antagonists, and modulators of the different muscarinic subtypes expressed in the CNS, and (b) investigating the neuronal dynamics and causality that regulate brain state transitions in the cerebral cortex and beyond. In particular, two-photon stimulation of PAI using pulsed infrared light<sup>30</sup> should enable deep penetration and subcellular resolution in three dimensions,<sup>70</sup> as recently demonstrated with endogenous mGlu<sub>5</sub>.<sup>71</sup> Compared to the local and often inhomogeneous expression patterns achieved with viral injections of optogenetic constructs, diffusible small molecules like PAI can in principle be applied to larger brain regions to control neuronal oscillations.<sup>72</sup> Thus, remote control of brain waves based on the photopharmacological manipulation of endogenous muscarinic receptors may reveal the complex three dimensional molecular signaling underlying brain states and their transitions, in order to link them with cognition and behavior in a diversity of wild-type organisms.

## CONCLUSION

A method for directly manipulating neural activity and brain rhythms with light is demonstrated. It is based on a photoswitchable muscarinic small molecule and does not require gene therapy. The photocontrol of endogenous receptors and their functions in the central nervous system, such as the transition between different brain states, is an achievement for neuromodulation technologies that is useful as tool in basic neuroscience research and in future brain therapies and stimulations. Thus, photopharmacological neuromodulation combined with implantable optoelectronic devices offers to exploit the untapped

potential of neuropharmacology, by controlling drug action in precise spatiotemporal patterns.

## EXPERIMENTAL SECTION

**Slice Preparation.** For the *in vitro* experiments we used isolated cortical slices from ferret, because they robustly reproduce the cortical SO compared with other animal models.<sup>73</sup> Twenty-five ferrets (4- to 6-month-old) were anesthetized with sodium pentobarbital (40 mg/kg) and decapitated. The entire forebrain was rapidly removed and placed in oxygenated cold (4–10 °C) bathing medium.<sup>74</sup> Ferrets were treated in accordance with protocols approved by the Animal Ethics Committee of the University of Barcelona, which comply with the European Union guidelines on the protection of vertebrates used for experimentation (Directive 2010/63/EU of the European Parliament and the Council of 22 September 2010). Coronal slices (400 μm thick) from primary visual cortex (V1) were used.<sup>75</sup> To increase tissue viability we used a modification of the sucrose-substitution technique,<sup>76</sup> such that during slice preparation, the tissue was placed in a solution in which NaCl was replaced with sucrose while maintaining the same osmolarity. After preparation, the slices were placed in an interface-style recording chamber (Fine Sciences Tools, Foster City, CA, USA). During the first 30 min the cortical slices were superfused with an equal mixture in volume of the normal bathing medium, artificial cerebral spinal fluid (ACSF) and the sucrose-substituted solution. Following this, normal bathing medium was added up to the recording chamber and the slices were superfused for 1–2 h; the normal bathing medium contained (in mM): NaCl, 126; KCl, 2.5; MgSO<sub>4</sub>, 2; Na<sub>2</sub>HPO<sub>4</sub>, 1; CaCl<sub>2</sub>, 2; NaHCO<sub>3</sub>, 26; dextrose,<sup>10</sup>; and was aerated with 95% O<sub>2</sub>, 5% CO<sub>2</sub> to a final pH of 7.4. Then, a modified slice solution was used throughout the rest of the experiment; it had the same ionic composition except for different levels of the following (in mM): KCl, 4; MgSO<sub>4</sub>, 1; and CaCl<sub>2</sub>, 1.<sup>74</sup> Bath temperature was maintained at 34–36 °C.

**Drug application and photostimulation in brain slices.** Iperoxo and PAI, both prepared as previously reported from commercially available starting materials<sup>30</sup> were bath-applied at the concentrations range of 1 nM to 100 nM for Iperoxo and 10 nM to 1 μM for PAI, as is mentioned in the Results section. We typically waited more than 1000 s after the application of the drug in order to let it act, to obtain a stable pattern of electrical activity, and to ensure a stable concentration in the bath, this being an interface chamber. PAI effectively photomodulates the activity of M2 receptors *in vitro* and *in vivo*: its dark-adapted state (*trans* form) behaves as a strong M2 agonist, then upon illumination with UV light (365 nm), PAI switches to its less active state (*cis* form). PAI can be switched back to its “full on-state” with WL, or using two-photon excitation with pulsed near-infrared light.<sup>30</sup> The high thermal stability of PAI *cis* form allows the administration of the less active drug (inactive in the cerebral cortex at concentrations lower than 1 μM) and subsequent activation of M2 receptors in the target region with WL.<sup>30</sup> We first investigated the efficacy of PAI in cortical neuronal circuits *in vitro* by obtaining the dose-response curves of *trans*- and *cis*-PAI solutions applied separately. The more active PAI isomer (*trans*) was tested by

applying its dark-adapted form (87% of *trans*-PAI), and *cis*-PAI was obtained by illuminating 1 mM stock solutions with 365 nm light (77% of *cis*-PAI, which is the maximum that can be achieved at the photo stationary state). Because of the high concentration of the stock solution (1 mM) and for the sake of having the maximal possible photoconversion of PAI into the *cis* form, UV light irradiation was performed over 10 min, even if it was demonstrated that the maximal percentage of the *cis* can be reached by a shorter time exposure to UV light (2 min).<sup>30</sup> Increasing concentrations of both *trans*- and *cis*-PAI (10 nM, 100 nM, 300 nM and 1  $\mu$ M) were bath applied in order to build up the dose-response curves.

**LFP recording and data analysis from in vitro recordings.** Our objective in this study was to identify the modulation of network dynamics exerted by photoswitchable muscarinic agonists. To this end, we obtained multiple LFP recordings and their correspondent multiunit activity (MUA) in the way described below. No single units were identified since we aimed at capturing the dynamics of the population and not of individual neurons. The recordings started after allowing at least 2 h of recovery of the slices. Extracellular recordings were obtained with flexible arrays of 16-electrodes arranged in columns as in **Figure 1A**. The multielectrode array (MEA) covered a large part of the area occupied by a cortical slice.<sup>77</sup> It consisted of six groups of electrodes positioned to record electrophysiological activity from superficial and from deep cortical layers (692  $\mu$ m apart) and from what should correspond to three different cortical columns (1500  $\mu$ m apart). The unfiltered field potential (raw signal) was acquired at 10 kHz with a Multichannel System Amplifier (MCS, Reutlingen, Germany) and digitized with a 1401 CED acquisition board and Spike2 software (Cambridge Electronic Design, Cambridge, UK). The MUA was estimated from the power of the frequencies between 200 and 1500 Hz in 5 ms windows.<sup>7,48</sup> The spectrum in this frequency band is a good estimate of the firing of the neuronal population, since it is proportional to the density of the Fourier components at high frequencies.<sup>78</sup> The MUA signal values were logarithmically scaled to compensate for the high fluctuations in the firing of neurons that are very close to the electrode, thus obtaining the logMUA signal (which we refer to as firing rate; FR). A bimodal distribution of the MUA the two peaks of the distribution corresponded to the samples of the activity network belonging to the Up and Down state, respectively. Thus, a threshold value separating the two modes of the distribution was set between the two peaks, such that samples belonged to the Up or to the Down states depending on their position with respect to this threshold. After Up and Down state detection, mean Up and Down state durations were obtained (Ruiz-Mejias et al., 2011). The frequency of the SO was the inverse of the duration of the entire Up-Down cycle. The Up state detection necessary was performed by setting a threshold in the log(MUA) time series as previously described to quantify frequency of the SO.<sup>7,48</sup> Firing rate (FR) of the Up states was quantified from the transformed log(MUA) signal as mean of absolute value of log(MUA). To study the variability of power spectral densities (PSD) of the local field potential, we used Welch's method with 50% overlapped Hamming window with a resolution of 1 Hz. All off-line estimates and analyses were implemented in MATLAB (The MathWorks Inc., Natick, MA, USA). All variables in the experimental conditions were compared with the control (no chemical added) condition.

**The *in vivo* preparation.** Cortical electrophysiology experiments were carried out in 2-3-month-old C57BL6/JR mice ( $n = 3$ ) in accordance with the European Union Directive 2010/63/EU and approved by the local ethics committee. Mice were kept under standard conditions (room temperature, 12:12-h light-dark cycle, lights on at 08:00 a.m). Anesthesia was induced by intraperitoneal injection of ketamine (30 mg/kg) and medetomidine (100 mg/kg). After this procedure, the mouse was placed in a stereotaxic frame, and air was enriched with oxygen. Body temperature was maintained at 37°C throughout the experiment.<sup>7</sup> A craniotomy was performed in each mouse: AP -2.5 mm, L 1.5 mm (primary visual cortex, V1).<sup>79</sup> Cortical recordings were obtained from infragranular layers with 1–2 MΩ single tungsten electrode insulated with a plastic coating except for the tip (FHC, Bowdoin, ME, USA). Spontaneous local field potential (LFP) recordings from the V1 area provided information about the local neuronal population activity—within 250 μm.<sup>80</sup> MUA estimation, Up-state detection and quantification of relative FR was performed as previously described. All these parameters were used to compare spontaneous activity during anesthesia (control), after application of the pre-illuminated, less active drug form (*cis*-PAI) and drug activation with WL (*trans*-PAI). *Cis*-PAI was locally delivered to the cerebral cortex surface and activity was recorded while applying a commercial red filter on the WL source to avoid the activation of the drug. The uncovered brain was illuminated with a WL source (Photonic Optics™ Optics Cold Light Source LED F1) in order to activate the drug *in situ* (*trans*-PAI). The electrophysiological signal was amplified with a multichannel system (Multi Channel Systems), digitized at 20 kHz with a CED acquisition board and acquired with Spike 2 software (Cambridge Electronic Design) unfiltered.<sup>81</sup>

**Statistical analysis for slice experiments.** Both *in vitro* and *in vivo* oscillatory frequency (OF) are reported as mean ± SEM. Measurements under different conditions were compared using the Friedman test and the Wilcoxon post-hoc tests corrected for multiple comparisons for the *in vitro* experiments.<sup>82</sup> *In vivo* statistical analysis were performed with the unpaired t test, significance values were established with a \* p-value < 5 · 10<sup>-2</sup>.

**AUTHOR INFORMATION.** Corresponding Author \*E-mail: pau@icrea.cat; msanche3@clinic.cat.

**Author Contributions.** † Almudena Barbero-Castillo and Fabio Riefolo contributed equally to this work. Notes The authors declare no competing financial interest.

**ACKNOWLEDGMENTS.** We thank Miquel Bosch for comments on the manuscript. This research received funding from European Union Research and Innovation Programme Horizon 2020 (Human Brain Project SGA2 Grant Agreement 785907, WaveScalES), European Research ERA-Net SynBio programme (Modulightor project), and financial support from Agency for Management of University and Research Grants/Generalitat de Catalunya (CERCA Programme; 2017-SGR-1442 project;), Ministry of Economy and Competitiveness (MINECO)/FEDER (Grant CTQ2016- 80066-R to PG and BFU2017-85048-R to MVS), the Fundaluce foundation, the Commission for Universities and Research of the Department of Innovation, Universities, and Enterprise of the Generalitat de Catalunya - AGAUR- (IU16-011508) and co-financed by the European Union Regional Development

Fund within the framework of the ERDF/FEDER Operational Program of Catalonia 2014-2020 with a grant of 50% of total eligible cost to PG and MVSV.

## REFERENCES

- (1) Andalman, A. S.; Burns, V. M.; Lovett-Barron, M.; Broxton, M.; Poole, B.; Yang, S. J.; Grosenick, L.; Lerner, T. N.; Chen, R.; Benster, T.; Mourrain, P.; Levoy, M.; Rajan, K.; Deisseroth, K. Neuronal Dynamics Regulating Brain and Behavioral State Transitions. *Cell* 2019, 177 (4), 970-985.e20. <https://doi.org/10.1016/j.cell.2019.02.037>.
- (2) Wang, S.; Tudusciuc, O.; Mamelak, A. N.; Ross, I. B.; Adolphs, R.; Rutishauser, U. Neurons in the Human Amygdala Selective for Perceived Emotion. *Proc. Natl. Acad. Sci. U. S. A.* 2014, 111 (30), E3110-9. <https://doi.org/10.1073/pnas.1323342111>.
- (3) Krehbiel, D.; Bartel, B.; Dirks, M.; Wiens, W. Behavior and Brain Neurotransmitters: Correlations in Different Strains of Mice. *Behav. Neural Biol.* 1986, 46 (1), 30-45. [https://doi.org/10.1016/S0163-1047\(86\)90872-1](https://doi.org/10.1016/S0163-1047(86)90872-1).
- (4) Obermayer, J.; Verhoog, M. B.; Luchicchi, A.; Mansvelder, H. D. Cholinergic Modulation of Cortical Microcircuits Is Layer-Specific: Evidence from Rodent, Monkey and Human Brain. *Frontiers in Neural Circuits. Frontiers Media S.A.* December 8, 2017, p 100. <https://doi.org/10.3389/fncir.2017.00100>.
- (5) Hanin, I. Central Neurotransmitter Function and Its Behavioral Correlates in Man. *Environ. Health Perspect.* 1978, 26, 135-141. <https://doi.org/10.1289/ehp.7826135>.
- (6) Peyrache, A.; Dehghani, N.; Eskandar, E. N.; Madsen, J. R.; Anderson, W. S.; Donoghue, J. A.; Hochberg, L. R.; Halgren, E.; Cash, S. S.; Destexhe, A. Spatiotemporal Dynamics of Neocortical Excitation and Inhibition during Human Sleep. *Proc. Natl. Acad. Sci. U. S. A.* 2012, 109 (5), 1731-1736. <https://doi.org/10.1073/pnas.1109895109>.
- (7) Ruiz-Mejias, M.; Ciria-Suarez, L.; Mattia, M.; Sanchez-Vives, M. V. Slow and Fast Rhythms Generated in the Cerebral Cortex of the Anesthetized Mouse. *J. Neurophysiol.* 2011, 106 (6), 2910-2921. <https://doi.org/10.1152/jn.00440.2011>.
- (8) Sanchez-Vives, M. V.; Mattia, M. Slow Wave Activity as the Default Mode of the Cerebral Cortex. *Arch. Ital. Biol.* 2014, 152 (2-3), 147-155. <https://doi.org/10.12871/000298292014239>.
- (9) Muller, L.; Reynaud, A.; Chavane, F.; Destexhe, A. The Stimulus-Evoked Population Response in Visual Cortex of Awake Monkey Is a Propagating Wave. *Nat. Commun.* 2014, 5 (1), 3675. <https://doi.org/10.1038/ncomms4675>.
- (10) McCormick, D. A.; Nestvogel, D. B.; He, B. J. Neuromodulation of Brain State and Behavior. *Annu. Rev. Neurosci.* 2020, 43 (1), annurev-neuro-100219-105424. <https://doi.org/10.1146/annurev-neuro-100219-105424>.
- (11) Lee, S.-H.; Dan, Y. Neuromodulation of Brain States. *Neuron* 2012, 76 (1), 209-222. <https://doi.org/10.1016/j.neuron.2012.09.012>.
- (12) Pinto, L.; Goard, M. J.; Estandian, D.; Xu, M.; Kwan, A. C.; Lee, S.-H.; Harrison, T. C.; Feng, G.; Dan, Y. Fast Modulation of Visual Perception by Basal Forebrain Cholinergic Neurons. *Nat. Neurosci.* 2013, 16 (12), 1857-1863. <https://doi.org/10.1038/nn.3552>.

- (13) Ramaswamy, S.; Colangelo, C.; Markram, H. Data-Driven Modeling of Cholinergic Modulation of Neural Microcircuits: Bridging Neurons, Synapses and Network Activity. *Front. Neural Circuits* 2018, 12, 77. <https://doi.org/10.3389/fncir.2018.00077>.
- (14) Hasselmo, M. E.; Sarter, M. Modes and Models of Forebrain Cholinergic Neuromodulation of Cognition. *Neuropsychopharmacology* 2011, 36 (1), 52–73. <https://doi.org/10.1038/npp.2010.104>.
- (15) Buzsàki, G.; Gage, F. H. The Cholinergic Nucleus Basalis: A Key Structure in Neocortical Arousal. *EXS* 1989, 57, 159–171.
- (16) Herrero, J. L.; Roberts, M. J.; Delicato, L. S.; Gieselmann, M. A.; Dayan, P.; Thiele, A. Acetylcholine Contributes through Muscarinic Receptors to Attentional Modulation in V1. *Nature* 2008, 454 (7208), 1110–1114. <https://doi.org/10.1038/nature07141>.
- (17) Thiele, A. Muscarinic Signaling in the Brain. *Annu. Rev. Neurosci.* 2013, 36 (1), 271–294. <https://doi.org/10.1146/annurev-neuro-062012-170433>.
- (18) Conner, J. M.; Culberson, A.; Packowski, C.; Chiba, A. A.; Tuszynski, M. H. Lesions of the Basal Forebrain Cholinergic System Impair Task Acquisition and Abolish Cortical Plasticity Associated with Motor Skill Learning. *Neuron* 2003, 38 (5), 819–829.
- (19) Kilgard, M. Cholinergic Modulation of Skill Learning and Plasticity. *Neuron* 2003, 38 (5), 678–680.
- (20) Ramanathan, D.; Tuszynski, M. H.; Conner, J. M. The Basal Forebrain Cholinergic System Is Required Specifically for Behaviorally Mediated Cortical Map Plasticity. *J. Neurosci.* 2009, 29 (18), 5992–6000. <https://doi.org/10.1523/JNEUROSCI.0230-09.2009>.
- (21) Winkler, J.; Suhr, S. T.; Gage, F. H.; Thal, L. J.; Fisher, L. J. Essential Role of Neocortical Acetylcholine in Spatial Memory. *Nature* 1995, 375 (6531), 484–487. <https://doi.org/10.1038/375484a0>.
- (22) Berg, R. W.; Friedman, B.; Schroeder, L. F.; Kleinfeld, D. Activation of Nucleus Basalis Facilitates Cortical Control of a Brain Stem Motor Program. *J. Neurophysiol.* 2005, 94 (1), 699–711. <https://doi.org/10.1152/jn.01125.2004>.
- (23) Kilgard, M. P.; Merzenich, M. M. Cortical Map Reorganization Enabled by Nucleus Basalis Activity. *Science* (80-. ). 1998, 279 (5357), 1714–1718. <https://doi.org/10.1126/science.279.5357.1714>.
- (24) Disney, A. A.; Aoki, C.; Hawken, M. J. Gain Modulation by Nicotine in Macaque V1. *Neuron* 2007, 56 (4), 701–713. <https://doi.org/10.1016/j.neuron.2007.09.034>.
- (25) Henny, P.; Jones, B. E. Projections from Basal Forebrain to Prefrontal Cortex Comprise Cholinergic, GABAergic and Glutamatergic Inputs to Pyramidal Cells or Interneurons. *Eur. J. Neurosci.* 2008, 27 (3), 654–670. <https://doi.org/10.1111/j.1460-9568.2008.06029.x>.
- (26) Donthamsetti, P. C.; Broichhagen, J.; Vyklicky, V.; Stanley, C.; Fu, Z.; Visel, M.; Levitz, J. L.; Javitch, J. A.; Trauner, D.; Isacoff, E. Y. Genetically Targeted Optical Control of an Endogenous G Protein-Coupled Receptor. *J. Am. Chem. Soc.* 2019, 141 (29), 11522–11530. <https://doi.org/10.1021/jacs.9b02895>.
- (27) Yamaguchi, H.; de Lecea, L. In Vivo Cell Type-Specific CRISPR Gene Editing for Sleep Research. *Journal of Neuroscience Methods*. Elsevier B.V. March 15, 2019, pp 99–102. <https://doi.org/10.1016/j.jneumeth.2018.10.016>.

- (28) Miesenböck, G. Optogenetic Control of Cells and Circuits. *Annu. Rev. Cell Dev. Biol.* 2011, 27 (1), 731–758. <https://doi.org/10.1146/annurev-cellbio-100109-104051>.
- (29) Scarr, E. Muscarinic Receptors: Their Roles in Disorders of the Central Nervous System and Potential as Therapeutic Targets. *CNS Neurosci. Ther.* 2012, 18 (5), 369–379. <https://doi.org/10.1111/j.1755-5949.2011.00249.x>.
- (30) Riefolo, F.; Matera, C.; Garrido-Charles, A.; Gomila, A. M. J.; Sortino, R.; Agnetta, L.; Claro, E.; Masgrau, R.; Holzgrave, U.; Batlle, M.; Decker, M.; Guasch, E.; Gorostiza, P. Optical Control of Cardiac Function with a Photoswitchable Muscarinic Agonist. *J. Am. Chem. Soc.* 2019, 141 (18), 7628–7636. <https://doi.org/10.1021/jacs.9b03505>.
- (31) Sanchez-Vives, M. V.; McCormick, D. A. Cellular and Network Mechanisms of Rhythmic Recurrent Activity in Neocortex. *Nat. Neurosci.* 2000, 3 (10), 1027–1034. <https://doi.org/10.1038/79848>.
- (32) McCormick, D. A. Cellular Mechanisms Underlying Cholinergic and Noradrenergic Modulation of Neuronal Firing Mode in the Cat and Guinea Pig Dorsal Lateral Geniculate Nucleus. *J. Neurosci.* 1992, 12 (1), 278–289.
- (33) Steriade, M.; Amzica, F.; Nunez, A. Cholinergic and Noradrenergic Modulation of the Slow (Approximately 0.3 Hz) Oscillation in Neocortical Cells. *J. Neurophysiol.* 1993, 70 (4), 1385–1400. <https://doi.org/10.1152/jn.1993.70.4.1385>.
- (34) Steriade, M. Cholinergic Blockage of Network- and Intrinsically Generated Slow Oscillations Promotes Waking and REM Sleep Activity Patterns in Thalamic and Cortical Neurons. *Prog. Brain Res.* 1993, 98, 345–355.
- (35) Jacobs, S. E.; Juliano, S. L. The Impact of Basal Forebrain Lesions on the Ability of Rats to Perform a Sensory Discrimination Task Involving Barrel Cortex. *J. Neurosci.* 1995, 15 (2), 1099–1109.
- (36) Xiang, Z.; Huguenard, J. R.; Prince, D. A. Cholinergic Switching within Neocortical Inhibitory Networks. *Science* 1998, 281 (5379), 985–988. <https://doi.org/10.1126/science.281.5379.985>.
- (37) Picciotto, M. R.; Higley, M. J.; Mineur, Y. S. Acetylcholine as a Neuromodulator: Cholinergic Signaling Shapes Nervous System Function and Behavior. *Neuron* 2012, 76 (1), 116–129. <https://doi.org/10.1016/j.neuron.2012.08.036>.
- (38) Zaghera, E.; McCormick, D. A. Neural Control of Brain State. *Curr. Opin. Neurobiol.* 2014, 29, 178–186. <https://doi.org/10.1016/j.conb.2014.09.010>.
- (39) Buhl, E. H.; Tamás, G.; Fisahn, A. Cholinergic Activation and Tonic Excitation Induce Persistent Gamma Oscillations in Mouse Somatosensory Cortex in Vitro. *J. Physiol.* 1998, 513 (1), 117–126. <https://doi.org/10.1111/j.1469-7793.1998.117by.x>.
- (40) Kuczewski, N.; Aztiria, E.; Gautam, D.; Wess, J.; Domenici, L. Acetylcholine Modulates Cortical Synaptic Transmission via Different Muscarinic Receptors, as Studied with Receptor Knockout Mice. *J. Physiol.* 2005, 566 (3), 907–919. <https://doi.org/10.1113/jphysiol.2005.089987>.
- (41) Wester, J. C.; Contreras, D. Differential Modulation of Spontaneous and Evoked Thalamocortical Network Activity by Acetylcholine Level in Vitro. *J. Neurosci.* 2013, 33 (45), 17951–17966. <https://doi.org/10.1523/JNEUROSCI.1644-13.2013>.

- (42) Compte, A.; Reig, R.; Descalzo, V. F.; Harvey, M. A.; Puccini, G. D.; Sanchez-Vives, M. V. Spontaneous High-Frequency (10-80 Hz) Oscillations during Up States in the Cerebral Cortex In Vitro. *J. Neurosci.* 2008, 28 (51), 13828–13844. <https://doi.org/10.1523/JNEUROSCI.2684-08.2008>.
- (43) Schmidt, S. L.; Chew, E. Y.; Bennett, D. V.; Hammad, M. A.; Fröhlich, F. Differential Effects of Cholinergic and Noradrenergic Neuromodulation on Spontaneous Cortical Network Dynamics. *Neuropharmacology* 2013, 72, 259–273. <https://doi.org/10.1016/j.neuropharm.2013.04.045>.
- (44) Castro-Alamancos, M. A.; Gulati, T. Neuromodulators Produce Distinct Activated States in Neocortex. *J. Neurosci.* 2014, 34 (37), 12353–12367. <https://doi.org/10.1523/JNEUROSCI.1858-14.2014>.
- (45) McCormick, D. A.; Williamson, A. Convergence and Divergence of Neurotransmitter Action in Human Cerebral Cortex. *Proc. Natl. Acad. Sci. U. S. A.* 1989, 86 (20), 8098–8102. <https://doi.org/10.1073/pnas.86.20.8098>.
- (46) Barocelli, E.; Ballabeni, V.; Bertoni, S.; Dallanocce, C.; De Amici, M.; De Micheli, C.; Impicciatore, M. New Analogues of Oxotremorine and Oxotremorine-M: Estimation of Their in Vitro Affinity and Efficacy at Muscarinic Receptor Subtypes. *Life Sci.* 2000, 67 (6), 717–723. [https://doi.org/10.1016/s0024-3205\(00\)00661-5](https://doi.org/10.1016/s0024-3205(00)00661-5).
- (47) Schrage, R.; Seemann, W. K.; Klöckner, J.; Dallanocce, C.; Racké, K.; Kostenis, E.; De Amici, M.; Holzgrabe, U.; Mohr, K. Agonists with Supraphysiological Efficacy at the Muscarinic M2 ACh Receptor. *Br. J. Pharmacol.* 2013. <https://doi.org/10.1111/bph.12003>.
- (48) Sanchez-Vives, M. V.; Mattia, M.; Compte, A.; Perez-Zabalza, M.; Winograd, M.; Descalzo, V. F.; Reig, R. Inhibitory Modulation of Cortical up States. *J. Neurophysiol.* 2010, 104 (3), 1314–1324. <https://doi.org/10.1152/jn.00178.2010>.
- (49) Yi, F.; DeCan, E.; Stoll, K.; Marceau, E.; Deisseroth, K.; Lawrence, J. J. Muscarinic Excitation of Parvalbumin-Positive Interneurons Contributes to the Severity of Pilocarpine-Induced Seizures. *Epilepsia* 2015, 56 (2), 297–309. <https://doi.org/10.1111/epi.12883>.
- (50) Hamilton, S. E.; Loose, M. D.; Qi, M.; Levey, A. I.; Hille, B.; McKnight, G. S.; Idzerda, R. L.; Nathanson, N. M. Disruption of the M1 Receptor Gene Ablates Muscarinic Receptor-Dependent M Current Regulation and Seizure Activity in Mice. *Proc. Natl. Acad. Sci.* 1997, 94 (24), 13311–13316. <https://doi.org/10.1073/pnas.94.24.13311>.
- (51) Steriade, M.; Contreras, D.; Curró Dossi, R.; Nuñez, A. The Slow (< 1 Hz) Oscillation in Reticular Thalamic and Thalamocortical Neurons: Scenario of Sleep Rhythm Generation in Interacting Thalamic and Neocortical Networks. *J. Neurosci.* 1993, 13 (8), 3284–3299.
- (52) Sakata, S.; Harris, K. D. Laminar Structure of Spontaneous and Sensory-Evoked Population Activity in Auditory Cortex. *Neuron* 2009, 64 (3), 404–418. <https://doi.org/10.1016/j.neuron.2009.09.020>.
- (53) Chauvette, S.; Volgushev, M.; Timofeev, I. Origin of Active States in Local Neocortical Networks during Slow Sleep Oscillation. *Cereb. Cortex* 2010, 20 (11), 2660–2674. <https://doi.org/10.1093/cercor/bhq009>.
- (54) Capone, C.; Rebollo, B.; Munoz, A.; Illa, X.; Giudice, P. Del; Sanchez-Vives, M. V.; Mattia, M. Slow Waves in Cortical Slices: How Spontaneous Activity Is Shaped by Laminar Structure. *Cereb. Cortex* 2019, 29 (1), 319–335. <https://doi.org/10.1093/cercor/bhx326>.

- (55) Beltramo, R.; D'Urso, G.; Dal Maschio, M.; Farisello, P.; Bovetti, S.; Clovis, Y.; Lassi, G.; Tucci, V.; De Pietri Tonelli, D.; Fellin, T. Layer-Specific Excitatory Circuits Differentially Control Recurrent Network Dynamics in the Neocortex. *Nat. Neurosci.* 2013, 16 (2), 227–234. <https://doi.org/10.1038/nn.3306>.
- (56) Koch, M.; Schmiedt-Fehr, C.; Mathes, B. Neuropharmacology of Altered Brain Oscillations in Schizophrenia. *International Journal of Psychophysiology.* Elsevier B.V. 2016, pp 62–68. <https://doi.org/10.1016/j.ijpsycho.2015.02.014>.
- (57) Cardin, J. A.; Carlén, M.; Meletis, K.; Knoblich, U.; Zhang, F.; Deisseroth, K.; Tsai, L.-H.; Moore, C. I. Driving Fast-Spiking Cells Induces Gamma Rhythm and Controls Sensory Responses. *Nature* 2009, 459 (7247), 663–667. <https://doi.org/10.1038/nature08002>.
- (58) Sohal, V. S.; Zhang, F.; Yizhar, O.; Deisseroth, K. Parvalbumin Neurons and Gamma Rhythms Enhance Cortical Circuit Performance. *Nature* 2009, 459 (7247), 698–702. <https://doi.org/10.1038/nature07991>.
- (59) Adesnik, H.; Naka, A. Cracking the Function of Layers in the Sensory Cortex. *Neuron.* Cell Press December 5, 2018, pp 1028–1043. <https://doi.org/10.1016/j.neuron.2018.10.032>.
- (60) Naka, A.; Veit, J.; Shababo, B.; Chance, R. K.; Risso, D.; Stafford, D.; Snyder, B.; Egladyous, A.; Chu, D.; Sridharan, S.; Mossing, D. P.; Paninski, L.; Ngai, J.; Adesnik, H. Complementary Networks of Cortical Somatostatin Interneurons Enforce Layer Specific Control. *Elife* 2019, 8. <https://doi.org/10.7554/eLife.43696>.
- (61) Hüll, K.; Morstein, J.; Trauner, D. In Vivo Photopharmacology. *Chemical Reviews.* American Chemical Society November 14, 2018, pp 10710–10747. <https://doi.org/10.1021/acs.chemrev.8b00037>.
- (62) Paulus, W. Transcranial Brain Stimulation: Potential and Limitations. *e-Neuroforum* 2014, 5 (2), 29–36. <https://doi.org/10.1007/s13295-014-0056-6>.
- (63) Pollok, B.; Boysen, A.-C.; Krause, V. The Effect of Transcranial Alternating Current Stimulation (TACS) at Alpha and Beta Frequency on Motor Learning. *Behav. Brain Res.* 2015, 293, 234–240. <https://doi.org/10.1016/j.bbr.2015.07.049>.
- (64) Lefaucheur, J.-P.; André-Obadia, N.; Antal, A.; Ayache, S. S.; Baeken, C.; Benninger, D. H.; Cantello, R. M.; Cincotta, M.; de Carvalho, M.; De Ridder, D.; Devanne, H.; Di Lazzaro, V.; Filipović, S. R.; Hummel, F. C.; Jääskeläinen, S. K.; Kimiskidis, V. K.; Koch, G.; Langguth, B.; Nyffeler, T.; Oliviero, A.; Padberg, F.; Poulet, E.; Rossi, S.; Rossini, P. M.; Rothwell, J. C.; Schönfeldt-Lecuona, C.; Siebner, H. R.; Slotema, C. W.; Stagg, C. J.; Valls-Sole, J.; Ziemann, U.; Paulus, W.; Garcia-Larrea, L. Evidence-Based Guidelines on the Therapeutic Use of Repetitive Transcranial Magnetic Stimulation (RTMS). *Clin. Neurophysiol.* 2014, 125 (11), 2150–2206. <https://doi.org/10.1016/J.CLINPH.2014.05.021>.
- (65) Zucca, S.; Pasquale, V.; Lagomarsino de Leon Roig, P.; Panzeri, S.; Fellin, T. Thalamic Drive of Cortical Parvalbumin-Positive Interneurons during Down States in Anesthetized Mice. *Curr. Biol.* 2019, 29 (9), 1481–1490.e6. <https://doi.org/10.1016/j.cub.2019.04.007>.
- (66) Gibbons, A. S.; Scarr, E.; McLean, C.; Sundram, S.; Dean, B. Decreased Muscarinic Receptor Binding in the Frontal Cortex of Bipolar Disorder and Major Depressive Disorder Subjects. *J. Affect. Disord.* 2009, 116 (3), 184–191. <https://doi.org/10.1016/j.jad.2008.11.015>.
- (67) Cannon, D. M.; Carson, R. E.; Nugent, A. C.; Eckelman, W. C.; Kiesewetter, D. O.; Williams, J.; Rollis, D.; Drevets, M.; Gandhi, S.; Solorio, G.; Drevets, W. C. Reduced Muscarinic Type 2 Receptor Binding in

Subjects With Bipolar Disorder. *Arch. Gen. Psychiatry* 2006, 63 (7), 741. <https://doi.org/10.1001/archpsyc.63.7.741>.

(68) Piggott, M. A.; Owens, J.; O'Brien, J.; Colloby, S.; Fenwick, J.; Wyper, D.; Jaros, E.; Johnson, M.; Perry, R. H.; Perry, E. K. Muscarinic Receptors in Basal Ganglia in Dementia with Lewy Bodies, Parkinson's Disease and Alzheimer's Disease. *J. Chem. Neuroanat.* 2003, 25 (3), 161–173.

(69) Dick, D. M.; Agrawal, A.; Wang, J. C.; Hinrichs, A.; Bertelsen, S.; Bucholz, K. K.; Schuckit, M.; Kramer, J.; Nurnberger, J.; Tischfield, J.; Edenberg, H. J.; Goate, A.; Bierut, L. J. Alcohol Dependence with Comorbid Drug Dependence: Genetic and Phenotypic Associations Suggest a More Severe Form of the Disorder with Stronger Genetic Contribution to Risk. *Addiction* 2007, 102 (7), 1131–1139. <https://doi.org/10.1111/j.1360-0443.2007.01871.x>.

(70) Wenzel, M.; Hamm, J. P.; Peterka, D. S.; Yuste, R. Acute Focal Seizures Start As Local Synchronizations of Neuronal Ensembles. *J. Neurosci.* 2019, 39 (43), 8562–8575. <https://doi.org/10.1523/JNEUROSCI.3176-18.2019>.

(71) Pittolo, S.; Lee, H.; Lladó, A.; Tosi, S.; Bosch, M.; Bardia, L.; Gómez-Santacana, X.; Llebaria, A.; Soriano, E.; Colombelli, J.; Poskanzer, K. E.; Perea, G.; Gorostiza, P. Reversible Silencing of Endogenous Receptors in Intact Brain Tissue Using 2-Photon Pharmacology. *Proc. Natl. Acad. Sci.* 2019, 116 (27), 13680–13689. <https://doi.org/10.1073/pnas.1900430116>.

(72) Zucca, S.; D'Urso, G.; Pasquale, V.; Vecchia, D.; Pica, G.; Bovetti, S.; Moretti, C.; Varani, S.; Molano-Mazón, M.; Chiappalone, M.; Panzeri, S.; Fellin, T. An Inhibitory Gate for State Transition in Cortex. *Elife* 2017, 6. <https://doi.org/10.7554/eLife.26177>.

(73) Sanchez-Vives, M. V.; Reig, R.; Winograd, M.; Descalzo, V. F. An Active Cortical Network in Vitro; Vol. 37.

(74) Mattia, M.; Sanchez-Vives, M. V. Exploring the Spectrum of Dynamical Regimes and Timescales in Spontaneous Cortical Activity. *Cogn. Neurodyn.* 2012, 6 (3), 239–250. <https://doi.org/10.1007/s11571-011-9179-4>.

(75) Krimer, L. S.; Goldman-Rakic, P. S. Prefrontal Microcircuits: Membrane Properties and Excitatory Input of Local, Medium, and Wide Arbor Interneurons. *J. Neurosci.* 2001, 21 (11), 3788–3796.

(76) Aghajanian, G. K.; Rasmussen, K. Intracellular Studies in the Facial Nucleus Illustrating a Simple New Method for Obtaining Viable Motoneurons in Adult Rat Brain Slices. *Synapse* 1989, 3 (4), 331–338. <https://doi.org/10.1002/syn.890030406>.

(77) D'Andola, M.; Rebollo, B.; Casali, A. G.; Weinert, J. F. .; Pigorini, A.; Villa, R.; Massimini, M.; Sanchez-Vives, M. V. Bistability, Causality, and Complexity in Cortical Networks: An In Vitro Perturbational Study. *Cereb. Cortex*, Vol. 28, Issue 7 2018, 2233–2242.

(78) Mattia, M.; Del Giudice, P. Population Dynamics of Interacting Spiking Neurons. *Phys. Rev. E* 2002, 66 (5), 051917. <https://doi.org/10.1103/PhysRevE.66.051917>.

(79) Golmohammadi, M. G.; Blackmore, D. G.; Large, B.; Azari, H.; Esfandiary, E.; Paxinos, G.; Franklin, K. B. J.; Reynolds, B. A.; Rietze, R. L. Comparative Analysis of the Frequency and Distribution of Stem and Progenitor Cells in the Adult Mouse Brain. *Stem Cells* 2008, 26 (4), 979–987. <https://doi.org/10.1634/stemcells.2007-0919>.

(80) Katzner, S.; Nauhaus, I.; Benucci, A.; Bonin, V.; Ringach, D. L.; Carandini, M. Local Origin of Field Potentials in Visual Cortex. *Neuron* 2009, 61 (1), 35–41.

(81) Castano-Prat, P.; Perez-Zabalza, M.; Perez-Mendez, L.; Escorihuela, R. M.; Sanchez-Vives, M. V. Slow and Fast Neocortical Oscillations in the Senescence-Accelerated Mouse Model SAMP8. *Front. Aging Neurosci.* 2017, 9, 141. <https://doi.org/10.3389/fnagi.2017.00141>.

(82) Benjamini, Y.; Hochberg, Y. Controlling the False Discovery Rate: A Practical and Powerful Approach to Multiple Testing. *Journal of the Royal Statistical Society. Series B (Methodological)*. WileyRoyal Statistical Society 1995, pp 289–300. <https://doi.org/10.2307/2346101>.

## Supporting Information

### Control of brain state transitions with a photoswitchable muscarinic agonist

Almudena Barbero-Castillo, Fabio Riefolo, Carlo Matera, Sara Caldas-Martínez, Pedro Mateos-Aparicio, Julia F. Weinert, Enrique Claro, Maria V. Sanchez-Vives, and Pau Gorostiza

#### Table of content

- 1. Competition binding experiments**
- 2. Autocorrelograms**
- 3. Additional references**

## 1. Competition binding experiment

### 1.1 Materials and Methods

Iperoxo (IPX) and Phthalimide-Azo-Iperoxo (PAI) were preliminarily assayed for their affinity to muscarinic receptors (mAChRs) by competition binding experiments in whole cortex of 3-4 months old female Wistar rat brain membrane, which contained a high density of all the subtypes of mAChRs.<sup>1</sup> [<sup>3</sup>H]Quinuclidinyl benzilate ([<sup>3</sup>H]QNB) is a muscarinic antagonist without subtype selectivity, which binds the muscarinic receptors with high selectivity. [<sup>3</sup>H]QNB is recognized to be excellent for such binding experiments,<sup>2,3</sup> and we performed them in order to test if IPX and PAI have the potential to modulate cortical brain states. Specific binding of IPX and PAI was defined by testing concentrations ranging from 10<sup>-9</sup> to 10<sup>-4</sup> M, and derivatizing the raw disintegrations per minute (dpm) data from the scintillation counter to obtain the total radioactivity values.<sup>1</sup>

**Results.** Competition binding experiments can show that both IPX and PAI have an interesting high binding affinity for mAChRs orthosteric site. IPX was found to have an IC<sub>50</sub> of 1.5 μM, trans-PAI of 47 nM and cis-PAI of 118 nM (**Figure S1**). Such preliminary results encouraged us to investigate further our muscarinic compounds activity on the dynamics of the isolated V1 cortical slices.

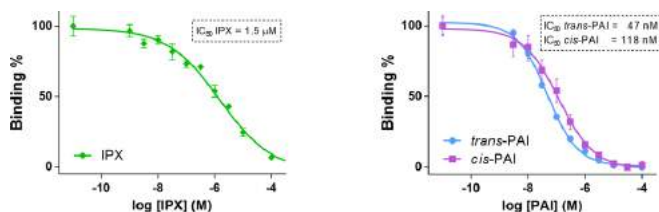


**Figure S1. Competitive binding experiments of IPX and PAI to Wistar rats' whole cortex containing all the mAChRs.** Competitive binding experiments of IPX and PAI to Wistar rats' whole cortex containing all the mAChRs. Competition for specific binding of 200 pM [<sup>3</sup>H]QNB to 3-4 months-old female Wistar rats brain membranes (whole cortex) containing high density of all the five mAChRs by IPX and PAI (n = 4 for each isomer). Data points were fitted using the "log(inhibitor) vs. normalized response - Variable slope (four parameters)" function in GraphPad Prism 6.

## 2. Autocorrelograms

### 2.1 Autocorrelograms at 200 nM of PAI (switching of PAI activity)

PAI (200 nM) was first applied in its less active isomer (*cis*-PAI, pre-irradiation with 365 nm light). The activity of *cis*-PAI at 200 nM (pink line) in cortical slices does not evoke strong changes in terms of oscillatory activity in comparison to the basal control situation (black line) without PAI application, as it is shown in the autocorrelograms graph (**Figure S2**). After white light (WL) application, PAI switches to its more active *trans* form (blue line), and

strong changes of the oscillatory activity are visible (**Figure S2**). The autocorrelograms are obtained by analyzing LFP from one channel.

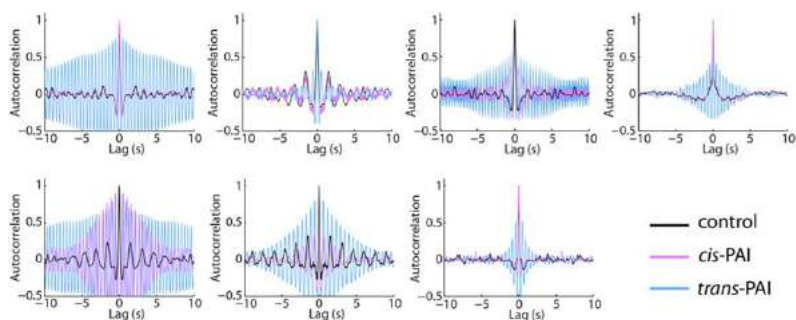


**Figure S2.** PAI can light-modulate the neuronal oscillatory activity in cortical ferret slices. Autocorrelograms of the rhythmicity of the neuronal oscillatory activity in basal condition (without PAI application, black line), under 200 nM *cis*-PAI application (pink line) and during white light irradiation (*trans*-PAI, blue line).

## 2.2 Autocorrelograms at 100 nM and 1 $\mu$ M of PAI

The activity of PAI at 100 nM and 1  $\mu$ M in cortical slices do not strongly differ between *trans* (**Figure S3**) and *cis* (**Figure S4**) in terms of oscillatory activity. 100 nM applications of *trans* and *cis* do not mostly produce changes in neuronal firing in comparison to the basal control situation (black line), as it is shown in the autocorrelograms graph (**Figure S3** and **S4**). At 1  $\mu$ M, both PAI isomers produce strong changes of the oscillatory activity (**Figure S3** and **S4**). The autocorrelograms graphs are obtained by analyzing LFP from one channel.

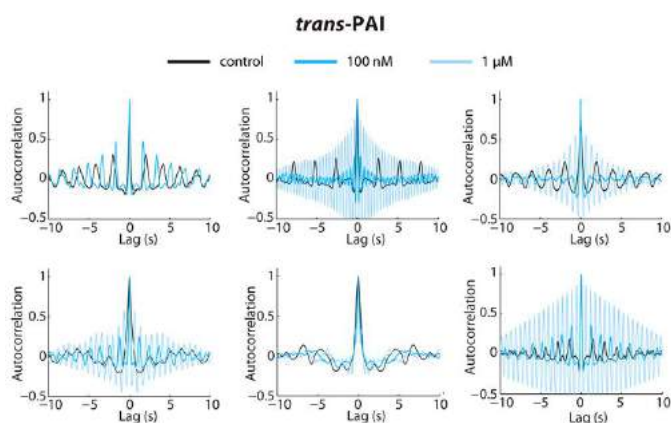


**Figure S3.** Autocorrelograms of the rhythmicity of the neuronal oscillatory activity in basal condition (without PAI application, black line), at 100 nM and 1  $\mu$ M of *trans*-PAI (blue lines) applications.

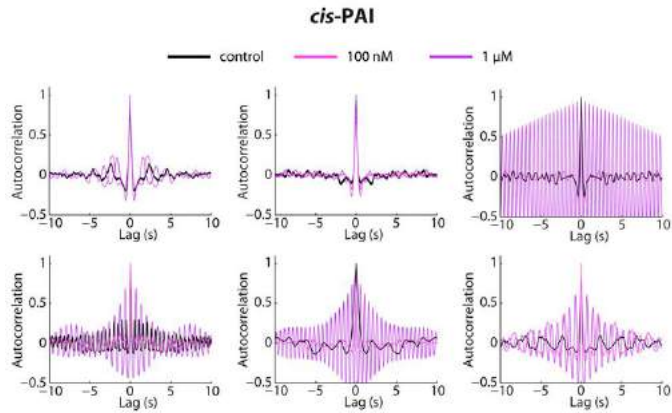


**Figure S4.** Autocorrelograms of the rhythmicity of the neuronal oscillatory activity in basal condition (without PAI application, black line), at 100 nM and 1  $\mu$ M of *cis*-PAI (pink lines) applications.

### 3. Additional references

- (1) E. Claro, *Biochem. Mol. Biol. Educ.* 2006, 34, 428–431.
- (2) H. I. Yamamura, S. H. Snyder, *Proc. Natl. Acad. Sci. U. S. A.* 1974, 71, 1725–9.
- (3) J. Sallés, M. A. Wallace, J. N. Fain, *J. Pharmacol. Exp. Ther.* 1993, 264.

## General Discussion

### Chapter III

The blending of hybridization and non-canonical azologization strategies allowed the creation of a promising light-sensitive muscarinic ligand in this chapter III. PAI activates M2 receptors in its *trans* conformation and can be photoisomerized to the less active *cis* form with ultraviolet light (365 nm). The back isomerization to the *trans* form can be successfully obtained using 420-460 nm wavelengths or with white light.

Although compounds that are active in their thermodynamically stable configuration display many advantages for basic research studies (Pittolo et al., 2019), dark-inactive ligands are in principle preferred for medical applications. PAI is active in the dark but the excellent thermal stability of its isomers can overcome this limitation. In particular, it allows administering the inactive *cis*-PAI in a living organism, and subsequently activating it to *trans* with spatiotemporal control. Moreover, we demonstrated the photoactivation of PAI with near-infrared (NIR) light under two-photon excitation (2PE) which is intrinsically constrained in three dimensions. Pulsed lasers are required for this purpose. The laser beam must possess a very short pulses width (femtoseconds) and be focused into a small volume (femtoliters). With these properties, it is possible to obtain a high photon density in this small volume, and to enhance the probability that a chromophore, in our case the azobenzene, absorbs two low-energy (IR) photons that allow performing the isomerization in a way equivalent to single high-energy photons using continuous UV light sources (**Figure 36**).

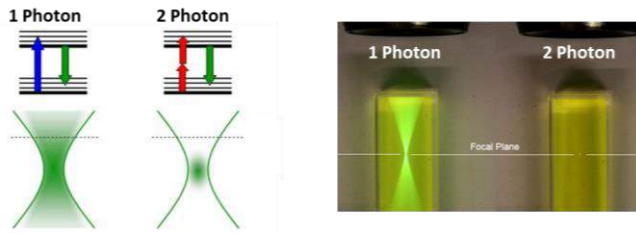


**Figure 36. One-photon and two-photon excitations.** With one-photon excitation, the fluorescence signals are equally generated above and below the focal plane. Differently, the two-photon excitation permits to confine the 80% of the total fluorescence signal to a region 1  $\mu\text{M}$  thick about the focal plane. Figure adapted from Weiß et al., 2009.

The wavelength to switch the photoresponsive drug can be chosen combining the energy of two photons, in order to span the energetic gap with the classical one-photon excitation. We used a pulsed laser together with a confocal microscope in order that PAI could activate M2 receptors under 840 nm illumination *in vitro* in calcium imaging assay. This result is promising and gets photopharmacology closer to clinical applications. Indeed, NIR wavelengths reside in the most suitable phototherapeutic window (650–850 nm) (**Figure 37**) where we can get the highest penetration into biological tissues with the lowest absorption and potential photodamage (Bort et al., 2013; Cabré et al., 2019a; Pawlicki et al., 2009; Svoboda and Yasuda, 2006; Zipfel et al., 2003).

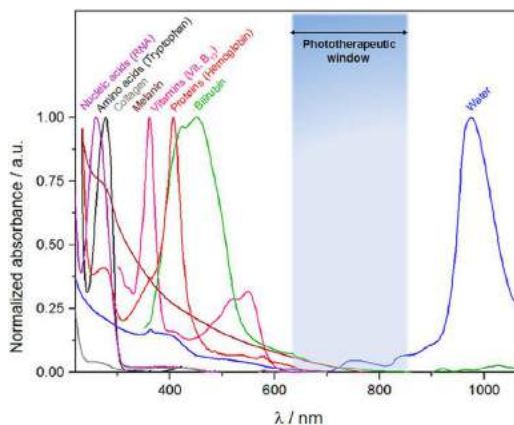


**Figure 37. Phototherapeutic window.** The spectral range of visible and near-infrared (NIR) light (650–850 nm) can penetrate deeper into human tissues than ultraviolet lights, causing less photodamages (Dąbrowski et al., 2016).

Furthermore, the photochemical properties of PAI can also be improved by the insertions of fluorine/s into the azobenzene, as these modifications can improve the two-photon absorption of the molecule (Cabr e et al., 2019a). Other ways to improve PAI regarding certain applications include the substitution of the azobenzene with a diazocine scaffold, which should afford dark-inactive derivatives.

In conclusion, PAI demonstrated the first photopharmacological manipulation of endogenous muscarinic receptors in living animals. With this drug, we photocontrolled important M2 functions in the cardiovascular system, where we opened the doors to innovative potential antiarrhythmic therapies, and in the brain, where we defined a new approach for studying cholinergic modulation in cognition and behavior. Besides, PAI can be used to photocontrol also other biological functions where M2 receptors are involved. The focalized stimulation of this drug with 2PE offers unique advantages *in vivo* both for research and clinical purposes. These improvements in the photochemical and pharmacological properties of PAI, together with progress in the miniaturization and performance of pulsed lasers may lead to advanced therapeutic applications of photopharmacology.



## CHAPTER IV

### Light-sensitive M1 Muscarinic Antagonists Designed with a Novel “Crypto-azologization” Method



## General Introduction

### Chapter IV

The list of approved muscarinic drugs in medicine is very short, mainly due to their adverse effects. In parallel to the development of novel photoswitchable agonists for such receptors, we also investigated the possibility of creating antagonists. We focused our studies on the M1 subtype, whose antagonists are used against the peptic ulcer disease and are also promising for the treatment of debilitating pathologies like Parkinson's disease (PD) (Xiang et al., 2012), some forms of cancer in animal models (Kruse et al., 2014; Magnon et al., 2013), or lethal events in the ischemic heart disease (Pedretti et al., 2003).

To design our light-sensitive derivatives, we considered the M1 antagonist pirenzepine as model because of its fascinating chemical structure. Pirenzepine belongs to the "privileged structures" family, as contains a fused three-ringed system. In general, the tricyclic core is present in many pharmaceutical agents. Such "privileged" drugs were intensely used in medicine for many different treatments, but their low selective properties cause undeniable side effects and toxicity that have progressively reduced their appeal in human therapies.

We designed a new strategy of azologization, named "crypto-azologization", and we applied it to design our pirenzepine derivatives. We replaced the three-ringed core with different azobenzene scaffolds. This novel design expands the azolog space and has the potential to produce drugs that are inactive in the thermodynamically stable *trans* configuration, which is a frequent concern in photopharmacology. Then, upon illumination with the correct wavelength, the obtained *cis* conformation can mimic the tricyclic geometry and accomplish the antagonist activity of the parent compound. This new azologization strategy can also be used for other members of the "privileged structures" family, such as the popular tricyclic antidepressant drugs (TCAs), in order

to improve their selectivity with the spatio-temporal photoactivation and reduce their unwanted side effects and toxicity.

First, to check our design strategy, we performed molecular docking simulations of a representative pirenzepine derivative structure at the inactive model of the human M1 receptor. The obtained results supported our hypothesis. Thus, we performed the synthesis and the photopharmacological characterization of four pirenzepine derivatives, named “cryptozepines”. We firstly studied their general affinity profile to mAChRs by competition binding experiments in rat brain membranes. Then, their photoswitchable antagonism was tested in real-time calcium imaging assays, using human M1 receptors expressed in cultured cells, and in cardiac atria *ex vivo*.

*This project has been developed at IBEC with collaborations at UAB for binding and ex vivo experiments. I personally carried out the design, the molecular docking simulations, the chemical syntheses, and the photochemical characterizations of all the compounds that are present in this work. I also performed the competition binding experiments on mAChRs, the development of the light-sensitive experimental set-up for the pharmacological studies, the design and the co-performance of all the in vitro and ex vivo experiments. I wrote the full draft of the manuscript. The results of this chapter have been recently submitted for publication and are currently under review. They are reproduced here in a journal article format with the corresponding supporting information. The reference of this work is:*

*“Rational design of photochromic analogs of tricyclic drugs”*

*Fabio Riefolo, Rosalba Sortino, Carlo Matera, Enrique Claro, Beatrice Preda, Simone Vitiello, Sara Traserra, Marcel Jiménez, and Pau Gorostiza*

*Submitted on the 27<sup>th</sup> of May 2020*

## Rational design of photochromic analogs of tricyclic drugs

Fabio Riefolo,<sup>†,‡</sup> Rosalba Sortino,<sup>†,‡,¶</sup> Carlo Matera,<sup>†,‡,¶</sup> Enrique Claro,<sup>§</sup> Beatrice Preda,<sup>†</sup> Simone Vitiello,<sup>†</sup> Sara Traserra,<sup>||</sup> Marcel Jiménez,<sup>||</sup> Pau Gorostiza<sup>†,‡,⊥,\*</sup>

<sup>†</sup>Institute for Bioengineering of Catalonia (IBEC), Barcelona Institute for Science and Technology (BIST), Barcelona, Spain.

<sup>‡</sup>Network Biomedical Research Center in Bioengineering, Biomaterials, and Nanomedicine (CIBER-BBN), Madrid, Spain.

<sup>§</sup>Institut de Neurociències and Departament de Bioquímica i Biologia Molecular, Unitat de Bioquímica de Medicina, Universitat Autònoma de Barcelona (UAB), Barcelona, Spain.

<sup>||</sup>Department of Cell Biology, Physiology and Immunology, Universitat Autònoma de Barcelona, Barcelona, Spain..

<sup>⊥</sup>Catalan Institution for Research and Advanced Studies (ICREA), Barcelona, Spain.

<sup>¶</sup>Contributed equally to this work.

**ABSTRACT:** Tricyclic chemical structures are the core of many important drugs targeting all neurotransmitter pathways. These medicines enable effective therapies to treat from peptic ulcer disease to psychiatric disorders. However, when administered systemically they cause serious adverse effects that limit their use. In order to obtain localized and on-demand pharmacological action using light, we have designed photoisomerizable ligands based on azobenzene that mimic the tricyclic chemical structure and display reversibly controlled activity. Several pseudo analogs of the tricyclic antagonist pirenzepine demonstrate that this is an effective strategy in muscarinic acetylcholine receptors, showing stronger inhibition upon illumination both *in vitro* and in cardiac atria *ex vivo*. These photoswitchable “crypto-azologs” of tricyclic drugs might open a general way to spatiotemporally target their therapeutic action while reducing their systemic toxicity and adverse effects.

## INTRODUCTION

Photopharmacology is a modern branch of pharmacology that aims to improve the efficacy and safety of drugs by directing their action to target organs and controlling their doses using light. It deals with molecular strategies to photo-regulate drug activity.<sup>1,2</sup> Most photoswitchable small molecule ligands developed in recent years have exploited the reduced size and robust photochromism of azobenzene, which allows two design approaches: (1) tailoring compounds through extension of the drug core (“azo-extension” approach), and (2) introducing an isosteric azobenzene photoswitch in the core (“azologization” approach).<sup>3,4</sup> The latter is the most straightforward design strategy and is generally preferred because it requires minimal modifications of the original structure, thus maintaining the drug-likeness of the parent compound and largely preserving its pharmacokinetic and pharmacodynamic properties.<sup>5,6</sup> If azologization motifs are not present, in some cases the drug structure can be extended with a photoswitchable moiety while retaining the drug activity.<sup>3,7</sup> However, these versatile and complementary strategies are not applicable to all drugs. This is often the case when azobenzene-like motifs are absent from a parent molecule that can only tolerate minor variations in size (i.e. non-azologizable and non-azo-extendable drugs), thus hampering the reach of photopharmacology. An important class of drugs that has not been endowed with photo-regulation is characterized by the general formula of **Figure 1A**, i.e. those fused tricyclic compounds which are known as “privileged structures” in medicinal chemistry.<sup>8</sup> This term was coined by Ben Evans in 1988 to recognize the potential of certain structural motifs as templates for derivatization and discovery of novel biological ligands.<sup>9</sup> A great diversity of tricyclic derivatives has been developed and are marketed for different clinical conditions. They include central nervous system agents such as tricyclic antidepressants used to treat psychiatric disorders<sup>10</sup> but also for other therapeutic indications such as loratadine (an antihistamine drug used to treat the symptoms of allergies), nevirapine (a non-competitive HIV-1 reverse transcriptase inhibitor), lonafarnib (a farnesyl transferase inhibitor used as anticancer), and pirenzepine (an antimuscarinic drug to treat peptic ulcers).<sup>11</sup>

An arylazo moiety (e.g., an azobenzene) in its *cis* configuration can quite resemble (at least in some of its conformations) the geometry of the tricyclic scaffold, whereas the corresponding *trans* isomer cannot. This is illustrated by the three-dimensional alignment of conformers in **Figure 1B**. Thus, we devised a way to mimic the tricyclic system of these drugs with a photochromic arylazo unit by means of two modifications: (1) the isosteric substitution of the two-atom bridge connecting the aryl rings with a –N=N– group to confer photochromic behavior, and (2) the cleavage (ring opening) of one of the two single bonds forming the one-atom bridge, to increase the flexibility and to enable greater changes in geometry upon photoisomerization. In this way, the photochromic pseudo-analog of the tricyclic drug should be able to maintain the pharmacological properties of the parent compound upon photoisomerization to the *cis* configuration. Conversely, the most thermodynamically stable *trans* isomer should display a reduced capacity to modulate its biological target. This situation would be particularly favorable to apply the inactive drug in the absence of illumination and to photoactivate it at the desired locations and times. We named this novel procedure to design photoswitchable small molecules “crypto-azologization” (where the prefix “crypto-” comes from the Ancient Greek word κρυπτός [kruptós], meaning “hidden”) because it expands the azologization strategy to compounds in which the potential photochromic scaffold is buried and must be sculpted out of the parent structure by a ring opening in addition to the canonical azosteric replacement.

As a test bed for our design strategy, we chose the muscarinic acetylcholine receptor (mAChR) antagonist pirenzepine (**Figure 1C**) both because of its tricyclic structure and therapeutic importance. Muscarinic receptors belong to the class A family of G-protein-coupled receptors (GPCRs) and are classified in five distinct subtypes.<sup>12,13</sup> The wide distribution of mAChRs in the body and the limited subtype selectivity of muscarinic drugs are the cause of their adverse effects, which have made these receptors an attractive target in photopharmacology.<sup>14-16</sup> Pirenzepine (Gastrozepine) is an M1-selective muscarinic antagonist marketed to treat peptic ulcers. In particular, it inhibits the parasympathetic nervous system “rest-and-digest” response, reducing gastric acid secretion and muscle spasm.<sup>17-20</sup> Other potential applications

have been considered, like slowing down myopia progression<sup>21</sup> and reducing the risk of lethal events in the ischemic heart disease.<sup>22</sup> The wide expression of M1 mAChRs in the hippocampus and medial prefrontal cortex suggests that M1-mediated signaling is important for cognitive and learning functions and plays a key role in several neurological disorders.<sup>12,13</sup> The development of photoswitchable M1 ligands is thus of great interest both for therapeutic and research purposes. Here, we report the synthesis of photoswitchable M1 mAChR antagonists designed by crypto-azologization of pirenzepine, and the characterization of their photopharmacological effects *in vitro* and *ex vivo*.

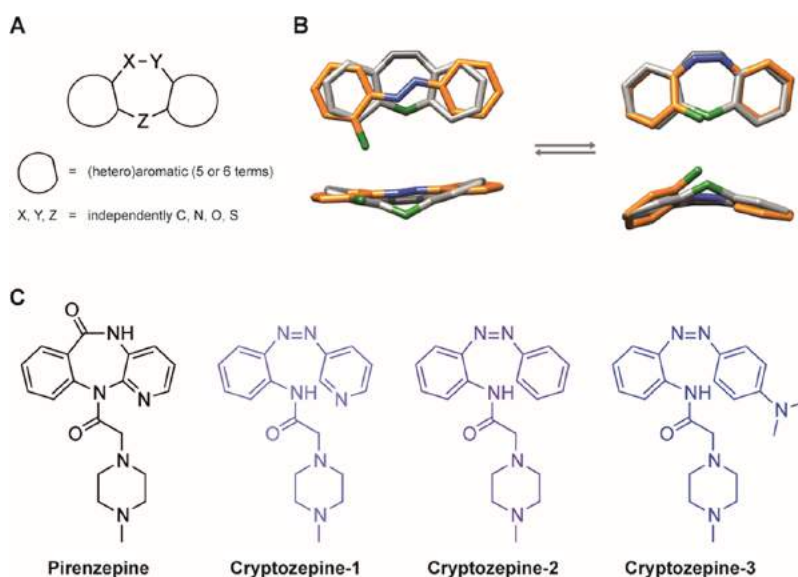


**Figure 1. Design strategy and structure of crypto-azologs.** (A) General scaffold of fused tricyclic drugs. (B) Best three-dimensional alignment of an azobenzene scaffold (*trans* on the left and *cis* on the right, both in orange) over a generic fused tricyclic system (in gray). For the sake of comparison, the carbon atom of the 1-atom bridge of the tricyclic system and the corresponding carbon atom of the azobenzene are indicated in green. Nitrogen atoms are in blue. (C) Chemical structure of the muscarinic M<sub>1</sub> antagonist pirenzepine and the cryptozepines, the photochromic derivatives discussed in this work.

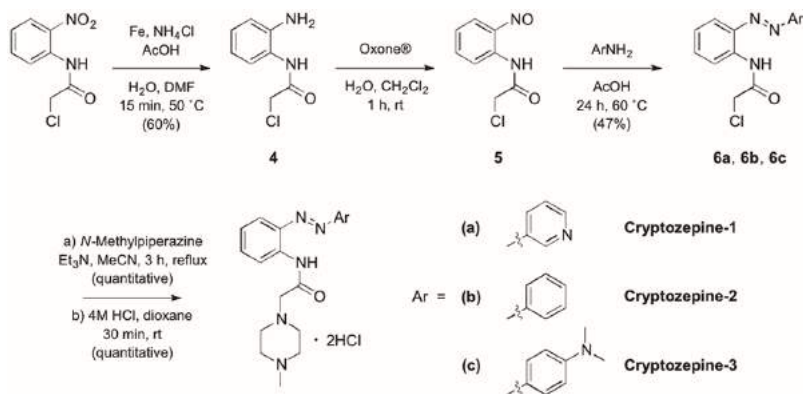
## RESULTS AND DISCUSSION

**Rational Design and Chemical Synthesis.** As an initial control for our design strategy, we performed docking simulations of a representative

structure at the M1 mAChR.<sup>23</sup> The results supported our hypothesis (see **SI** for details) and encouraged us to pursue the synthesis of a small set of pirenzepine crypto-azologs that were named “cryptozepines” (**Figure 1C**). Previous studies on pirenzepine congeners have shown how the nature and placement of accessory groups on the central core of the molecule determine the differences in receptor recognition and the binding process at mAChRs.<sup>19</sup> In particular, the positioning of the protonated nitrogen atom at the end of the piperazine, that is affected by the geometry of the whole structure, is crucial for the receptor recognition and the binding processes in M1 mAChRs.<sup>19,23,24</sup> On the other hand, certain structural modifications at the tricyclic core are tolerated. The endocyclic amide group is thought to participate in polar interactions at the binding site, therefore its replacement with a lipophilic function such as an ethylene bridge would likely produce a loss of affinity, whereas an azo group could be better accepted. The exocyclic amide group and the nitrogen atom in one of the two aromatic rings seem to have only a minor effect in terms of affinity and selectivity.<sup>19</sup> As such, we decided to conserve the essential 2-(4-methylpiperazin-1-yl)acetamide side chain in all the novel derivatives, while the endocyclic amide group was replaced with an azo group and the central 7-membered ring was “opened” to generate a fully unconstrained photochromic unit. In addition, structural variations at this unit were rationally designed in order to obtain analogs endowed with different photochemical properties. Cryptozepine-**1** and cryptozepine-**2** are straightforward crypto-azologs of pirenzepine and differ from one another in the presence of the nitrogen atom in one of the two aromatic rings. This feature should significantly reduce the half-life of thermal relaxation of the *cis* isomers, as well as an increase in the aqueous solubility of these derivatives. We expected though that these two derivatives would need ultraviolet (UV) light to undergo *trans*-to-*cis* isomerization, which is generally not convenient in biology.<sup>25</sup> Cryptozepine-**3** was designed to overcome this limitation by introducing an electron-donating group (–NMe<sub>2</sub>) at the *para* position of the benzene ring which is not directly connected to the side chain, in order to produce a red-shifting “push–pull” effect (**Figure 1C**).<sup>26</sup> As mentioned above, we hypothesized that the M1 mAChR should be able to properly accommodate the new ligands in their

*cis* configuration, while the *trans* geometry should hinder the rest of the molecule from entering the binding pocket.

Cryptozepines **1**, **2** and **3** were synthesized as illustrated in **Scheme 1** (see **SI** for detailed procedures). *N*-Chloroacetyl-2-nitroaniline was reduced to the corresponding amine (**4**) by treatment with iron in ammonium chloride and acetic acid. Oxidation with Oxone<sup>®</sup> gave the nitroso derivative (**5**), which was then coupled to the chosen arylamine under Mills conditions to yield the arylazo intermediates (**6a**, **6b**, **6c**). Nucleophilic substitution of the chlorine with 1-methylpiperazine and subsequent treatment with hydrochloric acid afforded the three final compounds as dihydrochloride salts (**1**, **2**, **3**). A fourth compound characterized by a different “push-pull” system was prepared, but because of its very low aqueous solubility at neutral pH we could not test its pharmacological properties. However, its physicochemical characterization is reported in the **SI** (compound **9**).



Scheme 1. The chemical synthesis of cryptozepines.

**Photochemical Characterization.** We then tested the ability of our photoswitchable compounds to effectively respond to light. First, we characterized the three cryptozepines by UV-Vis spectroscopy. Cryptozepines **1** and **2** displayed a clear photochromic behavior and the typical absorption bands of azobenzenes, with maxima at 318 nm and 433 nm due to the  $\pi$ - $\pi^*$  and  $n$ - $\pi^*$  transitions, respectively (**Figure 2** and **SI**). As expected, the presence of an electron-donating group in cryptozepine-**3** resulted in a strong red-shift of the  $\pi$ - $\pi^*$  transition band, with an

absorption maximum at 465 nm in aqueous solution. In this case, it was not possible to observe any change in the absorption spectrum with steady-state spectroscopy in aqueous solution since the thermal isomerization of this kind of azobenzenes in protic solvents occurs extremely fast and generally completes within milliseconds.<sup>27</sup> However, we proved the capacity of compound **3** to photoisomerize in a dry organic solvent (**Figure 2** and **SI**). We then determined the photostationary distribution of cryptozepines **1** and **2** by <sup>1</sup>H-NMR analysis.

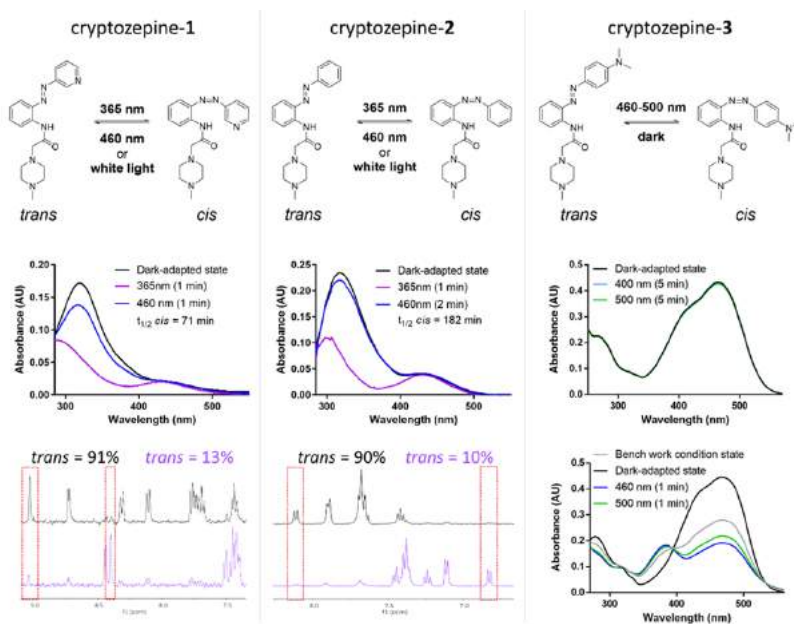


**Figure 2. Photochemical characterization.** Left column: absorption spectra (30  $\mu$ M in H<sub>2</sub>O) and quantification of cryptozepine-**1** photostationary state (PSS) by <sup>1</sup>H-NMR analysis (1 mM in D<sub>2</sub>O), showing the ratio between the two isomers in the dark-adapted state (*trans* = 91%) and after illumination with 365 nm light for 5 min (*trans* = 13%). Middle column: absorption spectra (30  $\mu$ M in H<sub>2</sub>O) and quantification of cryptozepine-**2** PSS by <sup>1</sup>H-NMR analysis (1 mM in D<sub>2</sub>O), showing the ratio between the two isomers in the dark-adapted state (*trans* = 90%) and after illumination with 365 nm light for 5 min (*trans* = 10%). Right column: absorption spectra in water (30  $\mu$ M, spectra above) and absorption spectra in anhydrous DMSO (30  $\mu$ M, spectra below) of cryptozepine-**3**. The switching of the red-shifted compound cryptozepine-**3** can be observed by UV-vis spectrophotometer analysis only in anhydrous solvent.

The distribution changed from about 90% in favor of the *trans* form in the dark to about 10% (90% in favor of the *cis* form) after illumination with UV light (365 nm) for both compounds. Compounds **1** and **2** also showed a

good thermal stability, with a half-life of thermal relaxation of 71 min and 182 min, respectively (**Figure 2** and **SI**).

**Competition Binding and Calcium Imaging Experiments at Muscarinic Receptors.** We determined the affinity of the cryptozepines for M1 mAChRs by radioligand competition binding assays. For this purpose, we used Wistar rat brain membranes (whole cortex), that contain a high density of M1 mAChRs,<sup>28</sup> and the non-selective muscarinic orthosteric antagonist [<sup>3</sup>H]quinuclidinyl benzilate ([<sup>3</sup>H]QNB) as competitive radioligand (see **SI**).<sup>28-31</sup> All cryptozepines showed good binding affinity in the low micromolar range, with cryptozepine-**2** emerging as the best ligand with an IC<sub>50</sub> of about 9 μM (see **SI**, **Figure S6.1**). No significant differences in affinity were observed between the *trans*- and the *cis*-enriched forms (named “*trans*” and “*cis*” from now on for the sake of simplicity) for the three compounds in these experimental conditions. These encouraging results suggested to retain cryptozepine-**2** (best binding affinity) and cryptozepine-**3** (best photochromic behavior) for further studies. We performed real-time calcium imaging experiments in transiently transfected HEK cells expressing M1 mAChR to study the antagonist behavior of our compounds (**Figure 3**). The calcium indicator OGB-1 AM (excitation at 494 nm and emission at 523 nm) was suitable for cryptozepine-**2**, while R-GECO1 (excitation at 561 nm and emission at 589 nm) was used for cryptozepine-**3** to avoid artifacts due to unwanted emission of fluorescence from OGB-1 AM upon illumination at 460 nm. The natural orthosteric agonist acetylcholine (ACh, 0.5 μM) was applied or co-applied to induce receptor activation. ACh alone induced reproducible cytosolic calcium oscillations, indicative of M1 agonism. Both cryptozepines-**2** and **3** (100 μM) showed an antagonistic behavior. Importantly, a complete recovery of ACh-induced activity was observed after the complete wash-out of the two antagonists. Cryptozepine-**2** reduced the total cell response by 42% in *trans* and by 58% in *cis*. Cryptozepine-**3** did not antagonize the ACh-induced response at 100 μM in *trans*, and it reduced the cell response by 14% under continuous illumination (*cis*-enriched form) with blue light (460 nm) (**Figure 3**). The antagonist activity and the significant differences observed between the

*trans* and *cis* states for both compounds are in agreement with the design. The stronger inhibition displayed by cryptozeptine-2 compared to cryptozeptine-3 at 100  $\mu$ M is probably due to the three-fold tighter binding of the former (see SI, Figure S6.1). The activity of *trans*-cryptozeptine-2 can also be attributed to its proximity to saturation at this concentration.

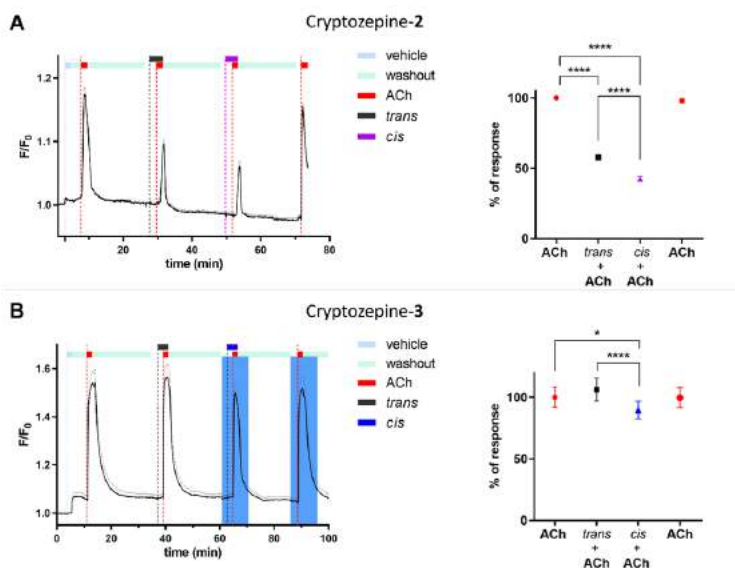


**Figure 3. Cryptozeptines-2 and 3 can antagonize ACh-induced activation of M1 mAChRs.** (A) Real-time calcium imaging traces from HEK cells expressing M1 mAChRs, which were loaded with the calcium indicator OGB-1 AM (10  $\mu$ M) (average of  $n = 289$  cells, grey band indicates the standard error of the mean (SEM)). The cell responses to ACh (0.5  $\mu$ M) were significantly reduced in the presence of cryptozeptine-2 (100  $\mu$ M). The quantification is presented in the right graph and shows a higher potency of the *cis* isomer. (B) Real-time calcium imaging traces from HEK cells co-expressing M1 mAChRs and R-GECO1 (average of  $n = 48$  cells, grey band indicates the standard error of the mean (SEM)). The cell responses to ACh (0.5  $\mu$ M) were significantly reduced in the presence of cryptozeptine-3 (100  $\mu$ M). The quantification is presented in the right graph and shows stronger inhibition of the *cis* isomer. Data were analyzed by one-way ANOVA with Tukey's multiple comparisons post-hoc test for statistical significance (p-value (\*) < 0.05 p-value (\*\*\*\*) < 0.0001; GraphPad Prism 6. Error bars are  $\pm$  SEM.

Correspondingly, cryptozeptine-3 is inactive in the dark and a (weak) inhibitor under illumination with blue light at the same concentration. We hypothesized that the electronic and/or steric properties of the additional group ( $-NMe_2$ ) on the terminal aromatic ring in cryptozeptine-3 might account for its loss of efficacy in comparison with cryptozeptine-2.

However, the efficiency of cryptozepine-**3** may be also limited by the relatively smaller population of *cis* isomer that is achieved upon irradiation as a consequence of its faster relaxation.

**Anticholinergic Effects in Mouse Isolated Atrium.** To validate cryptozologs in a physiologically relevant scenario (i.e. in tissue expressing a diversity of endogenous receptors) we tested the effect of cryptozepine-**2** on the mouse isolated atrium. Here, the excitation of muscarinic receptors induces arrest of the heartbeat.<sup>32-34</sup> This negative chronotropic effect in the atria is primarily mediated by mAChRs activation, including M1, and the anticholinergic activity of pirenzepine resumes the heart rate and rhythm.<sup>32-35</sup> We isolated the right atria from male mice and measured their spontaneous frequency of contraction (control), which was about 360 beats/min (see **SI**). Application of the muscarinic agonist carbachol (CCh, 1  $\mu$ M) strongly reduces the frequency to around 200 beats/min (**Figure 4**) and addition of pirenzepine (PNZ, 1  $\mu$ M) to the bath restores the frequency almost to control values (**Figure 4**). We used this robust assay to test the antagonist behavior of cryptozepine-**2** isomers. At the concentration of 100  $\mu$ M, the *trans* isomer was unable to antagonize CCh-induced bradycardia and was seemingly inert, whereas *cis*-cryptozepine-**2** readily induced the partial recovery of atrium contraction frequency (**Figure 4** and **SI**). This effect is in accord with the anticholinergic activity of pirenzepine in the atria<sup>32-35</sup> and further confirms our design and previous calcium imaging results.

Regarding future applications, the photopharmacological properties of cryptozepines could be enhanced by inserting fluorine in the ortho position(s) of the azobenzene. These modifications provide favorable photochromic properties like slow thermal back-isomerization and high two-photon cross section<sup>36</sup> and should preserve or even improve the antagonist potency by adding lipophilic contacts in the binding pocket.<sup>16</sup> Overall, the photopharmacological properties of cryptozepines set the stage for interesting assays *in vivo*. If they can be enterically administered in the inactive form (*trans*), these drugs could be remotely photoactivated at the desired location and time using the built-in LED of an endoscopy capsule,<sup>37</sup> potentially allowing to treat gastrointestinal tract diseases

without producing (adverse) effects in other regions or organs. More invasive applications include the manipulation of cardiac function *in vivo* using optoelectronic devices coupled to cardiac patches.<sup>14,38</sup>

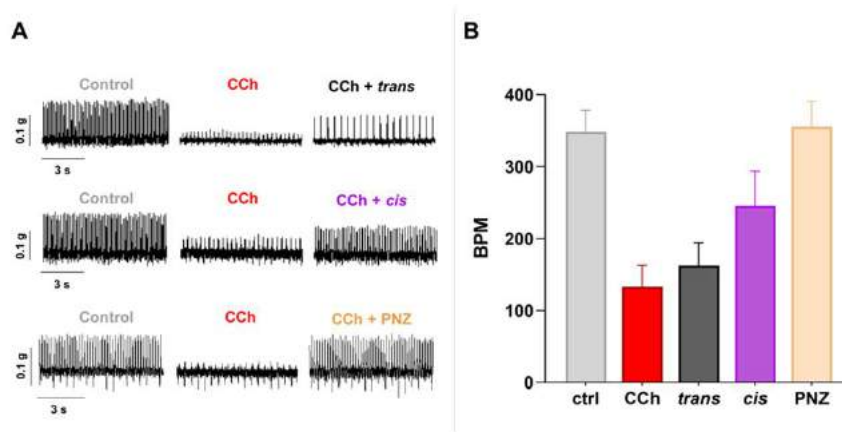


**Figure 4. Pirenzepine and cryptozepine-2 can antagonize CCh-induced bradycardia in mouse atria through M1 receptors.** Representative traces (Panel A) and quantification (Panel B) of mouse right atrium heart rate treated with Carbachol (CCh), pirenzepine (PNZ) and *trans/cis* cryptozepine-2. Spontaneous mechanical contractions of the mouse atria were recorded as control (ctrl) and defined as heartbeat frequency in beats/min (BPM). CCh 1  $\mu$ M decreased both the amplitude and BPM. The presence of PNZ ( $n = 6$ ) and *cis*-cryptozepine-2 (*cis*) ( $n = 2$ ) reversed the CCh-induced bradycardia. In contrast, *trans*-cryptozepine-2 (*trans*) ( $n=2$ ) did not reverse effect of CCh in terms of heartbeat frequency ( $n = 2$ ).

## CONCLUSION

In summary, we have expanded the rational design of photochromic ligands to the important class of tricyclic drugs. The proposed strategy involves two concomitant structural modifications to afford azobenzene derivatives that can mimic the tricyclic motif: (1) an isosteric replacement with a -N=N- group, and (2) a ring cleavage. We have demonstrated a proof of concept with a set of photoswitchable derivatives of the muscarinic antagonist pirenzepine that we named cryptozepines. Remarkably, these novel compounds retain micromolar binding and antagonist character despite the structural dissimilarity with the parent compound. The most potent photoswitchable compound (cryptozepine-2) displays negligible activity in mouse atrium in *trans* and M1 antagonism in *cis*, suggesting

therapeutic applications with high safety and localized efficacy. The high success rate obtained with this strategy opens the way to optimize the photochromic and pharmacological properties of these compounds, and to use it in other targets. This work provides a new toolbox to design photochromic drugs that significantly expands the scope of photopharmacology and its applications.

**AUTHOR INFORMATION.** Corresponding Author \*E-mail: pau@icrea.cat.

**Author Contributions.** †Rosalba Sortino and Carlo Matera contributed equally. Notes The authors declare no competing financial interest.

**ACKNOWLEDGMENTS.** The authors are grateful to Jean-Philippe Pin for providing the chimeric Gi/Gq protein clone. Molecular graphics and analyses were performed with the UCSF Chimera package. Chimera is developed by the Resource for Biocomputing, Visualization, and Informatics at the University of California, San Francisco (supported by NIGMS P41-GM103311). Mass spectrometry was performed at the IRB Barcelona Mass Spectrometry Core Facility, which actively participates in the BMBS European COST Action BM 1403 and is a member of Proteored, PRB2- ISCIII, supported by grant PRB2 (IPT13/0001 – ISCIISGEFI/FEDER). We thank Dr. Unai Elezcano and Dr. Sònia Varón from the Analysis and Chemistry Platform (PQA-PCB) at Barcelona Science Park for their help in HPLC-MS experiments throughout the project. This project has received funding from the EU Horizon 2020 Framework Programme for Research and Innovation under the Specific Grant Agreement 2 (Human Brain Project WaveScaleS SGA2 No. 785907), AGAUR/Generalitat de Catalunya (CERCA Programme, 2017-SGR-1442 and 2017-SGR-1548), FEDER funds, ERANET Syn-Bio MODULIGHTOR, Fundaluce foundation, MINECO (FPI fellowship BES-2014-068169 and project CTQ2016-80066R). We also acknowledge the CECH project co-financed by the European Union Regional Development Fund within the framework of the ERDF Operational Program of Catalonia 2014-2020. All animal procedures were experiments were approved by the Ethics Committee of the Universitat Autònoma de Barcelona (code EUT-MJ001). (Word Style “TD\_Acknowledgments”). Generally the last paragraph of the paper is the place to acknowledge people, organizations, and financing (you may state grant numbers and sponsors here). Follow the journal’s guidelines on what to include in the Acknowledgments section.

## REFERENCES

- (1) Lerch, M. M.; Hansen, M. J.; van Dam, G. M.; Szymanski, W.; Feringa, B. L. Emerging Targets in Photopharmacology. *Angew. Chemie Int. Ed.* 2016, 55 (37), 10978–10999. <https://doi.org/10.1002/anie.201601931>.
- (2) Hüll, K.; Morstein, J.; Trauner, D. In Vivo Photopharmacology. *Chemical Reviews. American Chemical Society* November 14, 2018, pp 10710–10747. <https://doi.org/10.1021/acs.chemrev.8b00037>.

- (3) Morstein, J.; Awale, M.; Reymond, J. L.; Trauner, D. Mapping the Azolog Space Enables the Optical Control of New Biological Targets. *ACS Cent. Sci.* 2019, 5 (4), 607–618. <https://doi.org/10.1021/acscentsci.8b00881>.
- (4) Pittolo, S.; Gómez-Santacana, X.; Eckelt, K.; Rovira, X.; Dalton, J.; Goudet, C.; Pin, J.-P.; Llobet, A.; Giraldo, J.; Llebaria, A.; Gorostiza, P. An Allosteric Modulator to Control Endogenous G Protein-Coupled Receptors with Light. *Nat. Chem. Biol.* 2014, 10 (10), 813–815. <https://doi.org/10.1038/nchembio.1612>.
- (5) Schoenberger, M.; Damijonaitis, A.; Zhang, Z.; Nagel, D.; Trauner, D. Development of a New Photochromic Ion Channel Blocker via Azologization of Fmocaine. *ACS Chem. Neurosci.* 2014, 5 (7), 514–518. <https://doi.org/10.1021/cn500070w>.
- (6) Matera, C.; Gomila, A. M. J.; Camarero, N.; Libergoli, M.; Soler, C.; Gorostiza, P. Photoswitchable Antimetabolite for Targeted Photoactivated Chemotherapy. *J. Am. Chem. Soc.* 2018, 140 (46), 15764–15773. <https://doi.org/10.1021/jacs.8b08249>.
- (7) Agnetta, L.; Decker, M. Photoresponsive Hybrid Compounds. In *Design of Hybrid Molecules for Drug Development*; Elsevier Inc., 2017; pp 279–315. <https://doi.org/10.1016/B978-0-08-101011-2.00011-8>.
- (8) Yet, L. *Privileged Structures in Drug Discovery*; John Wiley & Sons, Inc.: Hoboken, NJ, USA, 2018. <https://doi.org/10.1002/9781118686263>.
- (9) Evans, B. E.; Rittle, K. E.; Bock, M. G.; DiPardo, R. M.; Freidinger, R. M.; Whitter, W. L.; Lundell, G. F.; Veber, D. F.; Anderson, P. S.; Chang, R. S. L.; Lotti, V. J.; Cerino, D. J.; Chen, T. B.; Kling, P. J.; Kunkel, K. A.; Springer, J. P.; Hirshfield, J. *Methods for Drug Discovery: Development of Potent, Selective, Orally Effective Cholecystokinin Antagonists*. *J. Med. Chem.* 1988, 31 (12), 2235–2246. <https://doi.org/10.1021/jm00120a002>.
- (10) Marsh, W. Tricyclic Antidepressants. In *xPharm: The Comprehensive Pharmacology Reference*; Elsevier Inc., 2007; pp 1–3. <https://doi.org/10.1016/B978-008055232-3.61066-9>.
- (11) Fedi, V.; Guidi, A.; Altamura, M. Tricyclic Structures in Medicinal Chemistry: An Overview of Their Recent Uses in Non-CNS Pathologies. *Mini-Reviews Med. Chem.* 2008, 8 (14), 1464–1484. <https://doi.org/10.2174/138955708786786453>.
- (12) Matera, C.; Tata, A. Pharmacological Approaches to Targeting Muscarinic Acetylcholine Receptors. *Recent Pat. CNS Drug Discov.* 2014, 9 (2), 85–100. <https://doi.org/10.2174/1574889809666141120131238>.
- (13) Kruse, A. C.; Kobilka, B. K.; Gautam, D.; Sexton, P. M.; Christopoulos, A.; Wess, J. Muscarinic Acetylcholine Receptors: Novel Opportunities for Drug Development. *Nature Reviews Drug Discovery*. Nature Publishing Group 2014, pp 549–560. <https://doi.org/10.1038/nrd4295>.
- (14) Riefolo, F.; Matera, C.; Garrido-Charles, A.; Gomila, A. M. J.; Sortino, R.; Agnetta, L.; Claro, E.; Masgrau, R.; Holzgrabe, U.; Batlle, M.; Decker, M.; Guasch, E.; Gorostiza, P. Optical Control of Cardiac Function with a Photoswitchable Muscarinic Agonist. *J. Am. Chem. Soc.* 2019, 141 (18), 7628–7636. <https://doi.org/10.1021/jacs.9b03505>.
- (15) Agnetta, L.; Kauk, M.; Canizal, M. C. A.; Messerer, R.; Holzgrabe, U.; Hoffmann, C.; Decker, M. A Photoswitchable Dualsteric Ligand Controlling Receptor Efficacy. *Angew. Chem. Int. Ed. Engl.* 2017, 56 (25), 7282–7287. <https://doi.org/10.1002/anie.201701524>.

- (16) Agnetta, L.; Bermudez, M.; Riefolo, F.; Matera, C.; Claro, E.; Messerer, R.; Littmann, T.; Wolber, G.; Holzgrabe, U.; Decker, M. Fluorination of Photoswitchable Muscarinic Agonists Tunes Receptor Pharmacology and Photochromic Properties. *J. Med. Chem.* 2019, 62 (6), 3009–3020. <https://doi.org/10.1021/acs.jmedchem.8b01822>.
- (17) Hammer, R.; Berrie, C. P.; Birdsall, N. J. M.; Burgen, A. S. V.; Hulme, E. C. Pirenzepine Distinguishes between Different Subclasses of Muscarinic Receptors [28]. *Nature*. Nature Publishing Group 1980, pp 90–92. <https://doi.org/10.1038/283090a0>.
- (18) El-Obeid, H. A.; Babhair, S. A.; Al-Badr, A. A. Pirenzepine Dihydrochloride. *Anal. Profiles Drug Subst. Excipients* 1987, 16 (C), 445–506. [https://doi.org/10.1016/S0099-5428\(08\)60563-8](https://doi.org/10.1016/S0099-5428(08)60563-8).
- (19) Eberlein, W. G.; Engel, W. W.; Trummlitz, G.; Schmidt, G.; Hammer, R. Tricyclic Compounds as Selective Antimuscarinics. 2. Structure-Activity Relationships of M1 Selective Antimuscarinics Related to Pirenzepine. *J. Med. Chem.* 1988, 31 (6), 1169–1174. <https://doi.org/10.1021/jm00401a016>.
- (20) Encyclopedia of Psychopharmacology | Ian P. Stolerman | Springer <https://www.springer.com/gp/book/9783540687061#aboutAuthors> (accessed Apr 3, 2020).
- (21) Walline, J. J.; Lindsley, K.; Vedula, S. S.; Cotter, S. A.; Mutti, D. O.; Twelker, J. D. Interventions to Slow Progression of Myopia in Children. *Cochrane Database Syst. Rev.* 2011, No. 12. <https://doi.org/10.1002/14651858.cd004916.pub3>.
- (22) Pedretti, R. F. E.; Prete, G.; Foreman, R. D.; Adamson, P. B.; Vanoli, E. Autonomic Modulation during Acute Myocardial Ischemia by Low-Dose Pirenzepine in Conscious Dogs with a Healed Myocardial Infarction: A Comparison with  $\beta$ -Adrenergic Blockade. *J. Cardiovasc. Pharmacol.* 2003, 41 (5), 671–677. <https://doi.org/10.1097/00005344-200305000-00002>.
- (23) Thal, D. M.; Sun, B.; Feng, D.; Nawaratne, V.; Leach, K.; Felder, C. C.; Bures, M. G.; Evans, D. A.; Weis, W. I.; Bachhawat, P.; Kobilka, T. S.; Sexton, P. M.; Kobilka, B. K.; Christopoulos, A. Crystal Structures of the M1 and M4 Muscarinic Acetylcholine Receptors. *Nature* 2016, 531 (7594), 335–340. <https://doi.org/10.1038/nature17188>.
- (24) Murgolo, N. J.; Kozlowski, J.; Tice, M. A. B.; Hollinger, F. P.; Brown, J. E.; Zhou, G.; Taylor, L. A.; McQuade, R. D. The N4 Nitrogen of Pirenzepine Is Responsible for Selective Binding of the M1 Subtype Human Muscarinic Receptor. *Bioorganic Med. Chem. Lett.* 1996, 6 (7), 785–788. [https://doi.org/10.1016/0960-894X\(96\)00107-2](https://doi.org/10.1016/0960-894X(96)00107-2).
- (25) Dong, M.; Babalhavaeji, A.; Samanta, S.; Beharry, A. A.; Woolley, G. A. Red-Shifting Azobenzene Photoswitches for in Vivo Use. *Acc. Chem. Res.* 2015, 48 (10), 2662–2670. <https://doi.org/10.1021/acs.accounts.5b00270>.
- (26) Ghetti, F.; Griesbeck, A. G.; Oelgemöller, M. *CRC Handbook of Organic Photochemistry and Photobiology*; CRC Press, 2012.
- (27) Bandara, H. M. D.; Burdette, S. C. Photoisomerization in Different Classes of Azobenzene. *Chemical Society Reviews*. The Royal Society of Chemistry March 7, 2012, pp 1809–1825. <https://doi.org/10.1039/c1cs15179g>.
- (28) Claro, E. Analyzing Ligand Depletion in a Saturation Equilibrium Binding Experiment. *Biochem. Mol. Biol. Educ.* 2006, 34 (6), 428–431. <https://doi.org/10.1002/bmb.2006.494034062677>.
- (29) Yamamura, H. I.; Snyder, S. H. Muscarinic Cholinergic Binding in Rat Brain. *Proc. Natl. Acad. Sci. U. S. A.* 1974, 71 (5), 1725–1729. <https://doi.org/10.1073/pnas.71.5.1725>.

- (30) Sallés, J.; Wallace, M. A.; Fain, J. N. Differential Effects of Alkylating Agents on the Multiple Muscarinic Receptor Subtypes Linked to Activation of Phospholipase C by Carbachol in Rat Brain Cortical Membranes. *J. Pharmacol. Exp. Ther.* 1993, 264 (2).
- (31) Massoulié, J.; Carson, S.; Kato, G. Biochemical Characterization of Muscarinic Receptors: Multiplicity of Binding Components. *Prog. Brain Res.* 1979, 49 (C), 303–311. [https://doi.org/10.1016/S0079-6123\(08\)64642-7](https://doi.org/10.1016/S0079-6123(08)64642-7).
- (32) Heijman, J.; Kirchner, D.; Kunze, F.; Chrétien, E. M.; Michel-Reher, M. B.; Voigt, N.; Knaut, M.; Michel, M. C.; Ravens, U.; Dobrev, D. Muscarinic Type-1 Receptors Contribute to IK,ACh in Human Atrial Cardiomyocytes and Are Upregulated in Patients with Chronic Atrial Fibrillation. *Int. J. Cardiol.* 2018, 255, 61–68. <https://doi.org/10.1016/j.ijcard.2017.12.050>.
- (33) Süsskand, K.; Sewing, K.-F. Anticholinergic Effects of Pirenzepine on the Guinea-Pig Isolated Atrium. *Pharmacology* 1979, 19 (3), 163–164. <https://doi.org/10.1159/000137304>.
- (34) Woo, S. H.; Byung, H. L.; Kwon, K. Il; Chin, O. L. Excitatory Effect of M1 Muscarinic Acetylcholine Receptor on Automaticity of Mouse Heart. *Arch. Pharm. Res.* 2005, 28 (8), 930–935. <https://doi.org/10.1007/BF02973879>.
- (35) Hogan, K.; Markos, F. Muscarinic Type 1 Receptors Mediate Part of Nitric Oxide's Vagal Facilitatory Effect in the Isolated Innervated Rat Right Atrium. *Nitric Oxide - Biol. Chem.* 2007, 16 (1), 110–117. <https://doi.org/10.1016/j.niox.2006.05.005>.
- (36) Cabré, G.; Garrido-Charles, A.; Moreno, M.; Bosch, M.; Porta-de-la-Riva, M.; Krieg, M.; Gascón-Moya, M.; Camarero, N.; Gelabert, R.; Lluch, J. M.; Busqué, F.; Hernando, J.; Gorostiza, P.; Alibés, R. Rationally Designed Azobenzene Photoswitches for Efficient Two-Photon Neuronal Excitation. *Nat. Commun.* 2019, 10 (1), 1–12. <https://doi.org/10.1038/s41467-019-08796-9>.
- (37) Shrestha, R.; Mohammed, S. K.; Hasan, M. M.; Zhang, X.; Wahid, K. A. Automated Adaptive Brightness in Wireless Capsule Endoscopy Using Image Segmentation and Sigmoid Function. *IEEE Trans. Biomed. Circuits Syst.* 2016, 10 (4), 884–892. <https://doi.org/10.1109/TBCAS.2016.2546838>.
- (38) Feiner, R.; Engel, L.; Fleischer, S.; Malki, M.; Gal, I.; Shapira, A.; Shacham-Diamand, Y.; Dvir, T. Engineered Hybrid Cardiac Patches with Multifunctional Electronics for Online Monitoring and Regulation of Tissue Function. *Nat. Mater.* 2016, 15 (6), 679–685. <https://doi.org/10.1038/nmat4590>.



## Supporting Information

### Rational design of photochromic analogs of tricyclic drugs

Fabio Riefolo, Rosalba Sortino, Carlo Matera, Enrique Claro, Beatrice Preda, Simone Vitiello, Sara Traserra, Marcel Jiménez, Pau Gorostiza

#### Table of content

1. **Molecular docking simulations**
2. **Chemical synthesis**
3. **HPLC analyses and Mass Spectra**
4. **Photochemical characterization**
5. **NMR spectroscopy**
6. **In vitro radioligand competition binding experiments**
7. **In vitro calcium imaging experiments**
8. **Ex vivo mice atria tissue experiments**
9. **Additional references**

## 1. Molecular docking simulations

**Materials and methods.** Molecular docking simulations were performed using the crystal structure of the human M1 muscarinic acetylcholine receptor retrieved from the Protein Data Bank bound to the antagonist tiotropium (PDB code: 5CXV).<sup>1</sup> The protein pdb file was prepared for docking by removing co-crystallized ligands, non-complexed ions and water molecules, and finally applying the Dock Prep tool available in the free software package UCSF Chimera. This involved the addition of hydrogens and assigning partial charges (AMBER ff14SB method). The cryptozepine-2, *trans* and *cis*, structures were built with standard bond length and angles using ChemDraw and then energy minimized with Chem3D by the MM2 method. The minimized compounds were further prepared for docking studies with UCSF Chimera by adding hydrogens and assigning partial charges (AMBER ff14SB method). The necessary pdbqt files of ligands and receptor were prepared using AutoDock 4.2 software. The docking studies were carried out using the standard docking protocol applied for AutoDock Vina in PyRx 0.8 virtual screening software. Autodock Vina has been reported to be an effective tool capable of quickly and accurately predicting bound conformations and binding energies of ligands with macromolecular targets.<sup>2,3</sup> A grid box of size 18.68 × 17.35 × 13.64 Å, with x, y and z coordinates of -11.52, -12.61 and 37.05, respectively, was fixed to cover the entire orthosteric binding sites and accommodate the ligands to move freely. Docking studies were performed using an exhaustiveness value of 8 while all other parameters were maintained as defaults. All rotatable bonds within the ligands were allowed to rotate freely, and the receptor was considered rigid. The docking simulations were repeated three times for each ligand. The obtained poses were then ranked based on the predicted affinity docking scores (kcal/mol) and the best pose for each experiment was selected. The results were then analyzed using UCSF Chimera. Both isomers of the cryptozepine-2 and pirenzepine were docked into the orthosteric binding sites of the human M1 muscarinic acetylcholine receptor in its inactive conformation, bound to the antagonist tiotropium (PDB code: 5CXV). All the ligands were docked at this receptor model using a standard docking protocol with AutoDock Vina in the PyRx 0.8 software with a suitable grid box. We ran three/five simulations for each ligand isomer and selected the best pose obtained in each experiment based on the predicted binding affinity scores (kcal/mol).

**Molecular docking simulations of cryptozepine isomers.** In order to examine if the “cryptoazologization” concept was a reasonable strategy for developing light-sensitive cryptoazologs of pirenzepine, we firstly used molecular docking calculations. We docked cryptozepine-2, the crypto-azolog of pirenzepine with the simplest unsubstituted azobenzene as molecular switch, into the orthosteric binding site of the human M1 muscarinic acetylcholine receptor (inactive conformation bound to the antagonist tiotropium, PDB code: 5CXV).<sup>1</sup> We first validated the docking protocol with the parent compound pirenzepine. The obtained best poses and their average binding affinity (-8.3 kcal/mol) were in agreement with the results previously published for the same ligand (Figure S1 panel D).<sup>1</sup> The key elements for antagonist binding at the M1 receptor reside in the methylpiperazine amines.<sup>1,4-6</sup> This group must face and interact with the orthosteric site residues D105 and Y404 (transmembrane helices (TM) 3 and 7, respectively; residues

are numbered according to the human M1 receptor sequence PDB number 5CXV) (**Figure S1**). Additional confirmation that pirenzepine adopts the correct orientation in our calculations is provided by the tricyclic core oriented as the aromatic portions of tiotropium, which is free to create hydrophobic contacts with Y106 (TM3), W157 (TM4) and Y381 (TM6) (**Figure S1**).<sup>1</sup> We next studied cryptozepine-2 (**Figure S1**). Our calculations showed that the best poses of the *cis* isomer fit in the M1 orthosteric site in a similar way to pirenzepine (**Figure S1**), with favorable binding affinity values (-9.1 kcal/mol) (**Figure S1**, panel **E**). In contrast, a flipped orientation was favored for the majority of the *trans* isomer poses (**Figure S1**, panel **F**), which are likely incompatible with antagonism activity.<sup>1,4-6</sup> The planar *trans* geometry of cryptozepine-2 covers a larger space with the aromatic portions (8.7 Å) than its bent *cis* isomer (6.9 Å) and pirenzepine (7.1 Å) (**Figure S1**). This may hinder the correct placing into the binding pocket of the rest of the ligand and result in loss of antagonist behavior. Thus, computational results were in agreement with the “cryptoazologization” concept and encouraged to pursue the synthesis of a small library of cryptozepines.

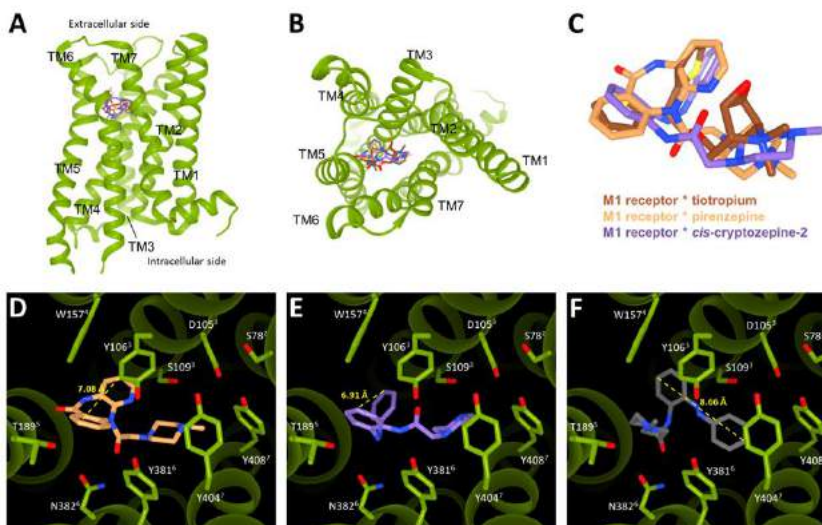


**Figure S1. Hypothetical binding mode of cryptozepine-2 (trans and cis isomers) in M1 mAChR.** **A** and **B**) Full view (panel **A**) and extracellular side view (panel **B**) of the M1 muscarinic structure (PDB code: 5CXV) colored in green, with our antagonists bound into the orthosteric site. **C**) Superimposition of binding poses of tiotropium from the M1 structure (PDB code: 5CXV), pirenzepine, and the *cis*-cryptozepine-2 from our simulations using the same receptor. **D**, **E** and **F**) Pirenzepine (panel **D**), *cis*- (panel **E**) and *trans*-cryptozepine-2 (panel **F**) poses in the M<sub>1</sub> receptor with the fundamental residues that contribute to the orthosteric binding site (several residues are omitted for clarity). The ligands are shown as sticks and colored according to element: carbon, beige for pirenzepine, brown for tiotropium, purple for *cis*-cryptozepine-2, dark grey for *trans*-cryptozepine-2; oxygen, red; nitrogen, dark blue; sulfur, yellow. Residues are numbered according to the human M1 receptor sequence (PDB code: 5CXV). Superscript numbers indicate the transmembrane (TM) helices of the M1 receptor. The yellow line and values indicate the length of the tricyclic core of pirenzepine, and the aromatic portions of *trans*- and *cis*-cryptozepine-2. Pirenzepine and cryptozepine-2 can antagonize CCh-induced bradycardia in mouse atria through M1 receptors.

## 2. Chemical synthesis

**Materials and methods.** All reagents and solvents were purchased from Sigma-Aldrich, Cyimit Química and ServiQuimia and were used without any further purification. TLC analyses were performed on commercial silica gel 60 F<sub>254</sub> aluminium foils (Merck); spots were further evidenced by spraying with a dilute alkaline potassium permanganate solution or a phosphomolybdic acid solution 5% in ethanol and, for tertiary amines and quaternary ammonium compounds, with the Dragendorff reagent. Flash chromatography was performed on PanReac AppliChem silica gel 60 (40-63 microns), Biotage® SNAP KP-C18-HS 12g or Biotage® SNAP KP-SIL 25g as stationary phases; mobile phases are specified

for each compound. UV-Vis spectra and experiments were recorded with a Shimadzu UV-1800 UV-VIS Spectrophotometer with standard quartz cuvettes (10 mm light path).  $^1\text{H}$ -NMR and  $^{13}\text{C}$ -NMR spectra were registered with a Varian Mercury 400 MHz (400 MHz for  $^1\text{H}$ -NMR and 101 MHz for  $^{13}\text{C}$ -NMR) and a Varian VNMR500 MHz instrument (500 MHz for  $^1\text{H}$ -NMR and 126 MHz for  $^{13}\text{C}$ -NMR) in  $\text{DMSO-}d_6$ ,  $\text{CDCl}_3$ ,  $\text{D}_2\text{O}$ . Residual signals of the deuterated solvents were used as an internal standard ( $\text{DMSO-}d_6$ :  $^1\text{H}$  2.50 ppm,  $^{13}\text{C}$  39.52 ppm;  $\text{CDCl}_3$ :  $^1\text{H}$  7.26 ppm,  $^{13}\text{C}$  77.16 ppm;  $\text{D}_2\text{O}$ :  $^1\text{H}$  4.79 ppm). Chemical shifts ( $\delta$ ) are expressed as parts-per-million (ppm) and coupling constants ( $J$ ) as hertz (Hz). HPLC analyses were performed with a Waters Alliance 2795 separation module (RP column: XSelect CSH C18, 50x4.6 mm, S-3.5  $\mu\text{m}$ , 1.6 ml/min; eluent: from 5% B to 100% B in 3.5 min using a linear gradient, A:  $\text{H}_2\text{O}$  0.1% formic acid, B: acetonitrile 0.1% formic acid) coupled to a Waters 2996 photodiode detector and a Waters 3100 mass spectrometer. High resolution mass spectroscopy measurements (ionization: NanoESI, positive ionization) were performed at the mass spectrometry core facility of the IRB (Barcelona, Spain) with a LTQ-FT Ultra (Thermo Scientific) for direct infusion (Automated Nanoelectrospray) of the sample. The NanoMate (AdvionBioSciences, Ithaca, NY, USA) aspirated the samples from a 384-well plate (protein Lobind) with disposable, conductive pipette tips, and infused the samples through the nanoESI Chip (which consists of 400 nozzles in a 20x20 array) towards the mass spectrometer. Spray voltage was 1.70 kV and delivery pressure was 0.50 psi. Data are reported as mass-to-charge ratio ( $m/z$ ) of the corresponding positively charged molecular ions.

**Abbreviations.** Solvents: EtOAc: ethyl acetate;  $\text{CH}_2\text{Cl}_2$ : dichloromethane; MeCN: acetonitrile; MeOH: methanol; EtOH: ethanol; THF: tetrahydrofuran;  $\text{Et}_2\text{O}$ : diethyl ether; DMSO: dimethylsulfoxide.

**Analytical characterizations:** NMR: d: doublet; dd: double doublet; ddd: double double doublet; dddd: doublet of doublet of doublet of doublets; dt: double triplet; m: multiplet; q: quartet; quin: quintet; s: singlet; t: triplet; m.p.: melting point;  $R_f$ : retention factor; r.t.: room temperature; RT: retention time.

## 2.1 Synthetic procedures

Cryptozepines (**1**, **2**, **3**) were synthesized as reported in **Scheme 1**. *N*-Chloroacetyl-2-nitroaniline was reduced to the corresponding amine (**4**) by treatment with iron in ammonium chloride and acetic acid.<sup>7</sup> Oxidation with Oxone<sup>®</sup> gave the nitroso derivative (**5**), which was then coupled to the chosen arylamine under Mills conditions to yield the arylazo intermediates (**6a**, **6b**, **6c**). Nucleophilic substitution of the chlorine with 1-methylpiperazine and subsequent treatment with hydrochloric acid afforded the three final compounds as dihydrochloride salts (**1**, **2**, **3**).

***N*-(2-aminophenyl)-2-chloroacetamide (4).** Fe (1.30 g, 23.30 mmol),  $\text{NH}_4\text{Cl}$  (124.63 mg, 2.33 mmol) and glacial acetic acid (0.270 mL, 4.66 mmol) were added into 10 mL  $\text{H}_2\text{O}$  and stirred at 50 °C for 15 min. A solution of 2-chloro-*N*-(2-nitrophenyl)acetamide (0.5 g, 2.33 mmol) in DMF (5 mL) was added into the above solution quickly, and stirring was continued at 50 °C for 15 min. Then the reaction solution was alkalized to pH 9 with aqueous  $\text{Na}_2\text{CO}_3$ . Subsequently the mixture was filtered, and the cake was washed with  $\text{H}_2\text{O}$  and EtOAc. The

combined filtrate was extracted with EtOAc. Then the combined organic layers were washed with brine, dried over anhydrous MgSO<sub>4</sub>, filtered, concentrated under reduced pressure. Purification of the crude product by chromatography on silica gel (cyclohexane/EtOAc, 4:6) afforded *N*-(2-aminophenyl)-2-chloroacetamide (**4**) as a white solid (260 mg, 60%). <sup>1</sup>H NMR (400 MHz, DMSO-*d*<sub>6</sub>) δ 8.19 (s, 1H), 7.31 (dd, *J* = 7.8, 1.5 Hz, 1H), 7.10 (td, *J* = 7.7, 1.5 Hz, 1H), 6.87 – 6.80 (m, 2H), 4.24 (s, 2H), 3.77 (s, 2H).

**2-Chloro-*N*-(2-nitrosophenyl)acetamide (5).** *N*-(2-aminophenyl)-2-chloroacetamide (**4**) (250 mg, 1.35 mmol) was suspended in 5 mL of CH<sub>2</sub>Cl<sub>2</sub>. Oxone<sup>®</sup> (630 mg, 2.05 mmol) in 20 mL of water was added and the resulting mixture was stirred vigorously for 1 h at room temperature. The organic phase was separated, and the aqueous phase was extracted with 10 mL of CH<sub>2</sub>Cl<sub>2</sub>. The combined organic phases were washed with 1 M HCl (50 mL), saturated aqueous NaHCO<sub>3</sub> (50 mL), and water (50 mL). Finally, it was dried over MgSO<sub>4</sub>, and evaporated under reduced pressure to afford the nitroso derivative (**5**) which was used in the next step without further purification.

**2-Chloro-*N*-(2-(pyridin-3-yl diazenyl)phenyl)acetamide (6a).** Compound **5** (155 mg, 0.78 mmol) and 3-aminopyridine (147 mg, 1.56 mmol) were dissolved in glacial acetic acid (30 mL) and stirred for 24 h at 60 °C. The solution was diluted with water and extracted with EtOAc. The organic phase was washed four times with water and once with brine and dried over MgSO<sub>4</sub>. The crude product was purified by chromatography (eluent: cyclohexane/EtOAc, 9:1) to yield **6a** (100 mg, 47%) as an orange solid. <sup>1</sup>H NMR (400 MHz, CDCl<sub>3</sub>) δ 10.96 (s, 1H), 9.23 (dd, *J* = 2.4, 0.8 Hz, 1H), 8.73 (dd, *J* = 4.7, 1.6 Hz, 1H), 8.68 (dd, *J* = 8.4, 1.3 Hz, 1H), 8.15 (ddd, *J* = 8.2, 2.4, 1.6 Hz, 1H), 7.92 (dd, *J* = 8.1, 1.6 Hz, 1H), 7.55 (ddd, *J* = 8.7, 7.2, 1.6 Hz, 1H), 7.48 (ddd, *J* = 8.2, 4.8, 0.8 Hz, 1H), 7.29 – 7.22 (m, 1H), 4.29 (s, 2H). <sup>13</sup>C NMR (101 MHz, CDCl<sub>3</sub>) δ 164.33, 152.27, 147.88, 147.31, 139.79, 135.65, 133.91, 127.05, 124.63, 124.31, 120.30, 120.05, 43.58.

**2-Chloro-*N*-(2-(phenyldiazenyl)phenyl)acetamide (6b).** Compound **5** (170 mg, 0.86 mmol) and aniline (159 mg, 1.71 mmol) were dissolved in glacial acetic acid (30 mL) and stirred for 4 days at room temperature. The solution was diluted with water and extracted with EtOAc. The organic phase was washed four times with water and once with brine and dried over MgSO<sub>4</sub>. The crude product was purified by chromatography (eluent: cyclohexane/EtOAc, 9:1) to yield **6b** (130 mg, 56%) as an orange solid. <sup>1</sup>H NMR (400 MHz, CDCl<sub>3</sub>) δ 11.03 (s, 1H), 8.66 (dd, *J* = 8.3, 1.3 Hz, 1H), 7.97 – 7.91 (m, 2H), 7.89 (ddd, *J* = 8.2, 1.6, 0.5 Hz, 1H), 7.56 – 7.46 (m, 4H), 7.22 (ddd, *J* = 8.2, 7.3, 1.3 Hz, 1H), 4.27 (s, 2H). <sup>13</sup>C NMR (101 MHz, CDCl<sub>3</sub>) δ 164.28, 152.51, 139.63, 135.29, 132.90, 131.66, 129.39, 124.46, 123.01, 120.08, 119.98, 43.52.

**2-Chloro-*N*-(2-((4-(dimethylamino)phenyl)diazenyl)phenyl)acetamide (6c).** Compound **5** (500 mg, 2.52 mmol) and 4-amino-*N,N*-dimethylaniline (514 mg, 3.78 mmol) were dissolved in glacial acetic acid (20 mL) and stirred for 30 minutes at room temperature. The solution was concentrated under reduced pressure and the crude product was purified by chromatography (eluent: cyclohexane/AcOEt, 8:2) to afford **6c** as a red solid in quantitative yield. <sup>1</sup>H NMR (400 MHz, CDCl<sub>3</sub>) δ 11.00 (s, 1H), 8.59 (dd, *J* = 8.3, 1.4 Hz, 1H), 7.94 – 7.87 (m, 2H), 7.83 (ddd, *J* = 8.1, 1.6, 0.5 Hz, 1H), 7.39 (dddd, *J* = 8.3, 7.3, 1.6, 0.5 Hz, 1H), 7.19 (dddd, *J* = 8.0, 7.3, 1.3, 0.5 Hz, 1H), 6.81 – 6.72 (m, 2H), 4.27 (s, 2H), 3.11 (s, 6H). <sup>13</sup>C NMR

(101 MHz, CDCl<sub>3</sub>) δ 164.04, 152.87, 143.71, 140.36, 134.62, 130.79, 125.35, 124.46, 119.78, 118.42, 111.73, 43.61, 40.43.

***(E)-2-(4-Methylpiperazin-1-yl)-N-(2-(pyridin-3-yl diazenyl)phenyl)acetamide***

***(Cryptozepine-1)***. Compound **6a** (100 mg, 0.364 mmol) was dissolved in 20 mL of MeCN. 1-Methylpiperazine (55 mg, 0.547 mmol) and triethylamine (55.3 mg, 0.546 mmol) were then slowly added to the solution. The mixture was stirred under reflux for 3 h. Upon completion, MeCN was removed under reduced pressure and the obtained oil was dissolved in EtOAc. The resulting organic solution was washed 4 times using 30 mL of saturated aqueous NaHCO<sub>3</sub>. The organic layer was dried over MgSO<sub>4</sub> and evaporated under reduced pressure to afford the final product (**1**) as a yellow solid (quantitative yield). <sup>1</sup>H NMR (400 MHz, CDCl<sub>3</sub>) δ 10.97 (s, 1H), 9.25 (dd, *J* = 2.4, 0.8 Hz, 1H), 8.78 (dd, *J* = 8.4, 1.3 Hz, 1H), 8.74 (dd, *J* = 4.8, 1.6 Hz, 1H), 8.26 (ddd, *J* = 8.2, 2.4, 1.6 Hz, 1H), 7.81 (dd, *J* = 8.2, 1.5 Hz, 1H), 7.58 – 7.44 (m, 2H), 7.15 (ddd, *J* = 8.4, 7.3, 1.3 Hz, 1H), 3.25 (s, 2H), 2.73 – 2.39 (m, 8H), 2.23 (s, 3H). <sup>13</sup>C NMR (101 MHz, CDCl<sub>3</sub>) δ 168.84, 151.95, 146.57, 139.99, 137.85, 134.10, 129.63, 128.23, 124.11, 123.65, 120.35, 116.24, 63.03, 55.04, 53.71, 45.95.

***(E)-1-Methyl-4-(2-oxo-2-((2-(pyridin-3-yl diazenyl)phenyl)amino)ethyl)piperazine-1,4-dium chloride (Cryptozepine-1 dihydrochloride)***

5 mL of 4 M HCl in dioxane were added slowly to compound **1** (10 mg, 0.03 mmol) at 0 °C. The mixture was stirred for 30 min at room temperature, then the solvent and excess of HCl were evaporated under reduced pressure and the resulting solid was washed 3 times with Et<sub>2</sub>O (30 mL). The so obtained orange solid was dried under vacuum to afford cryptozepine-1 dihydrochloride (quantitative yield). <sup>1</sup>H NMR (500 MHz, D<sub>2</sub>O) δ 9.23 (s, 1H), 8.88 (s, 1H), 8.70 (d, *J* = 8.4, 1.7 Hz, 1H), 8.09 (dd, *J* = 8.3, 5.4 Hz, 1H), 8.03 (d, *J* = 8.2 Hz, 1H), 7.82 (d, *J* = 8.2, 1.5 Hz, 1H), 7.72 (t, 1H), 7.44 (t, 1H), 3.61 (s, 2H), 3.58 – 3.00 (m, 8H), 2.88 (s, 3H). <sup>13</sup>C NMR (126 MHz, D<sub>2</sub>O) δ 170.19, 149.25, 145.58, 143.06, 140.05, 135.59, 134.71, 134.43, 127.04, 126.49, 124.01, 116.79, 59.48, 52.94, 49.49, 42.71. HR-MS (ESI, [M + H]<sup>+</sup>): calcd for C<sub>18</sub>H<sub>23</sub>N<sub>6</sub>O<sup>+</sup>, 339.19; found 339.1930.

***(E)-2-(4-Methylpiperazin-1-yl)-N-(2-(phenyldiazenyl)phenyl)acetamide (Cryptozepine-2)***

Compound **6b** (100 mg, 0.364 mmol) was dissolved in 20 mL of MeCN. 1-Methylpiperazine (55 mg, 0.547 mmol) and triethylamine (55.3 mg, 0.546 mmol) were then slowly added to the solution. The mixture was stirred under reflux for 3 h. Upon completion, MeCN was removed under reduced pressure and the obtained oil was dissolved in EtOAc. The resulting organic solution was washed 4 times using 30 mL of saturated aqueous NaHCO<sub>3</sub>. The organic layer was dried over MgSO<sub>4</sub> and evaporated under reduced pressure to afford the final product (**2**) as a yellow solid (quantitative yield). <sup>1</sup>H NMR (400 MHz, CDCl<sub>3</sub>) δ 10.94 (s, 1H), 8.77 (dd, *J* = 8.4, 1.3 Hz, 1H), 8.07 – 7.97 (m, 2H), 7.78 (dd, *J* = 8.2, 1.6 Hz, 1H), 7.58 – 7.44 (m, 4H), 7.12 (ddd, *J* = 8.3, 7.2, 1.3 Hz, 1H), 3.23 (s, 2H), 2.82 – 2.30 (m, 8H), 2.22 (s, 3H). <sup>13</sup>C NMR (101 MHz, CDCl<sub>3</sub>) δ 168.74, 152.75, 139.91, 137.41, 133.04, 131.31, 129.29, 123.49, 123.29, 120.09, 116.01, 63.02, 54.92, 53.73, 45.95.

***(E)-1-Methyl-4-(2-oxo-2-((2-(phenyldiazenyl)phenyl)amino)ethyl)piperazine-1,4-dium***

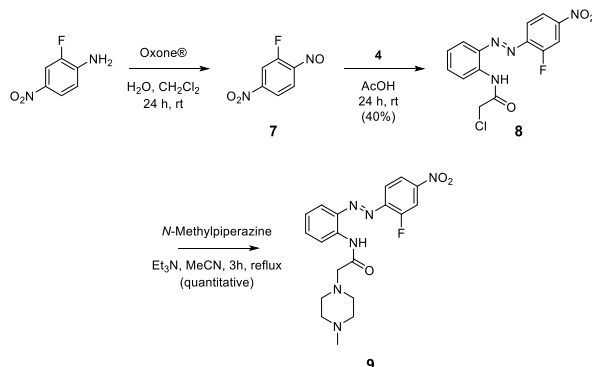
***chloride (Cryptozepine-2 dihydrochloride)***. 6 mL of 4 M HCl in dioxane were added slowly to compound **2** (50 mg, 0.15 mmol) at 0 °C. The mixture was stirred for 30 min at room temperature, then the solvent and excess of HCl were evaporated under reduced pressure and the resulting solid was washed 3 times with Et<sub>2</sub>O (30 mL). The so obtained orange solid was dried under vacuum to afford cryptozepine-2 dihydrochloride (quantitative yield). <sup>1</sup>H

NMR (400 MHz, DMSO-*d*<sub>6</sub>) δ 10.74 (s, 1H), 8.41 (d, *J* = 8.3 Hz, 1H), 8.06 – 7.91 (m, 2H), 7.84 – 7.55 (m, 5H), 7.32 – 7.25 (m, 1H), 3.52 – 2.87 (m, 10H), 2.69 (s, 3H). <sup>13</sup>C NMR (126 MHz, DMSO-*d*<sub>6</sub>) δ 153.28, 152.26, 136.30, 132.77, 131.81, 129.58, 128.87, 124.48, 122.98, 120.02, 116.13, 58.52, 50.68, 48.77, 41.88. HR-MS (ESI, [M + H]<sup>+</sup>): calcd for C<sub>19</sub>H<sub>24</sub>N<sub>5</sub>O<sup>+</sup>, 338.20; found 338.1968.

**(*E*)-*N*-(2-((4-(Dimethylamino)phenyl)diazanyl)phenyl)-2-(4-methylpiperazin-1-yl)acetamide (Cryptozepine-3).** Compound **6c** (20 mg, 0.063 mmol) was dissolved in 20 mL of MeCN. 1-Methylpiperazine (9.5 mg, 0.095 mmol) and triethylamine (9.58 mg, 0.095 mmol) were then slowly added to the solution. The mixture was stirred under reflux for 3 h. Upon completion, MeCN was removed under reduced pressure and the obtained oil was dissolved in EtOAc. The resulting organic solution was washed 4 times using 30 mL of saturated aqueous NaHCO<sub>3</sub>. The organic layer was dried over MgSO<sub>4</sub> and evaporated under reduced pressure to afford the final product (**3**) as a yellow solid (quantitative yield). <sup>1</sup>H NMR (400 MHz, CDCl<sub>3</sub>) δ 10.90 (s, 1H), 8.72 (dd, *J* = 8.4, 1.3 Hz, 1H), 8.03 – 7.98 (m, 2H), 7.75 (dd, *J* = 8.1, 1.6 Hz, 1H), 7.38 (ddd, *J* = 8.6, 7.3, 1.6 Hz, 1H), 7.11 (ddd, *J* = 8.3, 7.3, 1.4 Hz, 1H), 6.82 – 6.74 (m, 2H), 3.24 (s, 2H), 3.11 (s, 6H), 2.83 – 2.43 (m, 8H), 2.29 (s, 3H). <sup>13</sup>C NMR (101 MHz, CDCl<sub>3</sub>) δ 168.61, 152.65, 143.93, 140.49, 136.28, 131.02, 125.61, 123.56, 119.80, 115.65, 111.67, 63.13, 54.97, 53.78, 45.98, 40.43.

**(*E*)-1-(2-((2-((4-(Dimethylamino)phenyl)diazanyl)phenyl)amino)-2-oxoethyl)-4-methylpiperazine-1,4-dium (Cryptozepine-3 dihydrochloride).** 6 mL of 4 M HCl in dioxane were added slowly to compound **3** (10 mg, 0.026 mmol) at 0 °C. The mixture was stirred for 30 min at room temperature, then the solvent and excess of HCl were evaporated under reduced pressure and the resulting solid was washed 3 times with Et<sub>2</sub>O (30 mL). The so obtained orange solid was dried under vacuum to afford cryptozepine-3 dihydrochloride (quantitative yield). <sup>1</sup>H NMR (400 MHz, D<sub>2</sub>O) δ 8.01 (d, *J* = 8.2 Hz, 1H), 7.91 – 7.77 (m, 2H), 7.65 – 7.53 (m, 2H), 7.36 (d, 3H), 3.82 – 2.61 (m, 19H). <sup>13</sup>C NMR (101 MHz, D<sub>2</sub>O) δ <sup>13</sup>C NMR (101 MHz, D<sub>2</sub>O) δ 168.82, 149.08, 147.06, 141.60, 133.70, 131.88, 125.79, 125.00, 122.23, 116.67, 116.55, 59.48, 52.67, 49.44, 42.72, 42.67. HR-MS (ESI, [M + H]<sup>+</sup>): calcd for C<sub>21</sub>H<sub>29</sub>N<sub>6</sub>O<sup>+</sup>, 381.24; found 381.2387.

Compound **9** was synthesized as reported in **Scheme S2**. 2-fluoro-4-nitroaniline was oxidized with Oxone<sup>®</sup> to give the nitroso derivative (**7**), which was then coupled to the corresponding amine (**4**) under Mills conditions to yield the arylazo intermediate (**8**). Nucleophilic substitution of the chlorine with 1-methylpiperazine and subsequent treatment with hydrochloric acid afforded the compounds **9**.



Scheme S2. Chemical synthesis of compound 9.

**2-Fluoro-4-nitro-1-nitrosobenzene (7).** 2-Fluoro-4-nitroaniline (500 mg, 3.20 mmol) was suspended in 10 mL of CH<sub>2</sub>Cl<sub>2</sub>. Oxone® (2.46 g, 8.00 mmol) in 20 mL of water was then added and the resulting mixture was stirred vigorously for 24 h at room temperature. The organic phase was separated, and the aqueous phase was further extracted with 10 mL of CH<sub>2</sub>Cl<sub>2</sub> for 3 times. The combined organic phases were washed with 1 M HCl (50 mL), saturated aqueous NaHCO<sub>3</sub> (50 mL), and water (50 mL). Finally, it was dried over MgSO<sub>4</sub>, concentrated under reduced pressure, and purified by chromatography (eluent: cyclohexane/EtOAc, 9:1) to yield **7** as a green solid (300 mg, 55%) which was immediately used in the following step without further purification.

**2-Chloro-N-(2-((2-fluoro-4-nitrophenyl)diazenyl)phenyl)acetamide (8).** Compounds **4** (500 mg, 2.71 mmol) and **7** (250 mg, 1.47 mmol) were dissolved in glacial acetic acid (20 mL) and the resulting solution was stirred for 24 h at room temperature. The solution was then concentrated under reduced pressure and the crude material was purified by chromatography (eluent: cyclohexane/EtOAc, 9:1). The so obtained solid was further purified by crystallization from methanol to yield **8** as an orange solid (200 mg, 40%). <sup>1</sup>H NMR (400 MHz, CDCl<sub>3</sub>) δ 10.83 (s, 1H), 8.70 (dd, *J* = 8.5, 1.3 Hz, 1H), 8.33 – 8.08 (m, 2H), 7.95 (dd, *J* = 8.2, 1.6 Hz, 1H), 7.90 – 7.84 (m, 1H), 7.61 (ddd, *J* = 8.7, 7.4, 1.6 Hz, 1H), 7.30 – 7.24 (m, 1H), 4.29 (s, 2H). <sup>13</sup>C NMR (101 MHz, CDCl<sub>3</sub>) δ 164.35, 144.45, 140.28, 136.53, 135.36, 126.98, 124.83, 124.75, 120.49, 120.07, 119.85, 119.81, 119.23, 43.56.

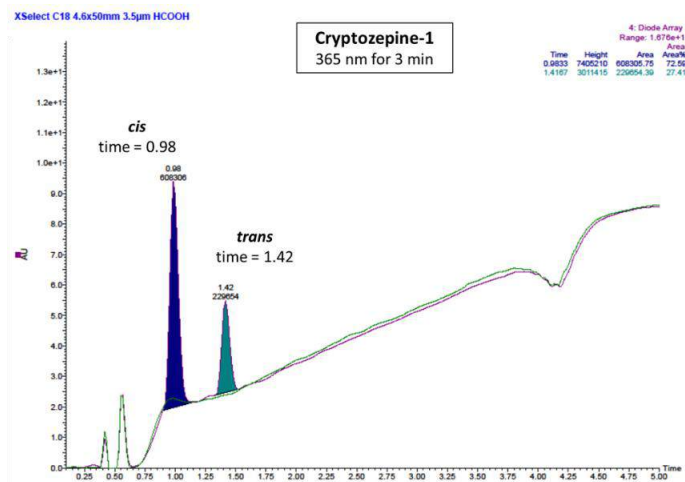
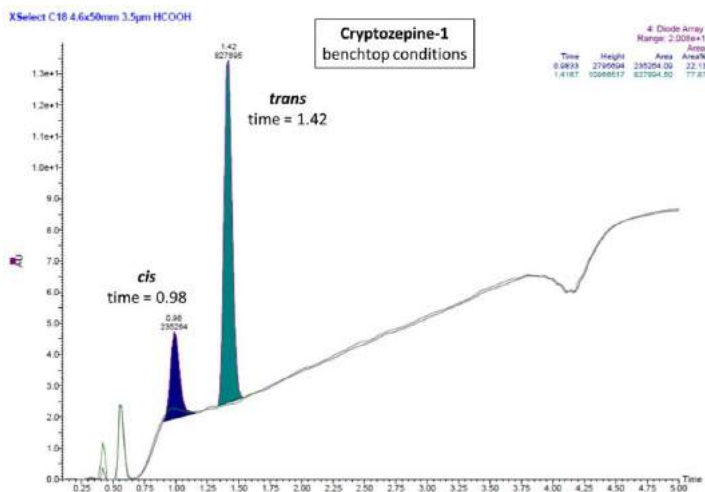
**(E)-N-(2-((2-Fluoro-4-nitrophenyl)diazenyl)phenyl)-2-(4-methylpiperazin-1-yl)acetamide (9).** Compound **8** (200 mg, 0.594 mmol) was dissolved in 20 mL of MeCN. 1-Methylpiperazine (89.24 mg, 0.891 mmol) and triethylamine (90.16 mg, 0.891 mmol) were then slowly added to the solution. The mixture was stirred under reflux for 3 h. Upon completion, MeCN was removed under reduced pressure and the obtained oil was dissolved in EtOAc. The resulting organic solution was washed 4 times using 30 mL of saturated aqueous NaHCO<sub>3</sub>. The organic layer was dried over MgSO<sub>4</sub> and evaporated under reduced pressure to afford the desired final compound (**9**) as an orange solid (quantitative yield). <sup>1</sup>H NMR (400 MHz, CDCl<sub>3</sub>) δ 10.94 (s, 1H), 8.80 (dd, *J* = 8.5, 1.3 Hz, 1H), 8.27 – 8.11 (m, 2H), 8.04 – 7.93 (m, 1H), 7.85 (dd, *J* = 8.3, 1.6 Hz, 1H), 7.58 (ddd, *J* = 8.6, 7.2, 1.6 Hz, 1H), 7.16 (ddd, *J* = 8.4, 7.2, 1.3 Hz, 1H), 3.26 (s, 2H), 2.80 – 2.30 (m, 8H), 2.21 (s, 3H). <sup>13</sup>C NMR (101 MHz, CDCl<sub>3</sub>) δ 168.86, 160.09, 157.48, 140.43, 138.63, 135.52, 123.79, 120.55,

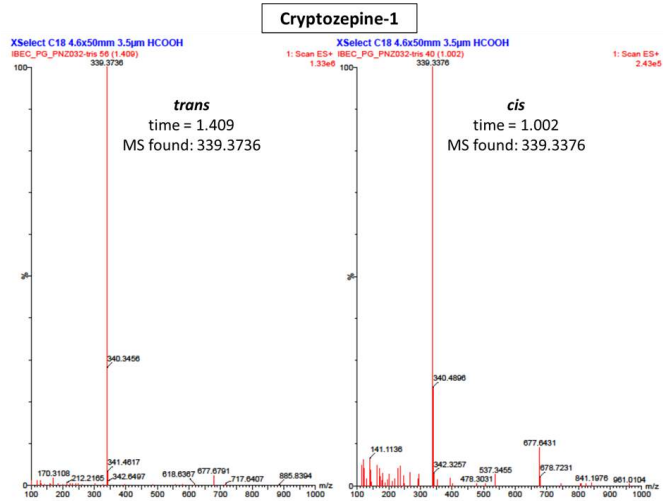
119.88, 119.43, 116.84, 113.78, 113.53, 62.93, 55.17, 53.63, 46.07. HR-MS (ESI,  $[M + H]^+$ ): calcd for  $C_{19}H_{22}FN_6O_3^+$ , 401.17; found 401.1732.

### 3. HPLC analyses and Mass Spectra

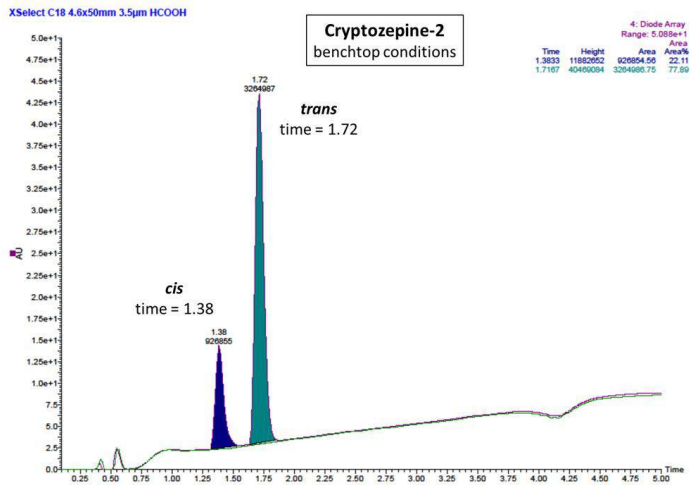
HPLC analyses were performed with a Waters Alliance 2795 separation module (RP column: XSelect CSH C18, 50x4.6 mm, S-3.5  $\mu$ m, 1.6 ml/min; eluent: from 5% B to 100% B in 3.5 min using a linear gradient, A:  $H_2O$  0.1% formic acid, B: acetonitrile 0.1% formic acid) coupled to a Waters 2996 photodiode detector and a Waters 3100 mass spectrometer (positive ionization analyses). PDA detector from 210 to 800 nm. Each HPLC analysis has been superimposed to the corresponding blank analysis. All the compound purities are  $\geq 95\%$ .

#### 3.1 Cryptozepine-1





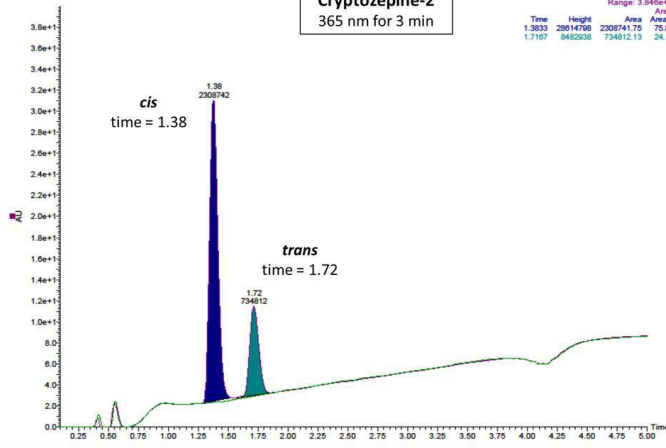
### 3.2 Cryptozepine-2



XSelect C18 4.6x50mm 3.5µm HCOOH

**Cryptozepine-2**  
365 nm for 3 min

4: Diode Array  
Range: 3.84e+1  
Area  
Time Height Area Area%  
1.383 29814798 23087412 75.85  
1.7167 8482038 734812.13 24.14

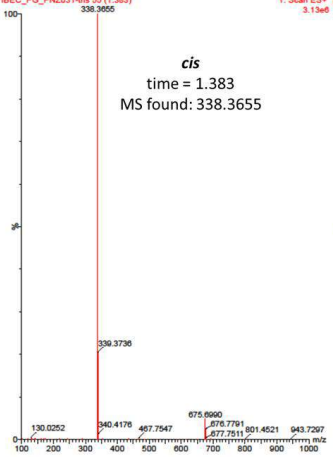


**Cryptozepine-2**

XSelect C18 4.6x50mm 3.5µm HCOOH

IBEC\_PG\_PNZ031-ins 55 (1.383)

*cis*  
time = 1.383  
MS found: 338.3655



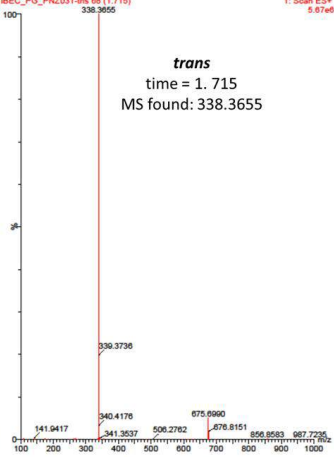
XSelect C18 4.6x50mm 3.5µm HCOOH

1: Scan ES+ IBEC\_PG\_PNZ031-ins 68 (1.715)

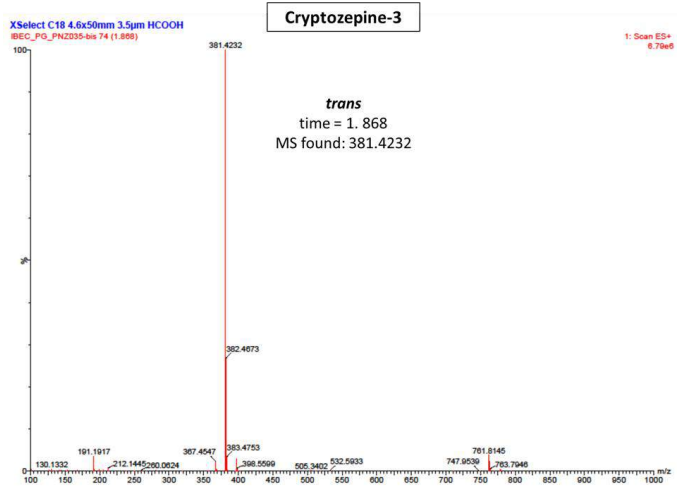
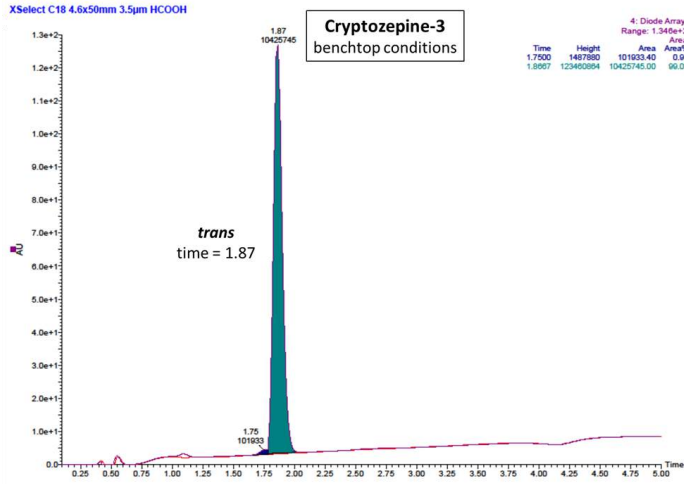
3.13e6

1: Scan ES+ 5.97e6

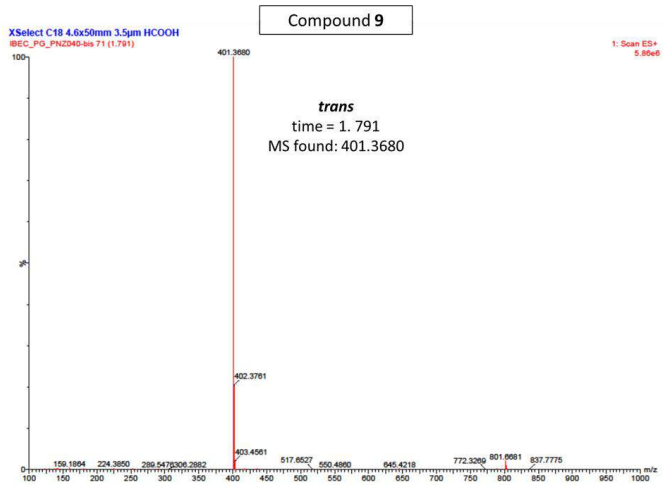
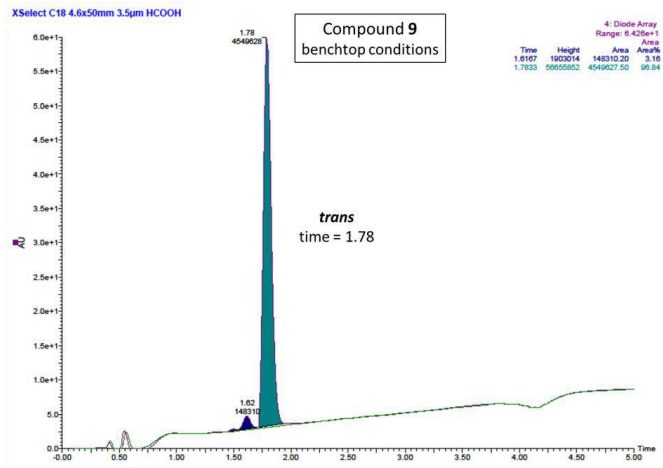
*trans*  
time = 1.715  
MS found: 338.3655



### 3.3 Cryptozepine-3



### 3.4 (E)-N-(2-((2-Fluoro-4-nitrophenyl)diazenyl)phenyl)-2-(4-methylpiperazin-1-yl)acetamide (9)



## 4. Photochemical characterization

An essential requirement for using our compounds as light-regulated M1 mAChRs antagonists is that they can effectively respond to light, which means that they can be quickly photoisomerized (from *trans* to *cis* and vice versa) between two different configurations with a relatively high degree of photoconversion (*trans/cis* ratio). We used UV-Vis spectroscopy and  $^1\text{H-NMR}$  to characterize their photochromic behavior.

### 4.1 Cryptozepine-1

Cryptozepine-1 revealed a clear photochromic behavior with the typical absorption bands of azobenzenes. Maximum absorption peaks in aqueous solution were observed at around 315 nm and 430 nm ( $\pi\text{-}\pi^*$  and  $n\text{-}\pi^*$  transitions, respectively) (Figure S4.1, panel B). Cryptozepine-1 can be effectively isomerized from *trans* to *cis* with ultraviolet light (365 nm), and back-isomerized from *cis* to *trans* with white (WL) or blue (460 nm) light. The process is reversible and can be repeated several times without any noticeable loss of photochromic behavior (Figure S4.1, panel D). We estimated a half-life of thermal relaxation of about 71 min at 37 °C in the dark for the *cis* isomer (30  $\mu\text{M}$  in water) obtained after illumination with 365 nm light (Figure S4.1, panel C).

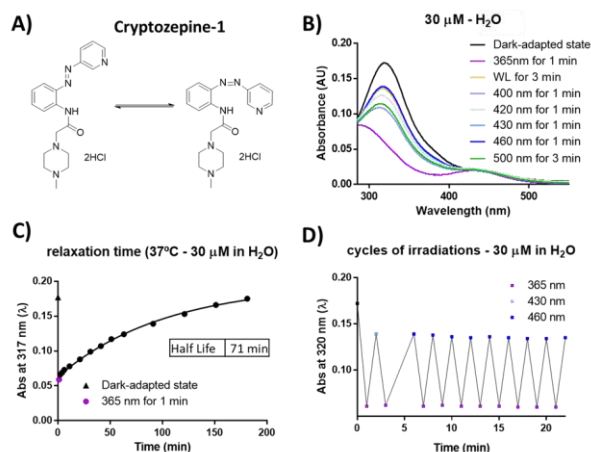


**Figure S4.1. Photochemical characterization of cryptozepine-1.** (A) Chemical structure of cryptozepine-1. (B) Absorption spectra in  $\text{H}_2\text{O}$  ( $30\ \mu\text{M}$ ). (C) Thermal stability: the photostationary state achieved after irradiation with 365 nm light in aqueous solution ( $30\ \mu\text{M}$ ) at  $37\ ^\circ\text{C}$  in the dark reverts to its dark-adapted state in less than 200 min. (D) Reversibility and stability of the photochromic behavior over several cycles of isomerization.

We next quantified by  $^1\text{H-NMR}$  the extent of photoisomerization for cryptozepine-1 ( $1\ \text{mM}$  in  $\text{D}_2\text{O}$ ) (Figure S4.1.1). The amount of the thermodynamically less stable *cis* isomer shifted from an initial value of 19% (as obtained under benchtop conditions) to 87% upon irradiation with 365 nm light for 5 minutes. After irradiation at 460 nm (10 min), the *trans* form reverted to a 58%. In the dark-adapted state the amount of *trans* isomer was 91%.

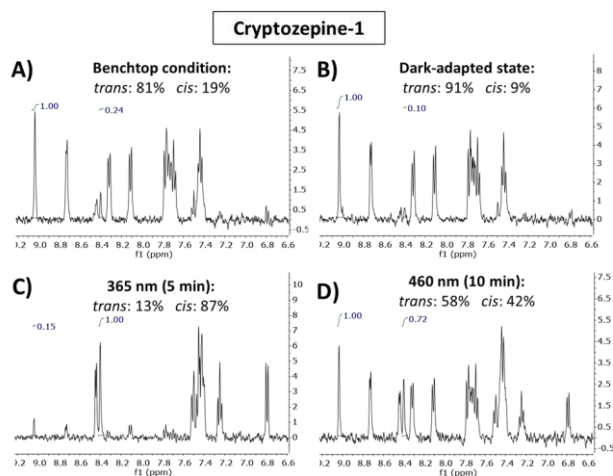


**Figure S4.1.1 Quantification of the photostationary state of cryptozepine-1.** (A) benchtop conditions, (B) dark-adapted state, (C) after 5 min of illumination with 365 nm light, and (D) after 10 min of illumination with 460 nm light.

## 4.2 Cryptozepine-2

Cryptozepine-2 revealed a clear photochromic behavior with the typical absorption bands of azobenzenes. Maximum absorption peaks in aqueous solution were observed at around 315 nm and 430 nm ( $\pi$ - $\pi^*$  and  $n$ - $\pi^*$  transitions, respectively) (Figure S4.2, panel B). Cryptozepine-2 can be effectively isomerized from *trans* to *cis* with ultraviolet light (365 nm), and completely back-isomerized from *cis* to *trans* with white (WL), blue (400-460 nm) or green (500 nm) light. The process is reversible and can be repeated several times without any noticeable loss of photochromic behavior (Figure S4.2, panel D). We estimated a half-life of thermal relaxation of about 180 min at 37 °C in the dark for the *cis* isomer (30  $\mu$ M in water) obtained after illumination with 365 nm light (Figure S4.2, panel C).

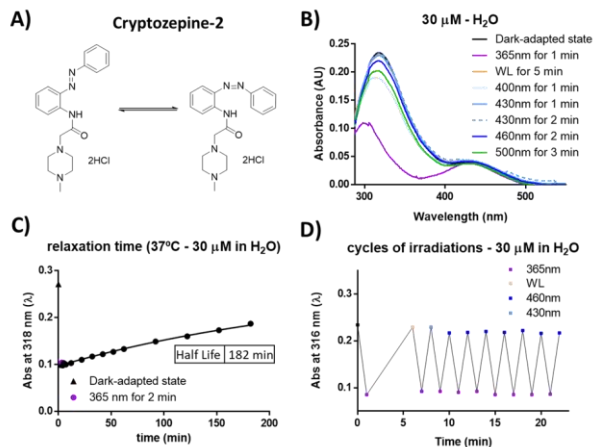


**Figure S4.2. Photochemical characterization of cryptozepine-2.** (A) Chemical structure of cryptozepine-2. (B) Absorption spectra in H<sub>2</sub>O (30 μM). (C) Thermal stability: the photostationary state achieved after irradiation with 365 nm light in aqueous solution (30 μM) at 37 °C in the dark has a half-life of 182 min. (D) Reversibility and stability of the photochromic behavior over several cycles of isomerization.

We next quantified by <sup>1</sup>H-NMR the extent of photoisomerization for cryptozepine-2 (1 mM in D<sub>2</sub>O) (**Figure S4.2.1**). The amount of the thermodynamically less stable *cis* isomer shifted from an initial value of 7% (as obtained under benchtop conditions) to 90% upon irradiation with 365 nm light for 5 minutes.

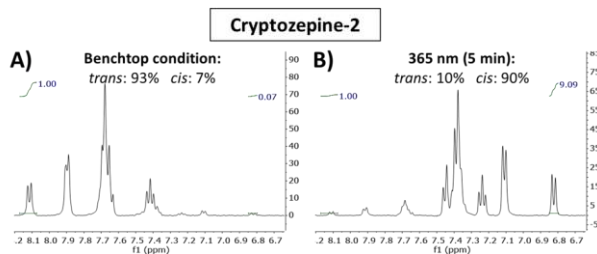


**Figure S4.2.1 Quantification of the photostationary state of cryptozepine-2.** (A) benchtop conditions, and (B) after 5 min of irradiation with 365 nm light.

### 4.3 Cryptozepine-3

Cryptozepine-3 revealed a clear photochromic behavior with the typical absorption bands of push-pull azobenzenes. The absorbance of the *trans* isomer is red shifted by ~100 nm and greatly decreases the thermal stability of the *cis* isomer, so its photoisomerization cannot be observed by steady-state UV-vis spectroscopy in aqueous solution. Maximum absorption peak in anhydrous DMSO (30  $\mu$ M) was observed at around 465 nm (**Figure S4.3**, panel B). Cryptozepine-3 can be effectively isomerized from *trans* to *cis* with blue (420-460 nm) and green (500 nm) light. The photostationary state achieved after irradiation with red lights reverts in 20 min at 37  $^{\circ}$ C in anhydrous DMSO in the dark (**Figure S4.3**, panel B).

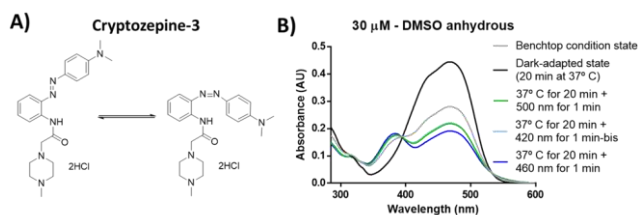


**Figure S4.3. Photochemical characterization of cryptozepine-3.** (A) Chemical structure of cryptozepine-3. (B) Absorption spectra in anhydrous DMSO (30  $\mu$ M).

### 4.4 Compound 9

Compound 9 revealed a clear photochromic behavior with the typical absorption bands of azobenzenes. Maximum absorption peaks in acidic water solution (pH 2) were observed at around 335 nm and 450 nm ( $\pi$ - $\pi^*$  and  $n$ - $\pi^*$  transitions, respectively) (**Figure S4.4**, panel B). Compound 9 can be effectively isomerized from *trans* to *cis* with ultraviolet light (365-380 nm), and back-isomerized from *cis* to *trans* with blue light (420-460 nm). The process is reversible and can be repeated several times without any noticeable loss of photochromic behavior (**Figure S4.4**, panel D). We estimated a half-life of thermal relaxation of about 68 min at 37  $^{\circ}$ C in the dark for the *cis* isomer (30  $\mu$ M, pH 2) obtained after illumination with 380 nm light (**Figure S4.4**, panel C).

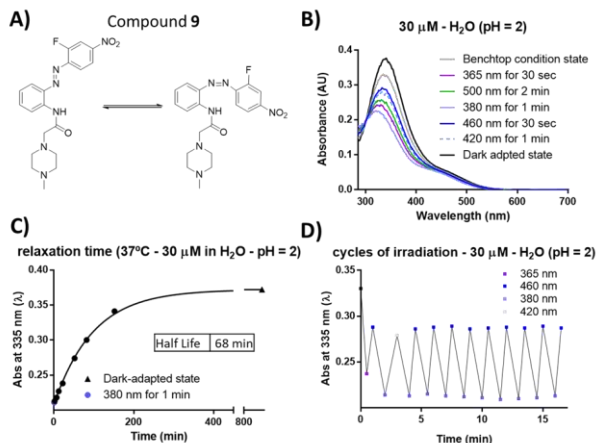


**Figure S4.4. Photochemical characterization of compound 9.** (A) Chemical structure of compound 9. (B) Absorption spectra in aqueous solution (30 μM, pH 2). (C) Thermal stability: the photostationary state achieved after irradiation with 380 nm light in aqueous solution (30 μM, pH 2) at 37 °C in the dark has a half-life of 68 min. (D) Reversibility and stability of the photochromic behavior over several cycles of isomerization.

We next quantified by <sup>1</sup>H-NMR the extent of photoisomerization for compound 9 (1.5 mM in D<sub>2</sub>O + HCl, pH 2) (**Figure S4.4.1**). The amount of the *cis* isomer shifted from an initial value of 18% (benchmark conditions) to 61% upon irradiation with 380 nm light (10 min). After irradiation with 460 nm (10 min), the *trans* form reverted to a 67%. In the dark-adapted state the amount of the *trans* isomer was about 93%.

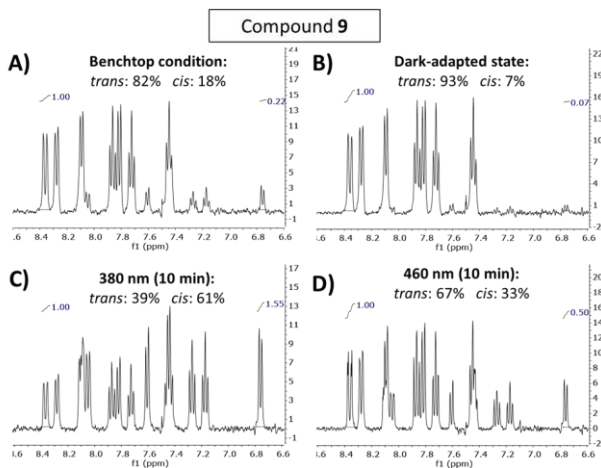


**Figure S4.4.1 Quantification of the photostationary state of compound 9.** (A) benchmark conditions, (B) dark-adapted state, (C) after 10 min of irradiation with 380 nm light, and (D) after 10 min of irradiation with 460 nm light.

## 5. NMR spectroscopy

### 5.1 NMR spectra of cryptozepine-1

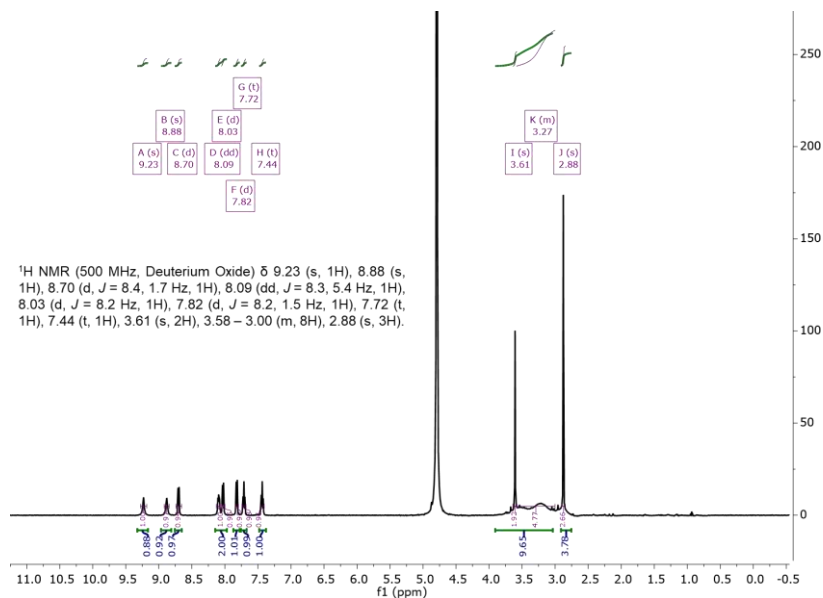


Figure S5.1. <sup>1</sup>H-NMR of cryptozepine-1 as obtained under benchtop conditions.

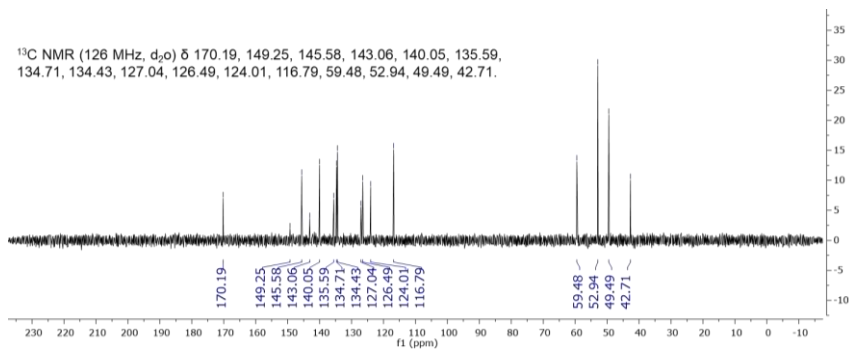


Figure S5.1.1 <sup>13</sup>C-NMR of cryptozepine-1 as obtained under benchtop conditions.

## 5.2 NMR spectra of cryptozepine-2

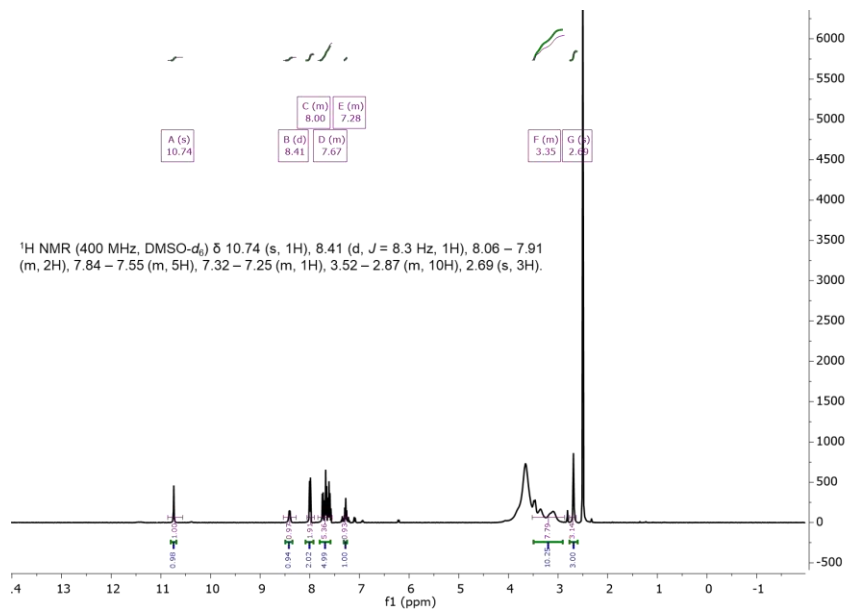


Figure S5.2 <sup>1</sup>H-NMR of cryptozepine-2 as obtained under benchtop conditions.

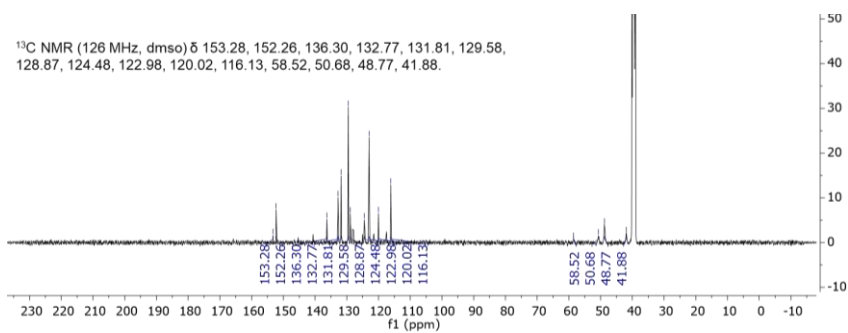


Figure S5.2.1 <sup>13</sup>C-NMR of cryptozepine-2 as obtained under benchtop conditions.

### 5.3 NMR spectra of cryptozepine-3

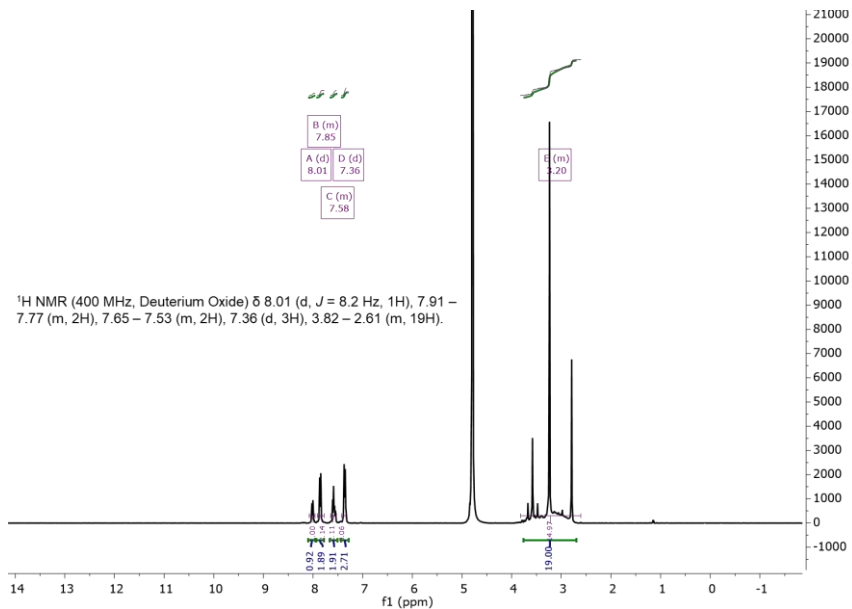


Figure S5.3 <sup>1</sup>H-NMR of cryptozepine-3 as obtained under benchtop conditions.

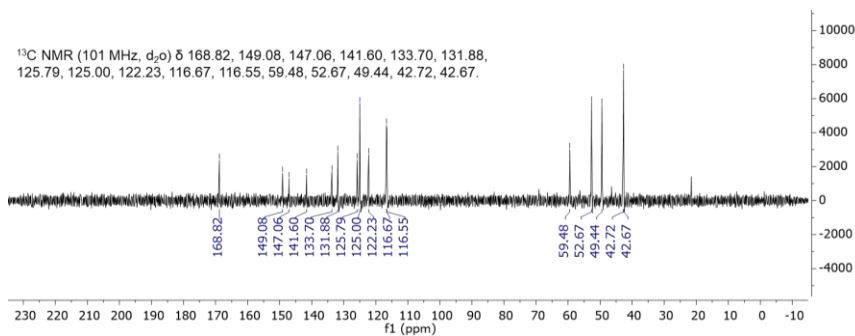


Figure S5.3.1 <sup>13</sup>C-NMR of cryptozepine-3 as obtained under benchtop conditions.

## 5.4 NMR spectra of compound 9

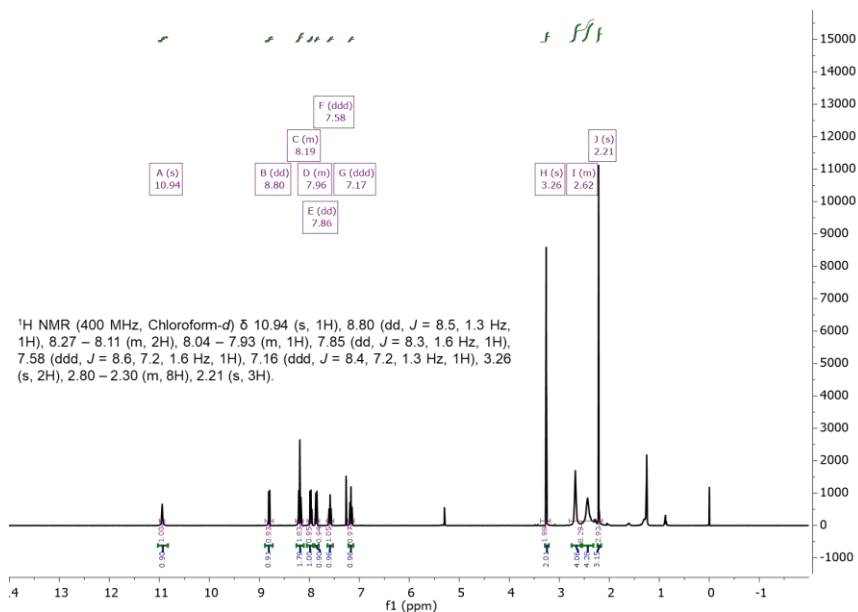


Figure S5.4 <sup>1</sup>H-NMR of compound 9 as obtained under benchtop conditions.

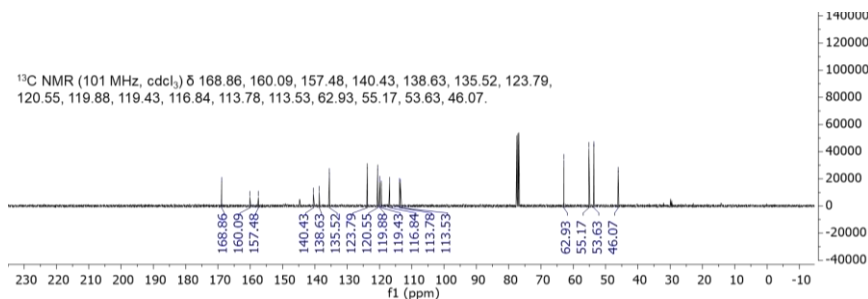
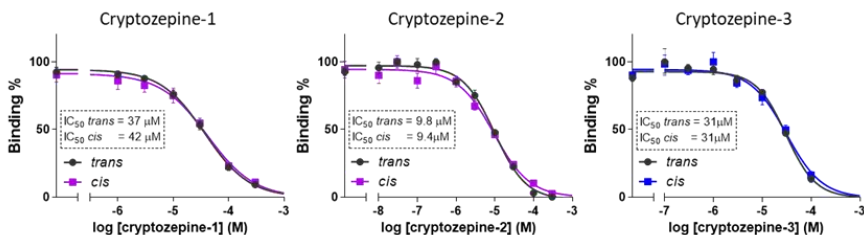


Figure S5.4.1 <sup>13</sup>C-NMR of compound 9 as obtained under benchtop conditions.

## 6. *In vitro* radioligand competition binding experiments

The affinity of our compounds for mAChRs was studied by radioligand competition binding experiments. Wistar rat brain membranes (whole cortex), that contain a high density of M1 mAChRs, were used for this assay.<sup>8</sup> The muscarinic antagonist [<sup>3</sup>H]quinuclidinyl benzilate ([<sup>3</sup>H]QNB) was used as competitive radioligand.<sup>9,10</sup> Specific binding was defined with the new ligands at total nominal concentrations ranging from 10 nM to 300  $\mu$ M, and derivatizing the raw disintegrations per minute (dpm) data from the scintillation counter to show the total radioactivity.<sup>8</sup>



**Figure S6.1. Competitive displacement of specific radioligand binding from mAChRs.** Competition for specific binding of 200 pM [<sup>3</sup>H]QNB to 3-4 months-old female Wistar rats brain membranes (whole cortex) containing high density of all five mAChRs by cryptozeprines-1, 2 and 3 (n = 4 for each isomer). Data points were fitted using the “log(inhibitor) vs. normalized response-variable slope (four parameters)” function in GraphPad Prism 6. Error bars are ± SEM.

## 7. *In vitro* calcium imaging experiments

**Cell culture and transfection for calcium imaging.** TsA201 cells were purchased from the European Collection of Authenticated Cell Culture. Cells were maintained at 37 °C in a humidified atmosphere with 5% CO<sub>2</sub> and grown in Dulbecco’s Modified Eagle’s Medium/Nutrient Mixture F-12 Ham (DMEM/F12 1:1, Life Technologies) medium, supplemented with 10% fetal bovine serum (FBS, Life Technologies) and antibiotics (1% penicillin/streptomycin, Sigma-Aldrich). Cells were transiently transfected with M1 receptor or co-transfected with M1 and R-GECO1 with X-tremeGENE 9 DNA Transfection Reagent (Roche Applied Science) following the manufacturer’s instructions. After 24 hours, cells were harvested with accutase (Sigma-Aldrich) and plated onto 16-mm glass coverslips (Fisher Scientific) pretreated with poly-L-Lysine (Sigma-Aldrich) to allow cell adhesion. Preconfluent cultures were used for experiments between 48 h and 72 h after transfection.

***In vitro* single-cell calcium imaging.** The bath solution used for single cell intracellular calcium recordings contained: 140 mM NaCl, 5.4 mM KCl, 1 mM MgCl<sub>2</sub>, 10 mM HEPES, 10 mM glucose and 2 mM CaCl<sub>2</sub> (pH 7.4). The calcium indicator used to test cryptozeprine-2 was OGB-1 AM (Life Technologies). Before each experiment, cells were mounted on the recording chamber (Open Diamond Bath Imaging Chamber for Round Coverslips from Warner Instruments) and loaded with OGB-1AM for 30 min at 37 °C with 5% CO<sub>2</sub>, at a final concentration of 10 μM in Ca<sup>2+</sup>-free bath solution. Cells were rinsed with fresh solution, and the recording chamber was filled with 1 mL recording solution and placed on an IX71 inverted microscope (Olympus) with a XLUMPLFLN 20XW x20/1 water immersion objective (Olympus). OGB-1 AM was excited during 50 ms at 488 nm by using a Polychrome V light source (Till Photonics) equipped with a Xenon Short Arc lamp (Ushio) and a 505-nm dichroic beam splitter (Chroma Technology). Emission at 510 nm was filtered by a D535/40 nm emission filter (Chroma Technology) and finally collected by a C9100-13 EM-CCD camera (HAMAMATSU). R-GECO1 was used as a Ca<sup>2+</sup> fluorescent indicator because it absorbs less than OGB1-AM at 460 nm, wavelength used to photoisomerize the compound cryptozeprine-3. R-GECO1 was excited during 50 ms at 562 nm by using a Polychrome V light source (Till Photonics) equipped with a Xenon Short Arc lamp (Ushio) and a 585-nm dichroic

beam splitter (Chroma Technology). Emission at 600 nm was filtered by ET630/75nm emission filter (Chroma Technology) and finally collected by a C9100-13 EM-CCD camera (HAMAMATSU). Images were acquired at room temperature with an imaging interval of 2 sec with the SmartLux software (HEKA), and the imaging analysis was done with FIJI (ImageJ). The agonist used to stimulate M1 in HEK tsA201 cells was acetylcholine (ACh, Sigma). Application of the compounds was carried out by manually pipetting a small volume during imaging acquisition into the accessory pool of the recording chamber for the final dilution of approximately 1:1000. Every application of 0.5 ACh  $\mu$ M was followed by the next application after a 20-min recovery time. The effect of M1 photoswitchable antagonists on the ACh-induced calcium signal was observed by applying for 2 minutes each compound (100  $\mu$ M) in its *trans* or *cis* form prior to the ACh application. In the case of pirenzepine, it was applied at decreasing concentrations ranging from 10 nM to 100  $\mu$ M, 2 minutes before ACh. Photoisomerization of cryptozepine-2 was achieved by pre-illuminating the compounds with Vilber Lourmat UV Lamp (365 nm, 6 W) for 2 min before application. Photoisomerization of cryptozepine-3 was achieved by continuously illuminating the specimen with 460 nm light. Numerical data were imported to GraphPad Prism version 6.00 for Windows (GraphPad Software, La Jolla, CA, USA). Statistical analysis was performed using the one-way ANOVA followed by the Tukey's multiple comparison post-hoc test. A value of  $p \leq 0.05$  was considered as statistically significant.

**Control experiments.** In order to assess the significance of cryptozepine-2 and -3 (photo)responses in M1 mAChR expressing cells, further control experiments were performed in tsA201 cells without the transfection with M1 receptor. No responses were observed after application of acetylcholine (ACh), cryptozepine-2 and 3, and under illumination at 460 nm, which excludes any response artifacts.

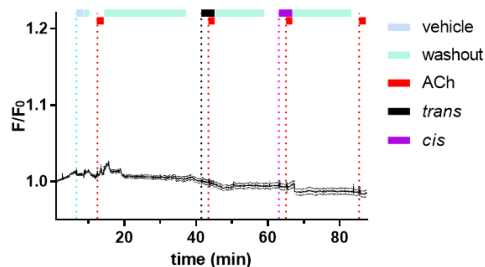
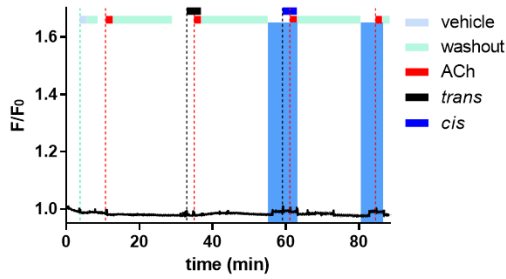
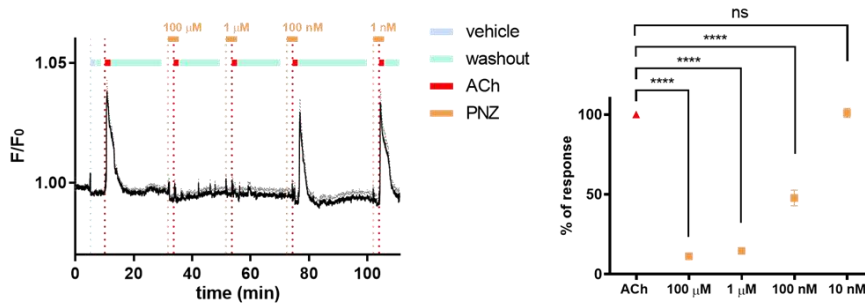


Figure S7.1. Control experiments for cryptozepine-2 with *in vitro* calcium imaging experiments in tsA201 cells without the presence of M1 receptor. No calcium oscillations were observed after application of ACh, cryptozepine-2 in the dark-adapted state (*trans*) and after 365 nm illumination (*cis*) ( $n = 50$  cells). Error bars are  $\pm$  SEM.



**Figure S7.2. Control experiments for cryptozepine-3 with *in vitro* calcium imaging experiments in tsA201 cells without the presence of M1 receptor.** No calcium oscillations were observed after application of ACh, cryptozepine-3 in the dark-adapted state (*trans*) and under 460 nm illumination (*cis*) ( $n = 50$  cells). Error bars are  $\pm$  SEM.

To validate our results, we performed calcium imaging recordings using the M1 antagonist pirenzepine (PNZ) (Sigma-Aldrich). We used pirenzepine at decreasing concentrations ranging from 10 nM to 100  $\mu$ M, 2 minutes prior to ACh application. As expected, at concentrations of 100  $\mu$ M, 1  $\mu$ M and 100 nM, we observed a significant inhibition of 89%, 85% and 52% of ACh-mediated calcium response respectively. However, the lowest concentration of PNZ (10 nM) had no significant effect.



**Figure S7.3. Pirenzepine (PNZ) antagonizes ACh-induced activation of M1 mAChRs.** Real-time calcium imaging traces from HEK cells expressing M1 mAChRs, which were loaded with the calcium indicator OGB-1 AM (10  $\mu$ M). Pirenzepine (PNZ) was used at concentrations ranging from 10 nM to 100  $\mu$ M. The cell responses to ACh (0.5  $\mu$ M) were significantly reduced in the presence of PNZ (100  $\mu$ M, 1  $\mu$ M and 100 nM). However, cell responses were recovered at lowest concentration (10 nM). Standard Error of the mean (SEM) is in gray. Quantification results are presented in the right graph ( $n = 94$  cells), one-way ANOVA with Tukey's multiple comparisons post-hoc test for statistical significance ( $p$ -value (\*) < 0.05  $p$ -value (\*\*\*) < 0.0001; GraphPad Prism 6. Error bars are  $\pm$  SEM.

## 8. Ex vivo mice atria tissue experiments

**Animals and tissue samples.** Ten CD1 male mice of 10-12 weeks old were used. Housing was under controlled conditions: constant temperature ( $22 \pm 2^\circ\text{C}$ ) and humidity ( $55 \pm 10\%$ ), 12-hour light/dark cycle and *ad libitum* access to water and food. Before euthanasia, heparin (100 units/kg IP) was administered. Animals were sacrificed by cervical dislocation under sedation with ketamine (80 mg/kg IP) and xylazine (10 mg/kg IP). For functional studies, heart was quickly removed and placed in carbogenated (95% O<sub>2</sub> and 5% CO<sub>2</sub>) Krebs solution (composition in mmol/L: glucose 10.10, NaCl 115.48, NaHCO<sub>3</sub> 21.90, KCl 4.61, NaH<sub>2</sub>PO<sub>4</sub> 1.14, CaCl<sub>2</sub> 2.50 and MgSO<sub>4</sub> 1.16) (pH 7.4). Functional experiments were approved by the Ethics Committee of the Universitat Autònoma de Barcelona (code EUT-MJ001).

**Functional studies.** Right atrium was isolated and mounted in a 10-mL chamber using a compact organ bath (Panlab sl). Tissue was bathed in a carbogenated Krebs solution maintained at  $37 \pm 1^\circ\text{C}$  using an external thermostat. Mechanical activity was measured with an isometric force transducer connected to a computer through an amplifier associated with PowerLab/800. LabChart software was used for data digitalization (1000 samples/s) and measurements. A tension of 0.2 g was applied, and tissue was allowed to equilibrate for 5 to 10 min, until spontaneous mechanical contractions were recorded. Carbachol  $10^{-6}$  M was added for 3 minutes and then pirenzepine (PNZ)  $10^{-6}$  M and  $10^{-5}$  M, *trans*-cryptozepine-2 (*trans*)  $10^{-5}$  M,  $3 \cdot 10^{-5}$  M and  $10^{-4}$  M or *cis*-cryptozepine-2 (*cis*)  $10^{-5}$  M,  $3 \cdot 10^{-5}$  M and  $10^{-4}$  M were applied. Amplitude and beats per minute (beats/min, bpm) were calculated before and after the addition of the drug.

**Results ex vivo.** Atrial contractions were recorded at a frequency of about 360 beats/min and a mean amplitude of 0.1 g. Carbachol (CCh) concentration dependently decreased both the amplitude and beats/min ( $n = 6$ ) with an EC<sub>50</sub> of about  $10^{-6}$  M. This concentration of CCh was used to activate muscarinic receptors in the bioassay and induces bradycardia. The presence of both pirenzepine (PNZ) ( $n = 6$ ) and *cis*-cryptozepine-2 (*cis*) ( $n = 2$ ) concentration-dependently reversed the effect of CCh  $10^{-6}$  M in terms of heartbeat frequency. In contrast, *trans*-cryptozepine-2 (*trans*) ( $n = 2$ ) did not reverse CCh-induced bradycardia ( $n = 2$ ) (Figures 4, S8.1 and S8.2).

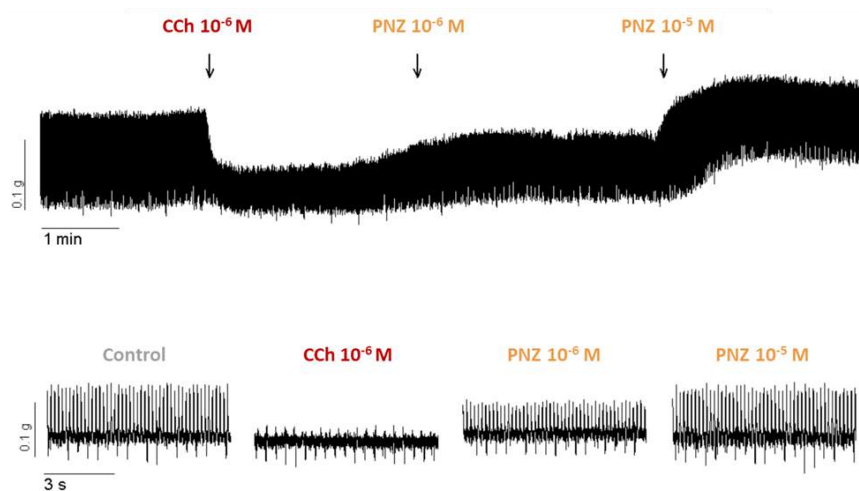


**Figure S8.1. Representative profile of the measured heart rate of a mouse right atrium treated with pirenzepine.** Spontaneous mechanical contractions were recorded as Control (ctrl). Carbachol (CCh) 10<sup>-6</sup> M decreased both the amplitude and beats/min (bpm). The presence of pirenzepine (PNZ) (n = 6) concentration-dependently reversed the bradycardic effect of CCh 10<sup>-6</sup>M.

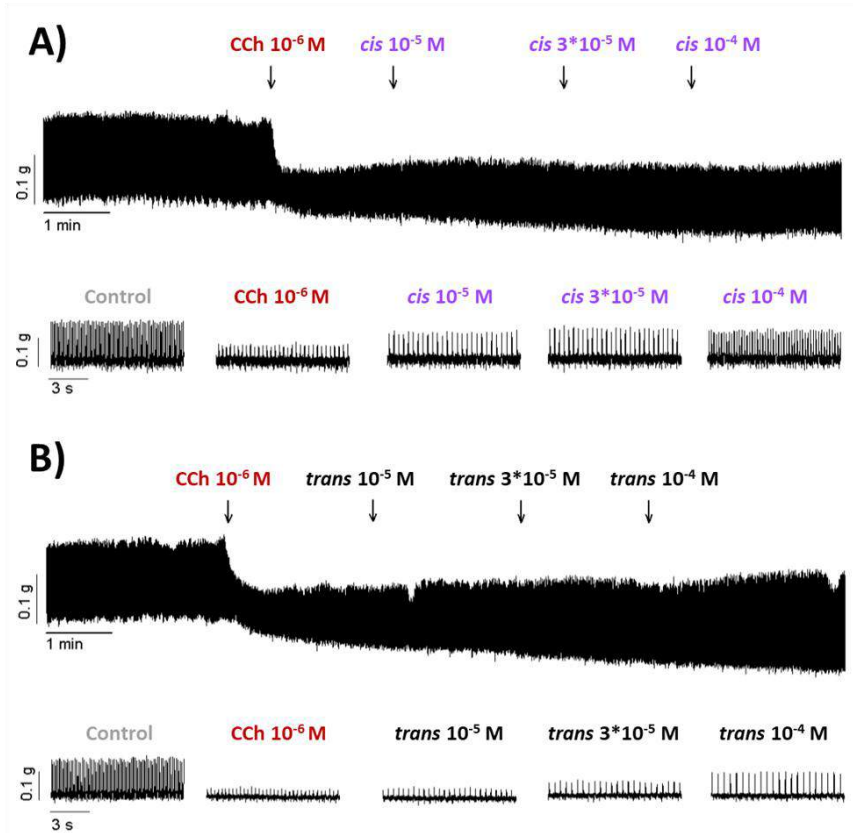


**Figure S8.2. Representative profile of the measured heart rate of a mouse right atrium treated with cryptozepine-2.** Spontaneous mechanical contractions were recorded as Control (ctrl). Carbachol (CCh)  $10^{-6}$  M decreased both the amplitude and beats/min (bpm). The presence of *cis*-cryptozepine-2 (*cis*) ( $n = 2$ ) concentration-dependently reversed the bradycardia induced by CCh  $10^{-6}$  M (Panel A), in line with the pirenzepine effect. In contrast, *trans*-cryptozepine-2 (*trans*) ( $n = 2$ ) did not reverse CCh effect in terms of heartbeat frequency ( $n = 2$ ) (Panel B).

## 9. Additional References

- (1) Thal, D. M.; Sun, B.; Feng, D.; Nawaratne, V.; Leach, K.; Felder, C. C.; Bures, M. G.; Evans, D. A.; Weis, W. I.; Bachhawat, P.; Kobilka, T. S.; Sexton, P. M.; Kobilka, B. K.; Christopoulos, A. Crystal Structures of the M1 and M4 Muscarinic Acetylcholine Receptors. *Nature* 2016, 531 (7594), 335–340. <https://doi.org/10.1038/nature17188>.
- (2) Morris, G. M.; Huey, R.; Lindstrom, W.; Sanner, M. F.; Belew, R. K.; Goodsell, D. S.; Olson, A. J. AutoDock4 and AutoDockTools4: Automated Docking with Selective Receptor Flexibility. *J. Comput. Chem.* 2009, 30 (16), 2785–2791. <https://doi.org/10.1002/jcc.21256>.

- (3) Dallakyan, S.; Olson, A. J. Small-Molecule Library Screening by Docking with PyRx. In *Methods in molecular biology* (Clifton, N.J.); 2015; Vol. 1263, pp 243–250. [https://doi.org/10.1007/978-1-4939-2269-7\\_19](https://doi.org/10.1007/978-1-4939-2269-7_19).
- (4) Lu, Z. L.; Saldanha, J. W.; Hulme, E. C. Transmembrane Domains 4 and 7 of the M1 Muscarinic Acetylcholine Receptor Are Critical for Ligand Binding and the Receptor Activation Switch. *J. Biol. Chem.* 2001, 276 (36), 34098–34104. <https://doi.org/10.1074/jbc.M104217200>.
- (5) Eberlein, W. G.; Engel, W. W.; Trummelitz, G.; Schmidt, G.; Hammer, R. Tricyclic Compounds as Selective Antimuscarinics. 2. Structure-Activity Relationships of M1 Selective Antimuscarinics Related to Pirenzepine. *J. Med. Chem.* 1988, 31 (6), 1169–1174. <https://doi.org/10.1021/jm00401a016>.
- (6) Murgolo, N. J.; Kozlowski, J.; Tice, M. A. B.; Hollinger, F. P.; Brown, J. E.; Zhou, G.; Taylor, L. A.; McQuade, R. D. The N4 Nitrogen of Pirenzepine Is Responsible for Selective Binding of the M1 Subtype Human Muscarinic Receptor. *Bioorganic Med. Chem. Lett.* 1996, 6 (7), 785–788. [https://doi.org/10.1016/0960-894X\(96\)00107-2](https://doi.org/10.1016/0960-894X(96)00107-2).
- (7) Song, Y.; Lin, X.; Kang, D.; Li, X.; Zhan, P.; Liu, X.; Zhang, Q. Discovery and Characterization of Novel Imidazopyridine Derivative CHEQ-2 as a Potent CDC25 Inhibitor and Promising Anticancer Drug Candidate. *Eur. J. Med. Chem.* 2014, 82, 293–307. <https://doi.org/10.1016/j.ejmech.2014.05.063>.
- (8) Claro, E. Analyzing Ligand Depletion in a Saturation Equilibrium Binding Experiment. *Biochem. Mol. Biol. Educ.* 2006, 34 (6), 428–431. <https://doi.org/10.1002/bmb.2006.494034062677>.
- (9) Yamamura, H. I.; Snyder, S. H. Muscarinic Cholinergic Binding in Rat Brain. *Proc. Natl. Acad. Sci. U. S. A.* 1974, 71 (5), 1725–1729. <https://doi.org/10.1073/pnas.71.5.1725>.
- (10) Sallés, J.; Wallace, M. A.; Fain, J. N. Differential Effects of Alkylating Agents on the Multiple Muscarinic Receptor Subtypes Linked to Activation of Phospholipase C by Carbachol in Rat Brain Cortical Membranes. *J. Pharmacol. Exp. Ther.* 1993, 264 (2).

## General Discussion

### Chapter IV

The method of “crypto-azologization” has the potential to substantially expand the repertoire of photoswitchable bioactive compounds in medicinal chemistry. Privileged structures typically display a “drug-like” profile and are able to target most neurotransmitter pathways, often with low selectivity. Such a dearth of specificity carries many undesirable side-effects. Sometimes, there are no true explanations about their mechanisms of action or why they are active against a particular group of targets. The recurrent strategy to diversify the pharmacological properties of the privileged structures exploits the insertion of chemically different side chains in different sites of the heterotricyclic core. This approach permits to create a huge number of different bioactive compounds able to preferentially act through more specific targets. However, even if the specificity of the binding properties can be remarkably improved by such chemical modifications, sometimes it is not enough to avoid off-target activity and toxicity (Borcherding et al., 2017; Crismon, 1994; Marsh, 2007).

Considering the cholinergic system, the tricyclic core is present in many anticholinergic agents, such as pirenzepine, otenzepad, telenzepine, propantheline, AFDX-116, or metantelina. They are characterized by different side chains that provide a moderate subtype selectivity among the muscarinic receptors. Some of these compounds are, or have been, marketed for different medical purposes, however their therapeutic use is fading due to their poor safety profile (Eglen, 2005; Kruse et al., 2014; Scarr, 2012).

We applied the new “crypto-azologization” concept to the M1 antagonist pirenzepine in order to produce a collection of photoswitchable muscarinic antagonists, and also to validate a new photoswitchable drug design strategy to that expands the breadth of photopharmacology. The

crypto-azologs obtained modulate muscarinic receptors reversibly, displaying stronger inhibitory activity upon illumination both *in vitro* and in cardiac atria *ex vivo*.

In comparison to the use of diazocines, which are also able to mimic the tricyclic structures, the “crypto-azologization” strategy has several advantages in medicinal chemistry. Diazocines exist as *cis* isomer in thermodynamically stable conditions in the dark, which appears to be most similar to the tricyclic structure (**Figure 38**, left). Thus, diazocine azologs of tricyclic drugs are predicted to behave as “dark-active” ligands (Siewertsen et al., 2009, 2011). Although this is generally not the desired situation for therapeutic purposes (Matera et al., 2018), this unexplored azologization strategy could be very useful for other applications like two-photon photopharmacology (Pittolo et al., 2019).

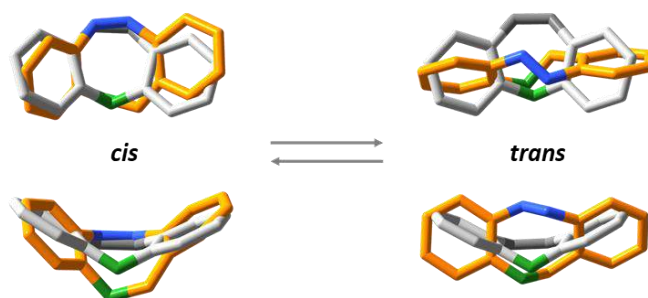


**Figure 38.** Three-dimensional alignment of a diazocine scaffold over a generic fused tricyclic system. Best three-dimensional alignment of a diazocine scaffold (dark-stable *cis* on the left and light-activated *trans* on the right, both in orange) over a generic fused tricyclic system (in gray). For the sake of comparison, the carbon atom of the 1-atom bridge of the tricyclic system and the corresponding carbon atom of the azobenzene are indicated in green. Nitrogen atoms are shown in blue.

Building on the experience with PAI, the application of cryptozepines to control brain waves is very interesting especially *in vivo*, as the dark-inactive ligands could be systemically administered and activated locally. These physiological experiments are under course in the laboratory of our collaborators at IDIBAPS (María Victoria Sánchez-Vives). In this regard, the two-photon excitation properties of these ligands would also be relevant, as they would permit the use of near-infrared (NIR) light to control their anticholinergic activity in the presence of endogenous neurotransmitter. Such wavelengths can penetrate deeper into the biological tissues and are

safer than violet lights, a great advantage for the potential clinical application of the drug. Furthermore, minimal chemical modifications of the structure of cryptozepine-**2** would suffice to improve both the potency (Agnetta et al., 2019) and the two-photon cross section (Cabr e et al., 2019a) of the drug, like the insertion of fluorine/s in the ortho positions of the azobenzene.

Last but not least, we envisage that combining the new photopharmacological crypto-azologization strategy with the systematic coupling of tricyclic scaffolds with different side chains to diversify their pharmacology would allow to optimize the action of a large number of “privileged” bioactive compounds that remain underexploited for both research and therapeutic applications.



## CHAPTER V

### Conclusions



## Conclusions

The main conclusions drawn from this work are summarized here.

*Chapter II* describes the development of light-regulated derivatives of the muscarinic agonist Iperoxo. The results indicate that:

- ❖ Azobenzenes are favorable molecular switches due to their small size and robust photochromism. Iperoxo, a potent muscarinic agonist, tolerates the azo-extension into its structure maintaining its original activity.
- ❖ Our iperoxo derivatives behave as more potent muscarinic agonists when coupled to the fluorinated azobenzenes than to the unsubstituted. This may be related to additional lipophilic contacts between the fluorines and the M1 residues near the orthosteric site, as suggested by our docking studies.
- ❖ Bivalent photoswitchable muscarinic agonists, IAI and F4-IAI, showed higher binding affinity and potency than the monovalent PI and F4-PI. Moreover, the bivalent nature confers a pronounced photoswitchable activity to these ligands, probably due to additional interactions at the allosteric site of the muscarinic receptors.
- ❖ The optimization of allosteric contacts might improve the photopharmacology of our muscarinic agonists.

Chapter III shows the development of light-regulated hybrid agonists for the M2 receptor. The results show that:

- ❖ The merger of hybridization and non-canonical azologization strategies forged the light-sensitive dualsteric agonist PAI. In this design, we included an azobenzene in the structure of the known M2 dualsteric ligand P-8-Iper, conserving the iperoxo-like orthosteric moiety and the M2-selective allosteric fragment.
- ❖ PAI is a potent M2 agonist in its *trans* form and can be photoisomerized into the less active *cis* isomer with ultraviolet light (365 nm). *Cis* to *trans* isomerization is achieved with 420-460 nm or white light. Both isomers of PAI have excellent thermal stability.
- ❖ In the heart, M2 receptor activation decreases heart rate and prolongs the atrio-ventricular conduction time. PAI demonstrated *in vitro* and *in vivo* the control of cardiac function with light and may pave the way to new therapies for various cardiopathies like atrial fibrillation.
- ❖ In the brain, M2 receptors modulate cognition, learning, memory, sensory, and motor functions. PAI can photocontrol the cortical network rhythmic activity *ex vivo* and in wildtype mice for the first time. This tool is innovative for basic neuroscience research and inspires new therapies against various brain disorders.
- ❖ Under two-photon excitation, PAI is sensitive to near-infrared light (840 nm), which can deeply penetrate biological tissue. This opens the way to advanced *in vivo* applications of our drug and other ligands containing related azobenzene cores.

*Chapter IV* is focused on the development of light-regulated M1 antagonists using the new “crypto-azologization” concept. The results demonstrate that:

- ❖ Many muscarinic antagonists have a heterotricyclic core, which is versatile but has not been controlled with light. Using photochromic arylazo scaffolds we mimicked the tricyclic system of the M1 antagonist pirenzepine. We named this strategy “crypto-azologization”.
- ❖ We developed four “crypto-azologs” of pirenzepine which inhibit M1 receptors upon illumination both *in vitro* and in cardiac atria *ex vivo*, demonstrating the efficacy of our strategy.
- ❖ The crypto-azologization mimics the heterotricyclic with the *cis* configuration, whereas the corresponding *trans* cannot. This allows the administration of inactive drugs and their localized photoactivation in tissue, enabling safer therapies with reduced side effects in other regions and organs.
- ❖ The “crypto-azologization” approach might control the action of many other tricyclic drugs clinically used as effective therapies for different conditions, like the tricyclic antidepressants, and provide an opportunity to reduce their side effects. This will expand the scope of photopharmacology and its applications.



## BIBLIOGRAPHY



- Adams, S.R., and Tsien, R.Y. (1993). Controlling cell chemistry with caged compounds. *Annu. Rev. Physiol.*
- Agnetta, L., Bermudez, M., Riefolo, F., Matera, C., Claro, E., Messerer, R., Littmann, T., Wolber, G., Holzgrabe, U., and Decker, M. (2019). Fluorination of photoswitchable muscarinic agonists tunes receptor pharmacology and photochromic properties. *J. Med. Chem.* *62*, 3009–3020.
- Aihara, T., Nakamura, Y., Taketo, M.M., Matsui, M., and Okabe, S. (2005). Cholinergically stimulated gastric acid secretion is mediated by M3 and M5 but not M1 muscarinic acetylcholine receptors in mice. *Am. J. Physiol. - Gastrointest. Liver Physiol.*
- Allen, T.G., and Brown, D.A. (1993). M2 muscarinic receptor-mediated inhibition of the Ca<sup>2+</sup> current in rat magnocellular cholinergic basal forebrain neurones. *J. Physiol.* *466*, 173–189.
- De Amici, M., Dallanoce, C., Holzgrabe, U., Tränkle, C., and Mohr, K. (2010). Allosteric ligands for G protein-coupled receptors: a novel strategy with attractive therapeutic opportunities. *Med. Res. Rev.*
- Anagnostaras, S.G., Murphy, G.G., Hamilton, S.E., Mitchell, S.L., Rahnama, N.P., Nathanson, N.M., and Silva, A.J. (2003). Selective cognitive dysfunction in acetylcholine M1 muscarinic receptor mutant mice. *Nat. Neurosci.*
- De Angelis, F., Bernardo, A., Magnaghi, V., Minghetti, L., and Tata, A.M. (2012). Muscarinic receptor subtypes as potential targets to modulate oligodendrocyte progenitor survival, proliferation, and differentiation. *Dev. Neurobiol.* *72*, 713–728.
- Antony, J., Kellershohn, K., Mohr-Andrä, M., Kebig, A., Prilla, S., Muth, M., Heller, E., Disingrini, T., Dallanoce, C., Bertoni, S., et al. (2009). Dualsteric GPCR targeting: a novel route to binding and signaling pathway selectivity. *FASEB J.*
- Aronstam, R.S., and Patil, P. (2009). Muscarinic receptors: autonomic neurons. In *Encyclopedia of Neuroscience*, (Elsevier Ltd), pp. 1141–1149.
- Asanuma, H., Liang, X., and Komiyama, M. (2000). Meta-aminoazobenzene as a thermo-insensitive photo-regulator of DNA- duplex formation. *Tetrahedron Lett.*
- Baillet, G., Giusti, G., and Guglielmetti, R. (1995). Study of the fatigue process and the yellowing of polymeric films containing spirooxazine photochromic compounds. *Bull. Chem. Soc. Jpn.*
- Bandara, H.M.D., and Burdette, S.C. (2012). Photoisomerization in different classes of azobenzene. *Chem. Soc. Rev.*
- Banghart, M.R., and Sabatini, B.L. (2012). Photoactivatable neuropeptides for spatiotemporally precise delivery of opioids in neural tissue. *Neuron.*
- Banghart, M., Borges, K., Isacoff, E., Trauner, D., and Kramer, R.H. (2004). Light-activated ion channels for remote control of neuronal firing. *Nat. Neurosci.*
- Banghart, M.R., Volgraf, M., and Trauner, D. (2006). Engineering light-gated ion channels. *Biochemistry.*
- Banghart, M.R., Mourot, A., Fortin, D.L., Yao, J.Z., Kramer, R.H., and Trauner, D. (2009). Photochromic blockers of voltage-gated potassium channels. *Angew. Chemie - Int. Ed.*
- Barocelli, E., Ballabeni, V., Bertoni, S., Dallanoce, C., De Amici, M., De Micheli, C., and Impicciatore, M. (2000). New analogues of oxotremorine and oxotremorine-M estimation of their in vitro affinity and efficacy at muscarinic receptor subtypes. *Life Sci.*
- Bartels, E., Wassermann, N.H., and Erlanger, B.F. (1971). Photochromic activators of the acetylcholine receptor. *Proc. Natl. Acad. Sci. U. S. A.*
- Bartus, R., Dean, R. 3rd, Beer, B., and Lippa, A. (1982). The cholinergic hypothesis of geriatric memory

dysfunction. *Science* (80).

Bautista-Barrufet, A., López-Gallego, F., Rojas-Cervellera, V., Rovira, C., Pericàs, M.A., Guisán, J.M., and Gorostiza, P. (2014). Optical control of enzyme enantioselectivity in solid phase. *ACS Catal.*

Beharry, A.A., Sadovski, O., and Woolley, G.A. (2011). Azobenzene photoswitching without ultraviolet light. *J. Am. Chem. Soc.*

Beker, F., Weber, M., Fink, R.H.A., and Adams, D.J. (2003). Muscarinic and nicotinic ACh receptor activation differentially mobilize Ca<sup>2+</sup> in rat intracardiac ganglion neurons. *J. Neurophysiol.* 90, 1956–1964.

Berg, R.H., Hvilsted, S., and Ramanujam, P.S. (1996). Peptide oligomers for holographic data storage. *Nature.*

Bermudez, M., Bock, A., Krebs, F., Holzgrabe, U., Mohr, K., Lohse, M.J., and Wolber, G. (2017). Ligand-Specific Restriction of Extracellular Conformational Dynamics Constrains Signaling of the M2 Muscarinic Receptor. *ACS Chem. Biol.*

Bertarelli, C., Bianco, A., Castagna, R., and Pariani, G. (2011). Photochromism into optics: opportunities to develop light-triggered optical elements. *J. Photochem. Photobiol. C Photochem. Rev.*

Bingen, B.O., Engels, M.C., Schaliq, M.J., Jangsangthong, W., Neshati, Z., Feola, I., Ypey, D.L., Askar, S.F.A., Panfilov, A. V., Pijnappels, D.A., et al. (2014). Light-induced termination of spiral wave arrhythmias by optogenetic engineering of atrial cardiomyocytes. *Cardiovasc. Res.*

Birnbaumer, L. (2007). Expansion of signal transduction by G proteins. The second 15 years or so: From 3 to 16  $\alpha$  subunits plus  $\beta\gamma$  dimers. *Biochim. Biophys. Acta - Biomembr.* 1768, 772–793.

Blevins, A.A., and Blanchard, G.J. (2004). Effect of Positional Substitution on the Optical Response of Symmetrically Disubstituted Azobenzene Derivatives. *J. Phys. Chem. B.*

Bock, A., Merten, N., Schrage, R., Dallanoce, C., Bätz, J., Klöckner, J., Schmitz, J., Matera, C., Simon, K., Kebig, A., et al. (2012). The allosteric vestibule of a seven transmembrane helical receptor controls G-protein coupling. *Nat. Commun.*

Bock, A., Bermudez, M., Krebs, F., Matera, C., Chirinda, B., Sydow, D., Dallanoce, C., Holzgrabe, U., De Amici, M., Lohse, M.J., et al. (2016). Ligand binding ensembles determine graded agonist efficacies at a G protein-coupled receptor. *J. Biol. Chem.*

Bonner, T.I., Young, A.C., Bran, M.R., and Buckley, N.J. (1988). Cloning and expression of the human and rat m5 muscarinic acetylcholine receptor genes. *Neuron.*

Borcherding, B., Rendleman, R.L., and Walkup, J.T. (2017). Neuropsychopharmacology. In Swaiman's Pediatric Neurology: Principles and Practice: Sixth Edition, p.

Borowiak, M., Nahaboo, W., Reynders, M., Nekolla, K., Jalinot, P., Hasserodt, J., Rehberg, M., Delattre, M., Zahler, S., Vollmar, A., et al. (2015). Photoswitchable inhibitors of microtubule dynamics optically control mitosis and cell death. *Cell.*

Bort, G., Gallavardin, T., Ogden, D., and Dalko, P.I. (2013). From one-photon to two-photon probes: “caged” compounds, actuators, and photoswitches. *Angew. Chemie - Int. Ed.*

Boyden, E.S., Zhang, F., Bamberg, E., Nagel, G., and Deisseroth, K. (2005). Millisecond-timescale, genetically targeted optical control of neural activity. *Nat. Neurosci.*

Boyle, P.M., Karathanos, T. V., and Trayanova, N.A. (2015). “Beauty is a light in the heart”: the transformative potential of optogenetics for clinical applications in cardiovascular medicine. *Trends Cardiovasc. Med.*

Brodde, O.E., and Michel, M.C. (1999). Adrenergic and muscarinic receptors in the human heart.

Pharmacol. Rev.

Brodde, O.E., Bruck, H., Leineweber, K., and Seyfarth, T. (2001). Presence, distribution and physiological function of adrenergic and muscarinic receptor subtypes in the human heart. *Basic Res. Cardiol.*

Brode, W.R., Gould, J.H., and Wyman, G.M. (1952). The relation between the absorption spectra and the chemical constitution of dyes. XXV. Phototropism and cis-trans isomerism in aromatic azo compounds. *J. Am. Chem. Soc.*

Broichhagen, J., Schönberger, M., Cork, S.C., Frank, J.A., Marchetti, P., Bugliani, M., Shapiro, A.M.J., Trapp, S., Rutter, G.A., Hodson, D.J., et al. (2014). Optical control of insulin release using a photoswitchable sulfonyleurea. *Nat. Commun.*

Broichhagen, J., Frank, J.A., and Trauner, D. (2015). A roadmap to success in photopharmacology. *Acc. Chem. Res.*

Brown, D.A., and Adams, P.R. (1980). Muscarinic suppression of a novel voltage-sensitive K<sup>+</sup> current in a vertebrate neurone. *Nature* 283, 673–676.

Brown, E. V., and Granneman, G.R. (1975). Cis-trans isomerism in the pyridyl analogs of azobenzene. A kinetic and molecular orbital analysis. *J. Am. Chem. Soc.*

Bruemann, T., Boyle, P.M., Vogt, C.C., Karathanos, T. V., Arevalo, H.J., Fleischmann, B.K., Trayanova, N.A., and Sasse, P. (2016). Optogenetic defibrillation terminates ventricular arrhythmia in mouse hearts and human simulations. *J. Clin. Invest.*

Bünemann, M., Meyer, T., Pott, L., and Hosey, M. (2000). Novel inhibition of G $\beta$ y-activated potassium currents induced by M2 muscarinic receptors via a pertussis toxin-insensitive pathway. *J. Biol. Chem.* 275, 12537–12545.

Bymaster, F.P., Shannon, H.E., Rasmussen, K., Delapp, N.W., Mitch, C.H., Ward, J.S., Calligaro, D.O., Ludvigsen, T.S., Sheardown, M.J., Olesen, P.H., et al. (1998). Unexpected antipsychotic-like activity with the muscarinic receptor ligand (5 R,6 R)6-(3-propylthio-1,2,5-thiadiazol-4-yl)-1-azabicyclo[3.2.1]octane. *Eur. J. Pharmacol.*

Byrne, D.P., Vonderach, M., Ferries, S., Brownridge, P.J., Evers, C.E., and Evers, P.A. (2016). CAMP-dependent protein kinase (PKA) complexes probed by complementary differential scanning fluorimetry and ion mobility-mass spectrometry. *Biochem. J.* 473, 3159–3175.

Cabré, G., Garrido-Charles, A., Moreno, M., Bosch, M., Porta-de-la-Riva, M., Krieg, M., Gascón-Moya, M., Camarero, N., Gelabert, R., Lluch, J.M., et al. (2019a). Rationally designed azobenzene photoswitches for efficient two-photon neuronal excitation. *Nat. Commun.*

Cabré, G., Garrido-Charles, A., González-Lafont, À., Moormann, W., Langbehn, D., Egea, D., Lluch, J.M., Herges, R., Alibés, R., Busqué, F., et al. (2019b). Synthetic photoswitchable neurotransmitters based on bridged azobenzenes. *Org. Lett.*

Callaway, E.M., and Katz, L.C. (1993). Photostimulation using caged glutamate reveals functional circuitry in living brain slices. *Proc. Natl. Acad. Sci. U. S. A.*

Canepari, M., Nelson, L., Papageorgiou, G., Corrie, J.E.T., and Ogden, D. (2001). Photochemical and pharmacological evaluation of 7-nitroindolyl- and 4-methoxy-7-nitroindolyl-amino acids as novel, fast caged neurotransmitters. *J. Neurosci. Methods.*

Caulfield, M.P. (1993). Muscarinic receptors-characterization, coupling and function. *Pharmacol. Ther.*

Caulfield, M.P., and Birdsall, N.J.M. (1998). International Union of Pharmacology. XVII. Classification of muscarinic acetylcholine receptors. *Pharmacol. Rev.* 50, 279–290.

Chambers, J.J., Banghart, M.R., Trauner, D., and Kramer, R.H. (2006). Light-induced depolarization of

- neurons using a modified Shaker K<sup>+</sup> channel and a molecular photoswitch. *J. Neurophysiol.*
- Chan, W.Y., McKinzie, D.L., Bose, S., Mitchell, S.N., Witkin, J.M., Thompson, R.C., Christopoulos, A., Lazareno, S., Birdsall, N.J.M., Bymaster, F.P., et al. (2008). Allosteric modulation of the muscarinic M4 receptor as an approach to treating schizophrenia. *Proc. Natl. Acad. Sci. U. S. A.*
- Chapple, C.R., and Nilvebrant, L. (2002). Tolterodine: selectivity for the urinary bladder over the eye (as measured by visual accommodation) in healthy volunteers. *Drugs R D.*
- Chapple, C.R., Rechberger, T., Al-Shukri, S., Meffan, P., Everaert, K., Huang, M., and Ridder, A. (2004). Randomized, double-blind placebo-and tolterodine-controlled trial of the once-daily antimuscarinic agent solifenacin in patients with symptomatic overactive bladder. *BJU Int.*
- Chiba, S., Zhang, L., and Lee, J.Y. (2010). Copper-catalyzed synthesis of azaspirocyclohexadienones from  $\alpha$ -azido- N -arylamides under an oxygen atmosphere. *J. Am. Chem. Soc.*
- Cho, A.K., Haslett, W.L., and Jenden, D.J. (1961). The identification of an active metabolite of tremorine. *Biochem. Res. Commun.*
- Choe, S. (2002). Ion channel structure: potassium channel structures. *Nat. Rev. Neurosci.*
- Christopoulos, A. (2002). Allosteric binding sites on cell-surface receptors: Novel targets for drug discovery. *Nat. Rev. Drug Discov.* *1*, 198–210.
- Clapham, D.E., and Neer, E.J. (1997). G protein  $\beta\gamma$  subunits. *Annu. Rev. Pharmacol. Toxicol.* *37*, 167–203.
- Clark, A.L., and Mitchelson, F. (1976). The inhibitory effect of gallamine on muscarinic receptors. *Br. J. Pharmacol.* *58*, 323–331.
- Claudio Viegas-Junior, Eliezer J. Barreiro, and Carlos Alberto Manssour Fraga (2007). Molecular hybridization: a useful tool in the design of new drug prototypes. *Curr. Med. Chem.*
- Conti, P., Dallanoce, C., De Amici, M., De Micheli, C., and Ebert, B. (1997). Synthesis and binding affinity of new muscarinic ligands structurally related to oxotremorine. *Bioorganic Med. Chem. Lett.*
- Cortés, R., Probst, A., Tobler, H.J., and Palacios, J.M. (1986). Muscarinic cholinergic receptor subtypes in the human brain. II. Quantitative autoradiographic studies. *Brain Res.*
- Costa, L.G., Guizzetti, M., Oberdoerster, J., Yagle, K., Costa-Mallen, P., Tita, B., Bordi, F., Vitalone, A., Palmery, M., and Valeri, P. (2001). Modulation of DNA synthesis by muscarinic cholinergic receptors. *Growth Factors* *18*, 227–236.
- Crismon, M.L. (1994). Tacrine: first drug approved for Alzheimer's disease. *Ann. Pharmacother.* *28*, 744–751.
- Cristofaro, I., Spinello, Z., Matera, C., Fiore, M., Conti, L., De Amici, M., Dallanoce, C., and Tata, A.M. (2018). Activation of M2 muscarinic acetylcholine receptors by a hybrid agonist enhances cytotoxic effects in GB7 glioblastoma cancer stem cells. *Neurochem. Int.*
- Cuello, A.C. (2009). Cholinergic pathways in CNS. In *Encyclopedia of Neuroscience*, (Elsevier Ltd), pp. 835–843.
- Dąbrowski, J.M., Pucelik, B., Regiel-Futyra, A., Brindell, M., Mazuryk, O., Kyzioł, A., Stochel, G., Macyk, W., and Arnaut, L.G. (2016). Engineering of relevant photodynamic processes through structural modifications of metallotetrapyrrolic photosensitizers. *Coord. Chem. Rev.*
- Dallanoce, C., Conti, P., De Amici, M., De Micheli, C., Barocelli, E., Chiavarini, M., Ballabeni, V., Bertoni, S., and Impicciatore, M. (1999). Synthesis and functional characterization of novel derivatives related to oxotremorine and oxotremorine-M. *Bioorganic Med. Chem.*

- Davis, A.A., Heilman, C.J., Brady, A.E., Miller, N.R., Fuerstenau-Sharp, M., Hanson, B.J., Lindsley, C.W., Conn, P.J., Lah, J.J., and Levey, A.I. (2010). Differential effects of allosteric M1 muscarinic acetylcholine receptor agonists on receptor activation, arrestin 3 recruitment, and receptor downregulation. *ACS Chem. Neurosci.* *1*, 542–551.
- Day, J.H. (1963). Thermochromism. *Chem. Rev.*
- Decker, M. (2017). Design of hybrid molecules for drug development.
- Dhein, S., Van Koppen, C.J., and Brodde, O.E. (2001). Muscarinic receptors in the mammalian heart. *Pharmacol. Res.*
- Doggrell, S.A., and Evans, S. (2003). Treatment of dementia with neurotransmission modulation. *Expert Opin. Investig. Drugs.*
- Dokić, J., Gothe, M., Wirth, J., Peters, M. V., Schwarz, J., Hecht, S., and Saalfrank, P. (2009). Quantum chemical investigation of thermal cis-to-trans isomerization of azobenzene derivatives: substituent effects, solvent effects, and comparison to experimental data. *J. Phys. Chem. A.*
- Donato, L., Mouro, A., Davenport, C.M., Herbivo, C., Warther, D., Léonard, J., Bolze, F., Nicoud, J.F., Kramer, R.H., Goeldner, M., et al. (2012). Water-soluble, donor-acceptor biphenyl derivatives in the 2-(o-nitrophenyl)propyl series: Highly efficient two-photon uncaging of the neurotransmitter  $\gamma$ -aminobutyric acid at  $\lambda=800$  nm. *Angew. Chemie - Int. Ed.*
- Dong, Q., Svoboda, K., Tiersch, T.R., and Todd Monroe, W. (2007). Photobiological effects of UVA and UVB light in zebrafish embryos: Evidence for a competent photorepair system. *J. Photochem. Photobiol. B Biol.*
- Eglen, R.M. (2005). Muscarinic receptor subtype pharmacology and physiology. *Prog. Med. Chem.*
- Eglen, R.M., and Nahorski, S.R. (2000). The muscarinic M5 receptor: A silent or emerging subtype? *Br. J. Pharmacol.*
- Eglen, R.M., and Watson, N. (1996). Selective muscarinic receptor agonists and antagonists. *Pharmacol. Toxicol.*
- Eglen, R.M., Hegde, S.S., and Watson, N. (1996). Muscarinic receptor subtypes and smooth muscle function. *Pharmacol. Rev.*
- Eglen, R.M., Choppin, A., Dillon, M.P., and Hegde, S. (1999). Muscarinic receptor ligands and their therapeutic potential. *Curr. Opin. Chem. Biol.*
- Eglen, R.M., Choppin, A., and Watson, N. (2001). Therapeutic opportunities from muscarinic receptor research. *Trends Pharmacol. Sci.*
- Ehlert, F.J. (1988). Estimation of the affinities of allosteric ligands using radioligand binding and pharmacological null methods. *Mol. Pharmacol.* *33*.
- Eljabu, F., Dhruval, J., and Yan, H. (2015). Incorporation of cyclic azobenzene into oligodeoxynucleotides for the photo-regulation of DNA hybridization. *Bioorganic Med. Chem. Lett.*
- Ellis, J., Huyler, J., and Brann, M.R. (1991). Allosteric regulation of cloned M1-M5 muscarinic receptor subtypes. *Biochem. Pharmacol.* *42*, 1927–1932.
- Ellis, J.L., Harman, D., Gonzalez, J., Spera, M.L., Liu, R., Shen, T.Y., Wypij, D.M., and Zuo, F. (1999). Development of muscarinic analgesics derived from epibatidine: Role of the M4 receptor subtype. *J. Pharmacol. Exp. Ther.*
- Everett, G.M., Blockus, L.E., and Shepperd, I.M. (1956). Tremor induced by tremorine and its antagonism by anti-Parkinson drugs. *Science* (80- ).

- Faulkner, M.A., and Hilleman, D.E. (2003). Pharmacologic treatment of chronic obstructive pulmonary disease: past, present, and future. *Pharmacotherapy*.
- Felder, C.C. (1995). Muscarinic acetylcholine receptors: signal transduction through multiple effectors. *FASEB J.* 9, 619–625.
- Felder, C.C., Bymaster, F.P., Ward, J., and DeLapp, N. (2000). Therapeutic opportunities for muscarinic receptors in the central nervous system. *J. Med. Chem.*
- Felizola, S.J.A., Maekawa, T., Nakamura, Y., Satoh, F., Ono, Y., Kikuchi, K., Aritomi, S., Ikeda, K., Yoshimura, M., Tojo, K., et al. (2014). Voltage-gated calcium channels in the human adrenal and primary aldosteronism. *J. Steroid Biochem. Mol. Biol.* 144, 410–416.
- Fenno, L., Yizhar, O., and Deisseroth, K. (2011). The development and application of optogenetics. *Annu. Rev. Neurosci.*
- Fino, E., Araya, R., Peterka, D.S., Salierno, M., Etchenique, R., and Yuste, R. (2009). RuBi-Glutamate: two-photon and visible-light photoactivation of neurons and dendritic spines. *Front. Neural Circuits*.
- Fisher, A., Brandeis, R., Haring, R., Bar-Ner, N., Kliger-Spatz, M., Natan, N., Sonogo, H., Marcovitch, I., and Pittel, Z. (2002). Impact of muscarinic agonists for successful therapy of Alzheimer's disease. In *Journal of Neural Transmission, Supplement*, p.
- Fisher, A., Pittel, Z., Haring, R., Bar-Ner, N., Kliger-Spatz, M., Natan, N., Egozi, I., Sonogo, H., Marcovitch, I., and Brandeis, R. (2003). M1 muscarinic agonists can modulate some of the hallmarks in alzheimer's disease: implications in future therapy. *J. Mol. Neurosci.*
- Forman, J., Dietrich, M., and Todd Monroe, W. (2007). Photobiological and thermal effects of photoactivating UVA light doses on cell cultures. *Photochem. Photobiol. Sci.*
- Fortin, D.L., Banghart, M.R., Dunn, T.W., Borges, K., Wagenaar, D.A., Gaudry, Q., Karakossian, M.H., Otis, T.S., Kristan, W.B., Trauner, D., et al. (2008). Photochemical control of endogenous ion channels and cellular excitability. *Nat. Methods*.
- Fortin, D.L., Dunn, T.W., Fedorchak, A., Allen, D., Montpeti, R., Banghart, M.R., Trauner, D., Adelman, J.P., and Kramer, R.H. (2011). Optogenetic photochemical control of designer K<sup>+</sup> channels in mammalian neurons. *J. Neurophysiol.*
- Frank, J.A., Moroni, M., Moshourab, R., Sumser, M., Lewin, G.R., and Trauner, D. (2015). Photoswitchable fatty acids enable optical control of TRPV1. *Nat. Commun.*
- Fraser, C.M., Wang, C.D., Robinson, D.A., Gocayne, J.D., and Venter, J.C. (1989). Site-directed mutagenesis of M1 muscarinic acetylcholine receptors: conserved aspartic acids play important roles in receptor function. *Mol. Pharmacol.* 36.
- Freissmuth, M., Casey, P.J., and Gilman, A.G. (1989). G proteins control diverse pathways of transmembrane signaling. *FASEB J.* 3, 2125–2131.
- Fujiwara, H., and Yonezawa, Y. (1991). Photoelectric response of a black lipid membrane containing an amphiphilic azobenzene derivative. *Nature*.
- García-Amorós, J., and Velasco, D. (2012). Recent advances towards azobenzene-based lightdriven real-time information-transmitting materials. *Beilstein J. Org. Chem.*
- Gautam, D., Heard, T.S., Cui, Y., Miller, G., Bloodworth, L., and Wess, J. (2004). Cholinergic stimulation of salivary secretion studied with M1 and M3 muscarinic receptor single- and double-knockout mice. *Mol. Pharmacol.*
- Gautam, D., Han, S.J., Hamdan, F.F., Jeon, J., Li, B., Li, J.H., Cui, Y., Mears, D., Lu, H., Deng, C., et al. (2006). A critical role for  $\beta$  cell M3 muscarinic acetylcholine receptors in regulating insulin release and blood glucose homeostasis in vivo. *Cell Metab.*

- Gegiou, D., Muszjat, K.A., and Fischer, E. (1968). Temperature dependence of photoisomerization. *J. Am. Chem. Soc.*
- Gomez, J., Shannon, H., Kostenis, E., Felder, C., Zhang, L., Brodtkin, J., Grinberg, A., Sheng, H., and Wess, J. (1999). Pronounced pharmacologic deficits in M2 muscarinic acetylcholine receptor knockout mice. *Proc. Natl. Acad. Sci. U. S. A.*
- Gorostiza, P., and Isacoff, E.Y. (2008). Optical switches for remote and noninvasive control of cell signaling. *Science* (80- ).
- Gregory, K., Sexton, P., and Christopoulos, A. (2007). Allosteric modulation of muscarinic acetylcholine receptors. *Curr. Neuropharmacol.* 5, 157–167.
- Griffiths, J. (1972). II. Photochemistry of azobenzene and its derivatives. *Chem. Soc. Rev.*
- Guo, M.L., Mao, L.M., and Wang, J.Q. (2010). Modulation of M4 muscarinic acetylcholine receptors by interacting proteins. *Neurosci. Bull.*
- Haga, K., Kruse, A.C., Asada, H., Yurugi-Kobayashi, T., Shiroishi, M., Zhang, C., Weis, W.I., Okada, T., Kobilka, B.K., Haga, T., et al. (2012). Structure of the human M2 muscarinic acetylcholine receptor bound to an antagonist. *Nature* 482, 547–551.
- Hall, D.A. (2000). Modeling the functional effects of allosteric modulators at pharmacological receptors: an extension of the two-state model of receptor activation. *Mol. Pharmacol.* 58, 1412–1423.
- Hamaoka, T., McCully, K.K., Quaresima, V., Yamamoto, K., and Chance, B. (2007). Near-infrared spectroscopy/imaging for monitoring muscle oxygenation and oxidative metabolism in healthy and diseased humans. *J. Biomed. Opt.* 12, 062105.
- Hamon, F., Djedaini-Pilard, F., Barbot, F., and Len, C. (2009). Azobenzenes-synthesis and carbohydrate applications. *Tetrahedron.*
- Hancock, J.T. (2010). Cell signalling.
- Hanna, V.S., and Hafez, E.A.A. (2018). Synopsis of arachidonic acid metabolism: a review. *J. Adv. Res.* 11, 23–32.
- Hartley, G.S. (1937). The cis-form of azobenzene. *Nature.*
- Hasselmo, M.E., and Sarter, M. (2011). Modes and models of forebrain cholinergic neuromodulation of cognition. *Neuropsychopharmacology* 36, 52–73.
- Hock, C., Maddalena, A., Raschig, A., Müller-Spahn, F., Eschweiler, G., Hager, K., Heuser, I., Hampel, H., Müller-Thomsen, T., Oertel, W., et al. (2003). Treatment with the selective muscarinic m1 agonist talsaclidine decreases cerebrospinal fluid levels of A $\beta$ 42 in patients with Alzheimer’s disease. *Amyloid.*
- Holschneider, D.P., Guo, Y., Wang, Z., Vidal, M., and Scremin, O.U. (2019). Positive allosteric modulation of cholinergic receptors improves spatial learning after cortical contusion injury in Mice. *J. Neurotrauma.*
- Holzgrabe, U., Bender, W., Botero Cid, H.M., Staudt, M., Pick, R., Pflutschinger, C., Balatková, E., Tränkle, C., and Mohr, K. (2000). Ligands for the common allosteric site of acetylcholine M2-receptors: development and application. In *Pharmaceutica Acta Helveticae*, p.
- Huang, X.P., and Ellis, J. (2007). Mutational disruption of a conserved disulfide bond in muscarinic acetylcholine receptors attenuates positive homotropic cooperativity between multiple allosteric sites and has subtype-dependent effects on the affinities of muscarinic allosteric ligands. *Mol. Pharmacol.*
- Huang, Y., and Thathiah, A. (2015). Regulation of neuronal communication by G protein-coupled receptors. *FEBS Lett.* 589, 1607–1619.

- Huang, C.-L., Feng, S., and Hilgemann, D.W. (1998). Direct activation of inward rectifier potassium channels by PIP2 and its stabilization by G $\beta$  $\gamma$ . *Nature* *391*, 803–806.
- Huang, X.P., Prilla, S., Mohr, K., and Ellis, J. (2005). Critical amino acid residues of the common allosteric site on the M2 muscarinic acetylcholine receptor: more similarities than differences between the structurally divergent agents gallamine and bis(ammonio)alkane-type hexamethylene-bis-[dimethyl-(3-phtha. *Mol. Pharmacol.*
- Hulme, E.C., Kurtenbach, E., and Curtis, C.A.M. (1991). Muscarinic acetylcholine receptors: Structure and function. In *Biochemical Society Transactions*, (Portland Press), pp. 133–138.
- Hvizdos, K.M., and Goa, K.L. (2002). Tiotropium bromide. *Drugs*.
- Irie, M. (2000). Diarylethenes for memories and switches. *Chem. Rev.*
- Ishimoto, T., Akiba, S., Sato, T., and Fujii, T. (1994). Contribution of phospholipases A2 and D to arachidonic acid liberation and prostaglandin D2 formation with increase in intracellular Ca<sup>2+</sup> concentration in rat peritoneal mast cells. *Eur. J. Biochem.* *219*, 401–406.
- Itier, V., and Bertrand, D. (2001). Neuronal nicotinic receptors: from protein structure to function. *FEBS Lett.* *504*, 118–125.
- Iwamoto, E.T., and Marion, L. (1993). Characterization of the antinociception produced by intrathecally administered muscarinic agonists in rats. *J. Pharmacol. Exp. Ther.*
- Iwamoto, M., Majima, Y., Naruse, H., Noguchi, T., and Fuwa, H. (1991). Generation of Maxwell displacement current across an azobenzene monolayer by photoisomerization. *Nature*.
- Izquierdo-Serra, M., Trauner, D., Llobet, A., and Gorostiza, P. (2013). Optical modulation of neurotransmission using calcium photocurrents through the ion channel LiGluR. *Front. Mol. Neurosci.*
- Izquierdo-Serra, M., Gascón-Moya, M., Hirtz, J.J., Pittolo, S., Poskanzer, K.E., Ferrer, È., Alibés, R., Busqué, F., Yuste, R., Hernando, J., et al. (2014). Two-photon neuronal and astrocytic stimulation with azobenzene-based photoswitches. *J. Am. Chem. Soc.*
- Izquierdo-Serra, M., Bautista-Barrufet, A., Trapero, A., Garrido-Charles, A., Diaz-Tahoces, A., Camarero, N., Pittolo, S., Valbuena, S., Perez-Jimenez, A., Gay, M., et al. (2016). Optical control of endogenous receptors and cellular excitability using targeted covalent photoswitches. *Nat. Commun.*
- Izuta, S., Yamaguchi, S., Kosaka, T., and Okamoto, A. (2019). Reversible and photoresponsive immobilization of nonadherent cells by spiropyran-conjugated PEG-lipids. *ACS Appl. Bio Mater.*
- Jakubik, J., Bacakova, L., El-Fakahany, E.E., and Tucek, S. (1995). Subtype selectivity of the positive allosteric action of alcuronium at cloned M1-M5 muscarinic acetylcholine receptors. *J. Pharmacol. Exp. Ther.*
- Jakubík, J., and El-Fakahany, E.E. (2010). Allosteric modulation of muscarinic acetylcholine receptors. *Pharmaceuticals*.
- Jakubík, J., and Tuček, S. (1995). Positive allosteric interactions on cardiac muscarinic receptors: effects of chemical modifications of disulphide and carboxyl groups. *Eur. J. Pharmacol. Mol. Pharmacol.*
- Jiménez, E., Gámez, M.I., Bragado, M.J., and Montiel, M. (2002). Muscarinic activation of mitogen-activated protein kinase in rat thyroid epithelial cells. *Cell. Signal.* *14*, 665–672.
- Jöhren, K., and Höltje, H.D. (2002). A model of the human M2 muscarinic acetylcholine receptor. *J. Comput. Aided. Mol. Des.*
- Jones, S.V.P. (1993). Muscarinic receptor subtypes: modulation of ion channels. *Life Sci.*
- Jung, S.R., Kushmerick, C., Seo, J.B., Koh, D.S., and Hille, B. (2017). Muscarinic receptor regulates

- extracellular signal regulated kinase by two modes of arrestin binding. *Proc. Natl. Acad. Sci. U. S. A.* **114**, E5579–E5588.
- Kale, R.P., Kouzani, A.Z., Walder, K., Berk, M., and Tye, S.J. (2015). Evolution of optogenetic microdevices. *Neurophotonics*.
- Kammer, H., Mayhaus, M., Albrecht, C., Andresen, B., Klaudiny, J., Demiralay, C., and Nitsch, R.M. (2000). Regulation of gene expression by muscarinic acetylcholine receptors: a comprehensive approach for the identification of regulated genes. *Ann. N. Y. Acad. Sci.* **920**, 305–308.
- Kardon, J.R., and Vale, R.D. (2009). Regulators of the cytoplasmic dynein motor. *Nat. Rev. Mol. Cell Biol.*
- Kawano, K., Ishii, T., Minabe, J., Niitsu, T., Nishikata, Y., and Baba, K. (1999). Holographic recording and retrieval of polarized light by use of polyester containing cyanoazobenzene units in the side chain. *Opt. Lett.*
- Kenakin, T. (2007). Allosteric agonist modulators. *J. Recept. Signal Transduct.* **27**, 247–259.
- Klán, P., Šolomek, T., Bochet, C.G., Blanc, A., Givens, R., Rubina, M., Popik, V., Kostikov, A., and Wirz, J. (2013). Photoremovable protecting groups in chemistry and biology: Reaction mechanisms and efficacy. *Chem. Rev.*
- Kleinlogel, S., Terpitz, U., Legrum, B., Gökbuget, D., Boyden, E.S., Bamann, C., Wood, P.G., and Bamberg, E. (2011). A gene-fusion strategy for stoichiometric and co-localized expression of light-gated membrane proteins. *Nat. Methods*.
- Koçer, A., Walko, M., Meijberg, W., and Feringa, B.L. (2005). Chemistry: a light-actuated nanovalve derived from a channel protein. *Science* (80- ).
- Komarov, I. V., Afonin, S., Babii, O., Schober, T., and Ulrich, A.S. (2018). Efficiently photocontrollable or not? Biological activity of photoisomerizable diarylethenes. *Chem. - A Eur. J.*
- Konrad, D.B., Frank, J.A., and Trauner, D. (2016). Synthesis of redshifted azobenzene photoswitches by late-stage functionalization. *Chem. - A Eur. J.*
- Kramer, R.H., Mourot, A., and Adesnik, H. (2013). Optogenetic pharmacology for control of native neuronal signaling proteins. *Nat. Neurosci.*
- Kruse, A.C., Hu, J., Pan, A.C., Arlow, D.H., Rosenbaum, D.M., Rosemond, E., Green, H.F., Liu, T., Chae, P.S., Dror, R.O., et al. (2012). Structure and dynamics of the M3 muscarinic acetylcholine receptor. *Nature*.
- Kruse, A.C., Kobilka, B.K., Gautam, D., Sexton, P.M., Christopoulos, A., and Wess, J. (2014). Muscarinic acetylcholine receptors: novel opportunities for drug development. *Nat. Rev. Drug Discov.*
- Kurtenbach, E., Pedder, E.K., Curtis, C.A.M., and Hulme, E.C. (1990a). The putative disulphide bond in muscarinic receptors. In *Biochemical Society Transactions*, (Portland Press), pp. 442–443.
- Kurtenbach, E., Curtis, C.A.M., Pedder, E.K., Aitken, A., Harris, A.C.M., and Hulme, E.C. (1990b). Muscarinic acetylcholine receptors. Peptide Sequencing identifies residues involved in antagonist binding and disulfide bond formation. *J. Biol. Chem.* **265**.
- Lachmann, D., Lahmy, R., and König, B. (2019). Fulgimides as light-activated tools in biological investigations. *European J. Org. Chem.*
- Langmead, C.J., Fry, V.A.H., Forbes, I.T., Branch, C.L., Christopoulos, A., Wood, M.D., and Herdon, H.J. (2006). Probing the molecular mechanism of interaction between 4-n-butyl-1-[4-(2-methylphenyl)-4-oxo-1-butyl]-piperidine (AC-42) and the muscarinic M1 receptor: Direct pharmacological evidence that AC-42 is an allosteric agonist. *Mol. Pharmacol.* **69**, 236–246.

- Langmead, C.J., Watson, J., and Reavill, C. (2008). Muscarinic acetylcholine receptors as CNS drug targets. *Pharmacol. Ther.*
- Lazareno, S., Gharagzoolo, P., Kuonen, D., Popham, A., and Birdsall, N.J.M. (1998). Subtype-selective positive cooperative interactions between brucine analogues and acetylcholine at muscarinic receptors: radioligand binding studies. *Mol. Pharmacol.* 53, 573–589.
- Lazareno, S., Popham, A., and Birdsall, N.J.M. (2000). Allosteric interactions of staurosporine and other indolocarbazoles with N-[methyl-3H]scopolamine and acetylcholine at muscarinic receptor subtypes: Identification of a second allosteric site. *Mol. Pharmacol.*
- Lazareno, S., Popham, A., and Birdsall, N.J.M. (2002). Analogs of WIN 62,577 define a second allosteric site on muscarinic receptors. *Mol. Pharmacol.*
- Lazareno, S., Doležal, V., Popham, A., and Birdsall, N.J.M. (2004). Thiochrome enhances acetylcholine affinity at muscarinic M4 receptors: receptor subtype selectivity via cooperativity rather than affinity. *Mol. Pharmacol.*
- Lazzaroni, M., Sangaletti, O., Parente, F., Imbimbo, B.P., and Bianchi Porro, G. (1986). Inhibition of food stimulated acid secretion by association of pirenzepine and ranitidine in duodenal ulcer patients. *Int. J. Clin. Pharmacol. Ther. Toxicol.*
- Lednev, I.K., Ye, T.Q., Abbott, L.C., Hester, R.E., and Moore, J.N. (1998). Photoisomerization of a capped azobenzene in solution probed by ultrafast time-resolved electronic absorption spectroscopy. *J. Phys. Chem. A.*
- Lee, S.H., and Dan, Y. (2012). Neuromodulation of brain states. *Neuron.*
- Lefaucheur, J.P. (2009). Treatment of Parkinson's disease by cortical stimulation. *Expert Rev. Neurother.*
- Lefaucheur, J.P., André-Obadia, N., Antal, A., Ayache, S.S., Baeken, C., Benninger, D.H., Cantello, R.M., Cincotta, M., de Carvalho, M., De Ridder, D., et al. (2014). Evidence-based guidelines on the therapeutic use of repetitive transcranial magnetic stimulation (rTMS). *Clin. Neurophysiol.*
- Lehár, J., Krueger, A.S., Avery, W., Heilbut, A.M., Johansen, L.M., Price, E.R., Rickles, R.J., Short, G.F., Staunton, J.E., Jin, X., et al. (2009). Synergistic drug combinations tend to improve therapeutically relevant selectivity. *Nat. Biotechnol.*
- Leirós, C.P., Rosignoli, F., Genaro, A.M., Sales, M.E., Sterin-Borda, L., and Borda, E.S. (2000). Differential activation of nitric oxide synthase through muscarinic acetylcholine receptors in rat salivary glands. *J. Auton. Nerv. Syst.* 79, 99–107.
- Lentes, P., Stadler, E., Röhrich, F., Brahms, A., Gröbner, J., Sönnichsen, F.D., Gescheidt, G., and Herges, R. (2019). Nitrogen bridged diazocenes: photochromes switching within the near-infrared region with high quantum yields in organic solvents and in water. *J. Am. Chem. Soc.*
- Lerch, M.M., Hansen, M.J., van Dam, G.M., Szymanski, W., and Feringa, B.L. (2016). Emerging targets in photopharmacology. *Angew. Chemie - Int. Ed.*
- Levey, A.I., Edmunds, S.M., Koliatsos, V., Wiley, R.G., and Heilman, C.J. (1995). Expression of M1-M4 muscarinic acetylcholine receptor proteins in rat hippocampus and regulation by cholinergic innervation. *J. Neurosci.*
- Lin, S., Kajimura, M., Takeuchi, K., Kodaira, M., Hanai, H., and Kaneko, E. (1997). Expression of muscarinic receptor subtypes in rat gastric smooth muscle: effect of M3 selective antagonist on gastric motility and emptying. *Dig. Dis. Sci.*
- Lohse, M.J. (1995). G-protein-coupled receptor kinases and the heart. *Trends Cardiovasc. Med.*
- Lohse, M.J., and Hoffmann, C. (2014). Arrestin interactions with G protein-coupled receptors. *Handb.*

Exp. Pharmacol.

Longo, F.M., and Massa, S.M. (2004). Neuroprotective Strategies in Alzheimer's Disease. *NeuroRx*.

Lu, B., Kwan, K., Levine, Y.A., Olofsson, P.S., Yang, H., Li, J., Joshi, S., Wang, H., Andersson, U., Chavan, S.S., et al. (2014).  $\alpha 7$  nicotinic acetylcholine receptor signaling inhibits inflammasome activation by preventing mitochondrial DNA release. *Mol. Med.* 20, 350–358.

Ludwig, M.G., and Seuwen, K. (2002). Characterization of the human adenylyl cyclase gene family: cDNA, gene structure, and tissue distribution of the nine isoforms. *J. Recept. Signal Transduct.* 22, 79–110.

Maeda, S., Qu, Q., Robertson, M.J., Skiniotis, G., and Kobilka, B.K. (2019). Structures of the M1 and M2 muscarinic acetylcholine receptor/G-protein complexes. *Science* (80-. ). 364, 552–557.

Magnon, C., Hall, S.J., Lin, J., Xue, X., Gerber, L., Freedland, S.J., and Frenette, P.S. (2013). Autonomic nerve development contributes to prostate cancer progression. *Science* (80-. ).

Marder, S.R., Kippelen, B., Jen, A.K.Y., and Peyghambarian, N. (1997). Design and synthesis of chromophores and polymers for electro-optic and photorefractive applications. *Nature*.

Marsh, W. (2007). Tricyclic antidepressants. In *XPharm: The Comprehensive Pharmacology Reference*, (Elsevier Inc.), pp. 1–3.

Matera, C., Flammini, L., Quadri, M., Vivo, V., Ballabeni, V., Holzgrabe, U., Mohr, K., De Amici, M., Barocelli, E., Bertoni, S., et al. (2014). Bis(ammonio)alkane-type agonists of muscarinic acetylcholine receptors: synthesis, in vitro functional characterization, and in vivo evaluation of their analgesic activity. *Eur. J. Med. Chem.*

Matera, C., Gomila, A.M.J., Camarero, N., Libergoli, M., Soler, C., and Gorostiza, P. (2018). Photoswitchable antimetabolite for targeted photoactivated chemotherapy. *J. Am. Chem. Soc.*

Matera, C., Bono, F., Pelucchi, S., Collo, G., Bontempi, L., Gotti, C., Zoli, M., De Amici, M., Missale, C., Fiorentini, C., et al. (2019). The novel hybrid agonist HyNDA-1 targets the D3R-nAChR heteromeric complex in dopaminergic neurons. *Biochem. Pharmacol.*

Matsui, H., Lazareno, S., and Birdsall, N.J.M. (1995). Probing of the location of the allosteric site on M1 muscarinic receptors by site-directed mutagenesis. *Mol. Pharmacol.*

Matsui, M., Motomura, D., Karasawa, H., Fujikawa, T., Jiang, J., Komiya, Y., Takahashi, S.I., and Taketo, M.M. (2000). Multiple functional defects in peripheral autonomic organs in mice lacking muscarinic acetylcholine receptor gene for the M3 subtype. *Proc. Natl. Acad. Sci. U. S. A.*

Mattingly, R.R., Sorisky, A., Brann, M.R., and Macara, I.G. (1994). Muscarinic receptors transform NIH 3T3 cells through a Ras-dependent signalling pathway inhibited by the Ras-GTPase-activating protein SH3 domain. *Mol. Cell. Biol.* 14, 7943–7952.

May, L.T., Lin, Y., Sexton, P.M., and Christopoulos, A. (2005). Regulation of M2 muscarinic acetylcholine receptor expression and signaling by prolonged exposure to allosteric modulators. *J. Pharmacol. Exp. Ther.* 312, 382–390.

Meerholz, K., Volodin, B.L., Sandalphon, Kippelen, B., and Peyghambarian, N. (1994). A photorefractive polymer with high optical gain and diffraction efficiency near 100%. *Nature*.

Merino, E. (2011). Synthesis of azobenzenes: The coloured pieces of molecular materials. *Chem. Soc. Rev.*

Messerer, R., Dallanoce, C., Matera, C., Wehle, S., Flammini, L., Chirinda, B., Bock, A., Irmen, M., Tränkle, C., Barocelli, E., et al. (2017). Novel bipharmacophoric inhibitors of the cholinesterases with affinity to the muscarinic receptors M1 and M2. *Medchemcomm.*

- De Min, A., Matera, C., Bock, A., Holze, J., Kloeckner, J., Muth, M., Traenkle, C., De Amici, M., Kenakin, T., Holzgrabe, U., et al. (2017). A new molecular mechanism to engineer protean agonism at a G protein-coupled receptor. *Mol. Pharmacol.*
- Miyamae, K., Yoshida, M., Murakami, S., Iwashita, H., Ohtani, M., Masunaga, K., and Ueda, S. (2003). Pharmacological effects of darifenacin on human isolated urinary bladder. *Pharmacology.*
- Mohr, K., Tränkle, C., Kostenis, E., Barocelli, E., De Amici, M., and Holzgrabe, U. (2010). Rational design of dualsteric GPCR ligands: quests and promise. *Br. J. Pharmacol.*
- Momotake, A., and Arai, T. (2003). A new class of azobenzene chelators for Mg<sup>2+</sup> and Ca<sup>2+</sup> in buffer at physiological pH. *Tetrahedron Lett.*
- Mosser, V.A., Jones, K.T., Hoffman, K.M., McCarty, N.A., and Jackson, D.A. (2008). Differential role of beta-arrestin ubiquitination in agonist-promoted down-regulation of M1 vs M2 muscarinic acetylcholine receptors. *J. Mol. Signal.* 3, 20.
- Mouro, A., Kienzler, M.A., Banghart, M.R., Fehrentz, T., Huber, F.M.E., Stein, M., Kramer, R.H., and Trauner, D. (2011). Tuning photochromic ion channel blockers. *ACS Chem. Neurosci.*
- Mouro, A., Fehrentz, T., Le Feuvre, Y., Smith, C.M., Herold, C., Dalkara, D., Nagy, F., Trauner, D., and Kramer, R.H. (2012). Rapid optical control of nociception with an ion-channel photoswitch. *Nat. Methods.*
- Nagel, G., Szellas, T., Huhn, W., Kateriya, S., Adeishvili, N., Berthold, P., Ollig, D., Hegemann, P., and Bamberg, E. (2003). Channelrhodopsin-2, a directly light-gated cation-selective membrane channel. *Proc. Natl. Acad. Sci. U. S. A.*
- Nathaniel, T.I., Umesiri, F.E., and Olajuyigbe, F. (2008). Role of M1 receptor in the locomotion behavior of the African mole-rat (*Cryptomys* sp). *J. Integr. Neurosci.*
- Nathanson, N.M. (2000). A multiplicity of muscarinic mechanisms: Enough signaling pathways to take your breath away. *Proc. Natl. Acad. Sci. U. S. A.* 97, 6245–6247.
- Nedoma, J., Dorofeeva, N.A., Tuček, S., Shelkovnikov, S.A., and Danilov, A.F. (1985). Interaction of the neuromuscular blocking drugs alcuronium, decamethonium, gallamine, pancuronium, ritebronium, tercuronium and d-tubocurarine with muscarinic acetylcholine receptors in the heart and ileum. *Naunyn. Schmiedebergs. Arch. Pharmacol.* 329, 176–181.
- Nedoma, J., Tuček, S., Danilov, A.F., and Shelkovnikov, S.A. (1986). Stabilization of antagonist binding to cardiac muscarinic acetylcholine receptors by gallamine and other neuromuscular blocking drugs. *J. Pharmacol. Exp. Ther.*
- Neher, E., Marty, A., Fukuda, K., Kubo, T., and Numa, S. (1988). Intracellular calcium release mediated by two muscarinic receptor subtypes. *FEBS Lett.* 240, 88–94.
- Nevola, L., Martín-Quirós, A., Eckelt, K., Camarero, N., Tosi, S., Llobet, A., Giral, E., and Gorostiza, P. (2013). Light-Regulated stapled peptides to inhibit protein-protein interactions involved in clathrin-mediated endocytosis. *Angew. Chemie Int. Ed.* 52, 7704–7708.
- Nuber, S., Zabel, U., Lorenz, K., Nuber, A., Milligan, G., Tobin, A.B., Lohse, M.J., and Hoffmann, C. (2016).  $\beta$ -Arrestin biosensors reveal a rapid, receptor-dependent activation/deactivation cycle. *Nature.*
- Ohtani, O., Furukawa, T., Sasai, R., Hayashi, E., Shichi, T., Yui, T., and Takagi, K. (2004). Effect of fluorinated ammonium counterions upon the reversibility in E-Z photoisomerization of azobenzene ion pair films. *J. Mater. Chem.*
- Oki, T., Takagi, Y., Inagaki, S., Taketo, M.M., Manabe, T., Matsui, M., and Yamada, S. (2005). Quantitative analysis of binding parameters of [<sup>3</sup>H]-methylscopolamine in central nervous system

- of muscarinic acetylcholine receptor knockout mice. *Mol. Brain Res.*
- Onali, P., and Olanas, M.C. (2002). Muscarinic M4 receptor inhibition of dopamine D1-like receptor signalling in rat nucleus accumbens. *Eur. J. Pharmacol.*
- Ortner, N.J., and Striessnig, J. (2016). L-type calcium channels as drug targets in CNS disorders. *Channels* 10, 7–13.
- Paulus, W. (2014). Transcranial brain stimulation: potential and limitations. *E-Neuroforum* 5, 29–36.
- Pawlicki, M., Collins, H.A., Denning, R.G., and Anderson, H.L. (2009). Two-photon absorption and the design of two-photon dyes. *Angew. Chemie - Int. Ed.*
- Pedretti, R.F.E., Prete, G., Foreman, R.D., Adamson, P.B., and Vanoli, E. (2003). Autonomic modulation during acute myocardial ischemia by low-dose pirenzepine in conscious dogs with a healed myocardial infarction: A comparison with  $\beta$ -adrenergic blockade. *J. Cardiovasc. Pharmacol.*
- Pemberton, K.E., and Jones, S.V.P. (1997). Inhibition of the L-type calcium channel by the five muscarinic receptors (m1-m5) expressed in NIH 3T3 cells. *Pflugers Arch. Eur. J. Physiol.* 433, 505–514.
- Pereira, L.S., Müller, V.T., da Mota Gomes, M., Rotenberg, A., and Fregni, F. (2016). Safety of repetitive transcranial magnetic stimulation in patients with epilepsy: A systematic review. *Epilepsy Behav.*
- Pianca, N., Zaglia, T., and Mongillo, M. (2017). Will cardiac optogenetics find the way through the obscure angles of heart physiology? *Biochem. Biophys. Res. Commun.*
- Pinto, L., Goard, M.J., Estandian, D., Xu, M., Kwan, A.C., Lee, S.H., Harrison, T.C., Feng, G., and Dan, Y. (2013). Fast modulation of visual perception by basal forebrain cholinergic neurons. *Nat. Neurosci.*
- Pittolo, S., Gómez-Santacana, X., Eckelt, K., Rovira, X., Dalton, J., Goudet, C., Pin, J.P., Llobet, A., Giraldo, J., Llebaria, A., et al. (2014). An allosteric modulator to control endogenous G protein-coupled receptors with light. *Nat. Chem. Biol.*
- Pittolo, S., Lee, H., Lladó, A., Tosi, S., Bosch, M., Bardia, L., Gómez-Santacana, X., Llebaria, A., Soriano, E., Colombelli, J., et al. (2019). Reversible silencing of endogenous receptors in intact brain tissue using 2-photon pharmacology. *Proc. Natl. Acad. Sci. U. S. A.*
- Posor, Y., Eichhorn-Grünig, M., and Haucke, V. (2015). Phosphoinositides in endocytosis. *Biochim. Biophys. Acta - Mol. Cell Biol. Lipids* 1851, 794–804.
- Post, M.J., Te Biesebeek, J.D., Doods, H.N., Wemer, J., Van Rooij, H.H., and Porsius, A.J. (1991). Functional characterization of the muscarinic receptor in rat lungs. *Eur. J. Pharmacol.*
- Pozhidaeva, N., Cormier, M.E., Chaudhari, A., and Woolley, G.A. (2004). Reversible photocontrol of peptide helix content: adjusting thermal stability of the cis state. In *Bioconjugate Chemistry*, p.
- Prado, M.A.M., Marchot, P., and Silman, I. (2017). Preface: Cholinergic Mechanisms. *J. Neurochem.* 142, 3–6.
- Preiksaitis, H.G., Krysiak, P.S., Chrones, T., Rajgopal, V., and Laurier, L.G. (2000). Pharmacological and molecular characterization of muscarinic receptor subtypes in human esophageal smooth muscle. *J. Pharmacol. Exp. Ther.*
- Prilla, S., Schrobang, J., Ellis, J., Höltje, H.D., and Mohr, K. (2006). Allosteric interactions with muscarinic acetylcholine receptors: Complex role of the conserved tryptophan M2422Trp in a critical cluster of amino acids for baseline affinity, subtype selectivity, and cooperativity. *Mol. Pharmacol.*
- Proška, J., and Tuček, S. (1994). Mechanisms of steric and cooperative actions of alcuronium on cardiac muscarinic acetylcholine receptors. *Mol. Pharmacol.*
- Purves, D., Augustine, G.J., Fitzpatrick, D., Hall, W.C., Lamantia, A.-S., McNamara, J.O., and Williams,

- S.M. (2011). *Neuroscience* (Sinauer Associates, Inc.).
- Qian, N.X., Russell, M., and Johnson, G.L. (1995). Acetylcholine muscarinic receptor regulation of the Ras/Raf/Map kinase pathway. *Life Sci.* *56*, 945–949.
- Ramaswamy, S., Colangelo, C., and Markram, H. (2018). Data-driven modeling of cholinergic modulation of neural microcircuits: bridging neurons, synapses and network activity. *Front. Neural Circuits*.
- Rapp, T.L., and Dmochowski, I.J. (2019). Ruthenium-cross-linked hydrogels for rapid, visible-light protein release. In *Methods in Enzymology*, p.
- Rasmussen, T., Fink-Jensen, A., Sauerberg, P., Swedberg, M.D.B., Thomsen, C., Sheardown, M.J., Jeppesen, L., Calligaro, D.O., Delapp, N.W., Whitesitt, C., et al. (2001). The muscarinic receptor agonist BuTAC, a novel potential antipsychotic, does not impair learning and memory in mouse passive avoidance. *Schizophr. Res.*
- Rau, H. (2002). Photoisomerization of azobenzenes. In *Photoreactive Organic Thin Films*, p.
- Raymo, F.M. (2003). Molecular devices and machines-A journey into the nanoworld. *ChemPhysChem*.
- Renuka, T.R., Robinson, R., and Paulose, C.S. (2006). Increased insulin secretion by muscarinic M1 and M3 receptor function from rat pancreatic islets in vitro. *Neurochem. Res.*
- Ricart-Ortega, M., Font, J., and Llebaria, A. (2019). GPCR photopharmacology. *Mol. Cell. Endocrinol.*
- Rosignoli, F., and Pérez Leirós, C. (2002). Activation of nitric oxide synthase through muscarinic receptors in rat parotid gland. *Eur. J. Pharmacol.* *439*, 27–33.
- Rowe, W.B., O'Donnell, J.P., Pearson, D., Rose, G.M., Meaney, M.J., and Quirion, R. (2003). Long-term effects of BIBN-99, a selective muscarinic M2 receptor antagonist, on improving spatial memory performance in aged cognitively impaired rats. *Behav. Brain Res.*
- Ruiz-Mejias, M., Ciria-Suarez, L., Mattia, M., and Sanchez-Vives, M. V. (2011). Slow and fast rhythms generated in the cerebral cortex of the anesthetized mouse. *J. Neurophysiol.*
- Rullo, A., Reiner, A., Reiter, A., Trauner, D., Isacoff, E.Y., and Woolley, G.A. (2014). Long wavelength optical control of glutamate receptor ion channels using a tetra-ortho-substituted azobenzene derivative. *Chem. Commun.*
- Rustler, K., Gomila, A., Maleeva, G., Gorostiza, P., Bregestovski, P., and König, B. (2020). Optical control of GABAA receptors with a fulgimide-based potentiator. *Chem. – A Eur. J.*
- Sadana, R., and Dessauer, C.W. (2009). Physiological roles for G protein-regulated adenylyl cyclase isoforms: insights from knockout and overexpression studies. *Neurosignals* *17*, 5–22.
- Sadovski, O., Beharry, A.A., Zhang, F., and Woolley, G.A. (2009). Spectral tuning of azobenzene photoswitches for biological applications. *Angew. Chemie - Int. Ed.*
- Samanta, S., Qin, C., Lough, A.J., and Woolley, G.A. (2012). Bidirectional photocontrol of peptide conformation with a bridged azobenzene derivative. *Angew. Chemie - Int. Ed.*
- Samanta, S., Beharry, A.A., Sadovski, O., McCormick, T.M., Babalhavaeji, A., Tropepe, V., and Woolley, G.A. (2013). Photoswitching azo compounds in vivo with red light. *J. Am. Chem. Soc.*
- Sanchez-Vives, M. V., and Mattia, M. (2014). Slow wave activity as the default mode of the cerebral cortex. *Arch. Ital. Biol.*
- Sandoz, G., Levitz, J., Kramer, R.H., and Isacoff, E.Y. (2012). Optical control of endogenous proteins with a photoswitchable conditional subunit reveals a role for TREK1 in GABAB signaling. *Neuron*.

- De Sarno, P., Shestopal, S.A., Zmijewska, A.A., and Jope, R.S. (2005). Anti-apoptotic effects of muscarinic receptor activation are mediated by Rho kinase. *Brain Res.* *1041*, 112–115.
- Scarr, E. (2012). Muscarinic receptors: their roles in disorders of the central nervous system and potential as therapeutic targets. *CNS Neurosci. Ther.*
- Schild, L. (2010). The epithelial sodium channel and the control of sodium balance. *Biochim. Biophys. Acta - Mol. Basis Dis.*
- Schmidt, R.F., and Thews, G. (1989). *Human physiology - Autonomic nervous system.*
- Schönberger, M., and Trauner, D. (2014). A photochromic agonist for  $\mu$ -opioid receptors. *Angew. Chemie - Int. Ed.*
- Schönberger, M., Damijonaitis, A., Zhang, Z., Nagel, D., and Trauner, D. (2014). Development of a new photochromic ion channel blocker via azologization of fomocaine. *ACS Chem. Neurosci.*
- Schönborn, J.B., and Hartke, B. (2014). Photochemical dynamics of E-methylfurylfulgide - Kinematic effects on photorelaxation dynamics of furylfulgides. *Phys. Chem. Chem. Phys.*
- Schrage, R., Seemann, W.K., Klöckner, J., Dallanoce, C., Racké, K., Kostenis, E., De Amici, M., Holzgrabe, U., and Mohr, K. (2013). Agonists with supraphysiological efficacy at the muscarinic M2 ACh receptor. *Br. J. Pharmacol.*
- Schwartz, T.W., and Holst, B. (2006). Allosteric modulation and other types of allostery in dimeric 7TM receptors. *J. Recept. Signal Transduct.* *26*, 107–128.
- Sekkat, Z., and Wolfgang, K. (2002). Photoreactive organic thin films.
- Shirey, J.K., Brady, A.E., Jones, P.J., Davis, A.A., Bridges, T.M., Kennedy, J.P., Jadhav, S.B., Menon, U.N., Xiang, Z., Watson, M.L., et al. (2009). A selective allosteric potentiator of the M1 muscarinic acetylcholine receptor increases activity of medial prefrontal cortical neurons and restores impairments in reversal learning. *J. Neurosci.*
- Siewertsen, R., Neumann, H., Buchheim-Stehn, B., Herges, R., Näther, C., Renth, F., and Temps, F. (2009). Highly efficient reversible Z-E photoisomerization of a bridged azobenzene with visible light through resolved S1( $n\pi^*$ ) absorption bands. *J. Am. Chem. Soc.*
- Siewertsen, R., Schönborn, J.B., Hartke, B., Renth, F., and Temps, F. (2011). Superior Z  $\rightarrow$  e and e  $\rightarrow$  Z photoswitching dynamics of dihydrodibenzodiazocine, a bridged azobenzene, by S1( $n\pi^*$ ) excitation at  $\lambda = 387$  and 490 nm. *Phys. Chem. Chem. Phys.*
- Song, P., Sekhon, H.S., Lu, A., Arredondo, J., Sauer, D., Gravett, C., Mark, G.P., Grando, S.A., and Spindel, E.R. (2007). M3 muscarinic receptor antagonists inhibit small cell lung carcinoma growth and mitogen-activated protein kinase phosphorylation induced by acetylcholine secretion. *Cancer Res.* *67*, 3936–3944.
- Stein, I.S., and Hell, J.W. (2010). CaMKII hinders down on the muscarinic M4 receptor to help curb cocaine-induced hyperlocomotion. *EMBO J.*
- Stein, M., Middendorp, S.J., Carta, V., Pejo, E., Raines, D.E., Forman, S.A., Sigel, E., and Trauner, D. (2012). Azo-propofols: photochromic potentiators of GABAA receptors. *Angew. Chemie - Int. Ed.*
- Stengel, P.W., Yamada, M., Wess, J., and Cohen, M.L. (2002). M3-receptor knockout mice: Muscarinic receptor function in atria, stomach fundus, urinary bladder, and trachea. *Am. J. Physiol. - Regul. Integr. Comp. Physiol.*
- Stockton, J.M., Birdsall, N.J., Burgen, A.S., and Hulme, E.C. (1983). Modification of the binding properties of muscarinic receptors by gallamine. *Mol. Pharmacol.* *23*.
- Strader, C.D., Sigal, I.S., Register, R.B., Candelore, M.R., Rands, E., and Dixon, R.A. (1987). Identification

- of residues required for ligand binding to the  $\beta$ -adrenergic receptor. *Proc. Natl. Acad. Sci. U. S. A.* *84*, 4384–4388.
- Strader, C.D., Gaffney, T., Sugg, E.E., Candelore, M.R., Keys, R., Patchett, A.A., and Dixon, R.A. (1991). Allele-specific activation of genetically engineered receptors. *J. Biol. Chem.* *266*.
- Striessnig, J., Ortner, N., and Pinggera, A. (2015). Pharmacology of L-type calcium channels: novel drugs for old targets? *Curr. Mol. Pharmacol.* *8*, 110–122.
- Subudhi, B., and Sahoo, S. (2016). Updates in drug development strategies against peptic ulcer. *J. Gastrointest. Dig. Syst.*
- Svoboda, K., and Yasuda, R. (2006). Principles of two-photon excitation microscopy and its applications to neuroscience. *Neuron*.
- Szymański, W., Beierle, J.M., Kistemaker, H.A.V., Velema, W.A., and Feringa, B.L. (2013). Reversible photocontrol of biological systems by the incorporation of molecular photoswitches. *Chem. Rev.*
- Tamai, N., and Miyasaka, H. (2000). Ultrafast dynamics of photochromic systems. *Chem. Rev.*
- Tang, Z., Johal, M.S., Scudder, P., Caculitan, N., Magyar, R.J., Tretiak, S., and Wang, H.L. (2007). Study of the non-covalent interactions in Langmuir-Blodgett films: An interplay between  $\pi$ - $\pi$  and dipole-dipole interactions. *Thin Solid Films*.
- Tansey, E.M. (2006). Henry Dale and the discovery of acetylcholine. *Comptes Rendus - Biol.* *329*, 419–425.
- Tian, H., and Wang, S. (2007). Photochromic bisthiénylene as multi-function switches. *Chem. Commun.*
- Tobin, A.B., and Budd, D.C. (2003). The anti-apoptotic response of the Gq/11-coupled muscarinic receptor family. In *Biochemical Society Transactions*, (Portland Press Ltd), pp. 1182–1185.
- Tränkle, C., Weyand, O., Voigtländer, U., Mynett, A., Lazareno, S., Birdsall, N.J.M., and Mohr, K. (2003). Interactions of orthosteric and allosteric ligands with [3H]dimethyl-W84 at the common allosteric site of muscarinic M2 receptors. *Mol. Pharmacol.*
- Tränkle, C., Dittmann, A., Schulz, U., Weyand, O., Buller, S., Jöhren, K., Heller, E., Birdsall, N.J.M., Holzgrabe, U., Ellis, J., et al. (2005). Atypical muscarinic allosteric modulation: cooperativity between modulators and their atypical binding topology in muscarinic M2 and M2/M5 chimeric receptors. *Mol. Pharmacol.*
- Tsutsumi, N., Yoshizaki, S., Sakai, W., and Kiyotsukuri, T. (1995). Nonlinear optical polymers. 1. Novel network polyurethane with azobenzene dye in the main frame. *Macromolecules*.
- Tyagi, S., Tyagi, P., Van-le, S., Yoshimura, N., Chancellor, M.B., and de Miguel, F. (2006). Qualitative and quantitative expression profile of muscarinic receptors in human urothelium and detrusor. *J. Urol.*
- Urban, J.D., Clarke, W.P., Von Zastrow, M., Nichols, D.E., Kobilka, B., Weinstein, H., Javitch, J.A., Roth, B.L., Christopoulos, A., Sexton, P.M., et al. (2007). Functional selectivity and classical concepts of quantitative pharmacology. *J. Pharmacol. Exp. Ther.* *320*, 1–13.
- Velema, W.A., Van Der Berg, J.P., Hansen, M.J., Szymanski, W., Driessen, A.J.M., and Feringa, B.L. (2013). Optical control of antibacterial activity. *Nat. Chem.*
- Velema, W.A., Szymanski, W., and Feringa, B.L. (2014). Photopharmacology: beyond proof of principle. *J. Am. Chem. Soc.* *136*, 2178–2191.
- Verde, E.M.R., Zayat, L., Etchenique, R., and Yuste, R. (2008). Photorelease of GABA with visible light using an inorganic caging group. *Front. Neural Circuits*.

- Vilaró, M.T., Palacios, J.M., and Mengod, G. (1994). Multiplicity of muscarinic autoreceptor subtypes? Comparison of the distribution of cholinergic cells and cells containing mRNA for five subtypes of muscarinic receptors in the rat brain. *Mol. Brain Res.*
- Voigtländer, U., Jöhren, K., Mohr, M., Raasch, A., Tränkle, C., Buller, S., Ellis, J., Höltje, H.D., and Mohr, K. (2003). Allosteric site on muscarinic acetylcholine receptors: identification of two amino acids in the muscarinic M2 receptor that account entirely for the M2/M5 subtype selectivities of some structurally diverse allosteric ligands in N-methylscopolamine-occupie. *Mol. Pharmacol.*
- Volgraf, M., Gorostiza, P., Numano, R., Kramer, R.H., Isacoff, E.Y., and Trauner, D. (2006). Allosteric control of an ionotropic glutamate receptor with an optical switch. *Nat. Chem. Biol.*
- Volgraf, M., Banghart, M., and Trauner, D. (2011). Switchable proteins and channels. In *Molecular Switches, Second Edition*, p.
- Wagner, G., Arion, V.B., Brecker, L., Krantz, C., Mieusset, J.L., and Brinker, U.H. (2009). Controllable selective functionalization of a cavitand via solid state photolysis of an encapsulated phenyl azide. *Org. Lett.*
- Wakamori, M., Yamazaki, K., Matsunodaira, H., Teramoto, T., Tanaka, I., Niidome, T., Sawada, K., Nishizawa, Y., Sekiguchi, N., Mori, E., et al. (1998). Single tottering mutations responsible for the neuropathic phenotype of the P-type calcium channel. *J. Biol. Chem.* 273, 34857–34867.
- Wang, H., Han, H., Zhang, L., Shi, H., Schram, G., Nattel, S., and Wang, Z. (2001). Expression of multiple subtypes of muscarinic receptors and cellular distribution in the human heart. *Mol. Pharmacol.*
- Waxenbaum, J.A., Reddy, V., and Varacallo, M. (2019). *Anatomy, autonomic nervous system* (StatPearls Publishing).
- Weber, M., Motin, L., Gaul, S., Beker, F., Fink, R.H.A., and Adams, D.J. (2005). Intravenous anaesthetics inhibit nicotinic acetylcholine receptor-mediated currents and Ca<sup>2+</sup> transients in rat intracardiac ganglion neurons. *Br. J. Pharmacol.* 144, 98–107.
- Wegener, M., Hansen, M.J., Driessen, A.J.M., Szymanski, W., and Feringa, B.L. (2017). Photocontrol of antibacterial activity: shifting from UV to red light activation. *J. Am. Chem. Soc.*
- Wegner, H.A. (2012). *Molecular switches. Second edition.* Edited by Ben L. Feringa and Wesley R. Browne. *Angew. Chemie Int. Ed.*
- Wein, A.J. (2005). Muscarinic acetylcholine receptor knockout mice: novel phenotypes and clinical implications. *J. Urol.*
- Weiner, D.M., Levey, A.I., and Brann, M.R. (1990). Expression of muscarinic acetylcholine and dopamine receptor mRNAs in rat basal ganglia. *Proc. Natl. Acad. Sci. U. S. A.*
- Weiße, T., Hildebrand, G., Schade, R., and Liefelth, K. (2009). Two-photon polymerization for microfabrication of three-dimensional scaffolds for tissue engineering application. *Eng. Life Sci.*
- Wess, J. (1993). Mutational analysis of muscarinic acetylcholine receptors: Structural basis of ligand/receptor/G protein interactions. *Life Sci.* 53, 1447–1463.
- Wess, J., Gdula, D., and Brann, M.R. (1991). Site-directed mutagenesis of the M3 muscarinic receptor: identification of a series of threonine and tyrosine residues involved in agonist but not antagonist binding. *EMBO J.* 10, 3729–3734.
- Wess, J., Maggio, R., Palmer, J.R., and Vogel, Z. (1992). Role of conserved threonine and tyrosine residues in acetylcholine binding and muscarinic receptor activation. A study with M3 muscarinic receptor point mutants. *J. Biol. Chem.* 267.
- Wess, J., Blin, N., Mutschler, E., and Blüml, K. (1995). Muscarinic acetylcholine receptors: structural basis of ligand binding and G protein coupling. *Life Sci.* 56, 915–922.

- Weston-Green, K., Huang, X.F., Lian, J., and Deng, C. (2012). Effects of olanzapine on muscarinic M3 receptor binding density in the brain relates to weight gain, plasma insulin and metabolic hormone levels. *Eur. Neuropsychopharmacol.*
- Wietek, J., Wiegert, J.S., Adeishvili, N., Schneider, F., Watanabe, H., Tsunoda, S.P., Vogt, A., Elstner, M., Oertner, T.G., and Hegemann, P. (2014). Conversion of channelrhodopsin into a light-gated chloride channel. *Science* (80- ).
- Xiang, Z., Thompson, A.D., Jones, C.K., Lindsley, C.W., and Conn, P.J. (2012). Roles of the M1 muscarinic acetylcholine receptor subtype in the regulation of basal ganglia function and implications for the treatment of Parkinson's disease. *J. Pharmacol. Exp. Ther.*
- Yamada, M., Basile, A.S., Fedorova, I., Zhang, W., Duttaroy, A., Cui, Y., Lamping, K.G., Faraci, F.M., Deng, C.X., and Wess, J. (2003). Novel insights into M5 muscarinic acetylcholine receptor function by the use of gene targeting technology. In *Life Sciences*, p.
- Yasuda, R.P., Ciesla, W., Flores, L.R., Wall, S.J., Li, M., Satkus, S.A., Weisstein, J.S., Spagnola, B. V., and Wolfe, B.B. (1993). Development of antisera selective for M4 and M5 muscarinic cholinergic receptors: distribution of M4 and M5 receptors in rat brain. *Mol. Pharmacol.*
- Yoshida, M., Muneyuki, E., and Hisabori, T. (2001). ATP synthase - A marvellous rotary engine of the cell. *Nat. Rev. Mol. Cell Biol.*
- Yu, L., Zhou, L., Cao, G., Po, S.S., Huang, B., Zhou, X., Wang, M., Yuan, S., Wang, Z., Wang, S., et al. (2017). Optogenetic modulation of cardiac sympathetic nerve activity to prevent ventricular arrhythmias. *J. Am. Coll. Cardiol.*
- Zacharias, P.S., Ameerunisha, S., and Korupoju, S.R. (1998). Photoinduced fluorescence changes on E-Z isomerisation in azobenzene derivatives. *J. Chem. Soc. Perkin Trans. 2.*
- Zemelman, B. V., Nesnas, N., Lee, G.A., and Miesenböck, G. (2003). Photochemical gating of heterologous ion channels: remote control over genetically designated populations of neurons. *Proc. Natl. Acad. Sci. U. S. A.*
- Zhang, F., Wang, L.P., Boyden, E.S., and Deisseroth, K. (2006). Channelrhodopsin-2 and optical control of excitable cells. *Nat. Methods.*
- Zhang, G., Liu, Y., Ruoho, A.E., and Hurley, J.H. (1997). Structure of the adenylyl cyclase catalytic core. *Nature* 386, 247–253.
- Zhang, X.Y., Jin, S., Ming, Y.F., Liang, Y.C., Yu, L.H., Fan, M.G., Luo, J., Zuo, Z.H., and Yao, S.D. (1994). Substituent effect on photochromism of indolinospirooxazines. *J. Photochem. Photobiol. A Chem.* 80, 221–225.
- Zhang, Y., Yue, J., Ai, M., Ji, Z., Liu, Z., Cao, X., and Li, L. (2014). Channelrhodopsin-2-expressed dorsal root ganglion neurons activates calcium channel currents and increases action potential in spinal cord. *Spine (Phila. Pa. 1976).*
- Zipfel, W.R., Williams, R.M., and Webb, W.W. (2003). Nonlinear magic: multiphoton microscopy in the biosciences. *Nat. Biotechnol.*
- Zlotos, D.P., Tränkle, C., Abdelrahman, A., Gündisch, D., Radacki, K., Braunschweig, H., and Mohr, K. (2006). 6H,13H-Pyrazino[1,2-a;4,5-a']diindole analogs: probing the pharmacophore for allosteric ligands of muscarinic M2 receptors. *Bioorganic Med. Chem. Lett.*

**SUMMARY**

in Spanish



## CAPÍTULO I

### INTRODUCCIÓN

La mayoría de los tratamientos médicos modernos se basan en la capacidad que los medicamentos farmacológicos tienen de interactuar con una diana molecular (por ejemplo, con los receptores) en el cuerpo humano para causar una respuesta fisiológica. Estas dianas se expresan en todo el cuerpo humano, en tejidos sanos y enfermos. Esto perjudica una interacción selectiva entre el fármaco y su diana en el estado de enfermedad, dando lugar a efectos no deseados en tejidos sanos y limitando la dosis efectiva en el sitio deseado. Los medicamentos regulados con la luz son moléculas pequeñas que se pueden ensayar, validar y aprobar mediante procedimientos estándar de desarrollo de medicamentos, y se pueden aplicar directamente a organismos silvestres, incluidos los humanos. Esta nueva disciplina se conoce como "fotofarmacología" y ofrece muchos beneficios para los tratamientos farmacológicos futuros. Un fármaco fotoconmutable reversible se podría controlar con la luz en todo el cuerpo, mejorando drásticamente su selectividad para una diana expresada en un sitio específico del organismo y reduciendo así los efectos secundarios en otras regiones.

Aún no se entienden completamente las complejas funciones de los receptores muscarínicos (mAChR) y la farmacología clínica del sistema muscarínico presenta importantes limitaciones. Estos receptores pertenecen a la clase A de receptores acoplados a proteína G (GPCR) y se clasifican farmacológicamente en cinco subtipos (M1-M5). Los compuestos bioactivos selectivos para el subtipo muscarínico pueden ser potencialmente muy efectivos para terapias contra la enfermedad de Alzheimer y Parkinson, asma, dolor, trastornos de la motilidad intestinal, enfermedades cardíacas y trastornos de la función urinaria. A pesar de varias décadas de estudios para identificar y desarrollar nuevos agonistas y antagonistas muscarínicos, aún no hemos logrado obtener todo el potencial terapéutico de esta clase de fármacos. La causa principal es la baja selectividad de subtipo de estos medicamentos. La elevada homología de la secuencia de aminoácidos en los sitios ortostéricos de todos los receptores M1-M5 limita el desarrollo de agentes adecuados. Son necesarios enfoques alternativos para conseguir una buena

especificidad de subtipo. El éxito de este desafío podría revolucionar la farmacología contra una gran variedad de enfermedades y trastornos, y lograr grandes avances en el conocimiento sobre el rol metabotrópico de la acetilcolina (ACh).

## **OBJETIVOS**

El gran objetivo de esta tesis es el desarrollo de ligandos fotoconmutables que permitan la modulación óptica de los receptores muscarínicos endógenos y de sus acciones fisiológicas, a través de estos objetivos específicos:

- 1) Desarrollo de agonistas muscarínicos fotoconmutables, aprovechando la extraordinaria actividad agonista de Iperoxo (*Capítulo II*);
- 2) Desarrollo de agonistas muscarínicos fotoconmutables mediante la hibridación molecular. Esta estrategia de diseño permite la creación de fármacos con mayor afinidad, eficacia, selectividad y seguridad que el ligando original (*Capítulo III*);
- 3) Obtención de antagonistas muscarínicos fotoconmutables mediante la nueva estrategia de "cripto-azologización", que imita la geometría del sistema heterocíclico de un antagonista del receptor M1, la pirenzepina (*Capítulo IV*);
- 4) Caracterización fotoquímica de todos los nuevos compuestos sintetizados (*Capítulos II, III y IV*);
- 5) Caracterización de la actividad farmacológica de los nuevos compuestos en receptores muscarínicos y de sus propiedades fotoconmutables en el entorno biológico (*Capítulos II, III, IV*);
- 6) Evitar el uso de la luz ultravioleta para estimular los nuevos ligandos muscarínicos fotoconmutables, para permitir una mayor penetración de la luz en los tejidos y reducir posibles daños celulares (*Capítulo II, III, IV*).

## CAPÍTULO II

### DESARROLLO DE AGONISTAS ORTOSTÉRICOS FOTOCONMUTABLES PARA CONTROLAR RECEPTORES MUSCARÍNICOS.

Iperoxo (IPX) es un ligando muscarínico muy atractivo. A pesar de su estructura química con un anillo isoxazolínico, que es atípica en comparación con la acetilcolina (ACh), este medicamento es uno de los agonistas muscarínicos más potentes que se conocen, aunque carece de selectividad de subtipo. En este capítulo hemos diseñado, sintetizado y caracterizado el perfil farmacológico de derivados fotoconmutables monovalentes (PI, F4-PI. Figura 1) y bivalentes (IAI, F4-IAI. Figura 1) de Iperoxo.

Para diseñar los nuevos compuestos, hemos extendido el nitrógeno de amonio cuaternario de Iperoxo con azobencenos no sustituidos (PI e IAI) y tetra-orto-fluorados (F4-PI y F4-IAI). Elegimos los azobencenos como interruptores moleculares debido a sus propiedades favorables, como la flexibilidad de diseño, los grandes cambios de geometría al isomerizar, la alta eficiencia de fotoisomerización, la gran estabilidad química y el buen perfil de seguridad que han demostrado en humanos.

Utilizamos los azobencenos tetraorto-fluorados por sus propiedades de fotoconversión *trans* / *cis*, que es muy completa y de lenta relajación térmica *cis* -> *trans*, gracias a la presencia de estos sustituyentes y sus propiedades electrónicas y estéricas.

Tras la síntesis química, hemos caracterizado las propiedades fotoquímicas de los nuevos compuestos, que deben comportarse como foto-interruptores reversibles. Inicialmente probamos la actividad farmacológica de estos ligandos mediante ensayos de unión específica a los receptores muscarínicos en membranas cerebrales de ratas. Posteriormente, evaluamos la actividad de estos derivados de iperoxo *in vitro* con la técnica de complementación de luciferasa en células en cultivo que expresan el mAChR M1 humano.

Por último, dimos una explicación de nuestros resultados farmacológicos mediante simulaciones computacionales de la unión entre ligandos y proteína, utilizando el modelo activo del receptor M1.

## Resultados y discusión del Capítulo II

En este primer estudio presentamos el fotocontrol de la actividad de los receptores muscarínicos utilizando la estrategia fotofarmacológica. Primero hemos demostrado que la extensión de iperoxo con azobenceno no compromete su actividad agonista. Este resultado no podía darse por supuesto y fue de fundamental importancia para el objetivo del proyecto. En el nuevo grupo de ligandos muscarínicos, solo el compuesto monovalente PI ha mostrado eficacia y potencia significativamente menores que el iperoxo. El perfil farmacológico de todos los demás derivados de iperoxo es comparable al del fármaco modelo.

Nuestros resultados *in vitro* muestran que los ligandos bivalentes (IAI y F4-IAI) son tan potentes como el iperoxo y pueden fotoconmutar farmacológicamente, a diferencia de los monovalentes (PI y F4-PI) que no muestran diferencias de actividad entre los fotoisómeros. En particular, los isómeros *trans* de IAI y F4-IAI han mostrado mayor potencia que sus formas *cis*. Estos resultados confirmaron la validez de la estrategia de extender la estructura de iperoxo con un grupo azobenceno para obtener ligandos que puedan fotocontrolar la actividad de los receptores muscarínicos.

Nuestros estudios computacionales revelaron que la actividad fotoconmutable de los derivados de iperoxo bivalentes parece estar causada por interacciones adicionales con el sitio alostérico del receptor muscarínico. Por lo tanto, el diseño de los próximos derivados de iperoxo debería hacer mayor hincapié en los contactos de los ligandos con la porción alostérica del receptor, para optimizar así el fotocontrol de los receptores muscarínicos.

*Este estudio se ha publicado en el artículo:*

*“Fluorination of Photoswitchable Muscarinic Agonists Tunes Receptor Pharmacology and Photochromic Properties.” Agnetta L., Bermúdez M., Riefolo F., et al. Journal of Medicinal Chemistry 2019 62 (6), 3009-3020. DOI: 10.1021/acs.jmedchem.8b01822.*

## CAPÍTULO III

### **AGONISTAS MUSCARÍNICOS FOTOCONMUTABLES OBTENIDOS MEDIANTE HIBRIDACIÓN MOLECULAR DE LIGANDOS ORTOSTÉRICOS Y ALOSTÉRICOS.**

En este capítulo investigamos si se puede mejorar el fotocontrol de la actividad muscarínica favoreciendo las interacciones entre los derivados de iperoxo y el sitio alostérico del receptor. Para el diseño de los nuevos ligandos hemos explorado la "hibridación molecular", una estrategia emergente para descubrir nuevos fármacos y que consiste en combinar los farmacóforos de diferentes moléculas bioactivas en una única estructura química. El nuevo compuesto híbrido que se obtiene puede mostrar un perfil farmacológico que también es "híbrido", con una mayor afinidad, eficacia, selectividad o seguridad de los fármacos originales. Los agentes híbridos muscarínicos convencionales se denominan "dualstericos" y unen en la misma estructura molecular los elementos fundamentales de un potente agonista ortostérico y un ligando alostérico selectivo a subtipo.

Entre los cinco subtipos muscarínicos, el receptor M2 constituye un prototipo esencial para estudiar el fenómeno del alosterismo de los GPCRs. Los agentes alostéricos W84 y Naphmethonium se han utilizado frecuentemente en combinación con Iperoxo para crear agonistas dualstéricos de M2. En este estudio, nos hemos centrado en los compuestos híbridos de M2 que han demostrado mayor eficacia farmacológica: Phthalimide-8-Iperoxo (P-8-Iper) y Naphthalimide-8-Iperoxo (N-8-Iper). A partir de estas estructuras químicas hemos desarrollado los correspondientes derivados fotoconmutables, reemplazando las cadenas de octano que separan las porciones ortostéricas y alostéricas de los ligandos originales con azobencenos. Así hemos sintetizado y caracterizados fotoquímicamente Phthalimide-Azobenceno-Iperoxo (PAI) y Naphthalimide-Azobenceno-Iperoxo (NAI) (Figura 2). PAI es el único que actúa como foto-interruptor farmacológico reversible, y hemos estudiado su actividad *in vitro* midiendo los cambios de calcio intracelular. Estos registros dan una indicación de la activación del receptor en células que sobrepresan los receptores M2 humanos. Una

vez demostrado el fotocontrol de M2 *in vitro*, hemos explorado las aplicaciones de PAI *in vivo* como instrumento de investigación biológica y por su potencial en terapias fotorreguladas.

### Resultados y discusión del Capítulo III

La combinación de la estrategia de hibridación con la inserción de un azobenceno en la estructura química ha permitido crear un ligando muscarínico sensible a la luz y muy prometedor farmacológicamente. PAI activa los receptores M2 en su conformación *trans* y se puede fotoisomerizar con luz ultravioleta (365 nm) a la forma *cis*, que es menos activa. La isomerización inversa de *cis* a *trans* se obtiene utilizando longitudes de onda de 420-460 nm o luz blanca.

Los receptores M2 están expresados en el corazón y su activación disminuye la frecuencia cardíaca. Por este motivo, los M2 se consideran una diana farmacológica para modular la función cardíaca. La fotorregulación espaciotemporal y reversible de funciones biológicas es una técnica que suscita mucho interés en el campo cardiovascular, en particular para enfermedades como la arritmia, en que las terapias clásicas como la estimulación eléctrica de los músculos cardíacos presentan varias e importantes limitaciones. Por lo tanto, la primera aplicación de PAI se centró en fotocontrolar la función cardíaca en dos modelos animales silvestres (renacuajo y rata).

*Este estudio se ha publicado en el artículo:*

*"Optical Control of Cardiac Function with a Photoswitchable Muscarinic Agonist." Riefolo, F. et al. Journal of the American Chemical Society 2019 141 (18), 7628-7636. DOI: 10.1021/jacs.9b03505.*

En segunda instancia, nos hemos centrado en las funciones cerebrales fundamentales que están dirigidas por el sistema colinérgico. Los receptores muscarínicos están abundantemente distribuidos en los tejidos cerebrales. La neuromodulación colinérgica es compleja y puede asociarse directamente con patrones característicos de actividad neuronal en la corteza cerebral, generalmente llamados "ondas cerebrales" o "estados cerebrales". Estas actividades oscilatorias neurales son incesantes y se consideran como importantes marcadores de los comportamientos y estados mentales humanos. El sistema colinérgico y otros neurotransmisores endógenos cooperan para controlar las transiciones entre diferentes patrones de oscilación neural, y por tanto entre diferentes comportamientos.

La manipulación de tales ondas cerebrales no solo es interesante para la investigación en neurociencia, sino que también ofrece gran potencial en medicina como una estrategia terapéutica moderna contra diferentes trastornos neurológicos y neurodegenerativos. Con esta segunda aplicación de PAI hemos demostrado por primera vez la posibilidad de fotocontrolar las transiciones entre estados cerebrales, en rodajas corticales aisladas y en ratones no manipulados genéticamente.

*Los resultados de este trabajo se han enviado recientemente a una revista científica, y se reproducen en esta tesis en formato de manuscrito "preprint" que está depositado online con referencia:*

*Control of brain state transitions with light. Barbero, A.\*; Riefolo, F.\* et al. bioRxiv 793927; doi: <https://doi.org/10.1101/793927>. \*co-first authors.*

Hemos demostrado que PAI puede emplearse para fotocontrolar la acción de los receptores muscarínicos del corazón y del cerebro de animales vivos. Estos resultados abren la puerta a nuevas terapias contra la arritmia y al estudio de los efectos colinérgicos en la cognición y el comportamiento. Además, la activación de PAI con luz infrarroja (dos fotones) permite salvar un importante obstáculo, la penetración profunda en tejidos biológicos sin causar daños, y hace posible aplicaciones no invasivas *in vivo*. En este sentido, se podría mejorar la capacidad de PAI de absorber dos fotones insertando un azobenceno fluorado puede ser considerado para ampliar sus aplicaciones fotofarmacológicas. Por otra parte, sería necesario simplificar los dispositivos ópticos de estimulación de dos fotones para miniaturizarlos y hacerlos más robustos, favoreciendo así las aplicaciones avanzadas de la fotofarmacología.

## CAPÍTULO IV

### DESARROLLO DE ANTAGONISTAS MUSCARÍNICOS DE M1 FOTOCOMMUTABLES MEDIANTE “CRIPTO-AZOLOGUIZACIÓN”

Paralelamente al desarrollo de los agonistas muscarínicos, también hemos investigado la creación de antagonistas foto-regulados. En este proyecto nos hemos centrado en los antagonistas del receptor M1, que se utilizan contra la úlcera péptica, y son terapias prometedoras para la enfermedad de Parkinson (EP), algunas formas de cáncer, o para reducir la mortalidad de cardiopatías isquémicas. Hemos elegido la pirenzepina como antagonista M1 modelo para diseñar nuestros derivados fotosensibles, debido a la su fascinante estructura química, perteneciente a la familia de las "estructuras privilegiadas". En general, estos medicamentos "privilegiados" contienen un sistema heterocíclico en su estructura química y se han usado en medicina para muchos tratamientos diferentes. De toda manera, la baja selectividad de estos compuestos causa muchos efectos secundarios y toxicidad que han reducido su uso clínico.

Diversos ligandos anticolinérgicos (pirenzepina, otenzepad, telenzepina, propantelina, AFDX-116 y metantelina) presentan un núcleo heterocíclico acoplado a diferentes cadenas laterales que producen una moderada selectividad de subtipo entre los cinco receptores muscarínicos. Algunos de estos medicamentos se han comercializado para diferentes usos médicos, pero su perfil de seguridad ha limitado las aplicaciones terapéuticas.

En este capítulo desarrollamos una nueva estrategia de diseño fotofarmacológico, la "criptoazologuización", que reemplaza el núcleo tricíclico de los fármacos privilegiados con diferentes azobencenos como foto-interruptores moleculares. Este método ofrece la ventaja de producir fármacos que son inactivos en la configuración *trans*, la más estable termodinámicamente. Solo al iluminar con la longitud de onda correcta se puede obtener el isómero *cis* que imita la geometría tricíclica del fármaco original y su efecto.

Para demostrar el potencial de esta nueva estrategia fotofarmacológica hemos desarrollado cuatro derivados de pirenzepina, llamándolos

"criptozepinas". Hemos estudiado la afinidad de estos nuevos compuestos por los receptores muscarínicos mediante ensayos de unión específica a los receptores muscarínicos en membranas cerebrales de ratas. Luego demostramos la actividad como antagonista fotoconmutable *in vitro*, registrando los cambios de calcio intracelular en células que sobreexpresan los receptores M1, y *ex vivo* en aurículas cardíacas.

## Resultados y discusión del Capítulo IV

En este estudio hemos validado la innovadora estrategia de "cripto-azologuización" mediante el desarrollo de derivados foto-conmutables de la pirenzepina, un conocido antagonista de M1. Nuestros "criptoazólogos" han demostrado que modulan reversiblemente la actividad de los receptores muscarínicos, mostrando una fuerte inhibición después de iluminarlos (forma *cis*) *in vitro* y en aurículas cardíacas *ex vivo*. La "criptoazologuización" podría permitir la administración de fármacos inactivos (forma *trans*) y su activación con luz solo en la ubicación corporal deseada y en el momento necesario, limitando así los efectos adversos en otras regiones y órganos. Otra ventaja de esta estrategia es que el uso de azobencenos clásicos como foto-interruptores permite hasta diez diferentes funcionalizaciones químicas, pero manteniendo una cierta simplicidad sintética.

Siguiendo el camino trazado por PAI, estamos aplicando las criptozepinas al control de las ondas cerebrales. En esta dirección, también serían relevantes las propiedades de estimulación infrarroja con láseres pulsados, que permitirían controlar su actividad anticolinérgica en presencia del neurotransmisor endógeno *in vivo* y de forma no invasiva. Se podría considerar la inserción de uno o más átomos de flúor en las posiciones orto del azobenceno para mejorar tanto su potencia farmacológica como la sección transversal de dos fotones del fármaco.

Esta nueva estrategia de cripto-azologuización fotofarmacológica permitiría optimizar la acción de muchos compuestos "privilegiados", por ejemplo mejorando la selectividad de los fármacos antidepresivos tricíclicos (ATC) mediante la foto-activación espacio-temporal. De este modo se podría reducir sus efectos secundarios y su toxicidad.

*Los resultados de este trabajo se han enviado recientemente a una revista científica, y se reproducen en esta tesis en formato de manuscrito: "Rational design of photochromic analogs of tricyclic drugs" Riefolo, F.; et al.*

## CAPÍTULO IV

### CONCLUSIONES

El *Capítulo II* describe el desarrollo de derivados foto-regulados del agonista muscarínico Iperoxo, y muestra que:

- El potente agonista muscarínico Iperoxo puede tolerar la extensión de su estructura con azobencenos sin cambiar su actividad original.
- La funcionalización de los azobencenos con flúor mejora la potencia de los derivados de iperoxo. Esto parece deberse a contactos lipofílicos adicionales entre los átomos de flúor y los residuos de M1, como indican nuestros estudios computacionales.
- Los agonistas fotoconmutables bivalentes (IAI y F4-IAI) han mostrado una mayor afinidad y potencia en los receptores muscarínicos que los monovalentes (PI y F4-PI), y también una actividad fotoconmutable más pronunciada. Este efecto probablemente se debe a interacciones en el sitio alostérico muscarínico que los bivalentes pueden hacer. Por lo tanto, una fuerte afinidad por los sitios alostéricos podría optimizar la fotofarmacología de esta clase de agonistas muscarínicos.

El *capítulo III* presenta el desarrollo de agonistas híbridos fotoconmutables del receptor M2. Los resultados muestran que:

- La fusión de las estrategias de hibridación y azologuización da lugar a PAI, un fuerte agonista M2 en su forma *trans* que se puede fotoisomerizar a la forma menos activa *cis* con luz ultravioleta (365 nm). La isomerización de *cis* a *trans* se obtiene con luz de 420-460 nm o blanca. Ambos isómeros de PAI tienen una excelente estabilidad térmica.
- La activación de los receptores M2 del corazón disminuye la frecuencia cardíaca y prolonga el tiempo de conducción auriculoventricular. En este contexto, PAI permite fotocontrolar la función cardíaca *in vivo*, y ofrece nuevas oportunidades terapéuticas contra diversas cardiopatías.
- Los receptores M2 del cerebro modulan varios procesos cognitivos, de aprendizaje, de la memoria, de las funciones sensoriales y

motoras. PAI permite controlar la actividad rítmica de la red cortical *ex vivo* y en ratones anestesiados. Estas propiedades son novedosas para la investigación básica en neurociencia e inspiran el desarrollo de nuevas terapias contra diversos trastornos cerebrales.

- La excitación con dos fotones de PAI permite activarlo con luz infrarroja, que penetra profundamente en los tejidos biológicos y causa daños mínimos. Estos resultados abren la puerta a aplicaciones fotofarmacológicas *in vivo* de forma no invasiva.

En el Capítulo IV, el desarrollo de antagonistas de M1 foto-regulados mediante método de la "criptoazologuización" demuestra que:

- El azobenceno permite imitar el sistema tricíclico del antagonista M1 pirenzepina. Esta estrategia de "criptoazologuización" se podría utilizar para controlar la actividad de muchos otros fármacos tricíclicos con luz.
- Los "criptoazólogos" de la pirenzepina que hemos desarrollado inhiben los receptores M1 con mayor potencia en el caso del fotoisómero *cis*, y lo hacen tanto *in vitro* como en las aurículas cardíacas *ex vivo*, demostrando la eficacia de esta estrategia.



